

Characterization of the protein phosphatase 1E (PPM1E)

Localization and truncation in brain tissue and effects on
neuronal morphology in primary neuronal culture

Dissertation

in partial fulfillment of the requirements
for the degree “Doctor rerum naturalium”
at the Georg August University Göttingen,
Faculty of Biology

submitted by

Anne Lene Jessen

born in

Kiel, Germany

Göttingen 2010

First Referee:

Prof. Dr. Nils Brose

Second Referee:

Prof.em. Dr. Rüdiger Hardeland

Advisor:

Dr. Heinz von der Kammer

Date of submission of the PhD thesis:

September 21, 2010

Date of thesis defence:

November 2, 2010

Declaration

This dissertation has been written independently and with no other sources and aids than quoted.

I hereby declare that this submission is my own work and that, to the best of my knowledge and belief, it contains no materials previously published or written by another person nor material which to a substantial extent has been accepted for the award of any other degree of the university or other institute of higher education, except where due acknowledgement has been made in the text.

Anne Lene Jessen

Göttingen, September 21, 2010

TABLE OF CONTENTS

ABSTRACT.....	7
ABBREVIATIONS.....	9
LIST OF FIGURES.....	13
LIST OF TABLES.....	16
1 INTRODUCTION.....	17
1.1 Alzheimer's disease.....	18
1.1.1 Cognitive phenotype, diagnostic and treatment.....	18
1.1.2 Ante-mortem diagnostic.....	18
1.1.3 Treatment of Alzheimer's disease – state of the art.....	19
1.1.4 Treatment of Alzheimer's disease - outlook.....	20
1.1.5 Histological phenotype.....	20
1.1.6 Post-mortem diagnostic.....	21
1.1.7 Etiology of Alzheimer's disease.....	22
1.2 Neuronal and dendritic spine morphology.....	24
1.2.1 Neurons in the hippocampus.....	24
1.2.2 Dendritic spine morphology.....	25
1.2.3 Dendritic spine motility.....	26
1.2.4 Synapses on dendritic spines.....	27
1.2.5 Compartmentalization and organelles in spines.....	27
1.2.6 The cytoskeleton.....	28
1.2.7 The actin cytoskeleton in dendritic spines and the neuronal nucleus.....	29
1.2.8 Synapse and dendritic spine morphogenesis.....	30
1.2.9 Synapse maturation.....	31
1.3 A screen for differentially regulated genes in early stages of Alzheimer's disease.....	31
1.4 The protein phosphatase 1E - PPM1E.....	34
1.4.1 A general introduction of phosphatases.....	34
1.4.2 The structure of the <i>PPM1E</i> gene and the PPM1E protein.....	36
1.4.3 Cellular localization and tissue specificity of PPM1E.....	37
1.4.4 Upstream effectors and regulators of the <i>PPM1E</i> gene.....	38
1.4.5 Proposed PPM1E effector kinases and binding partners.....	38
1.4.6 Phenotypes induced by PPM1E.....	45
1.5 Model systems and intentions of this study.....	45
1.5.1 Animal and cellular models for Alzheimer's disease.....	46
1.5.2 Intentions of this study.....	47

2	MATERIAL AND METHODS.....	48
2.1	Material.....	48
2.1.1	Chemicals and consumables.....	48
2.1.2	Biological material.....	48
2.1.3	Animals.....	48
2.1.4	Oligonucleotides.....	49
2.1.5	Vectors.....	54
2.1.6	Plasmids, as generated in this study.....	55
2.1.7	Antibodies and markers.....	56
2.2	Methods.....	58
2.2.1	General genetic, molecular biological and biochemical methods.....	58
2.2.2	His-hPPM1E protein expression, purification and <i>in vitro</i> activity determination.....	62
2.2.3	PPM1E Antibody production and characterization.....	64
2.2.4	Effects of PPM1E expression in <i>Drosophila melanogaster</i>	66
2.2.5	Influence of PPM1E in cell lines and primary neuronal culture.....	68
2.2.6	Expression and localization of PPM1E in human, rat and mouse brain.....	76
3	RESULTS.....	78
3.1	Characterization of tools for this study.....	78
3.1.1	Polymorphisms in the PPM1E sequence.....	78
3.1.2	Specificity of polyclonal anti-PPM1E antibodies.....	79
3.1.3	Endogenous and ectopic expression of PPM1E in different cell lines....	83
3.1.4	Characterization of human brain samples.....	84
3.2	Characteristic truncation and localization of the PPM1E phosphatase.....	88
3.2.1	PPM1E truncation and expression levels.....	88
3.2.2	Cellular and sub-cellular localization of endogenous PPM1E.....	94
3.3	Effects of PPM1E <i>in vitro</i> and in primary neuronal culture.....	106
3.3.1	Eukaryotically expressed PPM1E exhibits phosphatase activity <i>in vitro</i>	106
3.3.2	PPM1F levels do not compensate for PPM1E overexpression.....	107
3.3.3	Dephosphorylation of downstream kinases in primary neuronal culture	107
3.3.4	Increased PPM1E levels reduce mushroom spine density and dendritic arborization.....	118
3.3.5	Down-regulation of PPM1E with RNA interference affects spines and dendritic arborization.....	125
3.3.6	Coexpression of hARHGEF6 had no effect on dendritic spines.....	129
4	DISCUSSION.....	131

4.1	Characterization of PPM1E	131
4.1.1	Assessment of differential PPM1E expression is based on well-characterized human brain samples.....	131
4.1.2	The truncation of PPM1E is conserved in all investigated organisms ...	132
4.1.3	The levels of PPM1E are comparable in <i>R. norvegicus</i> and <i>H. sapiens</i>	133
4.1.4	The PPM1E expression rises during development	134
4.1.5	PPM1E changes its localization during development	136
4.1.6	PPM1E is enriched in the post-synaptic compartment and at sites of high metabolic activity.....	137
4.2	Effects of PPM1E	139
4.2.1	Suitability of rat primary neurons as a model system.....	139
4.2.2	Ectopic PPM1E expression affects the expression levels of CaMKIV and potentially of CaMKII α and PAK1	140
4.2.3	PPM1E expression affects the stabilization of dendritic spines.....	142
4.2.4	PPM1E expression affects the complexity of the dendritic arbor	145
5	CONCLUSIONS AND OUTLOOK	147
	APPENDIX.....	149
A 1.	Alignment of human PPM1E and PPM1F protein sequences	149
A 2.	Alignment of PPM1E transcripts	150
A 3.	Alignment of human and rat PPM1E protein sequences.....	151
A 4.	Alignment of human and rat ARHGEF6 protein sequences	152
A 5.	Alignment of human ARHGEF6 and ARHGEF7 protein sequences.....	153
A 6.	Alignment of human PPM1E with <i>D. melanogaster</i> CG10376-PA and Ppm1-PA	154
A 7.	Alignment of human ARHGEF6 with <i>D. melanogaster</i> rtGEF-PC	156
A 8.	Comparison of His-PPM1E purification by Ni-NTA and by size-exclusion chromatography.....	158
A 9.	PPM1E has no macroscopic effect on <i>D. melanogaster</i> neuronal cells.....	159
A 10.	Influence of growth substrate on PPM1E expression in primary hippocampal culture.....	162
	REFERENCE LIST.....	163
	ACKNOWLEDGEMENT	183
	CURRICULUM VITAE	185

ABSTRACT

Alzheimer's disease (AD) is a progressive neurodegenerative disorder, characterized by early deficits in learning and memory with eventual loss of higher cognitive functions. Although considerable progress in the understanding of the histological changes during the disease has been made, all therapies available today are symptomatic and the mechanisms which underly initial AD development are still unclear. In a screen of human brain tissue from different AD stages as represented by Braak staging, the brain-specific protein phosphatase 1E (PPM1E) stuck out for its strong up-regulation in early AD stages.

PPM1E has not been associated with neurological disorders or dementia before, however it was reported to negatively regulate the Ca^{2+} /calmodulin dependent kinases (CaMK) IV and II and the p21-activated kinase (PAK) 1. These kinases are important regulators of the actin cytoskeleton in dendritic spines and neuronal dendrites. The loss of dendritic spines and dystrophy of dendrites can be observed in the AD-affected brain. A negative regulation of the CaMKII, CaMKIV and PAK1 kinases might be potentially interrelated with these early changes. This study evaluated the influence of PPM1E on neuronal morphology in primary neuronal culture and aimed to characterize the previously poorly understood phosphatase in greater detail.

The present study showed that the elevation of PPM1E mRNA levels in human brain samples in early stages of Alzheimer's disease was also reflected on the protein level. PPM1E exhibited conserved subcellular, predominantly cytoplasmic localization and protein truncation in human brain tissue in different Braak stages, in rat brain tissues and in mature rat dissociated primary culture. The subcellular localization of PPM1E changed gradually during maturation of the dissociated primary culture from a predominantly nuclear localization during the first week, towards a predominantly cytoplasmic localization in more mature primary culture. Moreover PPM1E was enriched at sites of mitochondria accumulation in dendrites of mature dissociated hippocampal neurons.

Although CaMKII α , CaMKIV and PAK1 were proposed to be dephosphorylated by PPM1E, the present study found that increased PPM1E levels had no significant effect on the phosphorylation state of the kinases in mature dissociated primary neurons, whereas it significantly affected the overall CaMKIV expression. Further, increased levels of PPM1E had a degenerative effect on the number of dendritic mushroom

spines in mature neuronal culture, whereas downregulation of PPM1E lead to an increase in the number of stubby spines. The number of primary dendrites was negatively affected by down- as well as upregulation of PPM1E in these dissociated cultures.

Consequently, an early-onset dysregulation of PPM1E in Alzheimer's disease could negatively affect the dendrite and dendritic spine morphogenesis or homeostasis. Inhibiting PPM1E in an early stage of Alzheimer's disease may delay or at best even halt the progression of cognitive decline. PPM1E might therefore provide a promising new drug target for neurodegenerative diseases and especially for AD.

ABBREVIATIONS

A	alanine (Ala)
aa	amino acid(s)
AAV	adeno-associated virus
A β	amyloid beta
AD	Alzheimer's disease
a.k.a	also known as
AMPA	α -amino-3-hydroxyl-5-methyl-4-isoxazole-propionate
APP	amyloid precursor protein
ATP	adenosine triphosphate
ARHGEF6	Rac/Cdc42 guanine nucleotide exchange factor (GEF) 6 (α PIX)
ARHGEF7	Rac/Cdc42 guanine nucleotide exchange factor (GEF) 7 (β PIX)
au	arbitrary unit
BACE	β -site APP-cleaving enzyme 1
BLAST-N	basic local alignment search tool, for nucleotide sequences
BLAST-P	basic local alignment search tool, for polypeptide sequences
C	cysteine (Cys)
CaMK	Ca ²⁺ /calmodulin-dependent kinase
co	cortex / cortices
conc.	concentration(s)
COS-7	<u>C</u> V-1 (simian) in origin, <u>c</u> arrying the <u>S</u> V40 genetic material (kidney derived cell line)
COXII	cytochrome oxidase subunit II
CSF	cerebrospinal fluid
dbl	diffuse B-cell lymphoma
D	aspartic acid (Asp)
DAPI	4',6-diamidino-2-phenylindole
Dcvp	DNA containing viral rAAV particles
DG	dendate gyrus
DIV	day <i>in-vitro</i>
<i>D.melanogaster</i>	<i>Drosophila melanogaster</i>
DMSO	dimethyl sulfoxide
dNTP	deoxyribonucleotide
E	glutamic acid / glutamate (Glu)
E/Fhd domain	PPM1E/1F homology domain
EC ₅₀	half maximal effective concentration

ECL	enhanced chemiluminescence
EGFP	enhanced green fluorescence protein
EOAD	early-onset Alzheimer's disease
ER	endoplasmatic reticulum
EST	expressed sequence tag
F	phenylalanine (Phe)
FA	formaldehyde
F-actin	filamentous actin
G	glycine (Gly)
G-actin	globular actin
GAL	yeast transcription activator protein, specifically binds to UAS promoter region and activates transcription
GAPDH	glyceraldehyde 3-phosphate dehydrogenase
GEF	guanine nucleotide exchange factor
GFAP	glial fibrillary acid protein
h	hour(s)
H	histidine (His)
hc	hippocampus
hARHGEF6	<i>Homo sapiens</i> Rac/Cdc42 guanine nucleotide exchange factor 6
HBSS	Hanks's balanced salt solution
HeLa	human cervical cancer derived cell line (from patient <u>Henrietta Lacks</u>)
hshRNA	shRNA construct targeting rat PPM1E
<i>H.sapiens</i>	<i>Homo sapiens</i>
hPPM1E	<i>Homo sapiens</i> protein phosphatase 1E (PP2C domain containing)
hPPM1F	<i>Homo sapiens</i> protein phosphatase 1F (PP2C domain containing)
hSYN	human synapsin promoter
I	isoleucine (Ile)
JNK	c-Jun N-terminal kinase
K	lysine (Lys)
L	leucine (Leu)
LOAD	late-onset Alzheimer's disease
LTP	long-term potentiation
LTD	long-term depression
M	methionine (Met)

MAP2	microtubule associated protein 2
MCI	minimal/mild cognitive impairment
MEM	minimum essential medium
MWCO	molecular weight cut off
N	asparagine (Asn)
NBB	Netherlands Brain Bank
NCBI	National Center for Biotechnology Information
NeuN	neuron specific nuclear antigen
NFT	neurofibrillary tangles
NLS	nuclear localization signal
NMDA	N-methyl-D-aspartic acid
P	proline (Pro)
pAAV	plasmid DNA encoding elements for adeno associated virus production
PAGE	polyacrylamide gel electrophoresis
PAK	p21-activated kinase
PB	phosphate buffered saline
PCR	polymerase chain reaction
PMT	post-mortem delay time
PIIB	peptidylprolyl isomerase B (=cyclophilin B)
Q	glutamine (Gln)
qRT-PCR	quantitative real-time polymerase chain reaction
R	arginine (Arg)
RT	room temperature
rAAV	recombinant adeno associated virus
rARHGEF6	<i>Rattus norvegicus</i> Rac/Cdc42 guanine nucleotide exchange factor
<i>R.norvegicus</i>	<i>Rattus norvegicus</i>
RNA	ribonucleic acid
rPPM1E	<i>Rattus norvegicus</i> protein phosphatase 1E (PP2C domain containing)
rPPM1F	<i>Rattus norvegicus</i> protein phosphatase 1F (PP2C domain containing)
rr	ramp rate
rshRNA	shRNA construct targeting rat PPM1E
RT	room temperature
S	serine (Ser)

SA	spine apparatus
SDS	sodium dodecylsulfate
SEC	size exclusion chromatography
SER	smooth endoplasmic reticulum
Sf9	<i>Spodoptera frugiperda</i> cell line
shRNA	short hairpin ribonucleic acid
SYN	synapsin
SYP	synaptophysin
T	threonine (Thr)
TAMRA	tetramethyl-6-carboxyrhodamine dye
TRIM37	tripartite motif-containing protein 37
trunc.	truncated
UAS	upstream activation sequence
V	valine (Val)
W	tryptophan (Trp)
WHO	World Health Organization
WPRE	woodchuck postregulatory element
Y	tyrosine (Tyr)
zPPM1E	zebrafish protein phosphatase 1E (PP2C domain containing)

LIST OF FIGURES

	page
Figure 1.1: The hippocampus	25
Figure 1.2: Different types of dendritic spines	25
Figure 1.3 A: mRNA levels of (a) PPM1E, (b) ARHGEF6 and (c) PPM1F in human brain tissue samples from individuals corresponding to different Braak stages	32
Figure 1.3 B: mRNA levels of (a) PAK1 and (b) CaMKII α in human brain tissue samples from individuals corresponding to different Braak stages	33
Figure 1.4: Domain structure of human phosphatase PPM1E, its truncated version PPM1E(1-557) and PPM1F	36
Figure 1.5: Domain structure of the PPM1E target kinases CaMKII α , CaMKIV and PAK1	40
Figure 1.6: Nuclear and spine signaling pathways which regulate the actin cytoskeleton	41
Figure 1.7: Domain structure of ARHGEF6	44
Figure 2.1: Development of glial cells and neurons in primary hippocampal culture on day- <i>in-vitro</i> (DIV) 8 and 21	72
Figure 3.1: Specific detection of Myc_PPM1E with anti-PPM1E(AGC) (“AGC”) and anti-Myc-tag (“Myc”) antibodies	80
Figure 3.2: Myc_PPM1E expression in EGFP- and Myc-PPM1E-co-expressing and untransfected primary hippocampal neurons	81
Figure 3.3: Specificity of PPM1E(ENS) antibody in detection of endogenous PPM1E expression in human frontal cortex	82
Figure 3.4: Endogenous and ectopic expression of PPM1E in different cell lines	83
Figure 3.5: Linear regression between PPM1E mRNA levels and relevant properties of the analyzed human brain samples depicted in Table 3.1	86
Figure 3.6: Ectopic PPM1E(1-557) and PPM1E expression in H4 cells results in PPM1E bands with similar molecular weights	88
Figure 3.7: PPM1E levels in frontal human cortex samples classified into Braak stages 0 to 4	89
Figure 3.8: PPM1E protein levels in human frontal cortical brain samples	90

Figure 3.9: Linear correlation between PPM1E mRNA levels, normalized against cyclophilin B, and PPM1E(1-557) protein levels, normalized against α -Tubulin	91
Figure 3.10: Levels of PPM1E and PPM1E(1-554) in adult and embryonal day E17 rat brain tissues	92
Figure 3.11: Endogenous PPM1E expression during maturation of hippocampal neuronal culture	93
Figure 3.12: PPM1E is co-localized with the neuronal marker NeuN in human brain	94
Figure 3.13: PPM1E immunoreactivity in the human frontal cortex in different Braak stages shows similar cytoplasmatic expression of PPM1E in neurons in all analysed brain samples	95
Figure 3.14: No co-localization between glial cells and PPM1E(ENS) labeling	96
Figure 3.15: PPM1E is co-localized with the neuronal marker NeuN in rat frontal cortex and hippocampal dentate gyrus	97
Figure 3.16: Change in PPM1E localization during rat embryogenesis	98
Figure 3.17: PPM1E translocates from the nucleus to the cytoplasm during maturation of dissociated neuronal cultures from rat hippocampus (A) and cortex (B)	99
Figure 3.18: PPM1E is co-localized with EAAC1 in human frontal cortex	101
Figure 3.19: PPM1E is spacially close to GAD67 in human frontal cortex	101
Figure 3.20: PPM1E is not co-localized with the golgi apparatus	102
Figure 3.21: PPM1E is not co-localized with the endoplasmic reticulum	103
Figure 3.22: PPM1E is spatially closely correlated with synaptophysin and dendritic spines	104
Figure 3.23: PPM1E is co-localized with the mitochondrial protein COXII and not enriched at sites of F-actin accumulation in DIV 21 dissociated hippocampal neurons	104
Figure 3.24: Dephosphorylation of the peptide YGGMHRQEpTVDC by increased concentrations of purified His_PPM1E	106
Figure 3.25: PPM1F expression is independent from PPM1E expression under experimental conditions	107
Figure 3.26: PPM1E activity mutants	108
Figure 3.27: Expression of PPM1E and the activity mutants Myc_PPM1E(R241A) and Myc_PPM1E(D479N)	109
Figure 3.28: Efficiency of rAAV induced protein expression	110

Figure 3.29: Reduction of CaMKII α and β phosphorylation in dissociated wt and PPM1E overexpressing cortical neuronal cell culture	111
Figure 3.30: Influence of ectopic PPM1E expression on CaMKII α expression and phosphorylation in primary hippocampal culture	113
Figure 3.31: CaMKII α phosphorylation is visibly reduced in secondary dendrites which overexpress PPM1E	115
Figure 3.32: Influence of ectopic PPM1E expression on CaMKIV expression and phosphorylation in primary hippocampal culture	116
Figure 3.33: Influence of ectopic PPM1E expression on PAK1 expression and PAK phosphorylation in primary cortical culture	118
Figure 3.34: PPM1E reduces the number of mushroom spines in hippocampal neurons	120
Figure 3.35: Effects of EGFP, PPM1E and PPM1E(D479) expression on the (A) head diameter and (B) the spine length on hippocampal neurons	121
Figure 3.36: PPM1E expression decreases the number of mushroom-shaped spines in a concentration-dependent manner	122
Figure 3.37: PPM1E activity mutants have no influence on the arborization of primary hippocampal neurons	123
Figure 3.38: PPM1E overexpression significantly and concentration-dependent reduced the number of roots and the total neurite length	124
Figure 3.39: shRNA constructs down-regulate the expression of rat PPM1E	126
Figure 3.40: Downregulation of PPM1E increases the number and length and decreases the head diameter of stubby spines in hippocampal neurons	127
Figure 3.41: PPM1E overexpression as well as down-regulation reduce neuritic arborization	129
Figure 3.42: Overexpression of ARHGEF6 does not affect the number of spines nor does it increase the effect of PPM1E overexpression in mature hippocampal neurons	129

LIST OF TABLES

	page
Table 2.1: Oligonucleotides used in polymerase chain reaction (PCR) for cloning of different constructs used in this study	49
Table 2.2: Oligonucleotides used in quantitative real-time PCR (qRT-PCR) for the amplification of different genes	50
Table 2.3: Oligonucleotides for construction of shRNA constructs	53
Table 2.4: Oligonucleotides for sequencing of PPM1E and ARHGEF6 constructs	53
Table 2.5: DNA vectors which have been used in this study	54
Table 2.6: Plasmids generated for this study	55
Table 2.7: Antibodies and markers used in this study	56
Table 2.8: Sequences of the synthetic peptides used for immunization of rabbits and subsequent antibody isolation	65
Table 2.9: Cell lines cultivated in this study	69
Table 3.1: Human brain samples, which were classified as Braak 0 to 4, and analyzed for PPM1E mRNA levels previously	85

1 INTRODUCTION

Alzheimer's disease (AD) is a progressive neurodegenerative disorder, characterized by early deficits in learning and memory with eventual loss of higher cognitive functions. Although considerable progress in the understanding of the histological changes during the disease has been made, all treatment available today is symptomatic and the mechanisms which underly initial AD development are still unclear. Conventional approaches to identify drugs mainly addressed late stages of the disease and the nowadays available drugs fail to increase cognition in AD patients considerably. Moreover, it is likely that much of the neuronal damage, which is reflected in increased cognitive decline in late stages of AD, is presumably irreversible. It would therefore be desirable to prevent the disease before cognitive decline becomes apparent.

To identify genes that might be associated with the development of very early events in the disease, Evotec Neurosciences GmbH conducted a screen for genes that are differentially regulated in early AD. The brain-specific protein phosphatase 1E (PPM1E) stuck out in this screen for its strong up-regulation in early AD stages. PPM1E had not been associated with neurological disorders or dementia before, however it was reported to negatively regulate the Ca²⁺/calmodulin dependent kinases (CaMK) IV and II and the p21-activated kinase (PAK) 1. These kinases are important regulators of the actin cytoskeleton. Thus, negative regulation of these kinases and defects in the actin cytoskeleton in neurons in the AD-affected brain might be interrelated. This study evaluates the influence of PPM1E on the actin cytoskeleton in primary neuronal culture as model system and aims to characterize the previously poorly understood phosphatase in greater detail.

To provide a basis for the understanding of potential molecular links between PPM1E and Alzheimer's disease-related changes in the brain, this introduction will provide a short review of current AD research and clinical treatment. A screen of human brain tissues in different AD stages will be described afterwards, in which PPM1E expression is correlated with early disease development. Finally, the potential role which PPM1E might play in CaMK and PAK associated pathways and their respective relevance for spine development will be introduced.

1.1 Alzheimer's disease

Alzheimer's disease (AD) is a slowly progressing, heterogenous neurodegenerative disorder of uncertain etiology. It is the most common form of all brain degenerations and presumably caused by multiple factors. The greatest risk factor for AD is increasing age, wherefore AD becomes a major social and economic problem for the ageing society in post-industrialized countries. The total societal worldwide costs of dementia have been estimated to be \$422 billion in 2009 (Wimo et al., 2010).

1.1.1 Cognitive phenotype, diagnostic and treatment

Alzheimer's disease is characterized by a severe impairment of cognitive function while sensory and motor functions are very well preserved during early disease stages. Initially, AD is manifested as a series of mild cognitive impairments, deficits in short-term memories, loss of spatial memory and emotional imbalances (Selkoe, 2001). Declarative as well as nondeclarative memories become profoundly impaired during the course of the disease and are accompanied by a growing disability to learn new information. The ability for reasoning, abstraction and language also declines. During the progress of the disease, these symptoms become more severe, and ultimately result in the complete loss of executive functions.

1.1.2 Ante-mortem diagnostic

Progressive memory deficits are still the main diagnosis criterium for Alzheimer's disease¹ after elimination of other potential causes for dementia like vascular brain disease, Acquired immunodeficiency syndrome, morbus Parkinson and alcohol abuse. Other diagnostic approaches have advanced, namely the identification of biomarkers in the cerebrospinal fluid and *in vivo* positron emission tomography (PET) scans (Nordberg et al., 2010;Blennow et al., 2010;Dubois et al., 2007). The levels of A β and amyloid precursor protein (APP) isoforms, A β oligomers, and β -site APP-cleaving enzyme 1 (BACE1) levels in cerebrospinal fluid (CSF) have been proposed as biomarkers for AD (Zetterberg et al., 2010), but are not yet in clinical use. The relevance of APP, A β and BACE1 for the disease is described below in 1.1.7 *Etiology of Alzheimer's disease* (page 22).

PET scans have been successfully used for diagnostic purposes in clinical trials and are even able to distinguish Alzheimer's disease from other types of dementia with

¹ according to the "International Statistical Classification of Diseases and Related Health Problems 10, ICD-10 (F00-F03)", WHO

similar pathological brain alterations. However, diagnosis based on these physiological alterations remains difficult, because AD is a multifactorial disease and few AD-related physiological changes correlate consistently with the progress of dementia and can at the same time be diagnosed in the living patient with current technology. A significant correlation with cognitive disease progression has only consistently been described for the loss of dendritic spines and synapses on neurons and for the levels of soluble A β peptides in the interstitium² (spines and synapses: (Scheff et al., 2007;Lopez and DeKosky, 2003;Sisodia and St George-Hyslop, 2002;Terry et al., 1991); soluble A β peptides: (McLean et al., 1999;Lue et al., 1999)).

The diagnosis of AD is additionally complicated due the poor characterization of the transition modi between mild cognitive impairments (MCI) and AD. Currently, a diagnosis of MCI or mild physiological alterations in the brain is a poor predictor of disease development.

1.1.3 Treatment of Alzheimer's disease – state of the art

In addition to the outlined diagnostic challenges, no medical treatment is currently able to cure or prevent AD. However, some drugs which are able to delay disease progression or severity are used routinely for AD treatment. Today, five drugs are approved from the 'US Food and Drug Administration' (FDA): Four acetylcholinesterase inhibitors, which are applied for the enhancement of cognition and memory in moderate AD cases and which inhibit degradation of the neurotransmitter acetylcholin (Donepezil, ENA-713, Galantamine and Tacrine), and one 'N-methyl-D-aspartic acid' (NMDA) receptor antagonist, which is applied in moderate to severe cases and which modulates excess glutamatergic signaling (memantine). A number of alternative, but not FDA approved therapies are in use: Many patients additionally take antioxidants like Vitamin E or selenium, which are thought to be protective against damage caused by oxygen radicals. Women also take estrogen, which has been shown to reduce the risk of developing AD. Non-steroidal anti-inflammatory drugs (NSAIDs) may also be taken to prevent neuroinflammation-induced brain damage. However, neither antioxidants, nor estrogen, nor NSAIDs are proven to be beneficial in patients with manifested AD pathology.

² The relevance of A β peptides for the disease is described in 1.1.7 *Etiology of Alzheimer's disease*, page 22.

1.1.4 Treatment of Alzheimer's disease - outlook

Many drug trials have been discontinued during the last years, however a number of clinical trials in phase III are still running and represent the diversity of therapeutic approaches very well: anti-A β antibodies (AAB-001; Gammagard; Solanezumab), anti-oxidants (α -tocopherol, vitamine E), omega-3 fatty acids (docosahexanoic acid), estrogen (premarin), anti-inflammatory agents (ibuprofen), conditioners of cognitive function (Leuprolide acetate), γ -secretase inhibitors (LY450139 dihydrate), neuroprotectants (trans-3,4',5-trihydroxystilbene), anti-diabetics (rosiglitazone), 3-hydroxy-3-methylglutaryl-coenzyme-A-(HMG-CoA) reductase inhibitors (simvastatin) and agitation preventing agents (divalproex sodium) are currently tested for their effects on disease progression or severity.

A description of the whole range of proposed working mechanisms for these drugs is beyond the scope of this introduction. However, the roles of A β peptides and the γ -secretase in AD will be depicted below³.

1.1.5 Histological phenotype

On the histological level AD is generally characterized by the presence of two hallmark lesions: extracellular β -amyloid (A β)-containing neuritic plaques (Masters et al., 1985;Glenner and Wong, 1984a;Glenner and Wong, 1984b) and intracellular neurofibrillary tangles of hyperphosphorylated tau protein (Ballatore et al., 2007;Selkoe and Schenk, 2003;Brion et al., 2001;Braak and Braak, 1998;Hardy, 1997). Neuritic plaques are roughly spherical, extracellular deposits of amyloid β -protein (A β) fibrils, surrounded by dystrophic dendrites and axons, reactive astrocytes and activated microglia. A β peptides are cleavage products from the membrane protein 'amyloid precursor protein' (APP). Neurofibrillary tangles are non-membrane bound paired helical filaments in which hyperphosphorylated tau protein is enriched. They are mainly located in the perinuclear cytoplasm of many limbic and cortical neuronal cell bodies and cortical dystrophic dendrites.

The spatial and temporal connections between plaques and tangles are not completely understood. While hyperphosphorylated tau and insoluble tangles initially appear in the limbic system, i.e. the entorhinal cortex, hippocampus and dentate gyrus, and then progress to cortical areas, the plaques first appear in the frontal cortex to spread then over the entire cortical region (Smith, 2002;Braak and Braak, 1998;Bouras et al., 1994).

³ see 1.1.7 *Etiology of Alzheimer's disease*, page 22

While it has been observed that A β accumulation precedes and ultimately initiates the aggregation of wild-type tau protein in AD, the reverse sequence of pathogenesis has not been documented (Selkoe, 2002b).

A third invariant feature observed in AD patients, which has lately gained more attention in the research community, is the loss of multiple neuronal populations and synapses in selected brain regions (Lopez and DeKosky, 2003; Sisodia and St George-Hyslop, 2002; Terry et al., 1991).

In addition to neuritic dystrophies and eventual neuron loss, a progressive deprivation in dendritic spine numbers occurs on hippocampal pyramidal neurons (El Hachimi and Foncin, 1990; Ferrer and Gullotta, 1990; Scheibel, 1979), on dentate granule cells (Einstein et al., 1994; De Ruiter and Uylings, 1987; Gertz et al., 1987), and on neocortical pyramidal neurons (Baloyannis et al., 1992; Catala et al., 1988; Scheibel, 1983). Dendritic spines protrude from the dendrites of most principal neurons in the mammalian brain and represent the postsynaptic compartment for the majority of excitatory glutamatergic synapses (Carlisle and Kennedy, 2005; Sorra and Harris, 2000). Besides spine loss also morphological changes in dendritic spines were observed in the acoustic cortex of patients (Baloyannis et al., 2007).

A variety of other histological changes is observed in some AD patients. Among these changes are mild brain atrophy, 'diffuse' plaques with non-fibrillar accumulations of A β peptides and accumulation of A β in small blood vessels of the meninges and the cerebral cortex (Selkoe and Schenk, 2003).

1.1.6 Post-mortem diagnostic

Whether a dementia was of the Alzheimer type is usually assessed histologically in post-mortem tissue considering the presence of neuritic plaques and neurofibrillary tangles in neocortex and the limbic system (Ball and Murdoch, 1997). The severity of the disease is then expressed in scores determined in accordance with the '*Consortium to Establish a Registry for Alzheimer's Disease*' (CERAD) (Mirra et al., 1993; Mirra et al., 1991), and Braak criteria (Braak and Braak, 1991). The revised CERAD protocol diagnoses the probability for AD in a specific brain sample by semi-quantitative and age-related estimation of the frequency and relative proportions of both neuritic and diffuse plaques, which contain non-fibrillar A β , and on the basis of a clinical history in

dementia. The Braak staging makes use of differentiation between early, intermediate and late disease stages by semi-quantitative examination of neurofibrillary tangles.

1.1.7 Etiology of Alzheimer's disease

A great number of structural and biochemical changes in the brain during late-stage AD have been documented. However, only minor mechanistic insight into the initial development of the disease could be gained to date. The research has focussed to a great extent on the mechanisms underlying "familial" AD, also referred to as 'autosomal-dominant early-onset AD' (EOAD), presuming that they resemble those underlying the development of sporadic forms of AD. About 5 % of AD cases are "familial", in that they are associated with mutations in APP or presenilin genes.

Presenilins 1 and 2 are members of the catalytic core of the γ -secretase complex which is involved in APP cleavage (Selkoe and Wolfe, 2007;De Strooper, 2003). The normal physiological function of APP is unknown (Hardy, 2009). Most EOAD mutations alter APP processing, often resulting in increased levels of $A\beta_{1-42}$, a 42 amino acid peptide, which is more prone to aggregation and formation of plaques than other $A\beta$ fragments (Scheuner et al., 1996). $A\beta_{1-42}$ is proteolytically released from APP through cleavage by β -secretases (BACE) and subsequently by γ -secretases (Selkoe, 2001), whereas cleavage by α - and γ -secretases releases $APP_s-\alpha$ (Sisodia et al., 1990;Esch et al., 1990).

The amyloid hypothesis

Based on data derived from EOAD causing mutations and mouse models, which carry these mutations, the "amyloid hypothesis" was established (Tanzi and Bertram, 2005;Hardy and Selkoe, 2002). It suggests that elevation of $A\beta$ peptide levels, by increased production or decreased clearance, causes a series of events and triggers other deleterious changes including hyperphosphorylation of tau protein, which culminate in neuronal death and thus cause AD (Pimplikar, 2009;Hardy and Higgins, 1992;Selkoe, 1991).

However memory deficits and cognitive decline in AD patients do not correlate well with the $A\beta$ plaque burden and learning and synaptic dysfunction appear even before the formation of plaques (Selkoe, 2002a;Terry et al., 1991). Although two previous studies on AD animal models found correlations between amyloid plaque burden and cognitive decline (Gordon et al., 2001;Chen et al., 2000), most studies have failed to detect such

a correlation (Braak and Braak, 1998;Arriagada et al., 1992;Terry et al., 1991). Moreover, some mouse models show memory deficits even before plaques can be seen in the brain. This is frequently interpreted as evidence that amyloid plaques represent end-stage remains or byproducts of the pathological processes in AD.

The original amyloid hypothesis was adapted: Instead of amyloid plaques, soluble aggregates of toxic A β oligomers are thought to be the disease causing pathogenic agent (Walsh and Selkoe, 2007;Glabe, 2005;Walsh and Selkoe, 2004;Klein et al., 2001). This is supported by the fact that elevated levels of soluble A β peptides (McLean et al., 1999;Lue et al., 1999) correlate with cognitive decline. A growing amount of evidence suggests that soluble amyloid beta 1-42 (A β ₁₋₄₂) peptides are toxic and might induce synaptic dysfunction and neuronal death during the course of AD (Selkoe, 2002b).

As described above, dendritic spine loss and alterations, and the resulting loss of synapses, appear to be early events during the development of AD: Patients with mild AD already were described to have 55% less synapses in the stratum radiatum of the CA1 hippocampal area (Scheff et al., 2007). Additionally, the most prevalent early features found in cortical biopsies and animal models are synaptic loss and dysfunction (Coleman and Yao, 2003;Selkoe, 2002a).

The reduction in synapses during AD progression in humans also correlates well with tests for cognitive impairment, therefore dendritic spine and synapse alterations might be the structural correlates for cognitive decline (Scheff et al., 2007;Lopez and DeKosky, 2003;Sisodia and St George-Hyslop, 2002;Terry et al., 1991). Still other studies have shown correlations between abnormal dendritic spine morphology and brain dysfunction (Irwin et al., 2000;Wisniewski et al., 1991;Purpura et al., 1982).

It has been suggested that A β causes degeneration in presynaptic terminals and the loss of synapses and spines (Adalbert et al., 2007). Defects in axonal delivery of APP and in axosynaptic processing of APP have been proposed to be one cause for this process. A β -induced neuronal changes might also occur through direct binding of soluble A β peptides to excitatory synapses.

1.2 Neuronal and dendritic spine morphology

Changes in neuronal and dendritic spine morphology and numbers can be found in AD and many other cognitive disorders. Therefore neuronal morphology with a special focus on spine dynamics and morphogenesis is described in the following paragraph.

1.2.1 Neurons in the hippocampus

Neurons are highly specialized cells and can be distinguished into the signal receiving somatodendritic and the signal-transducing axonal compartment (reviewed in (Yoshihara et al., 2009;Sekino et al., 2007;Ethell and Pasquale, 2005;Yuste and Bonhoeffer, 2004)). Complex cell-cell interactions of single neurons and groups of synchronized neurons which create neuronal circuits are responsible for neurological processes. Neurons can be categorized according to their shape, size, neurochemical characteristics, connectivity and location.

Very well characterized and tightly organized neuronal circuits are found in the hippocampus, a structure of the mammalian limbic system in the medial temporal brain lobe, which is important for the formation of long-term memory (Figure 1.1). The hippocampus is one of the most plastic regions in the brain, and - together with the ventricular zone - the hippocampal dentate gyrus (DG) is one of only two structures in the brain known to retain the capability of de novo formation of neurons in the adult brain (Drew and Hen, 2007;Christie and Cameron, 2006;Goldman and Sim, 2005). The hippocampus is also one of the first affected brain regions during the development of AD, which is one of the reasons for the usage of primary dissociated hippocampal neurons as a model system for neurodegeneration in this study⁴. Densely packed pyramidal neurons and dentate granule cells of the DG constitute the majority of neurons in the hippocampus, however few inhibitory interneurons can also be found.

The neuronal circuits and populations in the hippocampus are well characterized (Morris and Johnston, 1995): The hippocampal DG receives the major afferent input from the entorhinal cortex (EC) via the perforant path (Figure 1.1 B). The axons of the granule cells of the dentate gyrus, the mossy fibers, in turn innervate the CA3 region. The pyramidal neurons of the CA3 region project via the Schaffer collaterals to the CA1 pyramidal neurons. The principal output of the hippocampus finally forms the connection of the CA1 to the subiculum (Sb) and on to the entorhinal cortex.

⁴ see also 1.5.1 Animal and cellular models for Alzheimer's disease, page 46

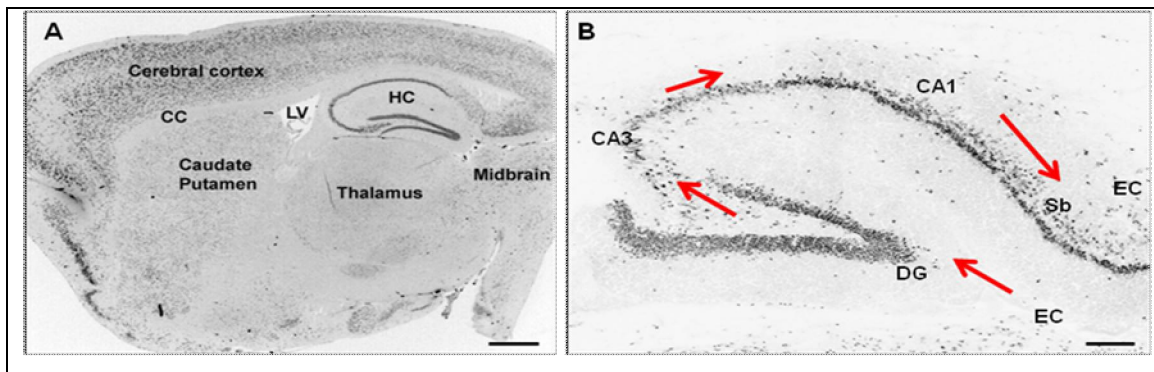


Figure 1.1: The hippocampus: (A) Saggital total mouse brain slice and (B) rat hippocampus slice. Neurons labeled by NeuN stain. (A) CC: Corpus callosum. LV: lateral ventricle. HC: hippocampus. (B) DG: dentate gyrus. Sb: subiculum. EC: entorhinal cortex. Arrows indicate the direction of neuronal circuits (compare text). Circuits adapted from (Morris and Johnston, 1995). Scale bars: (A) 1 mm, (B) 200 μm . (A, B) anti-NeuN labeled brain slices from this study.

1.2.2 Dendritic spine morphology

Dendritic spines are highly specialized actin-rich protrusions from the surface of dendrites (Figure 1.2 A, B). They were discovered by Santiago Ramon y Cajal in 1888, after visualization with a silver impregnation method developed by Golgi in 1873.

Spines have characteristic bulbous enlargements of their tips, the spine heads (Figure 1.2 B), and volumes between less than 0.01 up to 0.8 μm^3 (Harris and Kater, 1994). Spines receive about 90% of all glutamatergic excitatory presynaptic boutons in the mature central nervous system, and some inhibitory input (Harris and Kater, 1994). Mature neuronal dendrites can have up to 10 spines per μm .

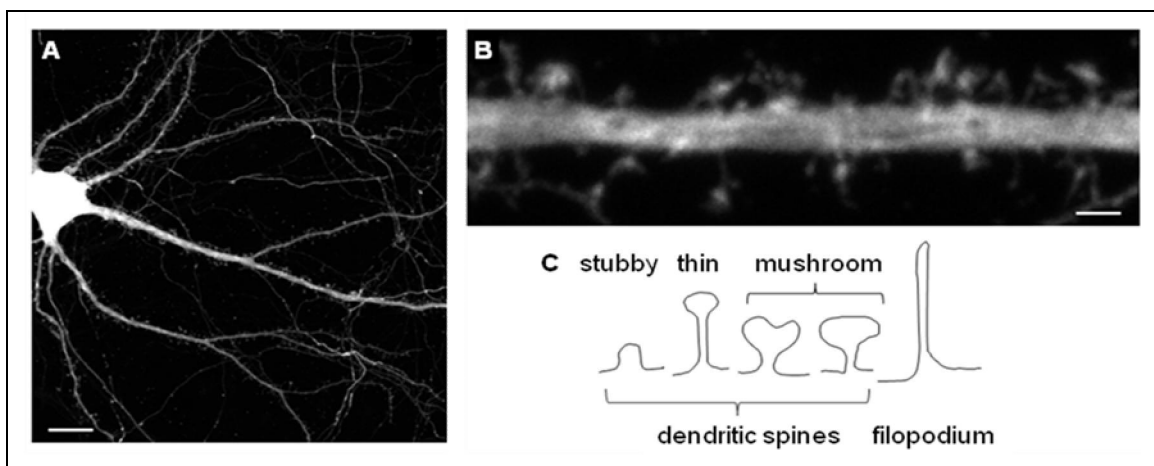


Figure 1.2: Different types of dendritic spines on an EGFP expressing neuron in dissociated hippocampal culture on day-*in-vitro* (DIV) 21 (A, B). (C) Schematic view of different spine types and a filopodium, adapted from Ethell and Pasquale (2005). (A, B) DIV 21, medium dense, dissociated primary hippocampal culture, transfected with pAAV/EGFP on DIV 7. Scale bars (A) 10 μm and (B) 1.5 μm .

Dendritic spines have been classified into thin, stubby and mushroom shaped spines based on their head-to-neck ratio (Peters and Kaiserman-Abramof, 1970). Thin spines have a small head and narrow neck with a head diameter of less than 0.6 μm (Figure 1.2 C). Their head is not bulbous. Stubby spines have no constriction between their head and their attachment to the dendritic shaft. Mushroom spines have a large irregular head which can have a diameter of more than 0.6 μm and a constricted narrow neck. Some mushroom spines have an irregularly shaped head (Yuste and Bonhoeffer, 2004). It has been suggested that mushroom spines represent more stable “memory” spines whereas thin spines could be “learning” spines (Tackenberg et al., 2009). Another type of dendritic protrusion is the dendritic filopodium, which is long, thin and headless and especially abundant in developing neurons, but also in adult neurons after certain events like induction of plasticity (Jourdain et al., 2003).

Irregularly shaped dendritic spines and abnormal spine densities or lengths have been also found in a number of cognitive disorders other than AD, like Fragile X syndrome, Down and Rett syndromes (Kaufmann and Moser, 2000).

1.2.3 Dendritic spine motility

Time-lapse imaging of spine dynamics shows that spines are not static, but can move along the dendrite and alter their morphology continuously even in the adult brain (Zuo et al., 2005; Holtmaat et al., 2005; Trachtenberg et al., 2002; Lendvai et al., 2000). Spine formation and remodelling in mature neurons can be induced by certain patterns of synaptic activity, learning and memory formation, hormonal fluctuations and changes in temperature (Roelandse and Matus, 2004; Yuste and Bonhoeffer, 2001; Engert and Bonhoeffer, 1999; Maletic-Savatic et al., 1999; Kirov and Harris, 1999; Hosokawa et al., 1995; Woolley et al., 1990; Fifkova and Delay, 1982). The activity of glutamate receptors, like α -amino-3-hydroxyl-5-methyl-4-isoxazole-propionate (AMPA) and NMDA receptors, is involved in this morphological change (Matus, 1999).

There is also evidence that the smaller spines preferentially undergo long-term potentiation (LTP), an experimentally induced strengthening of a synapse, while larger spines are more stable and show less plasticity (Matsuzaki et al., 2004). Classical mushroom-shape structures are more stable structures than thin and elongated spines (Bourne and Harris, 2008). Evidence suggests that activity and induction of plasticity participate in the selection of persistent spines.

Spine stability is developmentally regulated and increases during aging: In young mice 73 % of spines are persistent spines and have a lifetime longer than 8 days, whereas 96 % were stable in old animals (Holtmaat et al., 2005). This remarkable stability might indicate that neuronal circuits mature and stabilize, which might provide the structural basis for long-term memory.

1.2.4 Synapses on dendritic spines

Asymmetric chemical synapses are transcellular junctions capable of converting presynaptic changes in electrical charge into an extracellular chemical signal, which is received and integrated by the postsynaptic membrane. Presynaptic membrane depolarizations in the form of action potentials induce the opening of voltage dependent Ca^{2+} channels which allows Ca^{2+} influx. Then Ca^{2+} dependent exocytosis of presynaptic vesicles, filled with neurotransmitters, into the synaptic cleft between the post- and the presynaptic membrane is induced. The released neurotransmitters bind and activate receptors at the postsynaptic membrane which translate the chemical signal back to an electrical and to further signaling pathways.

The size of the post-synaptic spine head and the strength of the synapse correlate strongly, presumably associated with the higher levels of AMPA-type neurotransmitter-gated ion channels in larger spines (Kasai et al., 2003; Matsuzaki et al., 2001; Harris and Stevens, 1989; Harris and Stevens, 1988).

1.2.5 Compartmentalization and organelles in spines

One function of spines is to compartmentalize chemical and electrical changes within individual synapses (Nimchinsky et al., 2002; Yuste et al., 2000; Yuste et al., 1999; Segev and Rall, 1998; Svoboda et al., 1996). A correlation between the spine neck and the postsynaptic calcium response has been shown, implying that the spine serves as a calcium compartment (Korkotian and Segal, 2000). Ca^{2+} functions both as a charge carrier and as a signaling molecule (Nimchinsky et al., 2002; Yuste et al., 2000). It enters the spine either through neurotransmitter gated ion channels, like the NMDA receptor, AMPA receptor subtypes or voltage gated ion channels or through intracellular stores like the endoplasmic reticulum.

Electron microscopic investigation identified a dense structure, the post-synaptic density (PSD) below the postsynaptic membrane in the spine head juxtaposed to the active zone of the presynaptic terminal (Li and Sheng, 2003; Scannevin and Huganir,

2000); for review see (Kennedy, 1997). The PSD can be continuous or perforated (Tashiro and Yuste, 2003), and it is assembled from densely packed ion channels, cell surface receptors and cytoplasmic scaffolding and signaling proteins. Perforated PSDs are associated with more AMPA receptors than the non-perforated PSDs. Mushroom spines are more likely to have a perforated PSD whereas thin spines contain macular PSD, shaped like a disc (Sala, 2002). Dendritic filopodia do not contain a PSD (Jourdain et al., 2003).

Some dendritic spines contain smooth endoplasmic reticulum (SER), which assembles in larger spines into a structure named the spine apparatus (SA) consisting of two or more SER discs separated by electron-dense material (Nimchinsky et al., 2002), which possibly serves as Ca^{2+} ion, receptor protein and ion channel store (Tarrant and Routtenberg, 1979). The majority of mushroom-shaped spines contain SER, in contrast to only about 20% of the thin spines (Spacek and Harris, 1997). Since large spines are more likely to contain SER, their calcium concentrations can be regulated more tightly.

Polyribosomes and components of the endosomal-lysosomal pathway have also been found in spines, indicating that protein synthesis and degradation can occur locally (Steward and Schuman, 2001). Mitochondria are rarely found within spines in mature neurons but are essential for the formation and maintenance of spines and synapses (Li et al., 2004).

1.2.6 The cytoskeleton

The cellular morphology is stabilized by a dynamic network of filamentous specialized protein structures, which also facilitates the directed transport within the cell. Actin filaments, intermediate filaments and microtubuli interact in this meshwork. Actin filaments and microtubuli are built from F-actin and Tubulin subunits respectively. Actin filaments have especially important stabilizing functions below the plasma membrane and in membrane bulges like lamellopodia, microvilli, dendritic spines and during the dendritogenesis. Filamentous (F)-actin is enriched in dendritic spines (Kaeck et al., 1997;Wyszynski et al., 1997;Cohen et al., 1985;Matus et al., 1982), while microtubules are abundant only in the dendritic shaft and only few microtubule components have been detected in larger CA3 spines (Sorra and Harris, 2000;Van Rossum and Hanisch, 1999;Caceres et al., 1983;Westrum et al., 1980).

Neurofilament proteins, which are neuron-specific filaments related to intermediate filaments in other tissues, have also been detected in spines, but their function is poorly characterized (Walsh and Kuruc, 1992). The dynamic assembly and disassembly of the actin cytoskeleton in dendritic spines is highly regulated as described below.

Luo et al. (1996) were the first to suggest the significance of the actin cytoskeleton in dendritic spine formation. A disruption of the actin cytoskeleton, with the actin depolymerizing agent latrunculin A, during spine morphogenesis results in the global disassembly of synaptic structural elements (Zhang and Benson, 2001; Allison et al., 2000).

1.2.7 The actin cytoskeleton in dendritic spines and the neuronal nucleus

The importance of the actin cytoskeleton for spine morphology has been stressed above. A stringent regulation of the actin cytoskeleton is required for dendritic spine structural plasticity (Honkura et al., 2008; Cingolani and Goda, 2008) and while actin is one of the most abundant proteins in neurons as well as in muscle cells, it is very differently regulated in both cell types. Actin filaments, also known as microfilaments, are assembled from actin and a number of actin binding proteins. The actin protein is organized into two-stranded helical polymers with a diameter of 5 to 9 nm which can form linear bundles or fine meshworks. Although actin filaments are abundant throughout the cell, they are concentrated beneath the plasma membrane and in membrane protrusions. Most neuronal microfilaments are less than 1 μm in length.

Actin is present in a pool of soluble globular G-actin and filamentous F-actin polymers (Halpain, 2000; Rao and Craig, 2000). G-actin polymerizes fast *in vitro*, therefore G-actin binding proteins like thymosin β_4 sequester G-actin *in vivo* (Safer and Nachmias, 1994; Safer et al., 1990), and suppress its polymerization. The β - and γ -actin isoforms, which are selectively targeted to spines, are ubiquitously expressed and abundant in nervous tissue. The functional significance of the different genetic isotypes of actin is not clear because the genes are highly conserved in their intron-exon structure and in their sequence.

The actin filaments confer the characteristic spine morphology: In the spine neck and the core of the spine head F-actin forms longitudinal bundles, while it is arranged into a fine meshwork in the spine periphery (Landis and Reese, 1983; Fifkova and Delay, 1982; Matus et al., 1982).

The actin network is constantly rearranged and only 5% of the total actin in spines is stable, while most of it turns over within 2 min (Star et al., 2002). This constant turnover involves the treadmilling of existing filaments which have structural polarity, with polymerization on the fast growing “barbed” ends and depolymerisation at the “pointed” ends (Pollard and Borisy, 2003; Pantaloni et al., 2001; Woodrum et al., 1975). The fast growing ends are predominantly oriented towards the spine surface. The highest degree of actin dynamics is observed at the contact site to the presynaptic bouton, indicating a relation between the actin dynamics and synaptic transmission (Roelandse et al., 2003).

1.2.8 Synapse and dendritic spine morphogenesis

The molecular mechanisms that control the formation and elimination, motility and stability, size and shape of dendritic spines are still under investigation (Ethell and Pasquale, 2005). However, data from many experiments suggest that new spines can form by different mechanisms: *de novo* from a filopodium newly forming from a dendrite which then finds a presynaptic partner and subsequently evolves into a spine (Harris and Kater, 1994), or by constant outgrowth of spines directly, of which a few become stabilized by a presynaptic partner (Nimchinsky et al., 2002). New spines and functional synapses form, and non-activated synapses retract constantly (De Roo et al., 2008a; Nägerl et al., 2007).

Due to their high motility and flexibility it has been proposed that dendritic filopodia are involved in contacting new appropriate binding partners and then develop into spines. Filopodia form transient contacts with excitatory axons, some of which get stabilized and persist (Lohmann and Bonhoeffer, 2008). After that, filopodia can be morphologically and functionally transformed into spines (De Roo et al., 2008a; Zuo et al., 2005; Trachtenberg et al., 2002; Marrs et al., 2001; Maletic-Savatic et al., 1999). Meanwhile filopodia can also facilitate the establishment of synapses on the dendritic shaft (Fiala et al., 1998).

Finally, new protrusions also can appear directly as spines which typically have a long neck and small heads (Trachtenberg et al., 2002; Engert and Bonhoeffer, 1999). They are distinguished from filopodia by their head and severely reduced motility, but initially do not seem to have a PSD (De Roo et al., 2008b; Nägerl et al., 2007; Knott et al., 2006).

1.2.9 Synapse maturation

The stabilization of a synapse is likely facilitated and regulated by neural activity (Ehrlich et al., 2007). Hippocampal synapses undergo structural changes in size and shape after long-term potentiation *in vitro* and experience *in vivo* (Harvey and Svoboda, 2007; Holtmaat et al., 2006; Matsuzaki et al., 2004). This remodelling of spine size and morphology and synaptic strength is rendered possible by reorganization of the actin cytoskeleton and differential recruitment of receptors and ion channels to the postsynaptic membrane.

An increase in spine volume goes hand in hand with reorganization of the actin cytoskeleton from several actin pools in the spine (Honkura et al., 2008). Following induction of plasticity several proteins in the PSD are activated, among them the Ca²⁺/calmodulin-dependent kinase (CaMK) II which is activated through phosphorylation (Steiner et al., 2008). Rho GTPases such as Rac1 and Cdc42 appear to play central roles in spine remodelling and are regulated by several different signaling complexes including protein kinases such as CaMKK and CaMKI in a complex with GTPase exchange factor ARHGEF7 (β PIX) (Saneyoshi et al., 2008). An increase in spine volume correlates also with accumulation of additional AMPA receptors (Zito et al., 2009).

1.3 A screen for differentially regulated genes in early stages of Alzheimer's disease

In an endeavour to identify new drug potential drug targets for Alzheimer's disease, human cortical brain samples of different Braak stages were screened for genes that are differentially regulated in early stages of the disease (von der Kammer, 2009). Human brain samples from several 'brain banks' were analysed for their quality in respect to mRNA and protein degradation. Brain samples from the Netherlands Brain Bank (NBB) were found to be superior in these respects to samples from other sources (von der Kammer, personal communication). Histologically the individuals were grouped into different Braak stages and reflected the full range between Braak 0 and Braak 6⁵. These human brain tissue specimen from clinically and neuropathologically well characterized and age-matched individuals in frontal and inferior temporal cortex were analysed with real-time quantitative PCR (qRT-PCR) using gene-specific oligonucleotides.

⁵ compare 1.1.6 *Post-mortem diagnostic*, page 21

In total, five different donors with Braak stage 0, seven different donors with Braak stage 1, five different donors with Braak stage 2, four different donors with Braak stage 3, three different donors with Braak stage 4, six different donors with Braak stage 5 and four different donors with Braak stage 6 have been analysed. All values were normalized to Cyclophilin B values, a highly abundant 'housekeeping' gene.

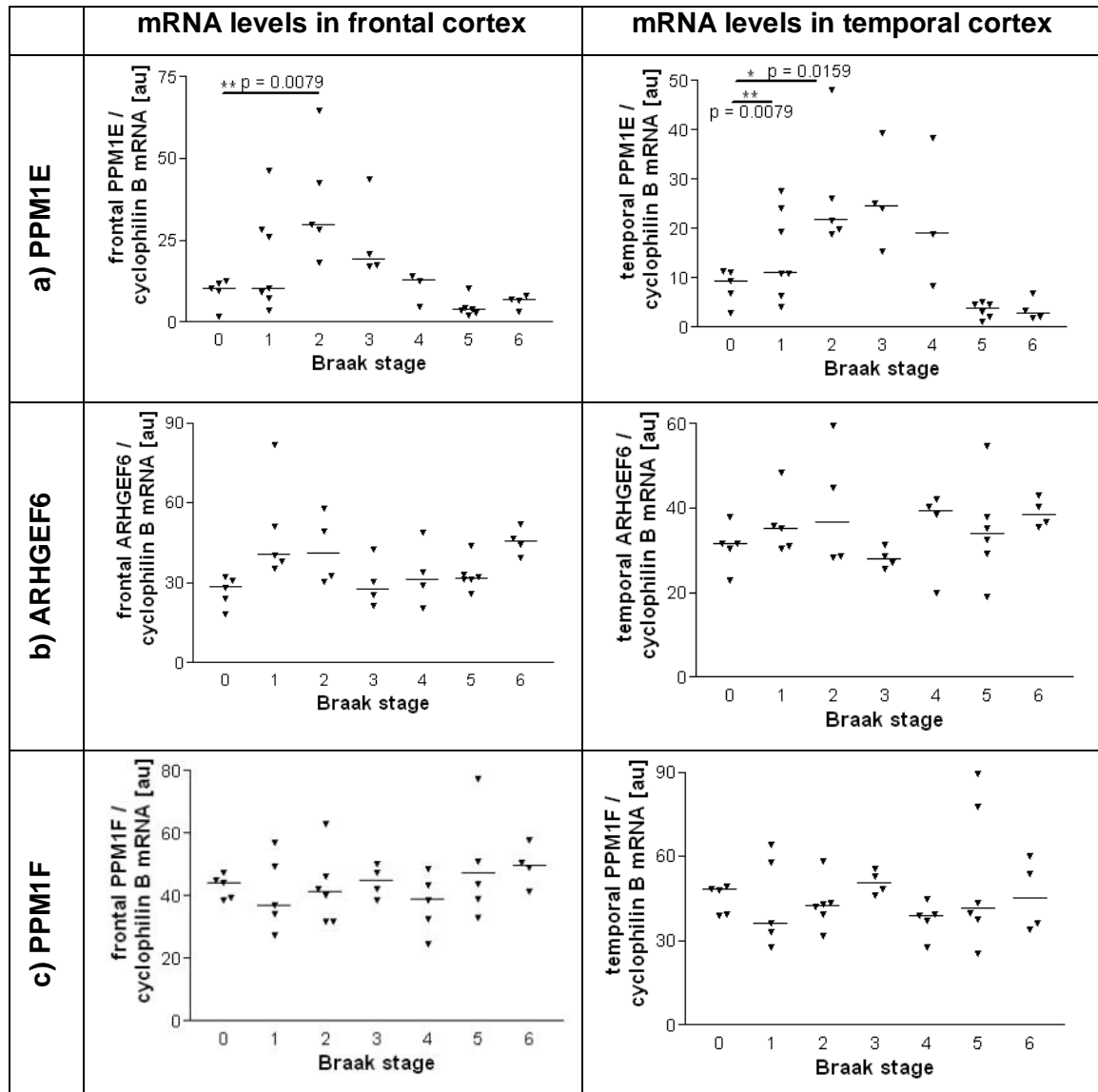


Figure 1.3 A: mRNA levels of (a) PPM1E, (b) ARHGEF6 and (c) PPM1F in human brain tissue samples from individuals corresponding to different Braak stages. mRNA levels of frontal (left) and temporal (right) cortex measured by quantitative RT-PCR analysis. Normalized to Cyclophilin B levels. au: arbitrary units. Horizontal lines represent the median. Statistical analysis with Mann-Whitney-U-test, 95 % confidence interval.

The levels of PPM1E mRNA stuck out from the mass of analysed genes for their quantitative correlation with AD progression as determined by Braak staging (Figure 1.3 A-a). Between samples of non-demented individuals staged in the lowest Braak

stage 0 and samples representing Braak stage 2 a significant increase in mRNA levels of PPM1E in frontal as well as inferior temporal cortex is detected. The PPM1E mRNA levels already show a slight increase by trend in Braak 1 compared with Braak 0, indicating that the upregulation of PPM1E starts early in the disease. As observed for the majority of analysed genes the PPM1E mRNA levels drop in later Braak stages.

The mRNA levels of the guanosine exchange factor ARHGEF6 (α PIX) are changing in a similar pattern throughout the disease stages (Figure 1.3 A-b). Interestingly, ARHGEF6 has been proposed to be a binding partner of PPM1E (Koh et al., 2002). ARHGEF6 levels increase in Braak 1 and 2 compared with Braak 0 controls. Meanwhile no changes were detected in the mRNA levels between Braak stages of the closest PPM1E homolog PPM1F (Figure 1.3 A-c).

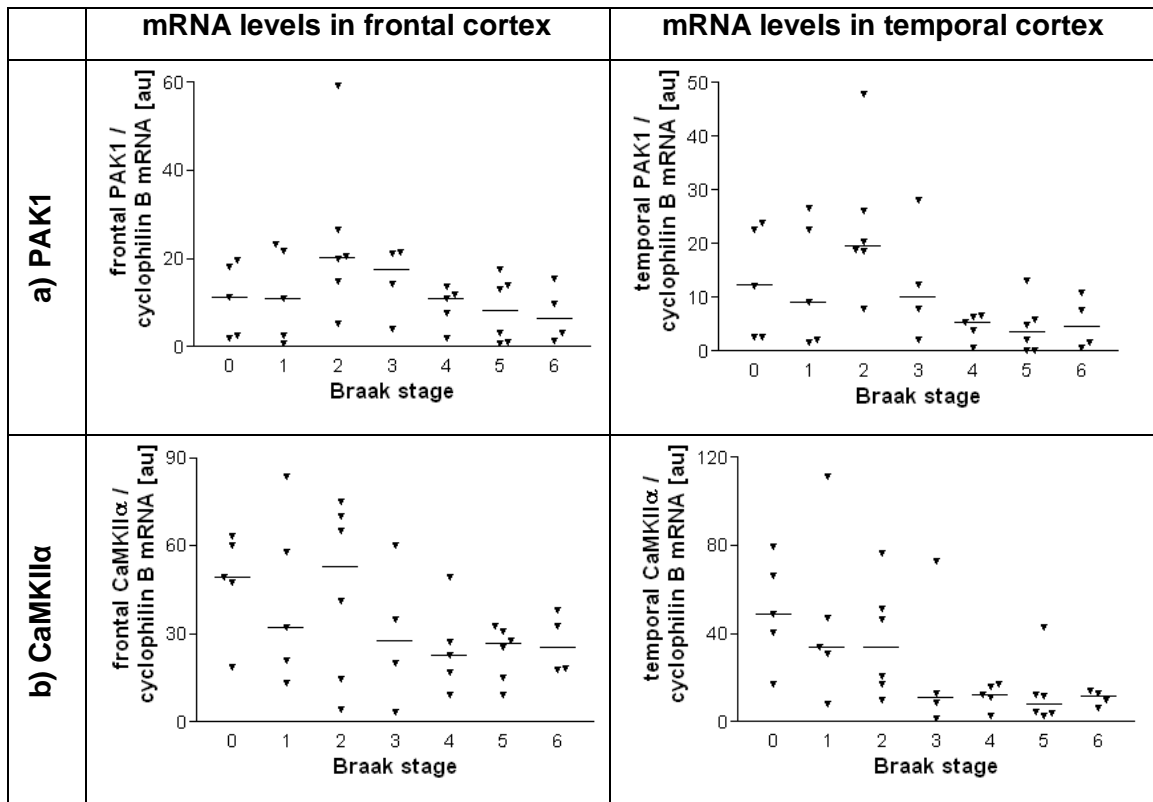


Figure 1.3 B: mRNA levels of (a) PAK1 and (b) CaMKII α in human brain tissue samples from individuals corresponding to different Braak stages. mRNA levels of frontal (left) and temporal (right) cortex measured by quantitative RT-PCR analysis. Normalized to Cyclophilin B levels. au: arbitrary units. Horizontal lines represent the median. Statistical analysis with Mann-Whitney-U-test, 95 % confidence interval.

The strong upregulation of PPM1E mRNA levels indicates that PPM1E might play a role during the initial development of the disease (von der Kammer, 2008). However,

the screen was not able to reveal whether this effect is supportive for disease progression or an adaptive cellular answer to slow cellular and brain damage.

Interestingly, the mRNA levels of the proposed effector kinases of PPM1E, PAK1 and CaMKII α , are not strongly regulated in Braak 0 to 3 and slightly reduced in later stages (Figure 1.3 B; von der Kammer, 2009). PAK1 mRNA levels are slightly upregulated by trend in Braak 2, however this effect is not significant (Figure 1.3 B-a). The expression of the third proposed PPM1E target kinase, CaMKIV, was not analysed in this screen (von der Kammer, 2009).

1.4 The protein phosphatase 1E - PPM1E

The protein phosphatase 1E (PPM1E) was identified in 2001 as '*Ca²⁺/calmodulin dependent kinase phosphatase with nuclear localization*' (CaMKP-N) as a homolog of PPM1F (CaMKP; POPX2) and is now also known as '*partner of pix*' (POPX) 1. PPM1E was shown to be a negative regulator of *Ca²⁺/calmodulin dependent kinases* (CaMK) II and IV as well as of p21-activated kinase (PAK) 1 (Kitani et al., 2006; Takeuchi et al., 2004; Koh et al., 2002; Takeuchi et al., 2001). It belongs to the PPM family of phosphatases, which are Mn^{2+}/Mg^{2+} - dependent and contains a PP2C-like phosphatase domain. The closest homolog, PPM1F, shares many structural and functional features with PPM1E and both are assumed to dephosphorylate CaMKII/IV and PAK1. PPM1E has long carboxy- and amino-terminal-stretches which are not present in PPM1F (Figure 1.4; Appendix A 1). More distant homologs for PPM1E are PPM1K and PPM1L, which are mitochondrial and endoplasmatic reticular localized Mn^{2+}/Mg^{2+} - dependent phosphatases respectively (Saito et al., 2008; Joshi et al., 2007).

Comparatively little research regarding PPM1E has been released to the public, therefore this section can give a fairly complete overview over the state of the art with respect to the phosphatase. In recent years some large-scale expression screens for cancer-affected tissue, among others, also came up with data about PPM1E. These will be excluded from the following literature review due to minor relevance to the project (compare for example Bianchini et al., 2007).

1.4.1 A general introduction of phosphatases

Phosphatases are important regulators of protein activity throughout the cellular interactome. Around 30 % of all human proteins are divalently linked to phosphate

(Cohen, 2000) and in a strictly guarded interplay these phosphorylations are regulated by protein kinases and phosphatases. Kinases covalently link a phosphate residue cleaved from adenosine triphosphate (ATP) to a specific amino acid residue and phosphatases catalyze the reversed reaction. While the human genome encodes 600 predicted kinases, only 200 phosphatases were predicted (Cohen, 2001). These numbers however equal when all possible combinations of holoenzymes are taken into account (Bollen and Beullens, 2002).

The amino acids serine, threonine and tyrosine are phosphorylated at their oxygen residue in mammalian proteins, and histidine can be phosphorylated at its nitrogen residue. The group of O-phosphatases are further subdivided into protein tyrosine phosphatases (PTPs), which also include a group of dual specific phosphatases, and serine/threonine phosphatases (Klumpp and Krieglstein, 2002). The latter can be grouped according to phylogenetic criteria into phosphoprotein phosphatases (PPP) and metal-dependent protein phosphatases (PPM). The serine/threonine phosphatases are further subdivided according to their biochemical properties: PP1 is inhibited by heat-resistant inhibitor proteins and dephosphorylates the β -subunit of the phosphorylase-kinase, while PP2 is not inhibited by these inhibitors and prefers the α -subunit. PP2A is auto-activated spontaneously, while PP2B is Ca^{2+} - and PP2C is $\text{Mg}^{2+}/\text{Mn}^{2+}$ -dependent (McGowan and Cohen, 1988). The PP2C phosphatases belong to the PPM family of phosphatases and are monomeric enzymes without known regulatory subunits (Barford et al., 1998; Barford, 1996; McGowan and Cohen, 1988). They share six conserved motives and are further distinguished into two groups by the amino acid sequence RXXME/QD or KXXXNED, which are designated 'motif I' (Komaki et al., 2003). PPM1E and PPM1F belong with PP2C α , PP2C β , FIN13/PP2C γ , PP2C δ , PP2C ϵ and Wip1 to the first group of PP2C phosphatases, PP2C ζ and NERPP-2 to the latter.

Although a structural model derived with X-ray crystallographic methods from PP2C α exists (Das et al., 1996), the catalytic mechanism of PP2C phosphatases is still not entirely clear (Jackson et al., 2003). The catalytically active, amino terminal domain of PP2C α consists of six α -helices and eleven β -sheets. In the catalytic center two Mn^{2+} ions are coordinated by four conserved aspartates, one glutamate and six water molecules (Barford et al., 1998; Das et al., 1996). This catalytic site is conserved in PPM1E and the Mn^{2+} and Mg^{2+} dependence of its catalytic activity has been demonstrated *in vitro* (Takeuchi et al., 2001). PPM1E activity is stronger correlated with the presence of Mn^{2+} than with that of Mg^{2+} ions. Additionally PPM1E and PPM1F

activity are stimulated by the presence of poly-cations like poly-L-lysine, probably depending on the polyglutamate stretch in the amino-terminal part of the two proteins (Tada et al., 2006; Takeuchi et al., 2001).

1.4.2 The structure of the *PPM1E* gene and the PPM1E protein

The *PPM1E* gene is located in chromosomal region 17q23.2 between bp 54188231 and 54417319 and codes for a 'protein phosphatase, Mg²⁺/Mn²⁺ dependent, 1E'. It is also known as CaMKP-N, POPX1, DKFZp781F1422, KIAA1072 and PP2CH.

The full-length PPM1E protein has a length of 755 amino acids and a calculated molecular weight of 84 kDa (for schematic view see Figure 1.4). The PPM1E protein is characterized by an amino-terminal domain of unknown function which contains characteristic repeats of glutamate and proline, a cluster of glutamate residues, and a cluster of proline residues (Appendix A 1). This domain is followed by a binding motif for the guanine nucleotide exchange factor ARHGEF (PIX) and a characteristic catalytic domain which is conserved in PPM1E and PPM1F (*PPM1E/1F* homology domain (E/Fhd)). The E/Fhd section comprises a PP2C-like phosphatase domain (Koh et al., 2002).

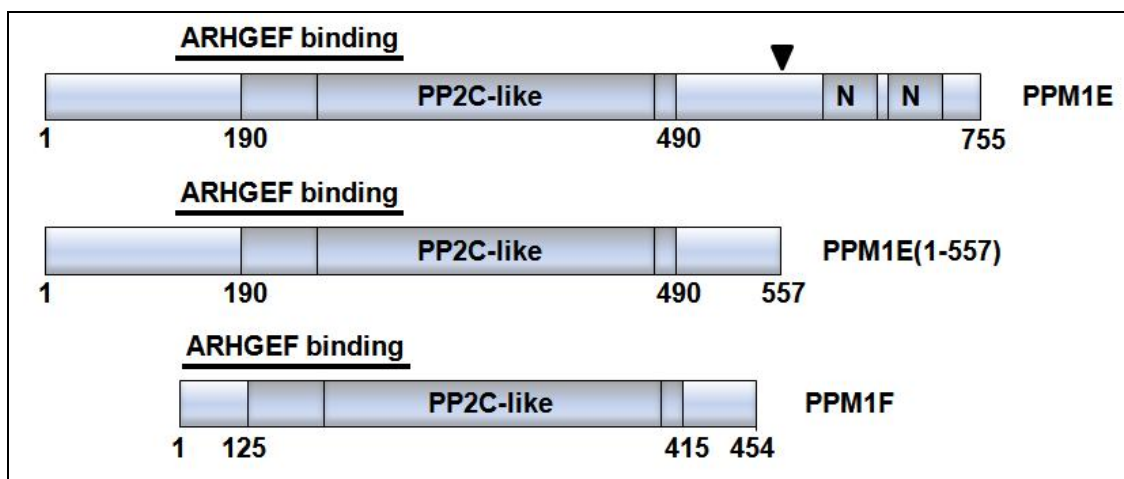


Figure 1.4: Domain structure of human phosphatase PPM1E, its truncated version PPM1E(1-557) and PPM1F. Postulated truncation site in PPM1E indicated by arrowhead. Region required for ARHGEF binding is indicated (Koh et al., 2002). PP2C-like: PP2C-like phosphatase domain. N: nuclear localization signal. *PPM1E/1F* homology domain (E/Fhd) between aa 190 – 490 (PPM1E variants) and 125 - 415 (PPM1F). Domain structures derived from Koh (2002), Takeuchi (2004) and Kitani (2006).

The homology between PPM1E and PPM1F is extended from the shared PP2C-like phosphatase domain towards the amino-terminal domain, suggesting that this domain

is required for recognition of shared substrates (Figure 1.4; Appendix A 1). The E/Fhd section is 59 % identical and 75 % conserved between PPM1E and PPM1F and was determined to comprise amino acid positions 200 to 490 of hPPM1E (Kitani et al., 2006). The catalytic domain is followed by a carboxy-terminal domain containing two nuclear localization signals (NLS) (Takeuchi et al., 2004).

The two carboxy-terminal NLS in PPM1E are located downstream from a cleavage site proposed to be at proline 557 in the human PPM1E sequence (Kitani et al., 2006; Takeuchi et al., 2004). Mass spectrometric analysis of rat PPM1E revealed that the protein runs at two apparent masses of 120 and 88 kDa in gelelectrophoresis. These correspond to the actual masses of an 83.4 kDa full length and a 61.1 kDa truncated form of PPM1E (Kitani et al., 2006). Rat PPM1E(1–554), truncated at the carboxyl side of proline 554 in rat PPM1E or in its vicinity, was estimated to be most likely the truncated form of PPM1E (Kitani et al., 2006). This corresponds to PPM1E(1-557) in the human PPM1E sequence which is encoded by NM_014906⁶.

1.4.3 Cellular localization and tissue specificity of PPM1E

Northern blot analysis revealed that PPM1E is enriched in brain tissue and testis, and very weakly expressed in heart, kidney and liver, while PPM1F is ubiquitously expressed in all examined tissues (Kitani et al., 2003; Takeuchi et al., 2001). Immunoblot analysis even detected expression of PPM1E exclusively in brain and none in testis or any other tested tissue (Kitani et al., 2006).

Endogenous PPM1E is expressed specifically in neurons and is enriched in the nucleus of day-*in-vitro* (DIV) 6, dissociated primary hippocampal neurons (Kitani et al., 2006), while it is mainly located in the cytoplasm in most neurons of the central nervous system, except for few large neurons of the facial and the mesencephalic trigeminal nuclei (Kitani et al., 2006).

PPM1E(1–554) contains - due to its C-terminal truncation - no NLS and is localized exclusively in the cytoplasm of COS-7 cells which encode ectopically for PPM1E(1-554) (Kitani et al., 2006). However it was shown by western blot analysis of cellular fractionates of rat brain, that truncated PPM1E is endogenously also present in the nucleus of cells, indicating that truncation of PPM1E can also occur in the nucleus (Kitani et al., 2006). The full length form of PPM1E was found in the nucleus as well as

⁶ NCBI (National Center for Biotechnology Information) GenBank accession number

in the cytoplasm. Of all analysed cellular fractions only the microsomal fraction did not contain PPM1E and PPM1E(1-554). Whether the proteolytic cleavage of PPM1E is mediated by a protease or in an autoproteolytic manner is currently unclear.

Moreover, the interrelation between protein truncation, localization and functional regulation of the phosphatase is largely unknown (Kitani et al., 2006; Takeuchi et al., 2004). It was hypothesized that PPM1E is the nuclear equivalent for cytosolic PPM1F in CaMK regulation, and nuclear CaMKIV and CaMKK α while PPM1F regulates CaMKI, CaMKII and CaMKK β (Kitani et al., 2003). CaMKI is localized in the cytosol but CaMKIV in the nucleus (Nakamura et al., 1995; Jensen et al., 1991) in rat CNS. This hypothesis would however not explain the cytosolic localization of PPM1E in neurons in most rat brain neuronal populations. Strong immunostaining of PPM1E was also observed at the synapse (Kitani et al., 2006).

1.4.4 Upstream effectors and regulators of the *PPM1E* gene

While no upstream regulators of the PPM1E protein have been identified so far, it is known that the *PPM1E* gene, which has 7 exons and 1 transcript (Dorkeld et al., 1999), is located in and regulated with the 17q23 amplicon (Pärssinen et al., 2007). The “*tripartite motif-containing protein 37*” (*TRIM37*) gene resides on the complementary strand and the *PPM1E* 3'UTR sequence overlaps with exon 25 of *TRIM37* (Hämäläinen et al., 2006). *TRIM37* has important functions in developmental patterning and oncogenesis. Transcribed from the opposite strands, *TRIM37b* and *PPM1E* could act as cis-encoded antisense transcripts and downregulate each other's expression (Hämäläinen et al., 2006).

1.4.5 Proposed PPM1E effector kinases and binding partners

Three target kinases were proposed to be dephosphorylated by PPM1E: PAK1, CaMKII and CaMKIV. The CaMKs and PAKs are not homologous in their overall primary or domain structures and the phosphorylated threonine residues which are dephosphorylated by PPM1E are not in similar contexts with respect to the primary sequence of the proteins (sequence alignments not shown).

Human PPM1E (hPPM1E) was described to form a complex with PAK1 and the ‘Rho guanine nucleotide exchange factor 6’ (ARHGEF6; α PIX), and to antagonize PAK1 activation by Cdc42 (cell division cycle 42) (Koh et al., 2002). PPM1E thereby inhibits actin stress fiber breakdown and morphological changes driven by Cdc42. Additionally

co-expression of PPM1E and PAK1 in COS-7 kidney-derived cells decreases PAK1 phosphorylation, indicating that this effect is mediated directly by PAK1 dephosphorylation. The binding site for ARHGEFs has been proposed to lie within the amino-terminal domain in PPM1E (Figure 1; Appendix A 1) (Koh et al., 2002).

Additionally, the rat and zebrafish homologues of PPM1E (rPPM1E and zPPM1E), designated as brain-specifically expressed 'CaM kinase phosphatase N' (CaMKP-N) and zCaMKP-N, were described to dephosphorylate specifically CaMKII and CaMKIV (Nimura et al., 2010; Nimura et al., 2007; Kitani et al., 2006; Takeuchi et al., 2004; Takeuchi et al., 2001). Recombinantly expressed rPPM1E and zPPM1E dephosphorylate full length CaMKIV and a synthetic phosphopeptide mimicking the phosphorylation site of CaMKII *in vitro* (Nimura et al., 2007; Kitani et al., 2003; Takeuchi et al., 2001). No mode of interaction between PPM1E and the CaMKs has been proposed so far. However, the homologous phosphatase PPM1F and a recombinant fusion protein, containing the amino-terminal part of PPM1F and the catalytic domain of PP2C α , exhibited comparable substrate activity towards CaM kinases *in vitro*, while PP2C α did not (Tada et al., 2006). This indicates that activity on CaMK involves the amino-terminal part of the shared E/Fhd domain (Figure 1.4). Additionally the direct interaction between CaMKII and multiple sites in PPM1F was proposed (Harvey et al., 2004).

1.4.5.1 Characterization of CaMKs and their effects on the actin cytoskeleton

The CaMK family kinases, including CaMKI, CaMKII, CaMKIV, and CaMK kinase (CaMKK), react to increases in intracellular Ca²⁺-levels by association with the Ca²⁺-binding protein calmodulin (Wayman et al., 2008). The CaMKs are activated by the binding of the Ca²⁺/calmodulin complex as well as by phosphorylation. The activated CaM kinases are known to be deactivated through dephosphorylation by ubiquitous multifunctional protein phosphatases such as protein phosphatases 1, 2A and 2C.

Structure of Ca²⁺/calmodulin-dependent kinases II and IV (CaMKII/IV)

CaMKII is a highly abundant serine/threonine kinase in the postsynaptic density of glutamatergic synapses (Colbran and Brown, 2004; Kennedy, 2000). Given its high abundance in dendritic spines CaMKII might have additional structural functions (Jourdain et al., 2003; Pratt et al., 2003; Shen et al., 1998). CaMKII is required for structural changes that are associated with LTP induction and can enhance the efficacy of synaptic transmission (reviewed in Lisman et al., 2002).

The CaMKII comprises 28 similar isoforms that are derived from α , β , γ and δ genes (Lisman et al., 2002). The major isoforms of CaMKII that are expressed in brain are CaMKII α and CaMKII β . These assemble in stochastic combinations into dodecameric heteromeric holoenzymes (Rosenberg et al., 2005). Each isoform consists of a catalytic kinase domain, an autoinhibitory regulatory domain (RD), a variable segment and a self-association domain (AD) (Figure 1.5). The catalytic domain contains the ATP-, substrate- and anchoring protein-binding sites and catalyses the phosphotransferase reaction. The autoinhibitory domain inhibits the catalytic activity by binding to the substrate binding site with a pseudosubstrate region. Binding of Ca²⁺/calmodulin to a region that overlaps with the substrate binding region inhibits binding of the inhibitory domain and facilitates autophosphorylation at Thr286 (CaMKII α) / Thr287 (CaMKII β). CaMKIV, also referred to as CaMK-GR, is structurally homolog to CaMKII but lacks a carboxyterminal association domain (Figure 1.5).

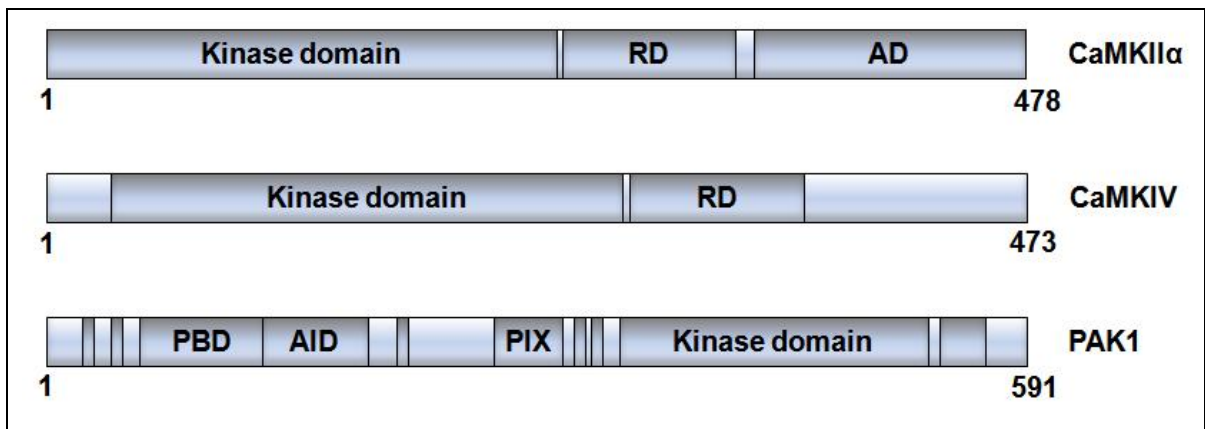


Figure 1.5: Domain structure of the PPM1E target kinases CaMKII α , CaMKIV and PAK1. RD: regulatory domain with calmodulin binding site. AD: association domain. PBD: p21 binding domain. AID: autoinhibitory domain. Small segments in PAK1: PXXP motif. Larger carboxy-terminal segment in PAK1: second part of kinase domain. Domain structures derived from: CaMK: (Soderling and Stull, 2001); PAK1: various publications (compare text).

Localization and function of Ca²⁺/calmodulin-dependent kinase II (CaMKII)

The β isoform of CaMKII binds to F-actin and is thereby responsible for the localization of CaMKII heterooligomers into dendritic spines (Jourdain et al., 2003; Pratt et al., 2003; Shen et al., 1998). Elevation of Ca²⁺ levels through NMDA receptors induce a reversible translocation of CaMKII from F-actin to the postsynaptic density, where CaMKII binding to the NR2B subunit of NMDA receptors prolongs the CaMKII kinase activity (Bayer et al., 2001; Shen et al., 2000; Shen and Meyer, 1999). Experimental enhancement of CaMKII signaling induces spine formation and increases synapse number (Jourdain et al., 2003; Bienvenu et al., 2000; Allen et al., 1998).

A number of substrates have been identified for CaMKII, including NMDA and AMPA receptors, scaffolding proteins like MAP2, tau and the PSD-95 family (Colbran and Brown, 2004;Mauceri et al., 2004;Yoshimura et al., 2000;Shen et al., 1998). CaMKII phosphorylates also the RacGEF kalirin-7 at threonine 95 and they form a signaling complex with PSD95 and AMPA-type glutamate receptors (Xie et al., 2007) (Figure 1.6). In primary hippocampal culture it has been shown that kalirin-7 recruitment to the synapse induces formation of a multiprotein complex consisting of AF-6/afadin, the Rho-family GTPase Rac1 and PAK which regulates spine head size (Xie et al., 2008). CaMKII mediated regulation of actin polymerization via this pathway has been proposed (Saneyoshi et al., 2010) (Figure 1.6).

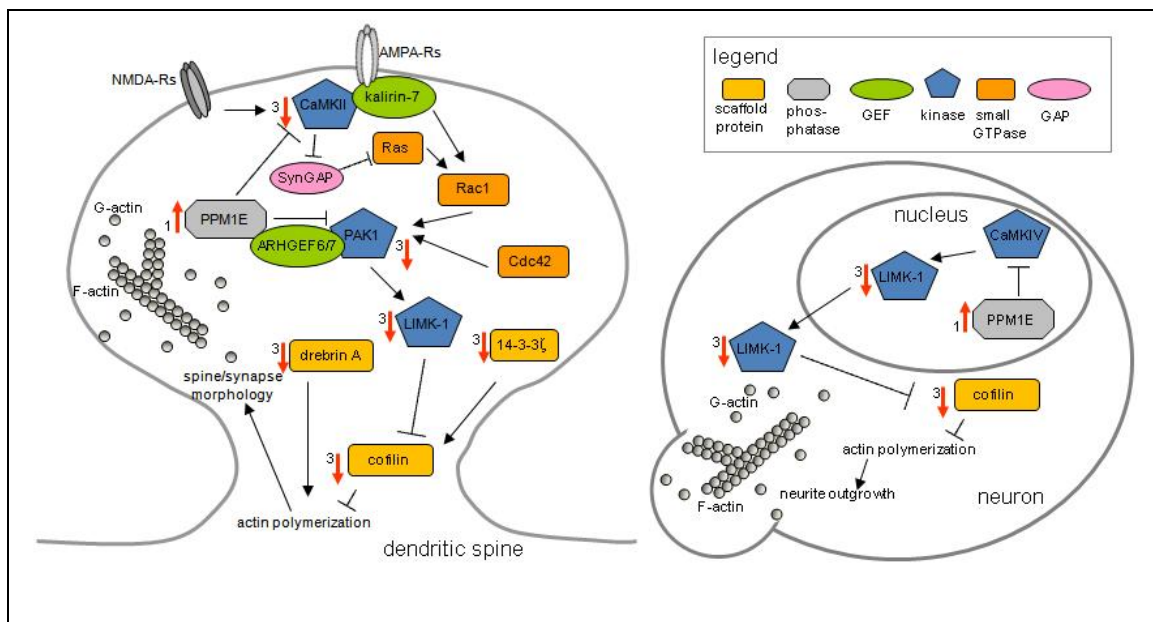


Figure 1.6: Nuclear and spine signaling pathways which regulate the actin cytoskeleton, adapted from Saneyoshi (2010) and Kitani (2003). PPM1E has been included based on the results from Kitani et al. (2006) and Koh et al. (2002). Red arrows and numbers indicate a differential gene regulation in Braak stages (von der Kammer, 2009). Spine and nucleus sizes not to scale.

CaMKII additionally phosphorylates and thereby inhibits SynGAP, which normally inactivates the Rho-family GTPase Ras by stimulating Ras-GTP hydrolysis (Carlisle et al., 2008;Oh et al., 2002;Chen et al., 1998) (Figure 1.6). Ras acts as a GTPase on Rac and its inhibition results in decreased turnover of GTP to GDP bound to Rac1.

Thus the kalirin-7- as well as the SynGAP-mediated effects of CaMKII culminate on Rac1: Rac1-GTP binds to and activates PAK1 and PAK3, which subsequently activate the serine-threonine kinase LIM kinase 1 (LIMK-1) by phosphorylation at threonine 508

(Figure 1.6). This residue is in the activation loop within the LIM kinase domain (Ohashi et al., 2000; Edwards et al., 1999; Maekawa et al., 1999; Yang et al., 1998b). Subsequently LIMK-1 phosphorylates and thereby inactivates the actin depolymerising proteins ADF and cofilin and thereby reduces filament turnover and cell motility.

Localization and function of Ca²⁺/calmodulin-dependent kinase IV (CaMKIV)

The related Ca²⁺/calmodulin-dependent kinase CaMKIV is predominantly located in the nucleus (Nakamura et al., 1995; Jensen et al., 1991), and its nuclear transport is facilitated by importin α (Kotera et al., 2005). CaMKIV is fully activated by CaMKK-mediated phosphorylation at threonine 196. CaMKIV directly activates LIMK-1 through phosphorylation at threonine 508 and thereby enables the induction of neurite outgrowth (Takemura et al., 2009) (Figure 1.6). Previous studies showed that knockdown or inhibition but also overexpression of LIMK-1 suppress neurite outgrowth and that these effects involve the phosphorylation of cofilin (Endo et al., 2007; Tursun et al., 2005; Rosso et al., 2004; Endo et al., 2003). LIMK-1 is also shown to localize to both nucleus and cytoplasm: The PDZ domain of LIMK-1 contains two leucine-rich nuclear export signals, which support preferentially cytoplasmic localization of LIMK-1 (Yang and Mizuno, 1999; Yang et al., 1998a), while the kinase domain contains a nuclear localization sequence (Yang and Mizuno, 1999). This way, CaMKIV activation in the nucleus can presumably translate to regulation of the cytoplasmic actin cytoskeleton.

A second function of activated CaMKIV is the phosphorylation of transcription factor CREB (cAMP response element-binding protein) at serine 133 (Silva et al., 1998a; Silva et al., 1998b; Bito et al., 1996a; Bito et al., 1996b; Nakamura et al., 1995; Matthews et al., 1994; Jensen et al., 1991), which then interacts with the transcription coactivator CBP (CREB-binding protein), resulting in the activation of CRE (cAMP response element)-mediated transcription through the recruitment of CBP to the promoter of CREB target genes (Impey et al., 2002; Chawla et al., 1998; Chrivia et al., 1993). CaMKIV mediated CREB activation also regulates dendritic growth (Redmond et al., 2002).

1.4.5.2 Characterization of PAK1 and its effects on the actin cytoskeleton

Six PAK isoforms have been identified, PAK1 to PAK6 (Abo et al., 1998; Sells and Chernoff, 1997; Lim et al., 1996; Manser et al., 1994), and are distinguished based on their domain architecture and regulatory mechanisms into group I (PAK1-3) and group II (PAK4-6) PAKs (Bokoch, 2003; Jaffer and Chernoff, 2002; Dan et al., 2001). In this study the group I PAKs are of special interest because they are structurally highly

conserved and PAK1 is an effector of PPM1E (Koh et al., 2002) and CaMKII as described above.

Structure of PAK1

PAK1 is maintained in an inactive, dimeric complex which is autoinhibited in *trans* (Parrini et al., 2002). It contains an amino-terminal regulatory domain and a highly conserved C-terminal catalytic kinase domain (Figure 1.5). The regulatory domain consists of a 'Cdc42 and Rac interactive binding' (CRIB) domain - also referred to as PBD (p21 binding domain), the ARHGEF binding motif and an autoinhibitory switch domain (AID) (Eswaran et al., 2008; Lei et al., 2000). In the homodimer of PAK1 one kinase domain binds to the AID domain in the second PAK1 (Parrini et al., 2002). The binding between AID and the kinase domain can be reversed by Cdc42 or Rac binding (Lei et al., 2000; Morreale et al., 2000; Zhao et al., 1998). Upon termination of autoinhibition PAK1 is autophosphorylated at several positions, among them threonine 423, and thereby fully activated (Gatti et al., 1999; Zenke et al., 1999; Yu et al., 1998). After activation through Cdc42, substrate binding and structural rearrangement PAK1 is active as a monomer.

PAK1 additionally contains five proline-rich motives (PXXP) which are distributed over the length of the regulatory domain and bind to SH3 (src homology 3) domains in Nck, Grb2 and ARHGEF. Four of these motives bind to Nck (Bokoch et al., 1996) and Grb2 (Puto et al., 2003), and one binds with high specificity to ARHGEF (also referred to as PIX). Nck and Grb2 are adaptor proteins which recruit PAK1 to the membrane after induction by growth receptors. ARHGEF is an exchange factor for the Rho family GTPases (Zhang et al., 2003), and a proposed cofactor for PPM1E action on PAK1 (Koh et al., 2002).

Function of PAK1

PAKs have various functions in regulation of the actin cytoskeleton at different cellular sites, but also in hormone signaling, apoptosis, gene transcription and cell cycle progression (Eswaran et al., 2008). Relevant to the pathway which is analysed in this study is mainly the PAK1-mediated phosphorylation of LIMK-1 (Ahmed et al., 2008; Edwards et al., 1999). As described above, the activation of LIMK-1 stabilizes F-actin through the subsequent inactivation of the F-actin-severing protein Cofilin (Figure 1.6).

1.4.5.3 The PPM1E binding protein ARHGEF

The PAK1 and PPM1E binding protein ARHGEF is a guanine nucleotide exchange factor (GEF) and was identified in 1997 as SH3 domain-containing protein and has two isoforms: ARHGEF6, also known as α PIX and p90-Cool-2, and ARHGEF7, also known as β PIX and p50/p85-Cool-1. Several splice variants exist for ARHGEF7, but so far only one has been identified for ARHGEF6 (Rhee et al., 2004; Kim et al., 2001; Kim et al., 2000). ARHGEF7 is a well established PAK1-interacting partner and it was shown that ARHGEF6 functions cooperatively with PAK3 in spine morphogenesis (Zhang et al., 2005; Zegers et al., 2003).

Structure of ARHGEFs

ARHGEF6 and 7 have similar domain structures except for an N-terminal 'calponin homology' (CH) domain which is only present in ARHGEF6 and is required for β -parvin binding and membrane localization (Rosenberger et al., 2003). C-terminally from that a SH3 domain, required for PAK and Cbl-b binding, is followed by 'Dbl homology' (DH) and 'pleckstrin homology' (PH) domains, which are required in interplay with the SH3 domain for calpain 4 binding (Figure 1.7). The amino-terminal SH3 domain in ARHGEF binds a conserved proline-rich 22 residue motif in PAK1/2/3 (Manser et al., 1998). At the C-terminal end a 'GIT1 binding domain' (GBD) and a 'coiled-coil' (CC) follow.

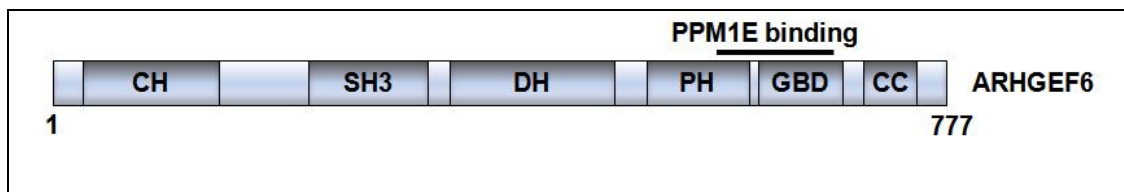


Figure 1.7: Domain structure of ARHGEF6. CH: calponin homology (not present in ARHGEF7). SH3: src homology 3. DH: dbl homology. PH: pleckstrin homology. GBD: Git-1 binding domain. CC: coiled coil. PPM1E binding region indicated (Koh et al., 2002). Domain structures derived from: Rosenberger et al., 2003; Koh et al., 2001; Kim et al., 2001.

ARHGEF7 is recruited to synaptic regions in hippocampal neurons by binding to the adaptor GIT1 (*G-protein-coupled receptor kinase interacting target 1*) (Zhang et al., 2003; Manser et al., 1998). GIT1 can activate PAK in a RhoGTPase independent manner by indirect binding to PAK together with ARHGEF (Loo et al., 2004). The CC domain at the very C-terminal end of ARHGEF is required for homo- and heterodimerisation of ARHGEFs (Koh et al., 2001; Kim et al., 2001). The presence of monomeric forms seems to be crucial for the GEF activity of ARHGEF6 towards Cdc42 and Rac1 (Feng et al., 2004). While monomers exhibit activity towards both Rho

GTPases, for the dimers only an activity towards Cdc42 could be demonstrated. PPM1E binding sites have been identified in the carboxy-terminal domain of ARHGEF and are conserved in ARHGEF6 and 7 (Figure 1.7; Appendix A 5) (Koh et al., 2002).

Function of ARHGEFs

ARHGEF recruits PAK to the cell membrane and is involved in PAK activation. ARHGEF6 is a strong activator of PAK, whereas ARHGEF7 splice variants have contradictory effects on PAK: The p50-Cool-1 splice variant inhibits Rac/Cdc42 stimulated PAK activity while p85-Cool-1 has a permissive effect on Rac/Cdc42 stimulated PAK activity (Feng et al., 2002). ARHGEFs also act as adaptor proteins or GEFs for GIT and Paxillin in the translocation of focal complexes and in cell adhesion processes (Rosenberger et al., 2005). Hence ARHGEFs are in more ways than one important regulators of the actin cytoskeleton.

1.4.6 Phenotypes induced by PPM1E

Although PPM1E targets on the molecular and cellular levels have been proposed, only very little insight into PPM1E-mediated phenotypes on the whole-organism level or in relevant cellular models has been gained to date. Additionally, no genetic disorders have been associated with PPM1E yet.

The only example of a phenotype associated with PPM1E is provided by the knock-down of the phosphatase during zebrafish embryogenesis (Nimura et al., 2007). Here the number of embryos with morphological and cellular abnormalities and apoptosis was significantly increased. The authors discuss that this could be attributed to impaired CaMKIV signaling, because the kinase is known to be important also for the regulation of apoptotic events (Walters et al., 2002; Sée et al., 2001; Wayman et al., 2000; McGinnis et al., 1998). However the results relating CaMKIV to apoptosis are contradictory, assigning CaMKIV pro- as well as anti-apoptotic properties (Nimura et al., 2007).

1.5 Model systems and intentions of this study

A transcriptional profiling of human temporal and frontal cortex in different Braak stages has revealed that the protein phosphatase 1E (PPM1E) is significantly up-regulated on the mRNA level with an early-onset already at Braak stage one. This and the affiliation of PPM1E with a major pathway regulating the actin cytoskeleton in neurons suggested a potential causative role in the early development of Alzheimer's disease.

1.5.1 Animal and cellular models for Alzheimer's disease

One major difficulty in AD research is the identification of the correct animal or cellular model for each question. Current mouse models for AD are based on early-onset AD (EOAD) mutations and ApoE4, which is a risk factor for sporadic AD. They replicate aspects of human AD, but none individually displays all AD hallmarks. Strains have been crossed to combine pathologies but whether and how these pathways interact on the molecular and cellular level to cause AD remains uncertain (Adalbert et al., 2007). Although other primates develop similar disease pathology with amyloid plaques, their plaques have different molecular compositions and the full Alzheimer's disease phenotype with cognitive defects is exclusively found in humans (Rosen et al., 2009).

Dissociated primary neuronal cultures

Due to the association of PPM1E with the above described CaMK/PAK pathway and actin cytoskeleton regulation, a model was sought after which would provide a straightforward analysis of effects on the cytoskeleton and would at the same time be close to the circumstances in the brain. One culture model for analysis of neuronal and spine morphology *ex vivo* are differentiated, dissociated cortical or hippocampal primary neurons. These permit visualization of dendritic spines by standard light or confocal microscopic techniques.

A relative comparability of the PPM1E effects in *Homo sapiens* and *Rattus norvegicus* is likely, because the inter-species homologies are considerable for PPM1E and its binding partner ARHGEF6: Rat and human PPM1E protein sequences are 88.6% identical (Appendix A 3). Within the PPM1E/1F homology domain (E/Fhd) the rat and human PPM1E proteins are 99% identical. As described above, it has been proposed that effects on CaMKs are mediated by this domain. The variability between human and rat PPM1E is greatest in the C-terminally truncated part of the PPM1E protein which contains 62% of all non-identical aa. However, the two nuclear localization signal-containing stretches in the C-terminal part of PPM1E are 77 and 74% identical between human and rat PPM1E. The ARHGEF binding site is conserved in human and rat PPM1E (Koh et al., 2002).

Rat and human ARHGEF6 are 98 % conserved with 82 % absolute sequence identity (Appendix A 4). The CH, DH, PH, GBD and DD domains as well as the SH3 domain, required for PAK binding, and amino acids 578 to 719 (human ARHGEF6), required for PPM1E binding, are conserved in the rat and human sequence and all ARHGEF7

splice variants (Appendix A 5). Moreover, also the putative target kinases CaMKII, CaMKIV and PAK1 do have rat homologues and the pathways are conserved in *Homo sapiens* and *Rattus norvegicus*.

1.5.2 Intentions of this study

The first objective of this study was to clarify whether the increase in PPM1E mRNA levels is an adaptive, protective answer of the brain, or whether the increased levels of PPM1E might support disease progression. For this purpose, effects of PPM1E on dendritic arborisation and dendritic spine morphogenesis were investigated to reveal whether PPM1E influences the neuronal actin cytoskeleton. Through PPM1E overexpression in dissociated primary neuronal culture this study shows that the phosphatase has a neurodegenerative effect: Dendritic mushroom spine density and dendritic arborization were significantly reduced. Knock-down of endogenous PPM1E meanwhile rather has a positive influence on dendritic spine morphogenesis or homeostasis, whereas it negatively influenced the complexity of the neuritic arbor.

A second objective was to clarify whether the PPM1E effects in the employed model system are attributable to a direct interaction with CaMKII, CaMKIV or PAK1. This study shows that increased PPM1E levels had an influence rather on the expression levels than on the phosphorylation state of the kinases.

Since PPM1E is relatively poorly characterized, further emphasis was placed on the elucidation of PPM1E localization. Amendatory to previously published results, which showed a nuclear localization of PPM1E in primary culture (Kitani et al., 2006), this study demonstrates that PPM1E changes localization depending on the developmental stage of the culture and that it is associated with sites of high metabolic activity in dendrites.

An early-onset dysregulation of PPM1E in Alzheimer's disease could negatively affect the dendrite and dendritic spine morphogenesis. Inhibiting PPM1E in an early stage of disease may delay or at best even prevent the progression of cognitive decline. PPM1E might therefore provide a promising new drug target for neurodegenerative diseases and especially for AD.

2 MATERIAL AND METHODS

2.1 Material

2.1.1 Chemicals and consumables

Unless otherwise mentioned, all chemicals were either purchased from Sigma-Aldrich (Steinheim, Germany), Merck (Darmstadt, Germany) or Invitrogen (Karlsruhe, Germany). Unless otherwise mentioned all consumables for cell culture were obtained from VWR (Darmstadt, Germany). Polyacrylamid electrophoresis gels and equipment were obtained from Invitrogen. Phosphate buffer (PB) was obtained from AppliChem (10x PBS buffer powder, #A0965,9010) for biochemical and from PAA (Dulbecco's PBS (1x), Pasching Austria, #H15-002) for cell culture applications.

2.1.2 Biological material

For description of primary rat neuronal cell culture and eukaryotic cell lines and their cultivation see 2.2.5 *Influence of PPM1E in cell lines and primary neuronal culture* (page 68). For *E.coli* competent bacterial strains see 2.2.1 *General genetic, molecular biological and biochemical methods* (page 58) and 2.2.2 *His-hPPM1E protein expression, purification and in vitro activity determination* (page 62). For Sf9 cell strains see 2.2.2 *His-hPPM1E protein expression, purification and in vitro activity determination* (page 62).

2.1.3 Animals

Timed-pregnant Wistar rats were purchased from University Medical Center Hamburg-Eppendorf (Hamburg, Germany) directly before preparation.

Wild type fruit flies were obtained from the Bloomington Stock Center (*Drosophila melanogaster*, w¹¹¹⁸) and maintained at 25°C and 65% relative humidity on a 12h/12h day/night cycle. The animals were reared in 175 ml breeding vials (Greiner Bio-One, Solingen, Germany) on an approximately 2 cm thick layer of commercial Nekton-*Drosophila*-food concentrate (Günter Enderle Nekton-Produkte, Pforzheim, Germany) with tap water and vinegar added.

2.1.4 Oligonucleotides

All synthetic oligonucleotides were synthesized externally (Metabion, Martinsried, Germany).

2.1.4.1 Oligonucleotides for polymerase chain reaction (PCR)

Primer ID	oligonucleotide primary sequence	included restriction site
hPPM1E		
#10	5'- <u>GCG GCC GCT</u> TAT TCT ATT TTA TAG CTC CAA GG-3'	<i>NotI</i>
#22	5'- <u>CTC GAG GGA TCC</u> TTA TTC TAT TTT ATA GCT CCA AGG-3'	<i>XhoI</i> / <i>BamHI</i>
#23	5'-CCA <u>GAA TTC</u> ATG CAT CAT CAT CAT CAC AGC-3'	<i>EcoRI</i>
#21	5'- <u>CAT ATG ATG</u> CAC CAC CAC CAC CAC GGC GGC TGC ATC CCT GAG-3'	<i>NdeI</i>
#9	5'- <u>GAA TTC</u> ATG GAA CAA AAA CTT ATT TCT GAA GAA GAT CTG GCC GGC TGC ATC CCT GAG-3'	<i>EcoRI</i>
#01	5'- <u>GGA TCC</u> ATG GCC GGC TGC ATC CCT GAG G-3'	<i>BamHI</i>
#02	5'- <u>GAA TTC</u> TTA TTC TAT TTT ATA GCT CCA AGG AAG ATC TGG-3'	<i>EcoRI</i>
hARHGFE6		
#30	5'- <u>AAG CTT</u> TTA CTT GTC ATC GTC GTC CTT GTA GTC TGG AAG AAT TGA GGT CTT GC-3'	<i>HindIII</i>
#03	5'- <u>GAA TTC</u> ATG AAT CCA GAA GAA CAA ATC G-3'	<i>EcoRI</i>
#04	5'- <u>CTC GAG</u> TTA TGG AAG AAT TGA GGT CTT GC-3'	<i>XhoI</i>
#28	5'- <u>CTC GAG</u> TTA CAG ATC TTC TTC AGA AAT AAG TTT TTG TTC TGG AAG AAT TGA GGT CTT GC	<i>XhoI</i>
rat PPM1E		
#05	5'- <u>GAA TTC</u> ATG GAA CAA AAA CTT ATT TCT GAA GAA GAT CTG GCG GGC TGC ATC CCT GAG G-3'	<i>EcoRI</i>
#06	5'- <u>AAG CTT</u> TTA AAT TTT ATA GTC CCA GGG AAG GTC TGG GC-3'	<i>HindIII</i>

Table 2.1 – part 1: Oligonucleotides used in polymerase chain reaction (PCR) for cloning of different constructs used in this study.

Primer ID	oligonucleotide primary sequence	included restriction site
rat ARHGEF6		
#07	5'-GAA TTC ATG AAT CCA GAA GAA CGC GT-3'	<i>EcoRI</i>
#08	5'-GGA TCC TTA CTT GTC ATC GTC GTC CTT GTA GTC CTG GAG AAT CGA GGT CTT G-3'	<i>BamHI</i>
hPPM1E(1-557)		
#31	5'-CTC GAG TTA GCT AGT TCT ATC AGT GAA TGA A-3'	<i>XhoI</i>
hPPM1E mutational primers (mismatching nucleotides in bold letters)		
#11	5'-CCA TGC CAT CAA AAA CAT GGC GAG GAA AAT GGA GGA CAA AC-3'	
#12	5'-GTT TGT CCT CCA TTT TCC TCG CCA TGT TTT TGA TGG CAT GG-3'	
#19	5'-GTG ATG CTG GGT CAA GTA ATA ACA TCA CGG TTA TTG-3'	
#20	5'-CAA TAA CCG TGA TGT TAT TAC TTG ACC CAG CAT CAC-3'	

Table 2.1 – part 2: Oligonucleotides used in polymerase chain reaction (PCR) for cloning of different constructs used in this study.

2.1.4.2 Oligonucleotides for real-time PCR

Primers complementary to rat genes	
Cyclophilin B	5'-TAG ACT GTG GCA AGA TCG AAG TG-3' 5'-CAG CTG TTT AGA GGG ATG AGG TC-3'
PPM1E	5'-GTT CTG GAT GGG ACT GAA GA-3' 5'-CAA GTG GTC AGA CAC AAC CTT-3'
PAK1	5'-GCA CTA TGA TTTG GAG CTG GCA-3' 5'-GGA TCG ATA GAA CCG GTC CTT C-3'

Table 2.2 – part 1: Oligonucleotides used in quantitative real-time PCR (qRT-PCR) for the amplification of different genes.

Primers complementary to rat genes	
PAK3	5'-GAC TGA CGT GGT CAC AGA AAC CT-3' 5'-TCC AAA GCT TGG AGG CAC TC-3'
LIMK-1	5'-CAA GGA CAA GCG GCT GAA CTT CA-3' 5'-GAC CCT CTG ACT CCA CGG GTA C-3'
Drebrin1	5'-TCC AGA AAT CGA CAT CAC CTG C-3' 5'-TAC TAA TCA CCA CCC TCG AA-3'
Primers complementary to human genes	
PPM1E	5'-GTT CTG GAT GGG ACC GAA GA-3' 5'-CAG GTG GTC GGA CAC AAC TTT-3'
Cyclophilin B	5'-ACT GAA GCA CTA CGG GCC TG-3' 5'-AGC CGT TGG TGT CTT TGC C-3'
14-3-3 β/α^1	5'-ACT CCC AGC AGG CTT ACC AG-3' 5'-GGC TAC AGG CCT TTT CAG GA-3'
14-3-3 ζ/δ^2	5'-TTG TAG GAG CCC GTA GGT CAT C-3' 5'-TCA GCA CCT TCC GTC TTT TGT-3'
ARHGEF6	5'-GGC AAA TCT TCC AGA CTA TGG C-3' 5'-CAG CTG GAT CAT TGG GCA G-3'
ARHGEF7	5'-GTT TTC ACT GGC CTC ACT CAG A-3' 5'-ATT TGG CCC CTC AAG CAA T-3'
CaMKII α	5'-TGG ACC GCA TGC CTT TTT AT-3' 5'-CCA ACC TGA CCC TTC TCA CAA -3'
Cofilin 1	5'-CCC TGG ATT TTC CTT CTC CC-3' 5'-TGC TTC AGC CCA AGA GGA AT-3'
Cofilin 2b	5'-TTG CAG TTC TGT GAG GCT TGA-3' 5'-ATC CGT GCT GCC ATA TCA CTA A-3'
Drebrin	5'-TCC AGA GAT CGA CAT CAC ATG C-3' 5'-CGC TAA TCA CCA CCC TCG AA-3'
LIMK-1	5'-CAA GGA CAA GAG GCT CAA CTT CA-3' 5'-CAC TCT CTG GCT CCA TGG GTA C-3'
MAP2	5'-CCT AGA TTC CAT AGC CCT TGG AT-3' 5'-GTG GTG GCT GGA AGG TAA TCA-3'

Table 2.2 – part 2: Oligonucleotides used in quantitative real-time PCR (qRT-PCR) for the amplification of different genes. ¹ tyrosine 3- /tryptophan 5-monoxygenase activating protein, beta/alpha polypeptide; ² tyrosine 3-/tryptophan 5 -monoxygenase activation protein, zeta/delta polypeptide;

Primers complementary to human genes	
MARK2	5'-GGA TGT GTG GAG CCT AGG AGT TAT-3' 5'-GGT TCT GTC CAT CAA AAG GCA-3'
PAK2	5'-GGC CAA ACC GTT ATC TAG CTT GA-3' 5'-TAT GAG GCC ACA GCA GTG ATG T-3'
PAK4	5'-CAT GAA TGT CCG AAG AGT GGC-3' 5'-GAA AAG AGG AGG CTG TCC AGG-3'
PAK6	5'-CTC CCA AGT CAG GCT GAA TGA-3' 5'-TGG ATG ACA CCC TGA GCA TG-3'
PAK1	5'-TTCCATTTGCAGAGAGCTTGG-3' 5'-TGATACCCTGCCAGCTGTGAG-3'
PAK3	5'-ACT CCA GAG CTC CAG AAT CCT G-3' 5'-TCG CCT ATC CAC ATC CAT CTC-3'
PAK5	5'-TTG CAT CGT CCC CCT CAT-3' 5'-CTA GCT TTG CCA CCT ACA CGA A-3'
PPM1F	5'-GAA GGG TTT ATC TGC GTT CGT CT-3' 5'-TTT CTG GCA TCT TGG GAC TTG T-3'
PSD-95	5'-CTT GGT CTG GAC TGA ATT GCC-3' 5'-AAT AAG AAG GGG TGG GAG GGA-3'
Rac1	5'-CAC CAG TGA GTT AGC AGC ACG T-3' 5'-TCT CCG CAA AAG CTG GTC A-3'
Synaptophysin	5'-GAG CTT CCA GAT GGG TTT TGT T-3' 5'-TCT TCT CAG GCC ACT TCC GT-3'
Primer complementary to AAV woodchuck postregulatory element (WPRE)	
WPRE ³	5'-CTA TGT TGC TCC TTT TAC GCT ATG-3' 5'-TCA TAA AGA GAC AGC AAC CAG GAT -3'

Table 2.2 – part 3: Oligonucleotides used in quantitative real-time PCR (qRT-PCR) for the amplification of different genes. ³. primer sequence kindly provided by Dr. Rolf Sprengel (Max Planck institute for medical research, Heidelberg, Germany).

2.1.4.3 Oligonucleotides for construction of shRNA constructs

shRNA constructs containing sequences complementary to the rat PPM1E gene	
rshRNA4	5'-GAT CCC <u>CCA TCA CTG TTATTG TGG TAT TCA AGA GAT ACC</u> <u>ACA ATA ACA GTG ATG TTT TTG GAA A-3'</u>
	5'-AGC TTT TCC AAA AAC ATC ACT GTT ATT GTG GTA TCT CTT GAA TAC CAC AAT AAC AGT GAT GGG G-3'
rshRNA6	5'-GAT CCC <u>CCA TCA CTG TTA TTG TGG TAT TCA AGA GAT ACC</u> <u>ACA ATA ACA GTG ATG TTT TTG GAA A-3'</u>
	5'-AGC TTT TCC AAA AAC ATC ACT GTT ATT GTG GTA TCT CTT GAA TAC CAC AAT AAC AGT GAT GGG G-3'
shRNA constructs containing sequences complementary to the human PPM1E gene	
hshRNA4	5'- GAT CCC <u>CCA TCA CGG TTA TTG TGG TAT TCA AGA GAT ACC</u> <u>ACA ATA ACC GTG ATG TTT TTG GAA A-3'</u>
	5'-AGC TTT TCC AAA AAC ATC ACG GTT ATT GTG GTA TCT CTT GAA TAC CAC AAT AAC CGT GAT GGG G-3'
hshRNA7	5'-GAT CCC <u>CAT ATA ATT GCC CTT CCT TTT TCA AGA GAA AAG</u> <u>GAA GGG CAA TTA TAT TTT TTG GAA A-3'</u>
	5'-AGC TTT TCC AAA AAA TAT AAT TGC CCT TCC TTT TCT CTT GAA AAA GGA AGG GCA ATT ATA TGG G-3'
scrambled shRNA construct*	
scram	5'- GAT CCC <u>CCC GCG ACT CGC CGT CTG CGT TCA AGA GAC GCA</u> <u>GAC GGC GAG TCG CGG TTT TTG GAA A -3'</u>
	5'- AGC TTT TCC AAA AA CCG CGA CTC GCC GTC TGC GTC TCT TGA ACG CAG ACG GCG AGT CGC GGG GG -3'

Table 2.3: Oligonucleotides for construction of shRNA constructs. The 5' and 3' single-stranded overhang of each aligned pair of oligonucleotides are complementary to *Bgl*I and *Hind*III restricted sites respectively. Sequences which are complementary to PPM1E sequences or scrambled are underlined. *(Vlachos et al., 2009).

2.1.4.4 Oligonucleotides for sequencing

hPPM1E	
hP_bp600_forward	5'-GGA GAT TGA GAC AGT GAA ATT GGC-3'
hP_bp1200_forward	5'-CTG TCG GTT TCC AGA GCT ATT GG-3'
hP_bp1800_forward	5'-GGT CCT GGT GCA CCA AAG AAA GC-3'
hP_bp200_reverse	5'-CTG GGC GAG TTT CGC GGA C-3'

Table 2.4 – part 1: Oligonucleotides for sequencing of PPM1E and ARHGEF6 constructs. Other constructs were sequenced with standard external T7, SP6 and CMV primers provided by the sequencing service (Qiagen, Hilden, Germany).

hPPM1E	
hP_bp800_reverse	5'-CTC ATA ATA AAG CTG GGG TC-3'
hP_bp1100_forward	5'-GCT TAA GAT GTG GGA CCA CA-3'
hP_bp420_forward	5'-CGG TTG AGG GTG AGG AGG-3'
hP_bp1350_reverse	5'-AGT GGA GGC AGA ATC TGC-3'
hARHGEF6	
hA_bp0_forward	5'-ATG AAT CCA GAA GAA CAA ATC G-3'
hA_bp598_forward	5'-GAA CAG GCT GGT TCC CCA G-3'
hA_bp1197_forward	5'-CTG AAA GCA ATC GTA GCA TTC-3'
hA_bp1801_forward	5'-CTA GGT TAT AAA GAG AGG ATG-3'

Table 2.4 – part 2: Oligonucleotides for sequencing of PPM1E and ARHGEF6 constructs. Other constructs were sequenced with standard external T7, SP6 and CMV primers provided by the sequencing service (Qiagen, Hilden, Germany).

2.1.5 Vectors

Vectors	Origin	Expression promoter (host)
pCR-BluntII-TOPO	Invitrogen, #K2800-20	SP6 (<i>E.coli</i>)
pET24a	Novagen, #69749-3	T7 (<i>E.coli</i>)
pFastBac1	Invitrogen, #10360-014 (Bac-to-Bac [®] Vector Kit)	Polyhedron (Sf9)
pFB-Neo-CMV	Stratagene, #217561, modified ² (Miller, 1997)	CMV (mammalian)
pFB-Neo-CMV-TO	pFB-Neo-CMV, modified ³	CMV under control of Tet repressor (mammalian)
pUAST	(Brand and Perrimon, 1993)	GAL UAS (<i>D. melanogaster</i>)
pAAV-6P-SEWB	(Kügler et al., 2003)	synapsin (mammalian neurons)
pcDNA3+	Invitrogen, # V790-20	
pSuper.basic	OligoEngine, #VEC-PBS-0001/0002	H1 (mammalian)
Helper plasmids	Origin	Viral product
pDP1rs	PlasmidFactory ¹ , #PF401 (Grimm et al., 2003)	AAV (serotype 1)
pDP2rs	PlasmidFactory ¹ , #PF402 (Grimm et al., 2003)	AAV (serotype 2)
pVPack VSV-G	Stratagene, #217567 (DuBridge et al., 1987)	Moloney Mouse Leukemia Virus (MMLV) – based (vesicular stomatitis virus G protein) virus

Table 2.5: DNA vectors which have been used in this study. ¹ produced under licence of the German Cancer Research Center, DKFZ; ² modified by A. Ebnet, Evotec Neurosciences GmbH, 2004 (exchange of T7 for CMV promoter); ³ modified by A. Ebnet, Evotec Neurosciences GmbH, 2004 (pFB-Neo-CMV with inclusion of tetR binding site).

2.1.6 Plasmids, as generated in this study

Construct under control of promoter	Cloned into vector	Host for expression
Myc_hPPM1E	pFB-Neo-CMV	mammalian cell lines
	pFB-Neo-CMV-TO	
	pUAST	<i>D.melanogaster</i>
	pAAV	mammalian neuron
His_hPPM1E	pET24a	<i>E.coli</i>
	pFastBac TM 1	<i>Sf9</i>
Myc_hPPM1E(1-557)	pFB-Neo-CMV	mammalian cell lines
Myc_rPPM1E	pFB-Neo-CMV	mammalian cell lines
Myc_hARHGEF6	pUAST	<i>D.melanogaster</i>
Flag_hARHGEF6	pAAV	mammalian neuron
Myc_hPPM1E (R241A)	pFB-Neo-CMV	CHO-K1
	pAAV	mammalian neuron
Myc_hPPM1E (D273A)	pFB-Neo-CMV	CHO-K1
	pAAV	mammalian neuron
Myc_hPPM1E (H275A)	pFB-Neo-CMV	CHO-K1
	pAAV	mammalian neuron
Myc_hPPM1E (G276D)	pFB-Neo-CMV	CHO-K1
	pAAV	mammalian neuron
Myc_hPPM1E (D479N)	pFB-Neo-CMV	CHO-K1
	pAAV	mammalian neuron

Table 2.6: Plasmids generated for this study. pCR-Blunt-TOPO constructs, which were only used as intermediates in the cloning procedure are not listed.

2.1.7 Antibodies and markers

Primary antibodies			
Antigen / clone	Manufacturer	Orderno.	Host
phospho-c-Jun N-terminal kinase (JNK) (Thr183/Thr185)	NEB	4668S	rabbit
CaMKII α (phospho T286) (22B1)	abcam	ab2724	mouse
CaMKII α / β	abcam	ab19223	rabbit
CaMKII α (6G9)	abcam	ab2725	mouse
CaMKII β	abcam	ab34703	rabbit
CaMKII (phospho T286(α)/T287(β))	abcam	ab32678	rabbit
CaMKIV	abcam	ab3557	rabbit
CaMKIV (phospho T196+T200)	abcam	ab59424	rabbit
cyclophilin B	abcam	ab16045	rabbit
EAAC1 (EAAT3)	Zymed	32-1000	mouse
Flag-tag (clone M2)	Sigma	F1804	mouse
GAD 67	Millipore	MAB5406	mouse
GAD 67	Chemicon	MAB5406	mouse
GAPDH (14C10)	Cell Signalling	2118	rabbit
GFAP	Chemicon	MAB360	mouse
GFP	Invitrogen	A6455	rabbit
GM130 (Golgi)	BD Transduct. Laboratories	610822	mouse
KDEL (10C3)	Stressgen	SPA-827	mouse
MAP2 (clone HM-2)	Sigma-Aldrich	M9942	mouse
MAP2	Millipore	Ab5622	rabbit
Myc-tag	MBL	562	rabbit
NeuN (clone A60)	Chemicon	MAB377	mouse
PAK1	Chemicon	AB3844	rabbit
PAK1/2/3 [phosphoThr ⁴²³]	Biosource	44-942G	rabbit
PAK1/2/3 [phosphoThr ⁴²³]	Rockland	600-401-413	rabbit
PAK1/2/3 [phosphoThr ⁴²³]	Sigma	P 7746	rabbit

Table 2.7 – part 1: Antibodies and markers used in this study. Antibodies were diluted for immunoblotting and immunolabeling of formaldehyde fixated specimens as recommended by the manufacturer if not otherwise stated.

Primary antibodies			
Antigen / clone	Manufacturer	Orderno.	Host
PSD-95 (6G9-1C9)	abcam	ab2723	mouse
Synaptophysin	Santa Cruz Biotechnology	sc-17750	mouse
α Tubulin	Dianova	DLN 15412	rabbit
Markers			
AlexaFluor488 ^R phalloidin	Invitrogen	A12379	
4'-6-diamino-2-phenylindole (DAPI) (5 mM)	Sigma	D9564	
DRAQ5	Cell Signaling	4084S	
Secondary anti-isotypic antibodies			
anti-mouse AlexaFluor [®] 647	Invitrogen	A21236	goat
anti-rabbit AlexaFluor [®] 488	Invitrogen	A11034	goat
anti-rabbit AlexaFluor [®] 555	Invitrogen	A21429	goat
anti-mouse IgG-HRP	Santa Cruz Biotechnology	sc-2031	goat
anti-rabbit IgG-HRP	Santa Cruz Biotechnology	sc-2030	goat

Table 2.7 – part 2: Antibodies and markers used in this study. Antibodies were diluted for immunoblotting and immunolabeling of formaldehyde fixated specimens as recommended by the manufacturer if not otherwise stated.

2.2 Methods

2.2.1 General genetic, molecular biological and biochemical methods

2.2.1.1 Tools for *in silico* genetic comparisons

Homology searches have been performed with resources of the NCBI (National Institute for Biotechnology Information, Rockville Pike, USA) using BLAST-N and BLAST-P algorithms (Altschul et al., 1997). Homology searches between human PPM1E (NM_014906) and ARHGEF6 (NM_004840) genes and the Drosophila genome have been performed with flybase (flybase.bio.indiana.edu) resources using BLAST-P algorithms (flybase.org/blast).

Homologies were displayed by alignment with ClustaW2 software (Larkin et al., 2007;Thompson et al., 1997). In the alignments (compare Appendix), “*” indicates residues that are identical in all sequences in the alignment; “:” indicates conserved substitutions within the groups of 1. small, hydrophobic and aromatic (without tyrosine) amino acids (aa), 2. acidic aa or 3. hydroxyl, amine, amide and basic aa. “.” Indicates semi-conserved substitutions between amino acids with similar shapes.

Searches for conserved domains have been performed with the Conserved domain database (CDD), a NCBI database of protein domains, families and functional sites (Marchler-Bauer et al., 2009).

2.2.1.2 Human and rat PPM1E and ARHGEF6 expression plasmid construction

The cDNA clones for hPPM1E and hARHGEF6 were purchased from Origene (Rockville, USA) and the German Resource Center for Genomic Research (rzpd; Berlin, Germany). Human PPM1E and ARHGEF6 were amplified by polymerase-chain-reaction (PCR), as described below, from human cDNA clone TC128041 (Origene, GeneID: NM_014906.3) and human Ultimate™ full length ORF expression clone IOH26187 (RZPD, GeneID: NM_004840) with the primer pairs #01 / #02 and #03 / #04 respectively.

rPPM1E and rARHGEF6 were amplified from rat primary hippocampal culture cDNA by means of PCR with the primer pairs #05 / #06 and #07 / #08 respectively. Neuronal mRNA was isolated from primary cell culture with RNeasy Plus Mini and QIAshredder kits (Qiagen, 74134 and 79656) as described further in 2.2.5.8 *Quantitative real-time*

PCR from isolated mRNA and transcribed into cDNA with Sensiscript II Reverse Transcriptase (205213, Qiagen) as described by the manufacturer.

All four constructs were ligated blunt into pCR-BluntII-TOPO as described in 2.2.1.3 *General DNA construct amplification and subcloning between vectors*.

2.2.1.3 General DNA construct amplification and subcloning between vectors

All DNA constructs were amplified with 25 units/ml *Pfu* Ultra DNA polymerase (Stratagene, #600670-51) in a thermal cycler (MJ Research) with 1-4 μ M forward and reverse primer concentration, 200 μ M dNTPs (Amersham Pharmacia Biotech, #27-2094) and with or without 5 % dimethyl sulfoxide (DMSO). Optimal temperature cycling parameters were adapted according to the primer pair and the amplified construct: The optimal annealing temperature lay usually 5°C below the predicted melting temperature of the primer pair, the length of amplification cycles at 72°C was 1 min per 500 basepairs of the construct, the denaturing temperature was 95°C. The temperature cycle was repeated 18 to 35 times avoiding longer reaction times than 6 hours. In some cases the DNA yield was raised through increasing the primer specificity by gradually lowering the annealing temperature in steps of 0.5°C in 8-12 cycles before carrying out 10-23 cycles at the optimal calculated annealing temperature.

Subcloning procedures for specific applications by means of restriction enzymes or of PCR into different expression plasmids (compare Tables 2.5 – Vectors, and 2.6 – Plasmids as generated in this study) and under addition of different affinity tags are described in the respective paragraph.

In all cases plasmid DNA was amplified in XL-1 blue competent *E.coli* cells (Stratagene, #200249) in lysogeny broth medium (5 g/l NaCl, 10 g/l tryptone and 5 g/l yeast extract) with 50 μ g/ml kanamycine or 100 μ g/ml ampicilline depending on the resistance gene carried by the vector. After 16 hours vigorously shaking at 37°C, the plasmids were purified with the QIAprep® Spin Miniprep or QIAfilter Plasmid Midi Kit (Qiagen #27106 and 12245). In cases where a change of buffer was necessary the PCR products were purified with the QIAquick PCR Purification Kit (Qiagen, #28106). DNA fragments were separated according to their size by agarose gelelectrophoresis and subsequent excision from gels. The excised fragments were purified with the QIAquick Gel Extraction Kit (Qiagen, #28706).

Constructs which were amplified by PCR were ligated blunt into pCR-BluntII-TOPO using the Zero Blunt® TOPO PCR Cloning Kit for sub-cloning according to the

manufacturer's advice (Invitrogen, #K2830-20). The constructs pCR-BluntII-TOPO / hPPM1E, / hARHGEF6 and / rPPM1E, among others, were constructed like this for further subcloning procedures. All constructs were confirmed by restriction digest with 2 to 3 appropriate restriction enzymes (Fermentas) and subsequent determination of fragment sizes on 1-2% agarose gelelectrophoresis in TAE buffer (AppliChem, TAE Puffer 50x, #A1691,5000CT). Suitable restriction sites were identified with NEBcutter V2.0 (Vincze et al., 2003). Constructs which were amplified by PCR were sequenced externally for verification (Qiagen sequencing service; compare Table 2.4 *Oligonucleotides for sequencing of PPM1E and ARHGEF6 constructs*). Constructs were subcloned through digest with restriction enzymes as specified in the respective paragraph according to manufacturer's protocol and ligated with T4 DNA Ligase (Fermentas, #EL0011) into the respective expression vector as recommended by the manufacturer.

2.2.1.4 Site-directed mutagenesis of hPPM1E and plasmid construction

pAAV / Myc-hPPM1E(R241A) and (D479N) mutants were constructed by a PCR overlap extension method (Ho et al., 1989) from pCR-BluntII-TOPO / hPPM1E with the gene primer pair #09 / #10 and the following mismatching primer pairs: (R241A): #11 / #12; (D479N): #19 / #20. Primer pairs for site-directed mutagenesis were designed using PrimerX[®] software (Lapid C., copyright 2003). PCR products were subcloned as described in 2.2.5 *Influence of PPM1E in cell lines and primary neuronal culture* (page 68).

2.2.1.5 shRNA design and plasmid construction

Short hairpin oligonucleotides were designed using siDESIGN software (Thermo Scientific) and the human (h) and rat (r) PPM1E sequences (NM_014906 and NM_198773 respectively) (Table 2.3 *Oligonucleotides for construction of shRNA constructs*). The antisense part of the sequences corresponds to sections in the coding sequence of rat or human PPM1E. The short hairpin RNAs (shRNAs) were expressed under control of the polymerase-III H1 gene promoter.

DNA encoding for short hairpin constructs was annealed from synthetic oligonucleotides and cloned as *Bgl*II / *Hind*III fragments into pSuper.basic (OligoEngine, USA). For expression of shRNAs, the transcriptional control units from pSuper.basic, containing the H1 promoter followed by the DNA encoding for the short hairpin constructs, were inserted as *Xba*I / *Xho*I fragments into pAAV-6P-SEWB

leaving the coding region and promoter for the EGFP gene intact (Shevtsova et al., 2005;Kügler et al., 2003).

2.2.1.6 Quantitative and qualitative immunoblotting

Cell culture lysates or protein solutions for immunoblotting were obtained as described in the respective paragraphs. Protein concentrations were determined with the BCA Protein Assay Kit (Thermo Scientific, #23225) using bovine serum albumin as standard. Equal amounts of protein (15–25 µg) from each cell culture lysate were dissolved in a mixture of sample and reducing sodium dodecylsulfate (SDS)-polyacrylamide gel electrophoresis (PAGE) buffer and heated at 70°C for 10 min as described by the manufacturer (Invitrogen, NuPAGE LDS sample buffer #NP0007 and reducing agent #NP0004).

The proteins were separated by SDS-PAGE on 10 % or 4-12 %-acrylamide gels (Invitrogen, NuPAGE Bis-Tris acrylamide gels), and transferred to PVDF membranes in transfer buffer containing 25 mM Tris, 200 mM glycine, 0.02% SDS and 20% methanol at 350 mA for 90 min.

For qualitative immunoblotting samples were separated by SDS-PAGE gels, and transferred to standard PVDF membranes (GE Healthcare, #RPN303F). Membranes were blocked in 10 % (w/v) milk powder in TBS-T (10mM Tris, 150 mM NaCl, 0.05 % Tween 20, pH 7.5). All further steps containing antibodies were carried out in 2.5 % (w/v) milk powder in TBS-T.

For quantitative immunoblotting five step 1:2 dilution series of each sample were separated by SDS-PAGE and transferred to ImmobilonTM-FL PVDF membranes (Millipore, #IPFL10100). Membranes were blocked with Sea blockTM blocking buffer (Pierce). All further steps containing antibodies were carried out in Sea blockTM blocking buffer.

All blots were incubated in primary and secondary antibodies for 1 hour each at room temperature and washed three times in TBS-T in between antibody incubations and before detection.

Qualitative immunoblots were detected with horseradish-peroxidase-labeled anti-isotypic antibodies and an ECL western blotting detection system according to manufacturer's instructions (GE Healthcare, #RPN2132) on chemiluminescence film

(GE Healthcare, #28906837). Films were developed with an automatic film processor (Amersham Hyperprocessor, GE Healthcare).

On quantitative immunoblots the bound primary antibodies were detected with fluorescently labeled Qdot^R-conjugated anti-isotypic antibody (Invitrogen) and visualized on the FMBIO^R II Fluorescent Image Scanning Unit (Ornberg et al., 2005). Analysis of fluorescence intensity was performed with ImageJ 1.38x (Abràmoff et al., 2004). Pictures were inverted and pixel intensities of the respective protein bands were measured. Values of the sample dilution series that are in the dynamic range of the fluorescence scan are averaged. Reported values were normalized to anti-Cyclophilin B or anti- α -Tubulin staining.

2.2.2 His-hPPM1E protein expression, purification and *in vitro* activity determination

2.2.2.1 Plasmid construction for and expression of His-hPPM1E protein in *E.coli*

pET24a / His-hPPM1E was constructed by PCR from pCR-BluntII-TOPO / hPPM1E with the primers #21 and #22. The PCR product was cloned as *Nde*I / *Xho*I fragment into pET24a (Novagen, #69749-3). His-hPPM1E was expressed in *E. coli*, BL21DE3 (Stratagene, #200131) or BL21-CodonPlus[®] -RIL and -RP(DE3) (Stratagene, #230245 and #230255) competent cells under control of the bacterial T7 promoter. *E.coli* was grown in 20 g/l tryptone, 10 g/l yeast extract, 5 g/l NaCl, 1 % Glucose, 20 mM K₂HPO₄ and 4 mM MgSO₄. Expression was induced with 0.5 mM Isopropyl- β -D-thiogalactopyranosid (IPTG) at OD_{600nm}=0.6 for 4 to 24 hours at 25 or 37°C. Cells were harvested by centrifugation at 17 000 g, suspended in 10 mM Tris-Cl pH 7.0, 150 mM NaCl with a general protease inhibitor mix (Complete, Roche, 11697498001) and disrupted by sonic oscillation. These and all following steps are performed on ice. A pinch of each DNase (Sigma, #D5025-150KU) and RNase (Sigma, #R4875-500MG) were added for 30 min on ice and cell debris was removed by centrifugation.

2.2.2.2 Plasmid construction for and expression of His-hPPM1E protein in Sf9 insect cells

His_PPM1E was expressed in the *Spodoptera frugiperda* cell line Sf9 under control of the polyhedrin promoter (Vaughn et al., 1977) (Cell Culture Service). The His_hPPM1E coding sequence was introduced into a baculovirus, AcNPV, using the Bac-To-BacBaculovirus Expression System with pFastBac 1 according to manufacturer's instructions with minor modifications (Gibco-BRL/Life Technologies, Gaithersburg, MD,

USA). pFastBac1 / His_hPPM1E was constructed by PCR from pCR-BluntII-TOPO / hPPM1E with the primers #23 and #22. The PCR product was cloned *EcoRI* / *XhoI* into pFastBac1.

Sf9 cells infected with the recombinant baculovirus were grown adherent at 27°C in TC100 medium (GIBCO, 13055-025) supplemented with 10% FCS, 1% sodium pyruvate (Sigma, S8636) and 0.83x Yeastolate (GIBCO, #18200-048). For protein expression 1×10^{10} cells in 1 l suspension culture with supplemented TC100 and 0.2 % pluronic F-68 (Sigma, # P5556), 10 U /ml penicillin, 10 mg/ml streptavidin (PAA, # P11-010) and 10 µg/ml gentamicin (Gibco, # 15710-049) were infected at multiplicity of infection (MOI) 5 to 8 in 2 l disposable PETG flasks (Nalgene, #4112-2000). After 72 hours the cells for protein production were harvested and disrupted as described in 2.2.2.1 *Plasmid construction for and expression of His-hPPM1E protein in E.coli*.

2.2.2.3 His-hPPM1E protein purification and detection

The His-tagged hPPM1E was purified using Ni-NTA chromatography with a 5 ml HisTrap™ HP column (GE Healthcare, #71-5027-68 AF) according to the manufacturer's instructions in 10 mM Tris-Cl pH 7.0, 150 mM NaCl using an ÄKTAprime™ plus system (GE Healthcare). His-PPM1E was eluted from the column with 150 mM imidazole (Fluka, #56750). After removal of imidazole by dialysis to 10 mM Tris-Cl pH 7.0, 150 mM NaCl in pleated dialysis tubing with a molecular weight cut off (MWCO) of 10 kDa (Pierce, #68100) the protein was concentrated to 1 mg/ml in Centriprep® centrifugal filters with MWCO of 10 kDa (Millipore, #4321) and subsequently stored with general protease inhibitor mix (Complete, Roche, 11697498001) in 4°C for several weeks.

Protein purifications were analyzed by SDS-PAGE and subsequent immunoblotting as described in 2.2.1.6 *Quantitative and qualitative immunoblotting*, or by subsequent general protein stain with Coomassie solution (0.78 g/l copper sulphate, 0.5 g/l serva blue R, 0.5 g/l crocein scarlet, 25 % 2-propanol, 10 % glacial acetic acid) for 1 h. Excess dye was removed in 18 % 2-propanol / 9 % glacial acetic acid.

2.2.2.4 His-hPPM1E phosphatase activity assay

His-hPPM1E activity was tested in two biochemical activity assays based on dephosphorylation of a phosphorylated peptide. A malachite green based assay detected subsequently released anorganic phosphate, while a polarization based

assay detected antibody binding to a tetramethyl-6-carboxyrhodamine dye (TAMRA)-labeled phosphorylated peptide.

In the malachite green based assay the PPM1E substrate peptide YGGMHRQEpTVDC (pT: phosphorylated threonine) containing the sequence around the autophosphorylation site of rat CaMKII α (281-289), and assay conditions are based on a PPM1E activity assay by (Takeuchi et al., 2001) with minor modifications. The phosphopeptides YGGMHRQEpTVDC and a shortened version MHRQEpTVDC were synthesized externally (Metabion, Germany). Reaction buffer consisted of 50 mM Tris-HCl pH 7.5, 2.5 mM MnCl₂, 2.5 mM MgCl₂, 0.125 mM EDTA, 0.0125 % Tween20 and 12.5 μ g/ml poly-L-lysine with 40 μ M phosphopeptide. Dephosphorylation was started by the addition of purified His_PPM1E at 30 °C to a reaction volume of 50 μ l and stopped by the addition of malachite green solutions according to manufacturer's instructions (R&D systems, #DY996). The release of inorganic phosphate was determined by the malachite green method of (Baykov et al., 1988) by measurement of absorbance at 620 nm on a Sapphire2 plate reader (Tecan, Switzerland) in 96 to 384 well plate format.

In the polarization based assay dephosphorylation of 10 nM TAMRA-labeled peptide TAMRA-MpTppYV was started by the addition of purified His-PPM1E under conditions as described above. An antibody raised against the phosphorylated c-Jun N-terminal kinase (JNK) and which binds to the phosphorylated assay peptide, was added in 1:20 dilution with 10 mM hydrogen peroxide to stop the reaction. Changes in fluorescence polarization are detected based on changes in abundance of large TAMRA-antibody complexes with a fluorescence correlation spectroscopy (FCS) reader (Evotec AG). The unspecific PPM1E inhibitor 1-Amino-8-naphtol-2,4-disulfonic acid was added as control (Calbiochem, 208775) (Sueyoshi et al., 2007).

2.2.3 PPM1E Antibody production and characterization

2.2.3.1 Anti-PPM1E and anti-ARHGEF6 antibody production

Rabbit polyclonal antibodies reactive to polypeptides corresponding to parts of the human PPM1E or ARHGEF6 sequence have been produced externally by immunization of rabbits with a synthetic peptide (Davids Biotechnologie, Regensburg, Germany).

<u>Antibody</u>	<u>synthetic peptide used for immunization</u>	<u>Peptide ID</u>	<u>Working concentration</u>
α PPM1E(AGC)	AGCIPEEKTYRRFLELFL	I	0.2-0.8 μ g/ml ¹
α PPM1E(GAA)	GAATAAAAPGHSAPPPPP	II	
α PPM1E(KLA)	KLARSVFSKLHEIC	III	
α PPM1E(ENS)	ENSFQGGQEDGGDDKENHGECK	IV	4 μ g/ml ²
α ARHGEF6(LLA)	LLAVNKATEDQLSERPCGR	V	
α ARHGEF6(SRR)	SRRDLEKLVRRLLKQTDE	VI	

Table 2.8: Sequences of the synthetic peptides used for immunization of rabbits and subsequent antibody isolation. ¹ dilution for immunoblotting with qualitative and quantitative detection respectively. ² dilution for immunolabeling of cell culture after formaldehyde fixation.

The amino acid sequences for anti-PPM1E immunization peptides nos. I (AGC), III (KLA) and IV (ENS) are conserved in human and rat PPM1E sequences (Appendix A 3). The peptide sequence II is specific for human PPM1E. The amino acid sequence for anti-ARHGEF6 immunization peptide nos. V (LLA) is conserved in human and rat, while the sequence IV (SRR) is specific for human ARHGEF6 (Appendix A 4).

Rabbits immunized with these peptides developed PPM1E-specific antibodies with different affinities and specificities. Antibodies were purified externally based on their affinity to the immunization peptides (Davids Biotechnologie, Regensburg, Germany).

2.2.3.2 Anti-PPM1E and anti-ARHGEF6 antibody characterization for immunoblot applications

Antibodies were tested on human frontal cortex samples (Netherlands Brain Bank) for their specificity in western blot applications. Protein samples and subsequent immunoblots were prepared as described in 2.2.1.6 *Quantitative and qualitative immunoblotting*. 25 μ g total protein per lane were detected with different concentrations of the respective antibodies. For specificity and signal intensity optimized antibody concentrations were then tested on several additional cell extracts and compared with signals of anti-affinity-tag antibodies in cell extracts of stable H4_Myc_PPM1E and H4_ARHGEF6_Flag cell lines.

2.2.3.3 Anti-PPM1E antibody characterization for immunofluorescence applications

The antibodies were tested on formaldehyde fixated primary neuronal culture and rat and human cryocut brain slices of frontal and temporal cortex. Antibody concentrations between 0.2 and 4 μ g/ml were incubated for 1 hour at room temperature or 4°C over

night. Unspecific non-epitopic antibody binding was ruled out by blocking the epitope-binding site by pre-incubation of the antibody with 10 µg/ml of the respective immunization peptide. Binding was subsequently detected with anti-isotypic fluorophore conjugated Alexa antibodies (Invitrogen) as described in 2.2.5 *Influence of PPM1E in cell lines and primary neuronal culture* (page 68). Samples were embedded in Fluoromount-G (Southern Biotech) and imaged using an inverse Olympus iX81 fluorescence microscope. Specific PPM1E staining pattern and background intensity were assessed.

2.2.4 Effects of PPM1E expression in *Drosophila melanogaster*

2.2.4.1 Cloning of pUAST injection vectors

pUAST is designed to direct GAL4-dependent transcription of a gene of choice in *D.melanogaster*. The respective sequence is subcloned into a polylinker situated downstream of five tandemly arrayed, optimized GAL4 binding sites, and upstream of the SV40 small t intron and polyadenylation site. Human PPM1E and ARHGEF6 were amplified by PCR from pCR-BluntII-TOPO / hPPM1E and / hARHGEF6. The used primer pairs, #09 / #22 and #03 / #28 respectively, included a N-terminal and C-terminal Myc-tag respectively. The genes were cloned as *EcoRI* / *XhoI* fragments into pUAST.

2.2.4.2 Establishment of transgenic *D.melanogaster* strains and fly rearing

w¹¹¹⁸ flies were employed as wild-type controls. The following fly lines were provided by the Bloomington Stock Center: wildtype control w¹¹¹⁸, double balancer [w^{*}; noc^{ScO}/CyO; Sb¹/TM3] and GAL4 driver P{GawB}elav^{C155}. Driver line P was kindly provided by Dr. Doris Kretzschmar (OHSU School of Medicine, Portland, USA). GAL4 in the driver lines is expressed in the eye under control of the glass multiple reporter (gmr) promoter (Freeman, 1996) or the neuron-specific elav promoter. As wildtype control the w¹¹¹⁸ fly stock and GAL4-driver lines crossed to w¹¹¹⁸ were used.

P-element mediated germline transformation of w¹¹¹⁸ flies was performed as described (Rubin and Spradling, 1982; Spradling and Rubin, 1982). Transgenes were created by injection of pUAST, containing the desired gene PPM1E or ARHGEF6, into w¹¹¹⁸ embryos. This led to random and stable integration of the gene on chromosome X, 2 or 3. Injection was carried out by Vanedis *Drosophila* Injection Service (Norway). For the establishment of stable fly lines, hatched transgenic flies were crossed to the double

balancer line and kept as stock as [w¹¹¹⁸; gene of interest/CyO] or [w¹¹¹⁸; +/+; gene of interest/Tm3] (“+”: wildtype chromosome).

Drosophila cultures were maintained on a 12–12 h light–dark cycle on standard corn meal yeast agar medium (160 g/l agar-agar, 0.044 % sugar beet molasses, 0.08 % malt extract, 0.08 % corn semolina, 0.018 % brewer's yeast, 0.01 % soy flour and 90 g/l methyl 4-hydroxybenzoate) at 25 °C in an environmental chamber (Mytrom, WB120K). All ingredients were purchased in public stores, except for methyl 4-hydroxybenzoate (nipagin, Sigma-Aldrich, #H3647). Cultures were transferred to a new vial every three to four days to avoid overcrowding.

For each transgene at least one strong and weak expressing cross to P{GawB}elav^{C155} and P{w; gmr-GAL4} was analyzed on western blot and for alterations in its eye and central nervous system respectively by visualization under the light microscope, surveillance of potential motor deficits and determination of the mean life span. Fly eyes in P{w; gmr-GAL4} were visualized directly without fixation and immunolabeling in a Zeiss Stemi 2000-C microscope after anesthetization with CO₂. The Lifespan of P{GawB}elav^{C155} crosses was evaluated in 70 flies per cross, the flies were collected within 16 hours after hatching, kept in groups of up to 25 individuals and their survival was evaluated thrice weekly after anesthetization with CO₂.

2.2.4.3 Immunoblot analyses of fly extracts

Ten flies were shock-frozen in liquid nitrogen. For analysis of gmr-GAL4 crosses the heads were separated from the torso by application of shock to the deep-frozen flies. The heads were transferred to 4°C ready-made RIPA buffer (0.5% deoxycholate, 0.1% SDS, 1% NP40 and 5 mM EDTA in PBS; Sigma, #R0278) including a cocktail of general protease inhibitors (Complete, Roche, #11697498001). They were homogenized with 10 blows in a 200 µl all glass tissue grinder (Wheaton, Neo-lab, #9-0906) and incubated on ice for 30 min. For analysis of Elav-GAL4 crosses whole flies were homogenized in the same manner. Soluble and insoluble fractions were separated by centrifugation at 16 000 g at 4 °C for 10 min. The supernatant was analyzed by SDS-PAGE and subsequent immunoblotting as described in 2.2.1.6 *Quantitative and qualitative immunoblotting*.

2.2.5 Influence of PPM1E in cell lines and primary neuronal culture

All cell culture reagents and media were obtained from PAA (Pasching, Austria), Sigma Aldrich (St. Louis, MO, USA) or Invitrogen (Karlsruhe, Germany). Culture plates in 75 and 175 cm² and 6-, 24- and 96-well plates with growth areas of 0.9, 1.9 and 9.6 cm² per well respectively and culture dishes with 15 cm diameter were purchased from greiner bio-one (Kremsmünster, Austria).

2.2.5.1 Plasmid construction

All plasmids for expression of recombinant proteins or shRNAs in neuronal cells were modified from pAAV-6P-SEWB. For expression of ARHGEF6_Flag the gene was amplified with Flag-tag from pCR-BluntII-TOPO / hARHGEF6 with primer pair #03 / #30 and cloned as *EcoRI* / *HindIII* fragment into pAAV-6P-SEWB. The *EcoRI* / *NotI* digested Myc_PPM1E_mutant inserts, constructed as described in 2.2.1.4 *Site-directed mutagenesis of hPPM1E and plasmid construction*, and an *EcoRI* / *NotI* Myc_PPM1E PCR fragment from PCR on pCR-BluntII-TOPO / hPPM1E with the following primer pair #09 / #10, were ligated to the *EcoRI* restricted site of an *EcoRI* / *BsrGI* digested pAAV-6P-SEWB. Single-strand DNA was complementarized with the DNA polymerase klenow fragment (Fermentas, #EP0051) and ligated blunt to gain a circular construct. Myc_PPM1E, Myc_PPM1E mutants and ARHGEF6_Flag were expressed under control of the human synapsin promoter. Control plasmid: pAAV-6P-SEWB, expression of EGFP (Table 2.5 *DNA vectors which have been used in this study*).

For expression in mammalian cell lines Myc_PPM1E or Myc_PPM1E mutants and ARGEF6_Flag were subcloned as *EcoRI* / *NotI* and *EcoRI* / *HindIII* fragments respectively from the respective pAAV-6P-SEWB construct into pFB-Neo-CMV and pFB-Neo-CMV-TO. Myc_hPPM1E(1-557) was amplified with Myc-tag from pCR-BluntII-TOPO / hPPM1E with the primer pair #09 / #31 and cloned as *EcoRI* / *XhoI* fragment into pFB-Neo-CMV. The genes of interest were expressed under control of the mammalian CMV promoter with and without Tet repression respectively. Control plasmid: pFB-Neo-CMV-EGFP, expression of EGFP (Table 2.5 *DNA vectors which have been used in this study*).

2.2.5.2 Cultivation of immortalized cell lines

All cell lines were obtained from the American Type Tissue Culture Collection (ATCC, Molsheim, France). Cultures were grown at 37°C in humidified atmosphere in 75 to 175 cm² cell culture dishes and as specified in Table 2.9. Cells in culture were split twice

weekly, with cell numbers as specified in Table 2.9. Cell numbers were determined with an automated Casy^R cell counting system (Innovatis, TT-2GB-1357). For long-time conservation 5×10^6 cells were stored in 95 % FCS (GIBCO) and 10 % DMSO in liquid nitrogen.

Cell line	Origin	Morphology	Growth medium ¹	CO ₂ conc.
CHO-K1 ¹⁰ / CHO-TRex ⁸	<i>Cricetulus griseus</i> (hamster, Chinese), ovary	epithelial- like	minimum essential medium (MEM, Gibco, 31095- 029)	5 %
HEK 293 GP ⁵ , ¹¹ / HEK 293 T17 ⁶	<i>Homo sapiens</i> , embryonic kidney	epithelial	DMEM (Sigma, D5796)	8 %
H4	<i>Homo sapiens</i> brain (neuroglioma)	epithelial	DMEM (Sigma, D5796)	8 %
RBL-1	<i>Rattus norvegicus</i> , peripheral blood (leukemia)	lymphoblast	DMEM F-12 (Sigma, D8437) ³ , 1xMEM NEAA (PAA, #M11- 003)	5 %
Pc-12 ²	<i>Rattus norvegicus</i> adrenal gland (pheochromocytoma)	polygonal, neuronal- like	RPMI 1640 (Sigma, #R8758), 5 % horse serum	5 %
Neuroscreen- 1 ⁷	Pc-12 subclone	polygonal, neuronal- like	RPMI 1650 (GIBCO ⁹), 25mM HEPES, 5 % horse serum, 2 mM L- Glutamine (Sigma, #G6784)	5 %
ST14A ⁴	embryonic day 14 rat striatal primordia, derived by retroviral transduction	polygonal, fibroblast- like	DMEM high glucose with NaPyruvat (PAA, #E15- 011), 2 mM L- Glutamine (Sigma, #G6784)	5 %

Table 2.9: Cell lines cultivated in this study. ¹ supplemented with 10 % fetal bovine serum (FBS, GIBCO) and 10 U / ml penicillin and 10 mg / ml streptomycin (Penicillin/Streptomycin (100 x), PAA, # P11-010); ² (Levi et al., 1985; Green et al., 1976); ³ supplemented with 15 % instead of 10% fetal bovine serum (FBS, GIBCO); ⁴ (Ehrlich et al., 2001); ⁵ packaging cell line for VSV-G production; ⁶ packaging cell line for AAV production; ⁷ Culture plates for Neuroscreen-1 cultivation are coated with 10x PBS diluted collagen solution (Sigma, #C8919); ⁸ supplemented with 5 µg/ml blasticidin; ⁹ not in stock anymore; ¹⁰ (Kao and Puck, 1968) ; ¹¹ (Graham et al., 1977).

All cell lines were cultured with 10 U / ml penicillin and 10 mg / ml streptomycin (Penicillin/Streptomycin (100 x), PAA, # P11-010), except for transfection or transduction purposes or directly after thawing of new culture stocks.

2.2.5.3 Transient transfection and establishment of stable transgenic cell lines

For transient transfection, plasmid lipofectamine 2000 particles were allowed to form for 20 minutes in a mixture of 100 μ l OptiMEM (Gibco, #31985-047), 1-4 μ l lipofectamine 2000 reagent (Invitrogen, #11668-027) and 1 μ g pFB-Neo-CMV or pFB-Neo-CMV-TO vector containing the gene of interest. The transfection mixture was added to 1.9 cm² confluent cells in 400 μ l of their respective culture medium. 24 hours after transfection of pFB-Neo-CMV-TO constructs, expression was induced by addition of 1 μ g/ml tetracycline.

For construction of a stable cell line, HEK 293 GP cells were incubated with transfection mixture as described above with minor modifications: 9.6 cm² confluent cells in 2 ml culture medium were transfected by addition of 500 μ l OptiMEM, 10 μ l lipofectamine 2000, 2 μ g pFB-Neo-CMV and 2 μ g pVPack VSV-G helper plasmid. After 48 hours the virus-containing supernatant was mixed with 10 μ g/ml DEAE-Dextran hydrochloride (Sigma, #D9885). 1 ml mixture was added to 9.6 cm² confluent cell culture of the respective cell line and supplemented with an equal amount of the respective culture medium after 3 hours. After 24 hours 400 μ g / ml G418 antibiotic was added for selection. For establishment of monoclonal cultures 1 cell / well was seeded in a 96 well plate in growth medium with G418 antibiotic for selection and amplified subsequently.

2.2.5.4 Immunolabeling and -blotting of monolayer culture of immortalized cell lines

For standard immunolabeling monolayer cells were fixed 4 to 24 hours after transfection or induction of construct expression with 4% formaldehyde (FA) in PB for 20 minutes at room temperature (RT) or in ice-cold methanol for 16 hours in -20 °C. Afterwards the cells were washed in PB and permeabilized and blocked in 0.5% Triton X-100 and 5 % normal goat serum in PB buffer for 30 min, then incubated with the primary antibodies for 1 hour in PB. After three washes in PB, antibody binding was detected for 1 hour with anti-isotypic fluorophore conjugated antibodies Alexa-488, Alexa-555 or Alexa-647 in a mixture with other desired autofluorescent or fluorophore-labeled markers (Table 2.7 – Antibodies and markers). For F-actin staining with AlexaFluor488^R labeled phalloidin the incubation time was extended to 2 hours. Cells

were then rinsed in PB and embedded in Aqua PolyMount (Polysciences Europe, #18606-20) on glass slides. Quantitative analysis of the number of transfected or infected cells was performed using an Olympus IX81 fluorescence microscope. Twenty fields per coverslip per experiment (n=3) were analyzed. Data were expressed as mean % of total cells per experiment \pm standard error of the mean.

For standard immunoblotting cells were washed with PB buffer and scraped off the culture dish or dissociated from the underground by trypsination (PAA, #L11-004) and solved in ready-made RIPA buffer (Sigma, #R0278) and a mix of general protease inhibitors (Roche, #11697498001). In cases where the preservation of the protein phosphorylation was necessary, the cells were directly lysed in above described buffer with a mix of phosphatase inhibitors (PhosStop, Roche, #04906845001) without a prior washing step in PB. Further sample preparation and immunoblotting was carried out as described in 2.2.1.6 *Quantitative and qualitative immunoblotting*.

2.2.5.5 Primary hippocampal neuronal culture

Primary rat hippocampal cultures were prepared from 17-day-old (E17) embryos of timed-pregnant Wistar rats as described previously (Wei et al., 2008;Zheng et al., 2002), with minor modification. In brief, the pregnant rats were anaesthetized with CO₂ (up to 80 %, 10 min) and then decapitated. The hippocampi (hc) or cortices (co) from the pup brain were then dissected in Hanks's balanced salt solution (HBSS) supplemented with 2 mM kynurenic acid, 10 mM hepes, 20 mM MgCl₂ and 0.6% glucose and digested with 20 units / ml papain (Fluka, #76216) in HBSS. The hc or co were washed with plating medium (MEM, 10 % ml FCS, 10 units / ml penicillin and 10 mg / ml streptomycin (Penicillin/Streptomycin (100 x), PAA, # P11-010) and 1% Glutamax), mechanically triturated and plated on either 96-well plates (4*10⁴ hc cells per well for survival/death assay), 24-well plates (7.5*10⁴ hc or 5*10⁵ co cells per well for biochemical analysis) or 13-mm round glass coverslips (VWR, #ECN 631-1578 or Marienfeld, #0111530) (7.5*10⁴ hc or 5*10⁵ co cells per coverslip for immunohistochemical staining and morphological analyses). VWR coverslips were etched in 65 % nitric acid for 24 h before usage. Plates and coverslips were coated with 0.1 mg/ml poly-L-lysine and 1 μ g/ml laminine. The cultures were grown at 37 °C in a 5 % CO₂ humidified atmosphere in Neurobasal medium supplemented with B27, 2 mM L-glutamine, 10 units/ml penicillin and 10 mg/ml streptomycin for 21 days. The medium was replaced 3 hours after plating and subsequently given half-changes twice weekly. Glial cell growth and mitosis was not inhibited to support the establishment of

good neuronal network (Figure 2.1). Neurons were transfected or infected on day in vitro (DIV) 7.

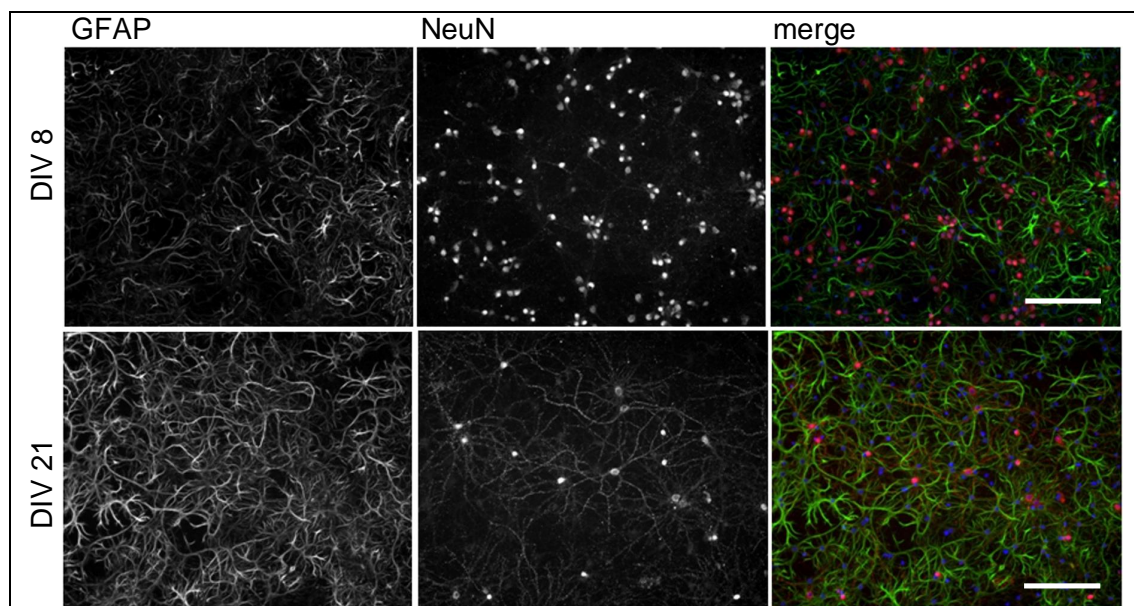


Figure 2.1: Development of glial cells (labelled with anti-GFAP antibody) and neurons (labelled with anti-NeuN antibody) in primary hippocampal culture on day-*in-vitro* (DIV) 8 and 21. GFAP: glial fibrillary protein. NeuN: neuron specific nuclear antigen. Merge: overlay of GFAP (green) and NeuN (red) stains. Scale bar: 200 μ m.

2.2.5.6 AAV vector production

AAV vector production was carried out in HEK 293 T17 cells and following a previously described calcium phosphate transfection protocol (Grimm et al., 1998). rAAVs were produced with serotype 1 and 2 packaging proteins both of which efficiently infect neuronal cells (Grimm et al., 2003). PPM1E is expressed under control of the neuron-specific promoter for human synapsin (hSYN) which induces exclusively neuronal expression (Kügler et al., 2003).

For preparative large-scale productions, 1.5×10^7 cells were seeded in each of ten 15-cm culture dishes and after adherence transfected with 21 μ g DNA. AAV vector and each of the helper plasmids pDP1 and pDP2 were transfected in equimolar amounts. Medium was changed after 24 hours and cells were incubated for 72 hours after infection and then scraped off the culture dish in 2.5 ml PB per 15 cm culture dish. Cells were pelleted, frozen and then thawed in 0.85 ml 50 mM Tris-Cl pH 8.0, 150 mM NaCl per 15 cm plate. Vector particles from large preparations were purified and concentrated by iodixanol density centrifugation as described by others with minor modifications (Zolotukhin et al., 1999). In brief, 0.85 μ l cell lysate was incubated with 40 units benzonase nuclease (Novagen, # 70746) and 0.6 % Na-deoxycholate for 30 min at 37°C, NaCl concentration was raised to 1 M and the suspension incubated 30 min at

56°C and frozen in dry ice. After complete freezing the pellet was thawed at 37°C, centrifuged at 7000 rpm for 30 min at 4°C and purified on a 3 ml 54% - 3 ml 30% - 3 ml 20% - 6 ml 5% iodixanol (OptiPrep[®] density gradient medium, Sigma, #D1556) / PB gradient, the 5% fraction containing 1 M NaCl. Tubes were sealed and centrifuged in a Type 1250 rotor (Sorvall Discovery 90SE Ultracentrifuge) at 271 000 g for 90 min at 12 °C. 2.5 ml from the border between the 54% and the 30% gradient step were aspirated with a syringe equipped with a 0.9 x 70 mm needle (Sterican), washed in 25 ml PB and concentrated in Amicon Ultra 15 Centrifugal Filter Devices (Millipore). The concentrated virus was filtered sterile through 0.45 µm filter (Millex-HV Syringe-Drive Filter (4 mm)) and stored at -80°C.

The number of DNA containing viral particles was estimated by real-time PCR with primers against the cis-acting woodchuck postregulatory regulatory element WPRE element in the viral DNA (Table 2.2 - Oligonucleotides used in quantitative real-time PCR).

2.2.5.7 Infection of neurons and subsequent analyses

1.9 cm² medium-density primary neurons were infected with 3*10⁸ DNA containing particles purified recombinant adeno-associated virus (rAAV) per ml on day *in-vitro* (DIV) 7 (compare (Grimm et al., 2003)). DIV 21 cells were lysed with self- or ready-made lysis buffer ((3% SDS, 20 mM Tris-Cl, pH 7.5, 10 mM EGTA, 2.5 mM MgCl₂) or RIPA (Sigma, #R0278)), containing a mix of general protease inhibitors (Roche, #11697498001). In cases where the preservation of the protein phosphorylation was necessary, the cells were directly lysed in above described buffer with PhosStop phosphatase inhibitor (Roche, #04906845001) and 10 µM CaMKP-Inhibitor (Calbiochem, #208775; (Sueyoshi et al., 2007)). Samples were analyzed in SDS-PAGE and immunoblotting as described in 2.2.1.6 *Quantitative and qualitative immunoblotting*.

2.2.5.8 Quantitative real-time PCR from isolated mRNA

mRNA was isolated from immortalized cell lines or primary cell culture with RNeasy Plus Mini and QIAshredder or 96 well TurboCapture mRNA kits (Qiagen, #74134, #79656 and #72251) and transcribed into cDNA with T₂₀ primers and Sensiscript II Reverse Transcriptase (Qiagen, #205213) as described by the manufacturer. General precautions to avoid RNase contamination, the usage of RNase free materials, cleaning with RNase decontamination solution (ZAP, Ambion, #9780) and breathing away from the samples were taken. Quantitative real-time PCR (qRT-PCR) was

performed with Sybr Green stain (Roche, #04707516001) on a LightCycler 480 (Roche). The PCR parameters were 95°C, 10 min then [95°C, 5 s (ramp rate (rr) 4.4°C/s) → 56°C, 5 s (rr 2.2°C/s) → 72°C, 5 s (rr 4.4°C/s)] for 50 cycles, then for melting curve determination 95°C, 1 s (rr 4.4°C/2) → 65°C, 15 s (rr 2.2°C/s) → 95°C continuous (rr 0.06°C). Melting curves were performed to document single product formation and additionally the product size was confirmed on a microfluidics-based platform (Agilent, 2100 Electrophoresis Bioanalyzer^R). In a typical run, samples were analyzed in triplicate for each primer pair (Table 2.2 – Oligonucleotides used in quantitative real-time PCR). Standard curves for each primer pair were derived from total brain cDNA dilution series with defined concentrations between 2 ng to 4 µg/µl. Total brain cDNA was polymerized as described above from total brain rat or human RNA purchased from Clontech (France). Samples were amplified with candidate gene and “housekeeping gene” cyclophilin B primers in separate reactions. The parameter Ct was derived for each cDNA sample and primer pair. Ct is an expression of amplification kinetics referring to the cycle at which log-phase amplification reaches the pre-determined threshold. Gene expression was expressed relative compared to cyclophilin B expression.

2.2.5.9 Transfection, immunostaining and imaging of primary neurons

Primary neurons growing on glass coverslips were transfected with pAAV-6-SEWB derived constructs on day-in-vitro (DIV) 7 and fixed on DIV21. The culture medium was changed to Neurobasal without additives and the conditioned culture supernatant was stored at 37 °C. Plasmid-Lipofectamine 2000 (Invitrogen, #11668-027) complexes were allowed to form for 20 minutes before application of 1 µg DNA in Neurobasal without additives to 1.9 cm² neuronal culture. After 1 hour the medium was changed to Neurobasal with 0.5 µM APV (Tocris), 5 % FCS, 10 units/ml penicillin and 10 mg/ml streptomycin (Penicillin/Streptomycin (100 x), PAA, # P11-010). After an additional hour the cells were washed with culture medium Neurobasal supplemented with B27, 2 mM L-glutamine, 10 units/ml penicillin and 10 mg/ml streptomycin, half of the volume was then replaced with the stored conditioned culture supernatant. All constructs coding for a protein were co-transfected in equal DNA volumes with EGFP expressing pAAV-6P-SEWB. To control for unspecific transfection effects a non-coding plasmid (pcDNA3+) was always co-transfected so that the total plasmid DNA summed up to 1 µg DNA per 1.9 cm² culture. EGFP was co-transfected to visualize the transfected neurons. All constructs coding for shRNAs contained the EGFP gene as well (see 2.2.1.5 *shRNA design and plasmid construction*).

Cells were fixed on DIV 21 with 4 % formaldehyde, 4 % sucrose in PB for 10 min at room temperature (RT). Samples were permeabilized with 0.1 % Triton[®] X-100 and blocked with 5 % normal goat serum in PB. Cells were stained with primary antibodies in PB for 1 hour at RT with the antibodies specified in Table 2.7 (Antibodies and markers). Detection with secondary antibodies was similarly performed for 45 minutes at RT, using anti-isotypic fluorophore conjugated antibodies Alexa-488, Alexa-555 or Alexa-647 in a mixture with other desired autofluorescent or fluorophore-labeled markers (Table 2.7 – Antibodies and markers). For F-actin staining with AlexaFluor488[®]-labeled phalloidin the incubation time was extended to 2 hours. Samples were embedded in Fluoromount-G (Southern Biotech).

For spine analysis samples were imaged using an inverse Leica SP2 microscope equipped with a 63x oil-immersion objective and connected to a Leica TCS SP2 AOBS confocal laser scanning setup. Z-stacks with 0.2 μm intervals, image resolution of 2048 x 2048 and 2x zoom were recorded. For general morphological analyses samples were imaged with an Olympus IX81 fluorescence microscope. For neurite outgrowth analysis samples were imaged with a 20x water-immersion objective in an Opera high content screening system (Perkin Elmer, #OP-QEHS-01)

2.2.5.10 Analysis of dendritic spines

To quantify the number and qualify the morphology of dendritic spines, one- or two-channel images were acquired using the same acquisition settings. Three dimensional stacks were built and spines along two secondary dendrites per neuron analyzed with Neuron Studio 0.9.44 software (Rodriguez et al., 2008). Results of the internal spine analysis tool were corrected manually. The spines were assigned to the group of mushroom, stubby or thin spines based on their head-to-neck size ratio (Peters and Kaiserman-Abramof, 1970). A total of 60 secondary dendrites from 30 neurons from three independent experiments were quantified for each transfection condition. For each dendrite an 80 to 200 μm segment was analyzed. In total more than 900 spines were counted for each analyzed condition.

2.2.5.11 Neurite analysis

The arborisation of neurons was evaluated in transfected 96well primary neuronal culture. 17 random pictures from GFP and DRAQ5 autofluorescence per well were taken with a 20x water-immersion objective and automatically evaluated with the NeuriteOutgrowth script from Acapella image analysis software (Perkin Elmer). A total of 17 pictures from 8 wells in one 96well plate for 3 independent experiments were

analyzed for each culture condition. In total over 300 transfected neurons were evaluated for each condition. Parameters were the following: maximal neurite width: 5 pixels (p); minimal neurite length: 10. Evaluated are the number of roots, i.e. segments having their origin in the neuron itself, and the total neurite length, i.e. the total length of the neurite structure in one neuron.

2.2.5.12 Statistical analysis

Statistical analyses were performed with R 2.10.1 (R foundation for statistical computing) and Prism 3.02 (GraphPad, La Jolla, CA, USA). Bars in figures indicate minima and maxima, boxes the 25 and 75% percentile with the median value. Statistical analyses of two groups were performed using two-tailed Mann Whitney U-test or Wilcoxon matched pairs test and 95% confidence intervals.

Correlation tests between parameters were performed by linear regression and estimation of the goodness of the fit from the coefficient of determination R^2 . The latter is a global effectiveness measure for the fit. To test the coefficient of determination R^2 statistically, it is tested against the $R^2=0$ hypothesis which would indicate that there is no correlation between parameters. If R^2 is significantly different from 0 then the parameters are assumed to correlate.

2.2.6 Expression and localization of PPM1E in human, rat and mouse brain

2.2.6.1 Cryosections, fixation and immunofluorescence of human and rat brain samples

Human, age-matched brain samples from healthy and Alzheimer's disease (AD)-affected donors were obtained deep-frozen from the Netherlands Brain Bank (NBB). Total rat brains were dissected from adult female Wistar rats. The rats were anaesthetized with CO_2 (up to 80 %, 10 min) and then decapitated.

Approximately 50 mg samples, separated from the deep-frozen human cortical brain specimen, or total deep-frozen adult rat brain hemispheres were embedded in O.C.T. Tissue-Tek^R compound medium (Sakura Finetek, The Netherlands) on dry ice. 14 μm cryosections were taken at 17 °C with a cryo-microtome (Leica CM3050 S) and mounted sequentially on glass slides (Superfrost Plus, Thermo Scientific, #J1800AMNZ) and stored in -80 °C.

For immunolabeling glass slides were dried 30 min at room temperature, washed three times in PB buffer and blocked 30 min in humid atmosphere in 10 % normal goat serum and 0.2 % Triton X-100 in PB buffer. Primary antibody was incubated over night at 4 °C. Then the glass slides were washed three times in 0.1 % Triton X-100 in PB, blocked in 3 % BSA / PB for 30 min and incubated with the secondary antibody 1:600 in 1 % BSA / PB for 2 h. Glass slides were washed in PB buffer twice before staining of neutral triglycerides and lipids with 1 % sudan black (Roth, #0292.1) in 70 % ethanol for 2.5 min and embedding in Fluoromount G (Southern Biotech).

2.2.6.2 Lysis of human and rat brain samples, SDS-PAGE and Immunoblot quantification

Approximately 50 mg human and rat brain samples were obtained as described above (2.2.6.1 *Cryosections, fixation and immunofluorescence of human and rat brain samples*), transferred to 4 °C ready-made RIPA lysis buffer (Sigma, #R0278), containing protease inhibitor Complete (Roche), and homogenized with 10 blows in a 7 ml all glass dounce tissue grinder (Kimble Chase). After 30 minutes incubation on ice, the protein lysate was separated from cell debris by centrifugation at 16 000 g. Measurement of protein concentration and subsequent SDS-PAGE and western blotting were carried out as described in 2.2.1.6 *Quantitative and qualitative immunoblotting*.

3 RESULTS

3.1 Characterization of tools for this study

This section will introduce tools which were essential for this study, and therefore needed careful characterization because they had not been discussed extensively in the literature before. Among them is the selection of primary sequences for rat and human PPM1E, the analysis of the specificity of anti-PPM1E antibodies, which were characterized during the course of this study, and the difficulties in the selection of suitable cell lines for investigation of PPM1E effects. The last paragraph will introduce the human brain samples, which are investigated in this study and which were analysed previously regarding their PPM1E mRNA levels (von der Kammer, 2009). Potential correlations between PPM1E mRNA levels in human brain samples and post-mortem delay time⁷ and other parameters will be critically reassessed.

3.1.1 Polymorphisms in the PPM1E sequence

Expression of the human PPM1E protein has been induced for different purposes in different cell lines and in primary neuronal culture during the course of this study. A critical first step was to determine the 'correct' PPM1E sequence from online database searches.

BlastP searches for human DNA sequences homologous to the PPM1E sequence, as derived from previous publications (Takeuchi et al., 2004; Koh et al., 2002; Takeuchi et al., 2001), revealed three slightly different PPM1E variants: *homo sapiens mRNA for KIAA1072 protein* (AB028995⁸, 759 amino acids (aa)), *homo sapiens PP2CH mRNA* (AF260269⁹, 766 aa) and *homo sapiens protein phosphatase 1E (PP2C domain containing) (PPM1E)* (NM_014906¹⁰, 755 aa) (Appendix A 2). The sequences of the encoded proteins differed in the number of glutamate-proline repeats within the amino-terminal part of the protein (11 in sequences AB028995 and AF260269, 10 in sequence NM_014906), in a 9 aa insertion (PLSERITPR) encoded only by the sequence AF260269, and in a valine at position 385 (NM_014906) / 389 (AB028995), which is replaced by an isoleucine (position 396) in AF260269. The sequence NM_014906 was used for all experiments discussed in this study. It was the most

⁷ post-mortem delay time (PMT): time between death of the donor and deep-freezing of the brain

⁸ NCBI (National Center for Biotechnology Information) GenBank accession number

⁹ NCBI GenBank accession number

¹⁰ NCBI GenBank accession number

commonly sequenced transcript, as judged from the number of expressed sequence tags (ESTs) in the NCBI database, and it was used in prior studies of PPM1E (Takeuchi et al., 2004; Koh et al., 2002; Takeuchi et al., 2001) (KIAA1072 of the Kazusa cDNA library = NM_014906).

The sequence of the PPM1E homolog in *Rattus norvegicus* was required in this study for the design and functional testing of short hairpin (sh) RNA constructs which were used to down-regulate rat PPM1E expression in rat primary neuronal cell culture. 'Rattus norvegicus protein phosphatase 1E (PP2C domain containing)' (Ppm1e; NM_198773¹¹, 750 aa), was amplified from mRNA isolated from the rat primary neuronal culture used in this study with terminally binding PCR primers. Others have characterized the PPM1E sequence 'Rattus norvegicus mRNA for calmodulin-dependent protein kinase phosphatase N' (AB081729¹², 750 aa) which is 100% identical to NM_198773 (Kitani et al., 2006).

3.1.2 Specificity of polyclonal anti-PPM1E antibodies

Since no commercial anti-PPM1E antibodies were available, polyclonal PPM1E antibodies were generated and purified by a service provider on behalf of this study. The polyclonal anti-PPM1E antibodies were generated by immunization of rabbits with synthetic peptides corresponding to the PPM1E sequence (Appendix A 3). Four peptides were used for immunization of two rabbits each. The purified polyclonal antibodies were characterized for immunoblotting and immunolabeling of formaldehyde fixed tissue and cell cultures in this study. The immunization with peptides I (AGC) and IV (ENS) resulted in the most specific polyclonal antibodies for these applications respectively. These specific anti-PPM1E antibodies are referred to as anti-PPM1E(AGC) and anti-PPM1E(ENS) according to the first three amino acids in the respective immunization peptide. Their sequences are conserved in human and rat PPM1E (Appendix A 3).

3.1.2.1 Anti-PPM1E(AGC) detects rat and human PPM1E specifically in immunoblotting

The specificity and suitable concentrations of all antibodies were initially tested in antibody dilution series on immunoblotted human cortical brain sample homogenates (data not shown). In this study concentrations of 0.2 to 0.8 µg / ml anti-PPM1E(AGC)

¹¹ NCBI GenBank accession number

¹² NCBI GenBank accession number

antibody were used for PPM1E detection in qualitative and quantitative immunoblotting respectively.

The antibodies were then tested for immunoblotting applications on day-*in-vitro* (DIV) 21 rat primary neuronal cell lysates from wildtype cultures and cultures in which Myc_PPM1E expression was induced by infection with recombinant adeno-associated viruses (rAAV) on DIV 7 (Figure 3.1). The antibody anti-PPM1E(AGC) revealed two specific bands at apparent masses around 120 and 80 kDa in Myc_PPM1E overexpressing cultures. The 120 kDa band is very weak and therefore only visible after longer exposure times of the light-sensitive film to the ECL-detected immunoblot (Figure 3.1: “1 min exposure”). The antibody specificity was controlled with an anti-Myc_tag antibody, which detected proteins with the same apparent molecular weights as anti-PPM1E(AGC) (Figure 3.1: “Myc”).

Kitani et al. (2006) predicted the truncation site of rat PPM1E to be located at proline 554. This site is homologous to proline 557 in the human PPM1E isoform (Appendix A 3, arrowhead). Rat PPM1E and PPM1E(1-554) run at 120 and 80 kDa in SDS-PAGE. These correspond to actual masses of 87.7 and 65.3 kDa respectively as demonstrated by mass

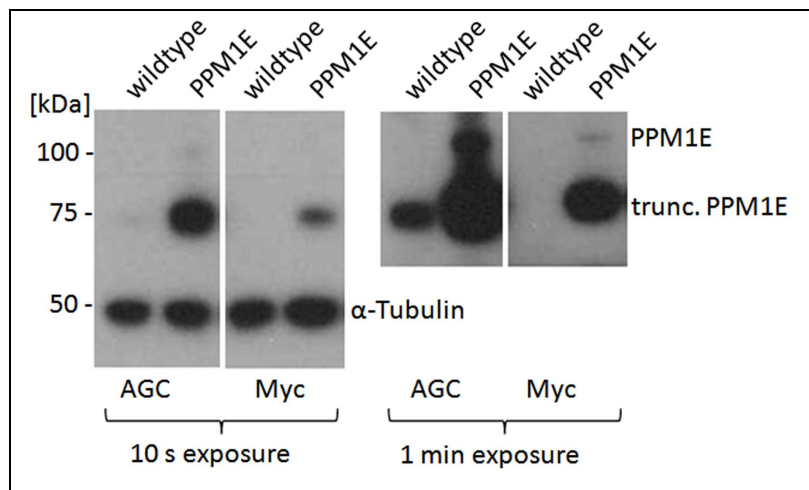


Figure 3.1: Specific detection of Myc_PPM1E with anti-PPM1E(AGC) (“AGC”) and anti-Myc-tag (“Myc”) antibodies. Wildtype and rAAV / Myc_PPM1E-infected dissociated primary rat hippocampal culture. Infection on DIV 7, analysis on DIV 21. Detection with anti-PPM1E(AGC) or anti-Myc-tag and anti- α -Tubulin antibody; 10 s (left) and 1 min (right) exposure of light-sensitive film to the same ECL-detected blot. trunc. PPM1E: truncated PPM1E (human PPM1E(1-557) or rat PPM1E(1-554)).

spectrometric analysis (Kitani et al., 2006). The authors did not speculate on a possible explanation for this unusual running behaviour in SDS-PAGE.

Human PPM1E and PPM1E(1-557) have predicted molecular weights of 84.0 and 61.4 kDa, but run also at apparent molecular weights of approximately 120 and 80 kDa (Figure 3.1) (Kitani et al., 2006; Takeuchi et al., 2001). In the wildtype primary hippocampal culture truncated PPM1E(1-554) is the predominant PPM1E species (Figure 3.1). However, extended anti-PPM1E(AGC) antibody detection revealed full-length as well as PPM1E(1-554) expression in these cultures (compare Figure 3.11).

3.1.2.2 Anti-PPM1E(ENS) detects PPM1E specifically in formaldehyde fixed specimen

Additionally the specificity proper concentration of polyclonal anti-PPM1E antibodies was tested in immunolabeling of formaldehyde (FA)-fixed, dissociated primary hippocampal culture and brain tissues (Figures 3.2 and 3.3 for anti-PPM1E(ENS); not shown for other polyclonal antibodies).

PPM1E detection with anti-PPM1E(ENS) in dissociated primary hippocampal culture

Primary hippocampal cell cultures were transfected on day-*in-vitro* (DIV) 7 with EGFP and Myc_PPM1E and analyzed on DIV 21 (Figure 3.2). The antibody anti-PPM1E(ENS) (4 μ g/ml) revealed a characteristic fragmented staining pattern in the dendrites of primary neurons which were transfected with Myc_PPM1E or untransfected (Figure 3.2 A). The fragmented detection was comparable with that of an anti-Myc_tag antibody of the same hippocampal culture batch (Figure 3.2 B).

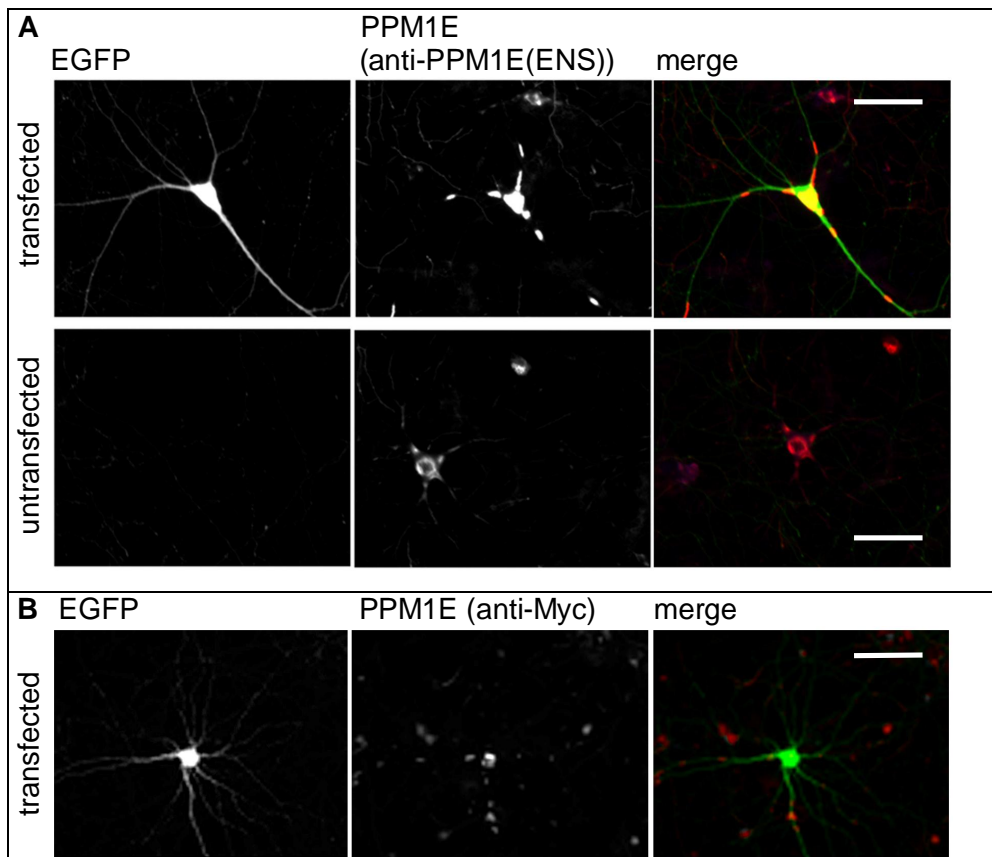


Figure 3.2: Myc_PPM1E expression in EGFP- and Myc-PPM1E-co-expressing and untransfected primary hippocampal neurons. Transfection on DIV 7, analysis on DIV 21. EGFP autofluorescence (left) and (A) anti-PPM1E(ENS) or (B) anti-Myc-tag stain; and merge of both: EGFP green, anti-Myc-tag or anti-PPM1E(ENS) red. Scale

bar: 50 μm .

Moreover, in young DIV 3 hippocampal neurons the primarily dendritic and somatic, non-nuclear staining pattern is comparable with one that has been shown previously by Kitani et al. (2006) (Figure 3.17 A).

The above described fragmented expression pattern of PPM1E was present in some but not all investigated cultures (compare Figures 3.2 and 3.17). The trigger for this fragmentation could not be identified in this study and occurred from time to time, depending on the culture batch, although due caution was taken to standardize the culture, fixation and immunolabeling procedures.

PPM1E detection with anti-PPM1E(ENS) in human cortical brain samples

In human frontal cortex tissue the antibody anti-PPM1E(ENS) detected PPM1E expression in neuronal nucleus and enriched in cytoplasm as indicated by NeuN co-labeling (Figure 3.3 A). A cytoplasmic enrichment of PPM1E has been shown before (Kitani et al., 2006).

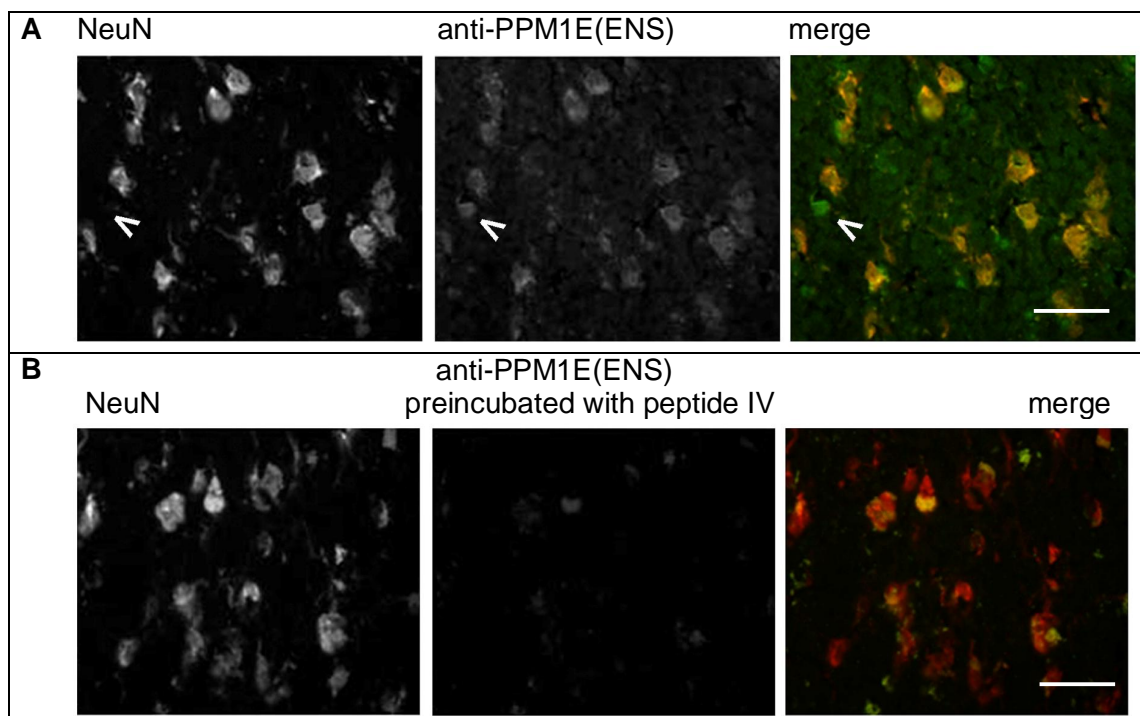


Figure 3.3: Specificity of PPM1E(ENS) antibody in detection of endogenous PPM1E expression in human frontal cortex. Detection with anti-NeuN (left) and anti-PPM1E(ENS) (middle) antibodies. Merge of NeuN (red) and anti-PPM1E(ENS) (green) detection (right). (A) Arrowhead indicates an example of a PPM1E(ENS)-positive, but NeuN-negative cell. (B) Preincubation with the corresponding immunization peptide blocks the anti-PPM1E(ENS) binding to the specimen. Scale bars: 50 μm

The anti-NeuN antibody specifically recognizes the DNA-binding, neuron-specific protein NeuN, which is present in the nucleus and cytoplasm. Occasionally cells can be found which are anti-PPM1E(ENS), but not anti-NeuN positive (Figure 3.3 A, arrowhead). Some neurons fail to be recognized by anti-NeuN: retinal cells, Cajal-Retzius cells, Purkinje cells, inferior olivary and dentate nucleus neurons, and sympathetic ganglion cells (Wolf et al., 1996; Mullen et al., 1992). Additionally anti-PPM1E(ENS) detected a diffuse stain which is visible as globular structures in higher magnification in between neuronal cell bodies¹³ (Figure 3.3 A). This diffuse stain and the soma detection of PPM1E could be blocked with the corresponding peptide ENSFQGGQEDGGDDKENHGEEK (Figure 3.3 B).

3.1.3 Endogenous and ectopic expression of PPM1E in different cell lines

Cell lines which express rat or human PPM1E would be a valuable tool to test the down-regulation of PPM1E by RNA interference and to evaluate PPM1E effects in a simple model system. Therefore a number of cell lines were tested for endogenous, immunoblot-detectable expression of PPM1E (Figure 3.4).

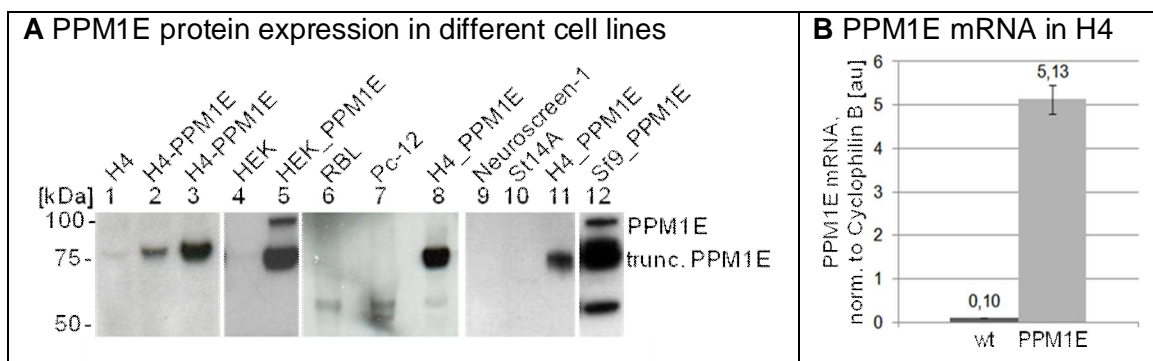


Figure 3.4: Endogenous and ectopic expression of PPM1E in different cell lines. (A) PPM1E is expressed in 1. wildtype H4, and after transfection (2, 5) or transduction (3, 8, 11, 12) with Myc_PPM1E (2, 3, 5, 8, 11) or His_PPM1E (12) constructs in H4, HEK and Sf9 cell lines in different PPM1E to PPM1E(1-557) ratios. In other cell lines with human or rat origin no PPM1E expression could be detected (4: HEK 293 GP; 6: RBL; 7: PC12; 9: NeuroscreenTM-1; 10: ST14A). 15 µg total protein per lane; immunoblot detection with anti-PPM1E(AGC). trunc. PPM1E: truncated PPM1E (PPM1E(1-557)). (B) PPM1E mRNA levels in H4 (wt) and H4_Myc_PPM1E (PPM1E) cell lines, normalized to Cyclophilin B levels. qRT-PCR analysis. au: arbitrary units; wt: wildtype.

However most analyzed cell lines did not express PPM1E in immunoblot-detectable amounts: Neither non-neuronal cell lines of human origin, namely human embryonic

¹³ for further investigation see paragraph 3.2.2.5 Co-localization of PPM1E with EAAC1 but not GAD67 in human cortical neurons

kidney cells (HEK 293 GP), nor cell lines of rat origin with neuron-like morphology like PC12 and NeuroscreenTM-1, or without neuron-like morphology like lymphoblast- (RBL-1) and fibroblast-resembling (ST14A) cells (Figure 3.4 A). The *Spodoptera frugiperda*-derived cell line Sf9 also did not – and was not expected to – express PPM1E.

A low endogenous PPM1E expression was however found in the human neuroglioma cell line H4 (Figure 3.4 A (1)). Quantitative real-time (qRT) PCR of H4 cells confirmed low levels of PPM1E mRNA (Figure 3.4 B). A H4 cell line, stably expressing Myc_PPM1E was established (H4_Myc_PPM1E), which revealed a fifty times increase in PPM1E expression (Figure 3.4 A (1, 3), B).

Ectopic expression of human PPM1E in H4, HEK or Sf9 cells by transfection or transduction resulted in expression of PPM1E in different ratios of truncated and full-length form (Figure 3.4 A (2, 3, 5, 8, 11, 12)). Obviously the mechanism of PPM1E truncation is neither restricted to neuronal, nor to mammalian cells. In H4 cells only PPM1E(1-557) is detected (Figure 3.4 A (1-3, 8, 11)), whereas in transiently Myc_PPM1E expressing HEK and Sf9 cells both forms, PPM1E and PPM1E(1-557), are present (Figure 3.4 A (5,12)). The truncated PPM1E(1-557) is in all analyzed samples the predominant PPM1E species.

In Sf9 cells in which expression of PPM1E is induced by a baculovirus which encodes human PPM1E, a third, shortened form appears, which has a molecular weight of approximately 60 kDa (Figure 3.4 A (12)). This has been observed before in attempts to express PPM1E in Sf9 cells (Takeuchi et al., 2001).

No rat cell line with a sufficiently high endogenous PPM1E expression to test shRNA constructs was identified, therefore transient overexpression of PPM1E in HEK cells was used for this purpose as described below¹⁴.

3.1.4 Characterization of human brain samples

Human frontal and temporal cortex samples in different Braak stages were obtained from the Netherlands Brain Bank (NBB; Amsterdam, The Netherlands). The mRNA and protein quality of the brain samples was controlled previously (von der Kammer, 2009) and the donors are age-matched between 63 and 91 years. PPM1E mRNA levels

¹⁴ compare 3.3.5 *Down-regulation of PPM1E with RNA interference affects spines and dendritic arborization*, page 125

were determined by means of quantitative real-time PCR (qRT-PCR) for frontal and temporal cortex before (von der Kammer, 2009) (Figure 1.3 A-a and Table 3.1).

NBB ID	PMT [min]	Brain mass	pH CSF	sex	age	Braak stage	Diagnosis	PPM1E mRNA in frontal / temporal cortex ¹	PPM1E protein in frontal cortex IB ²	PPM1E protein in frontal cortex IHC ³
93-105	420	1405	6.75	m	80	0	NDC	9.50 / 11.18	0.65	yes
93-110	525	1346	6.11	m	73	0	NDC	12.03 / 6.87	0.61	yes
00-090	465	1560	6.46	m	70	0	NDC	10.40 / 11.41		
01-004	515	1169	6.4	f	64	0	NDC	1.76 / 2.97	0.58	yes
00-067	45	1267	--	m	73	0	NDC	12.46 / 9.46	0.86	yes
94-124	330	967	6.60	m	63	1	CVE	28.47 / 24.11		
00-032	390	1047	7.02	f	78	1	NDC	26.23 / 19.43		
01-005	1185	1149	6.21	f	77	1	NDC	46.47 / 27.75	0.97	yes
01-006	345	1088	6.49	f	91	1	NDC	7.33 / 11.03	0.98	
01-016	505	1138	7.19	m	77	1	NDC	10.41 / 6.44	0.83	
00-137	435	1031	7.00	f	92	1	NDC	3.77 / 4.15		
00-142	330	1280	6.6	f	82	1	NDC	9.26 / 10.99	1.07	
96-044	350	1101	7.00	f	90	2	NDC	64.68 / 48.12	1.37	yes
00-030	426	1468	6.66	m	82	2	NDC	28.39 / 21.79	0.86	
01-094	330	1220	6.76	m	86	2	NDC	42.59 / 19.81		
01-139	815	1249	6.3	f	73	2	NDC	29.88 / 18.87	0.97	
96-075	345	1449	7.31	m	76	2	Dsicc	18.09 / 26.24		
96-051	290	1256	6.65	f	71	3	NDC	43.73 / 15.48	0.96	yes
00-070	285	1150	6.54	m	80	3	Dsicc	20.80 / 24.05	0.82	
01-030	540	1199	6.54	f	85	3	Dsicc	17.63 / 25.29	0.76	
03-006	320	1106	6.51	f	91	3	NDC	17.09 / 39.54	0.98	
92-088	415	1378	6.55	m	83	4	AD	14.06 / 19.04	0.89	yes
01-039	300	1213	6.49	m	88	4	AD	12.80 / 38.41	0.81	
00-104	360	1377	6.38	m	86	4	AD	4.73 / 8.42	0.97	

Table 3.1: Human brain samples, which were classified as Braak 0 to 4, and analyzed for PPM1E mRNA levels previously (von der Kammer, 2008). ¹ PPM1E mRNA normalized against cyclophilin B mRNA, determined by qRT-PCR [arbitrary units] (von der Kammer, 2009). ² PPM1E(1-557) protein levels normalized against α -Tubulin (for details see section 3.2.1, page 88 ff). ³ for details see section 3.22, page 94ff. NBB: Netherlands Brain Bank. PMT: post-mortem delay time between death of donor and freezing of brain. NDC: non-demented control. CVE: control with vascular encephalopathy. Dsicc: dementia with senile involutive cortical changes. IB: PPM1E protein expression analyzed by immunoblotting of human frontal cortical brain samples in the present study. IHC: PPM1E protein expression analyzed by immunolabeling of FA-fixed human cortical brain samples.

To test against possible process-inherent effects on the degradation-sensitive mRNA, a possible correlation between post-mortem delay time (PMT) - the period between death of the brain donor and the deep-freezing of the brain - and mRNA levels of PPM1E was assessed. No significant correlation between either frontal or temporal mRNA expression and the PMT was found (Figure 3.5 A). Tested against the $R^2=0$ hypothesis (no correlation), the probability for a correlation with the post-mortem time is $p=0.95$ and $p=0.38$ for temporal and frontal PPM1E expression respectively, hence no significant correlation was found (95 % confidence interval).

Moreover, no correlation was found between other potentially relevant parameters for mRNA stability, which were documented for the brain samples (Table 3.1), and either frontal or temporal PPM1E mRNA levels, neither for age of the donor, nor for pH in cerebrospinal fluid (CSF), nor for the brain mass (Figure 3.5 B-D).

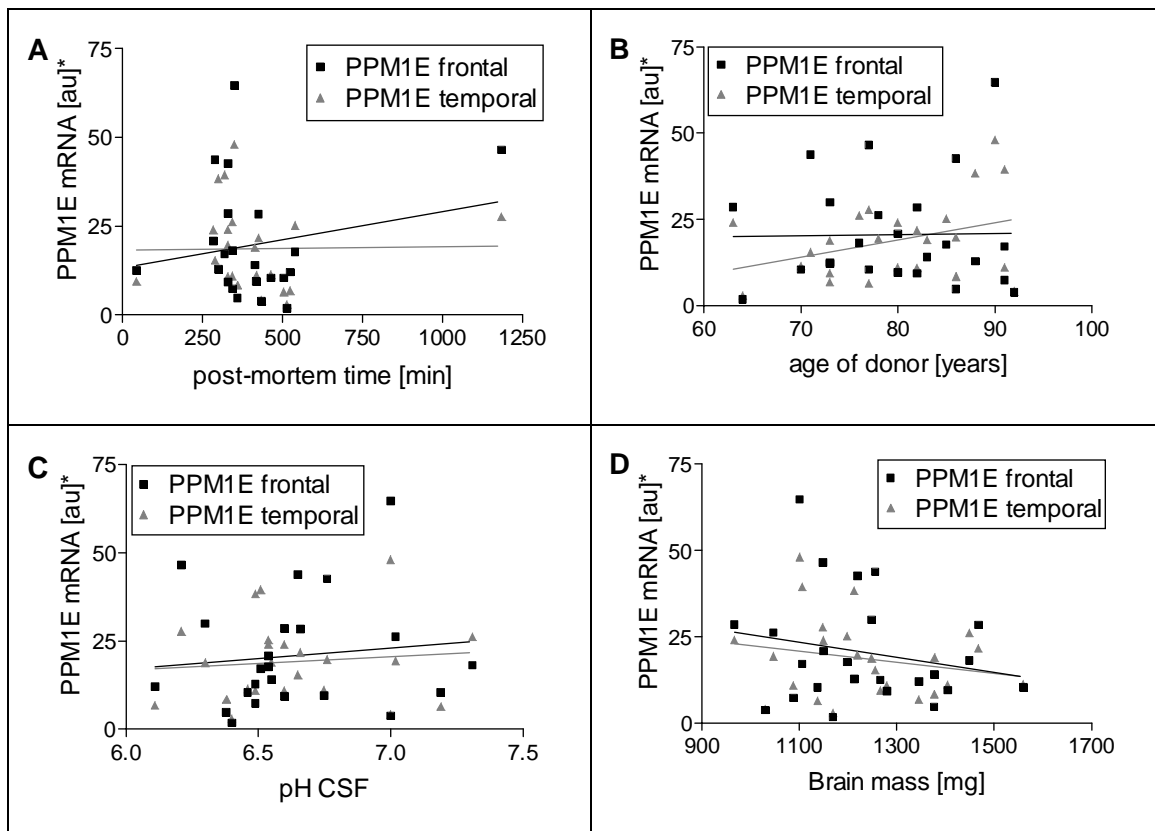


Figure 3.5: Linear regression between PPM1E mRNA levels and relevant properties of the analyzed human brain samples depicted in Table 3.1. Correlation with (A) post-mortem delay time; (B) age of donor; (C) pH in cerebrospinal fluid and (D) brain mass. Linear regression analysis for frontal and temporal cortex respectively: $R^2 = 0.0394 / 0.0002$ (PMT); $0.0003 / 0.1370$ (age of donor); $0.0126 / 0.0100$ (pH CSF); $0.0445 / 0.0446$ (brain mass). All parameter pairs were tested against $R^2 = 0$, and were not significantly correlated. au: arbitrary units. *PPM1E mRNA normalized to cyclophilin B mRNA levels.

The brain samples were therefore, and due to previous histological and biochemical analysis (von der Kammer, 2009), regarded as sufficiently well preserved in respect to protein and mRNA quality. The microscopic integrity of the tissues was good as determined previously during Braak staging analysis by the NBB.

3.2 Characteristic truncation and localization of the PPM1E phosphatase

3.2.1 PPM1E truncation and expression levels

The human PPM1E protein exists in a full-length form with a length of 755 aa and a form which is truncated after proline 557 (PPM1E(1-557)). This truncation site was proposed on the basis of mass spectrometric data for the rat PPM1E isoform, which indicated that the phosphatase is truncated carboxyterminally from the homologous proline at position 554 in rat PPM1E(554). No regulatory or mechanistic insights into the mechanism of truncation exist yet. Therefore the expression of PPM1E and PPM1E(1-557) in different tissues was investigated further.

3.2.1.1 PPM1E expression in H4 neuroglioma cells

Kitani et al. (2006) predicted the truncation site of rat PPM1E to be located at proline 554. Therefore this study tested whether the homologous truncated protein PPM1E(557) would exhibit a comparable running behaviour than truncated full length PPM1E in ectopically expressing cells.

Human neuroglioma H4 cell lines stably expressing the full-length Myc_PPM1E or the truncated Myc_PPM1E(1-557) were established. In accordance with predictions from Kitani et al. (2006) for the rat PPM1E (CaMKP-N) homolog, one specific PPM1E band at an apparent mass of approximately 80 kDa was detected in either cellular lysate (Figure 3.6).

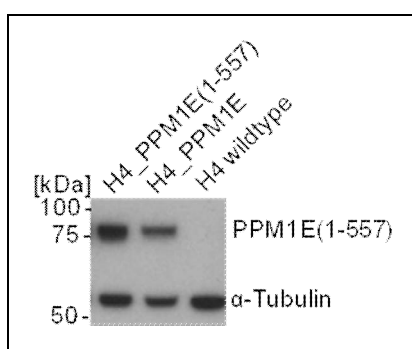


Figure 3.6: Ectopic PPM1E(1-557) and PPM1E expression in H4 cells results in PPM1E bands with similar molecular weights. 15 µg total protein per lane; immunoblot detection with anti-PPM1E(AGC) and anti- α -Tubulin antibodies.

The endogenous PPM1E expression in H4 cells is very low. However the molecular weight of the endogenous PPM1E is also comparable to that of the induced Myc_PPM1E(1-557) expression (compare Figure 3.4 A (1) and Figure 3.6).

3.2.1.2 PPM1E expression in human frontal cortex

To investigate whether PPM1E protein levels are also differentially regulated in early Braak stages, like the mRNA levels, samples from a subset of previously analyzed donors were subjected to quantitative immunoblot analyses of the PPM1E protein levels.

The analysis of PPM1E protein expression in this study was focused on brain samples which are classified as Braak 0 to 4. In these the PPM1E mRNA levels were differentially regulated and therefore they were regarded as most relevant to the cause of the present study. Human brain samples which represent very late Alzheimer stages (Braak 5 and 6, compare Figure 1.3) were not analysed. This study quantitatively evaluated the protein levels of PPM1E in frontal cortex from 18 donors.

In human frontal cortex protein extracts from 18 donors, the full-length as well as PPM1E(1-557) were detected and analyzed. PPM1E(1-557) was shown to be the predominant PPM1E species in all analyzed samples, except sample 01-005, although the ratio between truncated and full-length PPM1E was subject to considerable changes between the donors (Figure 3.7).

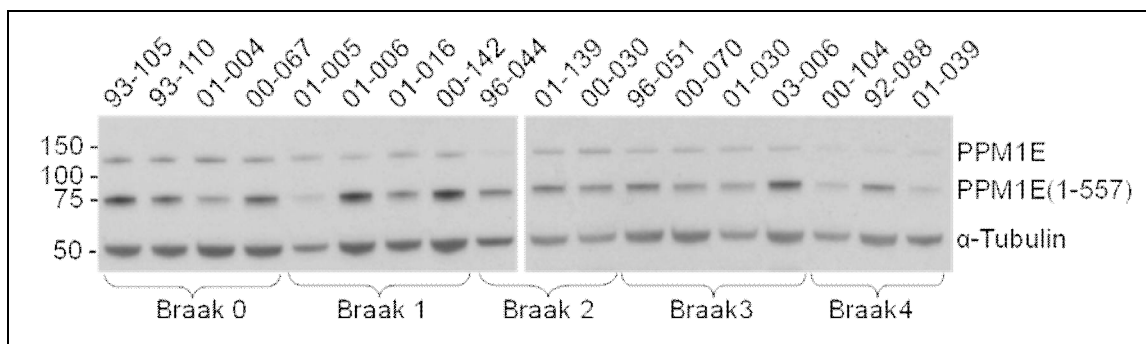


Figure 3.7: PPM1E levels in frontal human cortex samples classified into Braak stages 0 to 4. Qualitative Western blot detection with anti-PPM1E(AGC) and anti- α -Tubulin. 15 μ g protein of frontal cortex per lane. The samples are labeled with the donor ID from the NBB (see Table 3.1 for donor characterization).

The exact PPM1E protein levels were determined with quantitative immunoblots to investigate whether early changes of PPM1E mRNA levels are reflected in the protein concentration. All investigated samples were derived from human frontal cortex. However, due to the limited availability of brain samples not all samples could be matched with respect to the region in frontal cortex.

The overall expression of PPM1E and PPM1E(1-557) was determined from five-step dilution series of frontal cortex protein extracts of each of 18 donor samples (Figure 3.8 A, example blots). Values in the dynamic range of antibody binding and detection for PPM1E(1-557) were averaged for each sample and normalized to equally derived levels of the “housekeeping” protein α -Tubulin¹⁵ (Figure 3.8 B). α -Tubulin is a component of microtubules and due to the high abundance of microtubules in eukaryotic cells it is a suitable protein for normalization.

Approximate values were similarly derived for full-length PPM1E, however the signal was too low in several samples to achieve detection in the dynamic range (Figure 3.7 and 3.8 C). Therefore no conclusive statement on the levels of full-length PPM1E during the development of Alzheimer’s disease can be made here. However it can be said, that the expression of full-length PPM1E does not appear to follow the same regulatory pattern through the Braak stages as PPM1E(1-557) levels (Figure 3.7).

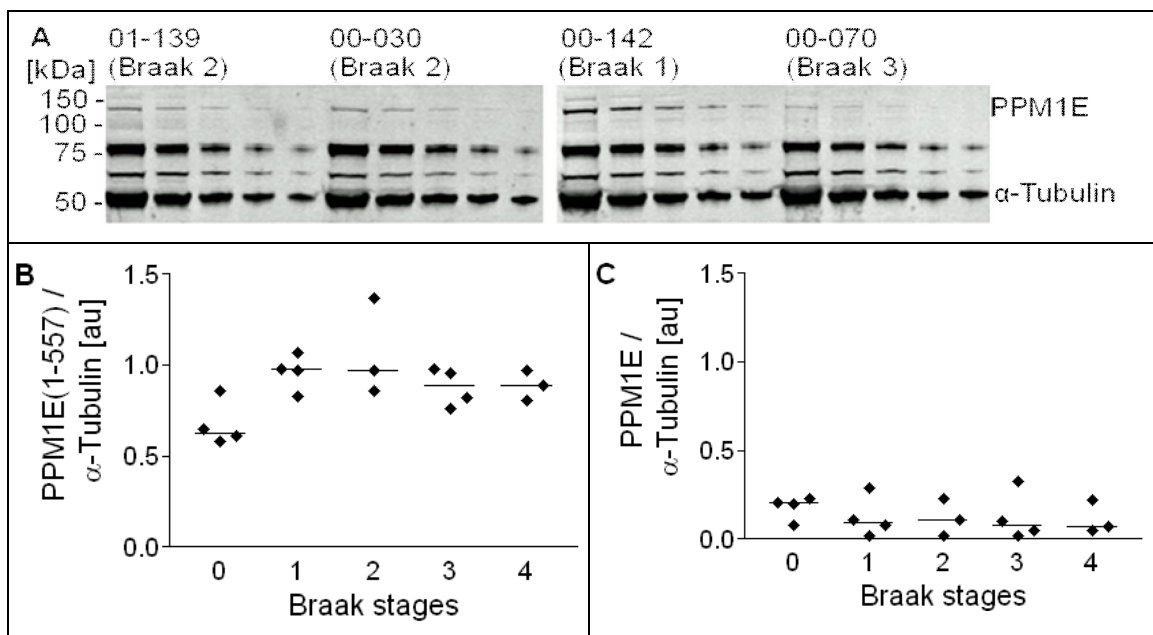


Figure 3.8: PPM1E protein levels in human frontal cortical brain samples. (A) Example blots with 1:2, 5-step, dilution series of brain samples; 15 μ g protein per lane in highest dilution. Detection with anti-PPM1E(AGC) and anti- α -Tubulin antibodies. (B) Mean values from the dynamic values of quantitative dilution series PPM1E(1-557), normalized to α -Tubulin, and (C) values for full-length PPM1E from the highest protein concentration in the dilution series (15 μ g protein), normalized against α -Tubulin. Horizontal lines represent the median for each Braak stage cohort.

¹⁵ For a more detailed description of the quantification procedure see 3.3.3.3 *Immunoblot quantification of protein levels*, page 111, and 2.2.1.6 *Quantitative and qualitative immunoblotting*, page 61.

The PPM1E(1-557) levels in Braak 1 and 2 are considerably higher than those in Braak 0 samples (Figure 3.8 B). These differences in PPM1E(1-557) levels are statistically not significant, potentially due to the low number of samples. However, the changes in levels of PPM1E(1-557) obviously reflect the changes in concentration of PPM1E mRNA through the investigated Braak stages 0 to 4 (Figure 3.9, compare also Figures 1.3 A-a and 3.8 B). The PPM1E(1-557) protein levels correlate linearly significantly ($p=0.045$) with the PPM1E mRNA levels in frontal cortex.

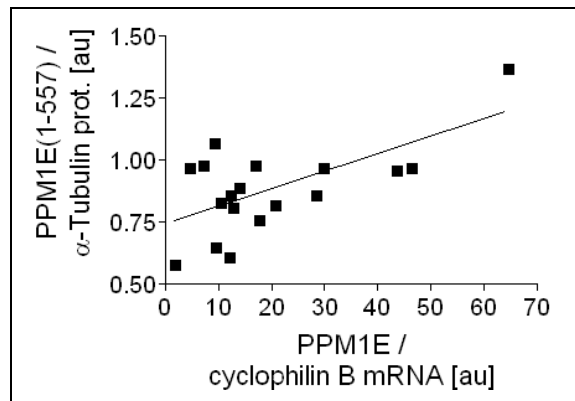


Figure 3.9: Linear correlation between PPM1E mRNA levels, normalized against cyclophilin B, and PPM1E(1-557) protein levels, normalized against α -Tubulin. $p=0.045$, linear regression.

3.2.1.3 PPM1E expression in rat brain

The model system for neuronal morphogenesis in this study was dissociated rat hippocampal culture. Therefore the PPM1E expression in adult rat was also investigated to verify that the expression with respect to truncation and localization was comparable with the expression of PPM1E in human brain tissue. The PPM1E expression in embryonal day 17 (E17) rat and younger embryonal stages was analyzed as an additional reference for the dissociated culture which is prepared from 17-days-old embryos. Additionally embryonal day 9 and 13 were analyzed because initial synapse development during rat embryogenesis happens around E10 (Li and Sheng, 2003).

The PPM1E expression in adult and embryonal rat brain tissue was investigated in tissue homogenates from the brain regions frontal cortex, cerebellum, hippocampus and olfactory bulb for adult rats and embryonal day 17 (E17) (Figure 3.10 A). Due to their small size the E9 and E13 embryos were analyzed as whole embryos. Head and limbs of E13 embryos were additionally analyzed separately.

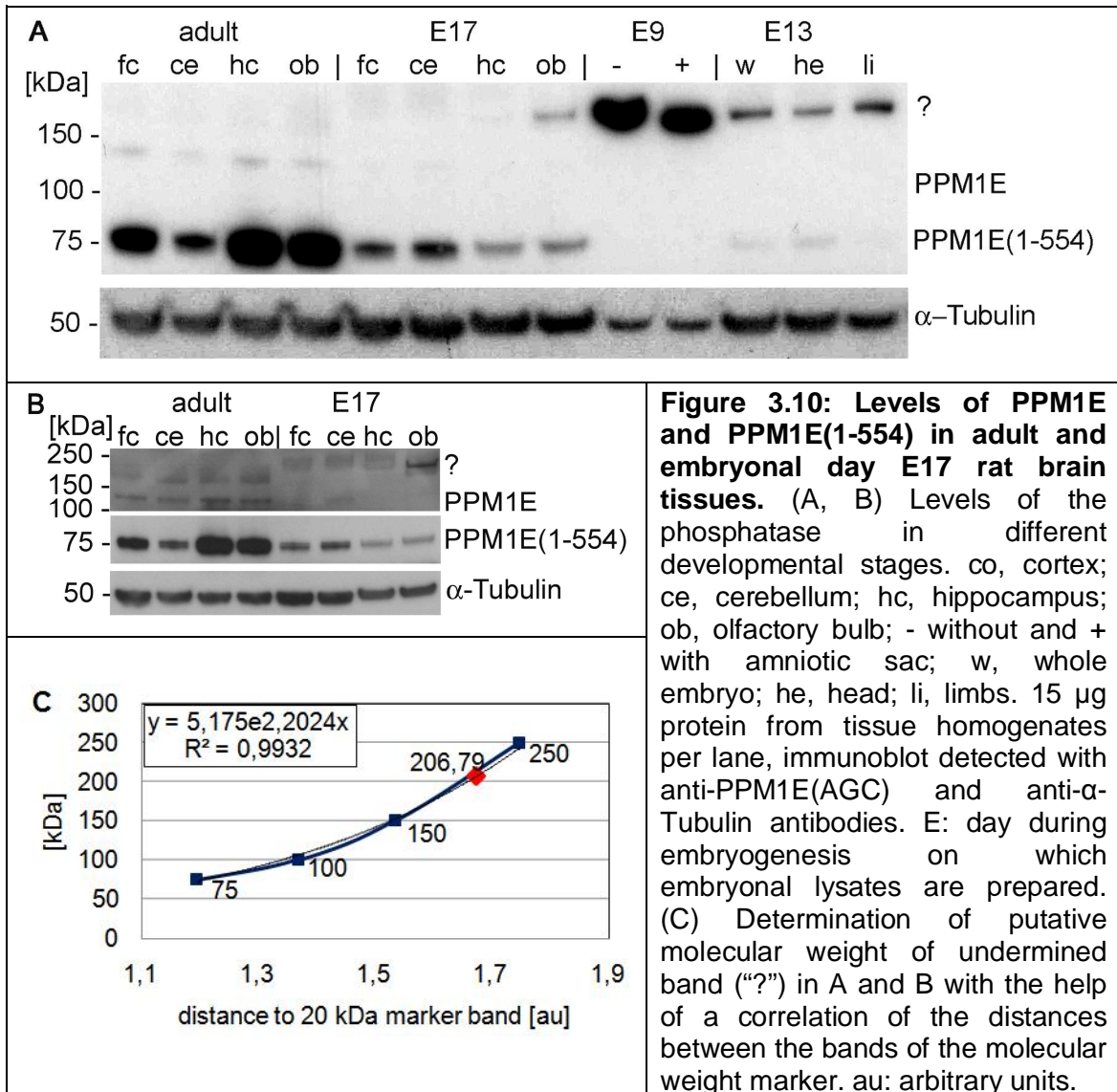


Figure 3.10: Levels of PPM1E and PPM1E(1-554) in adult and embryonal day E17 rat brain tissues. (A, B) Levels of the phosphatase in different developmental stages. co, cortex; ce, cerebellum; hc, hippocampus; ob, olfactory bulb; - without and + with amniotic sac; w, whole embryo; he, head; li, limbs. 15 μ g protein from tissue homogenates per lane, immunoblot detected with anti-PPM1E(AGC) and anti- α -Tubulin antibodies. E: day during embryogenesis on which embryonal lysates are prepared. (C) Determination of putative molecular weight of undermined band (“?”) in A and B with the help of a correlation of the distances between the bands of the molecular weight marker. au: arbitrary units.

The ratio between full-length and the predominant truncated form of PPM1E was comparable with that in *Homo sapiens* cortical samples (Figure 3.10 A: adult, e.g. “fc”: frontal cortex). The levels of expression differed considerably between the analyzed brain areas and ages: The PPM1E(1-554) expression was considerably lower in all four analyzed brain areas in E17 embryos than in adult rat, and full length PPM1E was only detectable in adult rat homogenates (Figure 3.10 A), potentially due to lower PPM1E expression levels. The expression of PPM1E(1-554) is especially high in hippocampus and olfactory bulb in the adult rat, whereas in E17 embryos the PPM1E expression is higher in the frontal cortex and the cerebellum. In E9 complete embryo homogenates no PPM1E or PPM1E(1-554) signal can be detected, whereas a low concentration of PPM1E(1-554) was present in E13 whole embryo and embryonal head homogenates (Figure 3.10 A). It cannot be excluded that PPM1E expression is present, but too diluted, because the E9 embryos measured only approximately 50 mm in diameter and

were therefore analyzed in whole. Also the E13 “head” sample is diluted by other constituent parts of the head other than the evolving brain.

A previously unknown signal with a mass of approximately 200 kDa appears very strongly in all E9 and weaker in the E13 samples and is also present in E17 olfactory bulb (Figure 3.10 A – “?”). To verify that the signal in E17 olfactory bulb is no technical artifact the immunoblot was repeated without adjacent E9 homogenates (Figure 3.10 B). The new anti-PPM1E(ENS) detected signal had a size of approximately 206.79 kDa as determined in relation to the marker bands by measuring the relative distance to the 20 kDa band of the same marker (Figure 3.10 C). However, a 207 kDa protein or protein complex has not been described in the literature in conjunction with PPM1E and this study could not identify whether this signal a specific detection of a PPM1E complex.

Finally it can be stated that the PPM1E expression rises considerably between the embryonal stages and the adult rat.

3.2.1.4 PPM1E expression in rat primary hippocampal culture

The development of PPM1E expression during the maturation of rat primary hippocampal culture which was prepared from E17 rat embryonal hippocampi was also analyzed in immunoblots. The endogenous PPM1E expression rises considerably with increasing culture age (Figure 3.11). No expression of PPM1E(1-554) is detected on day-*in-vitro* (DIV) 1, and

after that the expression rises and remains relatively constant between DIV 8 and 20.

Subsequently the expression of PPM1E(1-554) at least doubles

and again remains constant between DIV 21 and 25. Post-DIV 25 cultures were not investigated in this study. The exact age at which PPM1E expression would undergo the last steep increase in expression varied slightly between cultures between DIV 20 and 21 (data not shown). These changes in expression are conserved in full-length



Figure 3.11: Endogenous PPM1E expression during maturation of hippocampal neuronal culture¹⁶. Qualitative immunoblot detected with anti-PPM1E(AGC) and anti- α -Tubulin antibodies. DIV: day-*in-vitro*.

¹⁶ The exposure time of the light sensitive film to the qualitative example blot in Figure 3.10 was ten times longer for detection of full-length PPM1E than for detection of PPM1E(1-554) and α -Tubulin.

PPM1E, although its levels are considerably lower¹⁶. The ratio between PPM1E and PPM1E(1-554) does not change significantly during the maturation.

3.2.2 Cellular and sub-cellular localization of endogenous PPM1E

It was previously reported that day-*in-vitro* (DIV) 6 rat primary hippocampal neurons show a different distribution of PPM1E expression than the majority of human brain neurons, including those in the hippocampal CA1 region (Kitani et al., 2006). The PPM1E expression is neuron-specific and cytoplasmatic in most neuronal brain populations, but enriched in the nucleus in primary hippocampal neurons on DIV 6 (Kitani et al., 2006). To understand why PPM1E shows different localization in these neurons, the sub-cellular localization of PPM1E was investigated in this study.

3.2.2.1 Localization of PPM1E in human frontal cortex

Co-detection with NeuN revealed that PPM1E is enriched in neuronal soma also in the human frontal cortex samples which were investigated in the present study (Figure 3.12). This observation confirmed data from Kitani et al. (2006). The PPM1E levels in nuclei are considerably lower, as shown by co-labelling with the DNA binding marker DAPI (4',6-diamidino-2-phenylindole) (Figure 3.12, arrowheads). Additionally anti-PPM1E(ENS) detects small globular structures in between the neurons which are described in further detail below¹⁷. These are visible as diffuse stain in lower magnification (Figure 3.12).

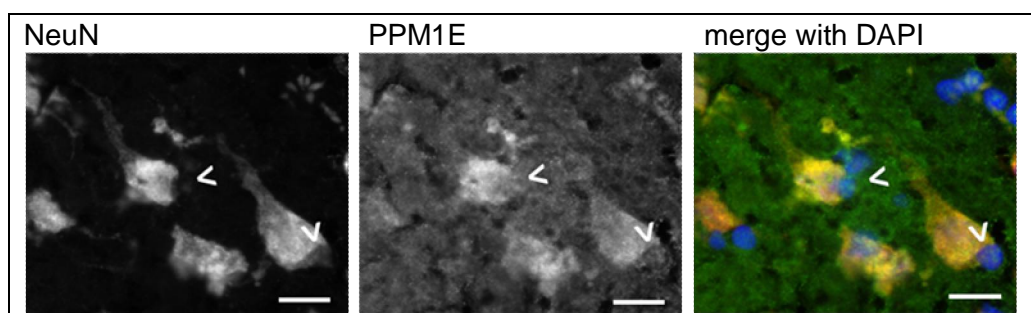


Figure 3.12: PPM1E is co-localized with the neuronal marker NeuN in human brain. Example picture from human frontal cortex, Braak 0 donor 93-105. Merge: anti-NeuN detection red; anti-PPM1E(ENS) detection green; DAPI detection blue. Arrowheads indicate nuclei. Scale bar 20 μ m.

To analyze whether PPM1E localization does change during the development of Alzheimer's disease as reflected by Braak staging, a subset of the previously described brain samples was analyzed. Eight donor samples were picked based on their PPM1E

¹⁷ see paragraph 3.2.2.5 Co-localization of PPM1E with EAAC1 but not GAD67 in human cortical neurons , page 100

protein expression levels, to represent the whole range of expression levels (Figure 3.13). Frontal cortical samples were co-immunolabeled with anti-PPM1E(ENS) and anti-NeuN antibodies and superficial cortical layers were imaged. The superficial cortical regions could not be entirely matched due to the restricted availability of brain samples.

The localization of PPM1E is not changed in samples of different Braak stages (Figure 3.13). PPM1E is consistently co-localized with NeuN in healthy brain donors as well as in Alzheimer's disease patients. Higher PPM1E protein levels are not visibly reflected by a higher degree of PPM1E(ENS) immunolabeling in these frontal cortex specimen.

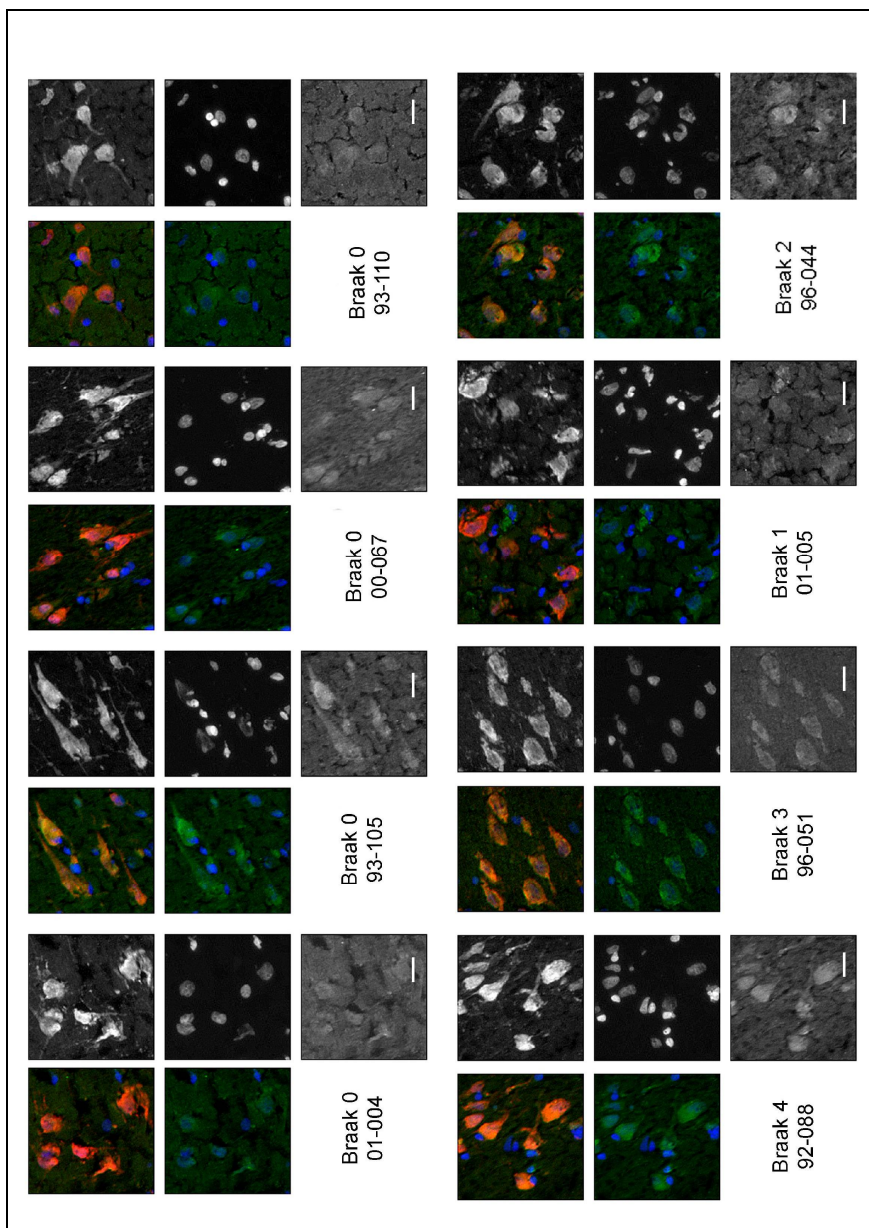


Figure 3.13: PPM1E immunoreactivity in the human frontal cortex in different Braak stages shows similar cytoplasmatic expression of PPM1E in neurons in all analysed brain samples. Brain tissue donor number ("XX-XXX") and Braak stage indicated. The donors are sorted in ascending order according to rising PPM1E protein levels (as determined by immunoblot quantification). Five pictures for each donor are (clockwise, starting with upper right picture) 1. anti-NeuN stain; 2. nuclear DAPI stain; 3. anti-PPM1E(ENS) stain; 4. Merge of DAPI (blue) and anti-PPM1E(ENS) (green); 5. Merge of DAPI (blue) and anti-NeuN (red). Scale bar 20 μ m.

Occasionally very few cells in human cortex are anti-PPM1E(ENS) but not anti-NeuN positive (compare Figure 3.3, arrowheads). However, co-immunolabeling of PPM1E(ENS) and glial cells revealed that PPM1E was not present in glial cells of human frontal cortex (Figure 3.14). The glia cells were detected with a monoclonal antibody directed against GFAP (glial fibrillary acidic protein).

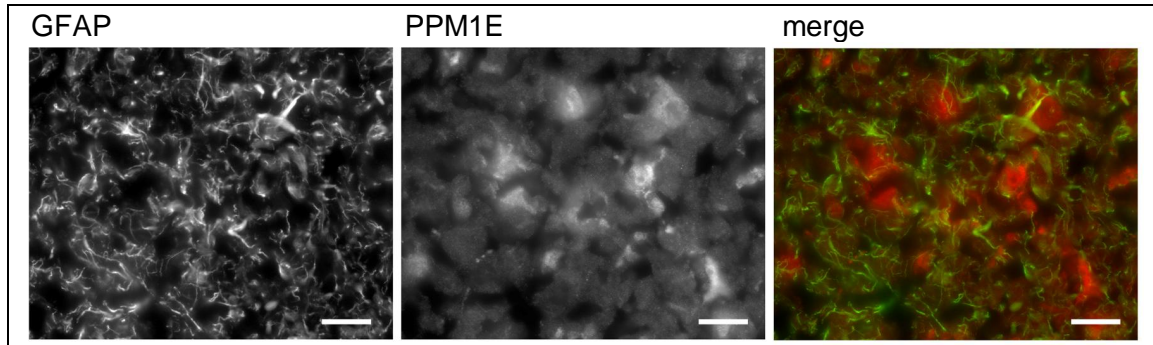


Figure 3.14: No co-localization between glial cells and PPM1E(ENS) labeling. Detection with anti-GFAP and anti-PPM1E(ENS) antibody. merge: GFAP green, PPM1E(ENS) red. Scale bar 20 μ m.

As described previously, NeuN fails to detect some neurons. Therefore it is not unlikely that the cells which are NeuN negative and PPM1E positive might be neurons.

3.2.2.2 Localization of PPM1E in rat hippocampus and cortex

The investigation of PPM1E expression in rat hippocampus and frontal cortex revealed that PPM1E is concentrated in the neuronal soma and weakly also in the nucleus as derived from co-immunolabeling with NeuN protein (Figure 3.15). The NeuN protein is localized mainly in the nucleus of embryonic neurons and is distributed throughout the nucleus and cytoplasm in mature neurons. The co-localization of PPM1E and NeuN is conserved in frontal cortex and dentate gyrus (DG) samples.

As described for human frontal cortex PPM1E is also in rat brain samples additionally diffusely distributed between neuronal cell bodies (see “background” stain in Figure 3.15 B). The expression pattern in human and rat brain samples appear to be comparable.

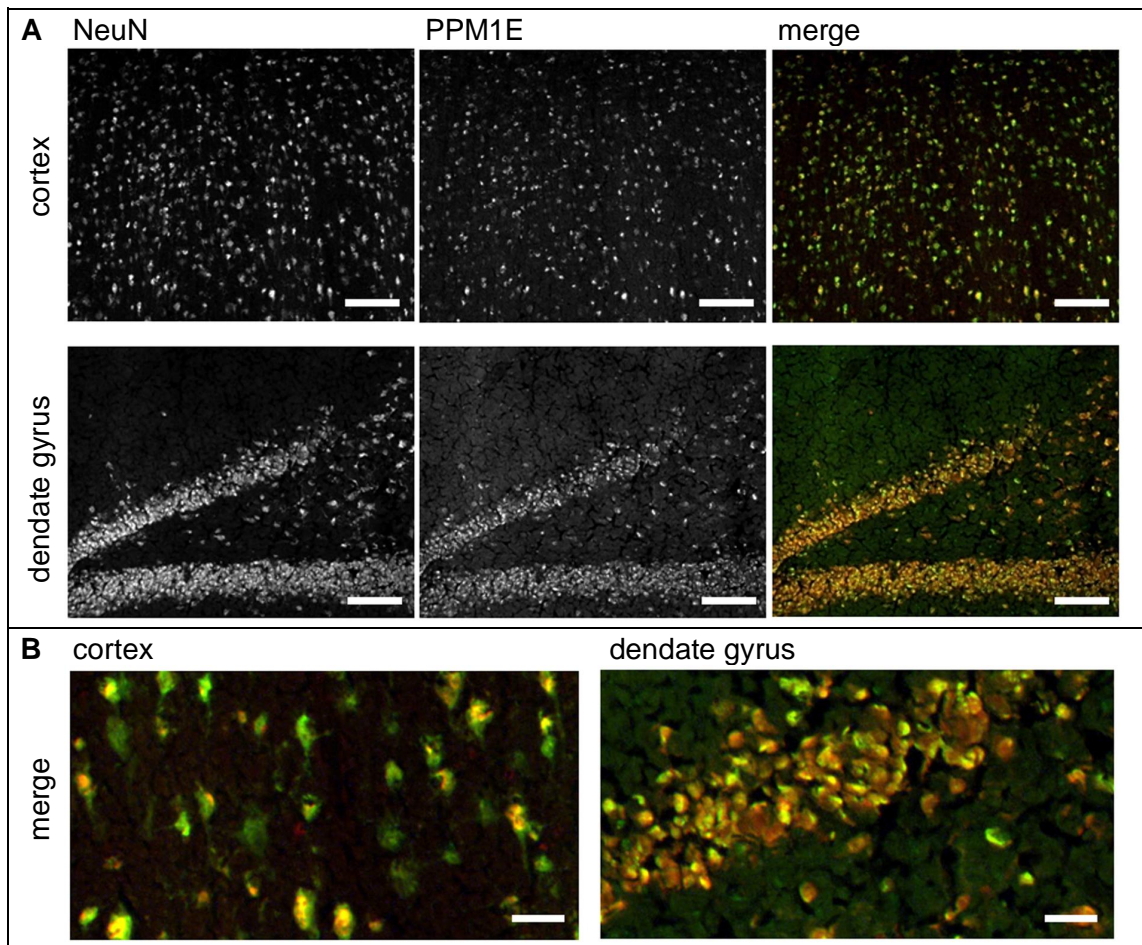


Figure 3.15: PPM1E is co-localized with the neuronal marker NeuN in rat frontal cortex and hippocampal dentate gyrus. PPM1E is enriched in the cytoplasm. merge: PPM1E(ENS) green; NeuN red. Cortex: frontal cortex. (B) Zooms from merged pictures in Figure 3.15 A. Scale bar (A) 120 μm , (B) 40 μm .

3.2.2.3 Localization of PPM1E during rat embryogenesis

The distribution of PPM1E during rat embryogenesis was analyzed in immunolabeled cryosections. While PPM1E was readily detected with the anti-PPM1E(ENS) antibody in E17 specimen, the signal strength was markedly reduced in specimen of earlier days of embryonic development E9 and E13 (Figure 3.16, considerably longer exposure times for PPM1E in E9 and E13 specimen).

This difference in signal strength confirms the immunoblotting results described above, which detected no PPM1E(1-554) or full length PPM1E in specimen taken during early embryogenesis on E9. However the comparison of PPM1E expression in E9 embryos interestingly showed a distinctly different distribution from E17 and adult rat specimen. PPM1E appears diffusely mainly in the cytoplasm and to a minor extend also in the nuclei of E9 and E13 neurons, like in the adult rat as described above, while it shows a

strong nuclear and diffuse cytoplasmic stain during later stages of embryonic development in E17 neurons.

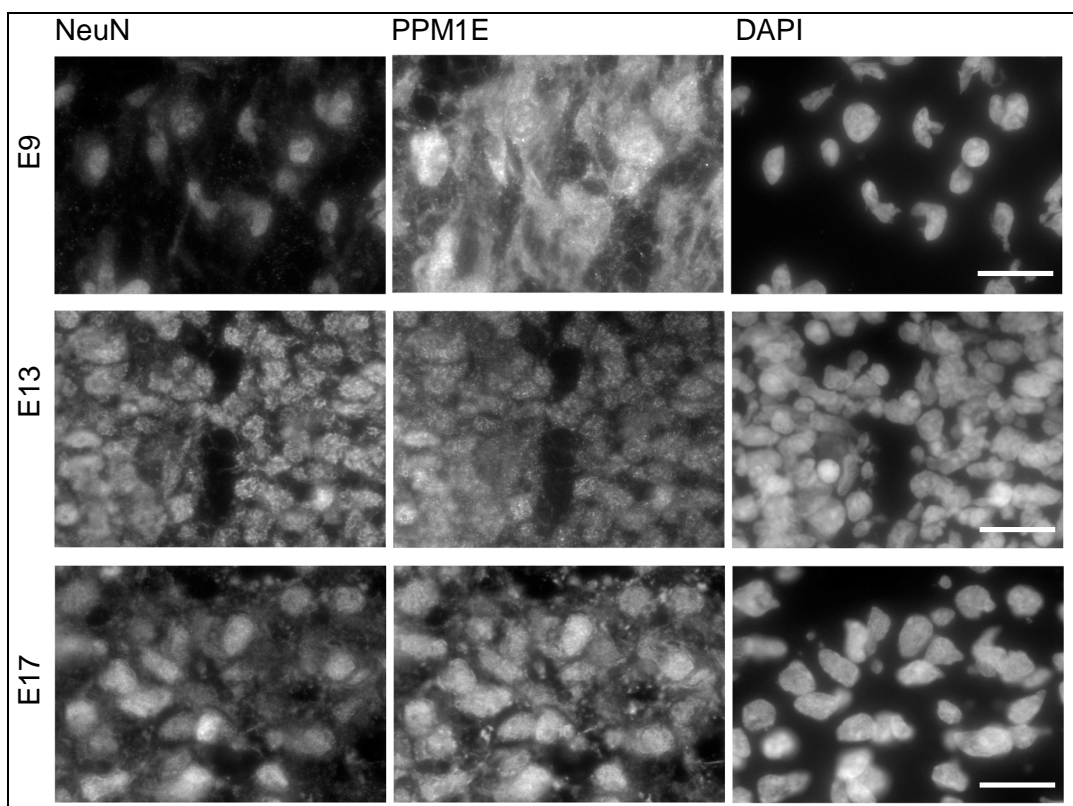


Figure 3.16: Change in PPM1E localization during rat embryogenesis. Immunolabeling of cryosections of rat embryonal brain tissue with anti-PPM1E(ENS) and anti-NeuN antibodies and DAPI. E: day in rat embryogenesis. Scale bar 20 μ m.

3.2.2.4 Localization of PPM1E in rat primary neuronal culture

The primary dissociated cultures which were investigated in this study were medium-dense, mixed hippocampal or cortical cultures, which contain neuronal but also glial cells (Figure 2.1). Glial growth and mitosis was not inhibited in favour of consistent neuronal development: The glial cells improved the growth conditions for neurons and supported the establishment of a differentiated neuritic network.

The hippocampal neuronal culture usually appeared healthier for a longer time than cortical culture of the same age¹⁸. It showed less signs of cell detachment and neurite death. Therefore the culturing period was restricted to 17 days-*in-vitro* (DIV) for cortical neurons, while hippocampal neurons were kept in culture for 21 to 22 days.

¹⁸ Primary cortical neurons were cultivated only for the biochemical analysis of PAK phosphorylation in this study. For further details see 3.3.3.6 *PPM1E affects PAK1 expression but not phosphorylation*, page 117.

Immunolabeling of mixed rat hippocampal and cortical primary culture showed that PPM1E was consistently expressed in all neurons of the primary neuronal culture (Figure 3.17). Neurons were detected with co-immunolabeling of the microtubule-associated protein 2 (MAP2). Seldom non-neuronal cells showed also PPM1E expression, (Figure 3.17 B, DIV 17, green arrow).

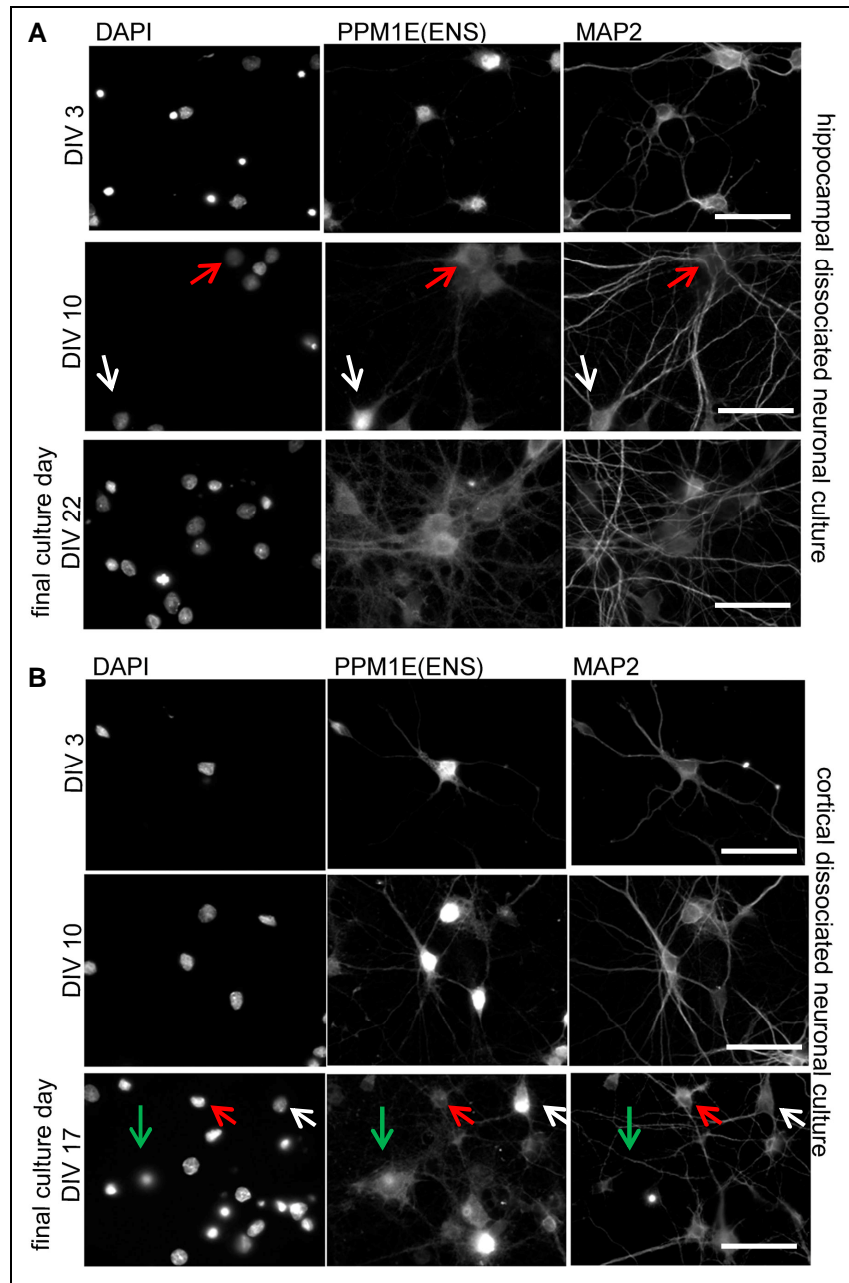


Figure 3.17: PPM1E translocates from the nucleus to the cytoplasm during maturation of dissociated neuronal cultures from rat hippocampus (A) and cortex (B). Neurons are labeled by anti-MAP2 antibody detection, nuclei are stained with DAPI. Red and white arrows indicate neurons in which PPM1E is enriched in the cytoplasm and nucleus respectively. Green arrow indicates a PPM1E(ENS)-positive non-neuronal cell. Scale bar 100 μ m.

In accordance with the literature PPM1E was mainly located in the nucleus in young primary hippocampal and cortical neurons on DIV 3 (Kitani et al., 2006) (Figure 3.17: DIV 3). However during culture maturation the localization was gradually shifting in an increasing number of cells towards the cytoplasm (Figure 3.17: DIV 10 to DIV 17 / 22). During the maturation of cortical neurons this shift in localization occurred usually later than in hippocampal cultures. On DIV 17 some cortical neurons still showed nuclear PPM1E expression while PPM1E was translocated to the cytoplasm in almost all hippocampal neurons by DIV 10.

The distribution of PPM1E was however different between culture batches, in that the ratio of nuclear to cytoplasmic PPM1E on DIV 21 was in some cases almost 1 as determined by visual inspection, while in other culture batches, the cytoplasmic fraction of PPM1E was much bigger than the nuclear (e.g. Figure 3.17 A). As discussed before additionally the dendritic expression appeared in some culture batches in a fragmented and in other in smooth fashion.

The reported differential distribution of PPM1E in intact mature brain tissue and dissociated culture is thus abolished in the comparison with mature neuronal cultures.

3.2.2.5 Co-localization of PPM1E with EAAC1 but not GAD67 in human cortical neurons

In addition to the enrichment of PPM1E in the cytoplasm or the nucleus, it has also been reported that electron microscopic immunolabeling detects enrichment of the phosphatase at the post-synaptic density (Kitani et al., 2006). In cortical tissue, beyond and within the borders of the neuronal soma and in dendrites diffuse PPM1E-containing globular structures are detected as indicated above.

Interestingly, PPM1E was partly co-localized with the high affinity glutamate transporter EAAC1 (excitatory amino acid carrier 1) in human frontal cortex (Figure 3.18). EAAC1 is responsible for re-uptake of the neurotransmitter glutamate from the synaptic cleft. EAAC1 is specific for glutamatergic, excitatory neurons and purkinje cells, specifically enriched in cortex, hippocampus and caudate-putamen and confined to presynaptic and postsynaptic elements. The co-localization of PPM1E and EAAC1 supports the results from Kitani et al. (2006) who stated that PPM1E is specifically present in the post-synaptic compartment of excitatory, asymmetric synapses.

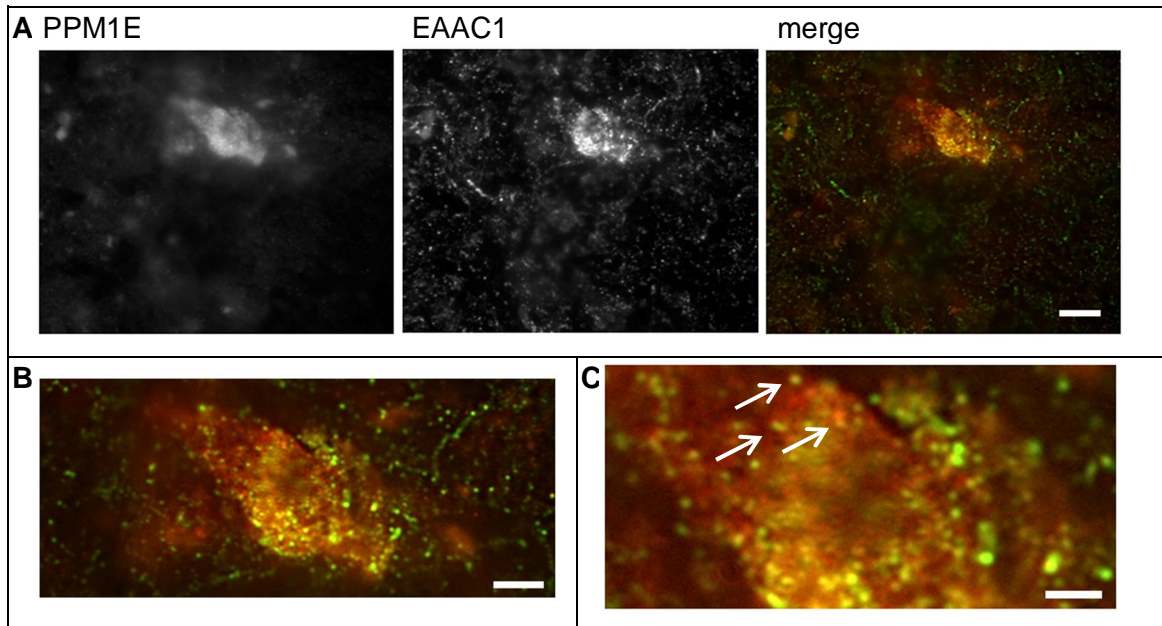


Figure 3.18: PPM1E is co-localized with EAAC1 in human frontal cortex. merge: PPM1E red, EAAC1 green. (C) Arrows indicate co-localization. Scale bar (A) 20 μm , (B) 10 μm , (C) 4 μm .

However PPM1E was not co-localized with GAD67 (glutamic acid decarboxylase 67-kDa isoform) (Figure 3.19), which catalyzes the conversion of glutamate to GABA (gamma-aminobutyric acid), the principal inhibitory neurotransmitter in the brain (Fong et al., 2005). GAD67 is thought to be diffusely distributed through the nerve cell body of GABAergic inhibitory neurons and is shown to be targeted to axonal nerve terminals and enriched at presynaptic clusters (Kanaani et al., 1999).

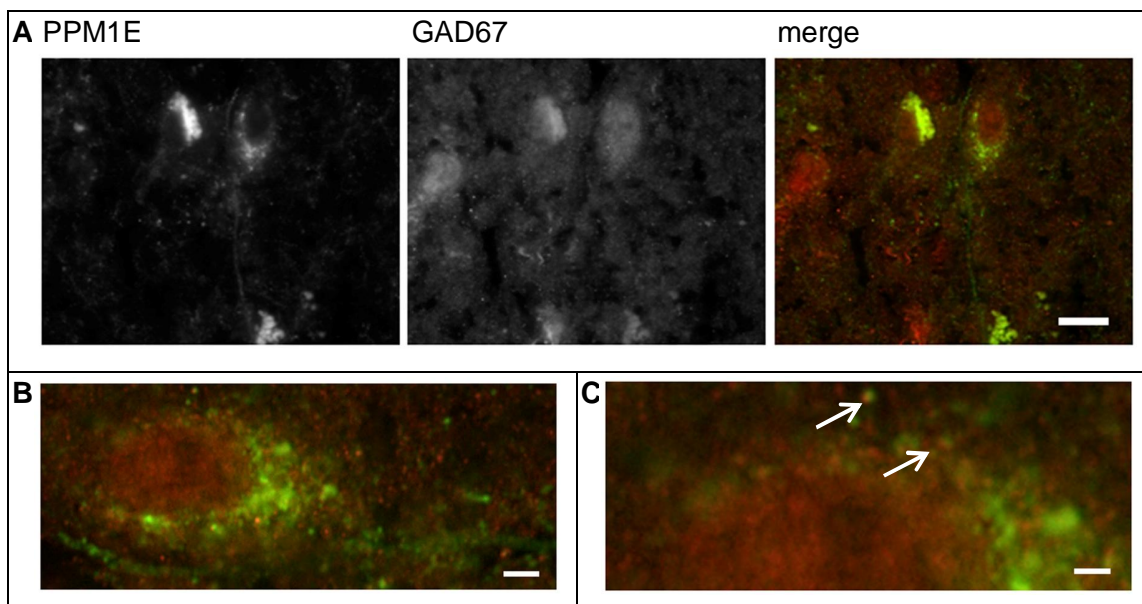


Figure 3.19: PPM1E is spatially close to GAD67 in human frontal cortex. Arrows indicate close spatial localization. merge: PPM1E red, GAD67 green. (B, C) Zooms are turned 90° counter-clockwise. (C) Arrows indicate close spatial localization of PPM1E and GAD67. Scale bar (A) 25 μm , (B) 6 μm , (C) 2.5 μm .

PPM1E and GAD67 signals were in some cases spatially very close, which might imply that the PPM1E accumulation is not restricted to excitatory synapses, but also present in the postsynaptic compartment of inhibitory synapses (Figure 3.19, arrows).

3.2.2.6 Localization of PPM1E in dissociated primary hippocampal neurons

The resolution of pre- and postsynaptic structures in monolayer culture is considerably better than in the investigated brain slices. Therefore possible co-localizations between PPM1E and cellular organelles and the association of PPM1E with the post-synaptic compartment were closer investigated in dissociated rat hippocampal neurons.

No co-localization between PPM1E and golgi apparatus or ER

PPM1E is not co-localized with elements of larger organelles like the golgi apparatus or the endoplasmic reticulum (ER), even though the occasionally fragmented dendritic localization indicated a possible co-localization with larger cellular organelles (Figure 3.20 and 3.21). The potential co-localization with golgi apparatus was tested by co-immunolabeling of PPM1E and GM130, the 'golgi matrix protein of 130 kDa' (Figure 3.20). PPM1E is not present in or associated with the golgi apparatus.

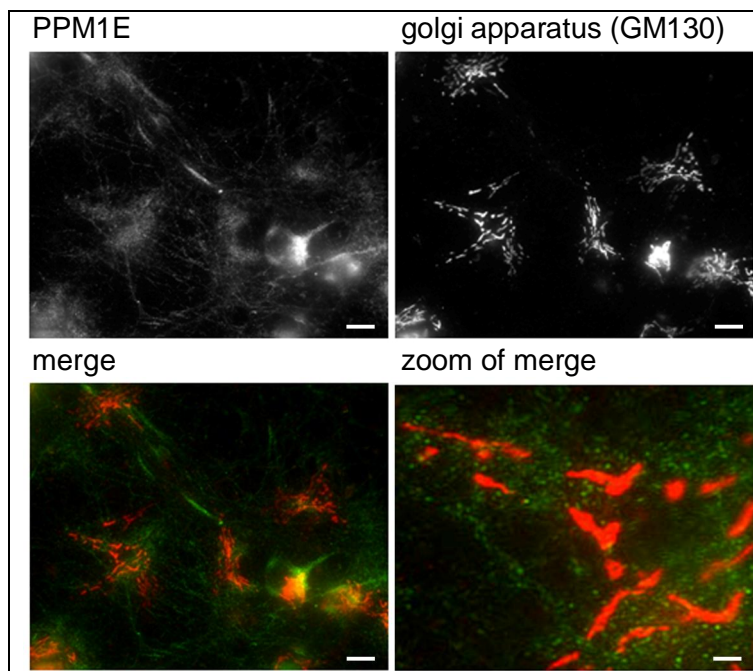


Figure 3.20: PPM1E is not co-localized with the golgi apparatus. Co-detection with anti-PPM1E(ENS) and anti-GM130. Merge: PPM1E(ENS) green; GM130 red. Primary hippocampal cell culture DIV 21. Scale bar 20 μm , zoom: 3.3 μm .

A co-localization with the endoplasmic reticulum was investigated by co-immunolabeling of PPM1E and an antibody against the KDEL tetrapeptide (Figure 3.21). The sequence KDEL is located at the carboxy-terminus of luminal proteins and serves as essential retrieval motif during the sorting of these proteins along the secretory pathway. PPM1E is not transported into or associated with the endoplasmic-reticulum (Figure 3.21).

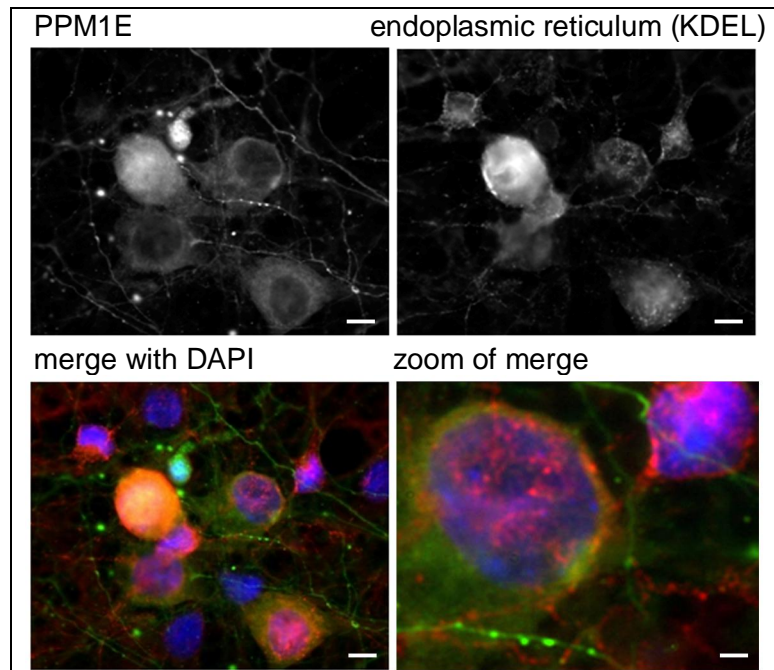


Figure 3.21: PPM1E is not co-localized with the endoplasmic reticulum. Co-detection with anti-PPM1E(ENS), anti-KDEL and DAPI. Merge: PPM1E(ENS) green; KDEL red; DAPI blue. Primary hippocampal cell culture DIV 21. Scale bar 12 μm , zoom 3 μm .

Close spatial localization of PPM1E and synaptophysin in primary neuronal culture

The synaptic localization of PPM1E which was found in cortical brain tissue is conserved in primary neuronal culture. Small globular enrichment of PPM1E can be found opposed to synaptophysin and localized in close spatial relation to dendritic spines of dissociated DIV 21 hippocampal neurons (Figure 3.22). Synaptophysin is a characteristically enriched in presynaptic vesicles.

As described above the small globular PPM1E enrichment is not restricted to the spines, but can also be seen in the dendritic shaft. In some cultures these globular structures form clusters within a dendrite, which appear like a fragmented distribution in lower magnification (Figure 3.22, merge, zoom 1).

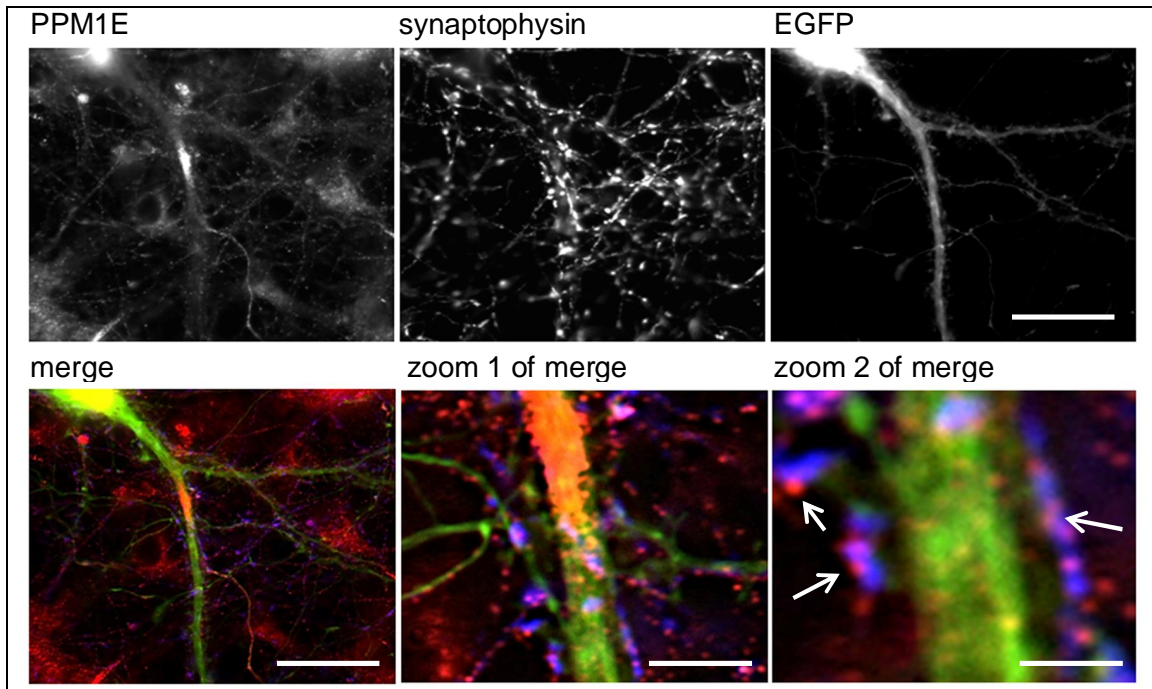


Figure 3.22: PPM1E is spatially closely correlated with synaptophysin and dendritic spines. Primary hippocampal cell culture DIV 21, transfected on DIV 7 with 0.2 μg pAAV / PPM1E and / EGFP. Merge: EGFP green; synaptophysin blue, PPM1E red. Scale bar 45 μm , zoom 1: 9 μm , zoom 2: 3 μm .

Co-localization of PPM1E with mitochondria in dendritic shaft

Due to the globular structure of PPM1E agglomerations the co-localization with mitochondria was investigated. Indeed, the sites of PPM1E enrichment in dendrites overlap with sites of COXII (cytochrome oxidase subunit II) accumulation (Figure 3.23). COX catalyzes the reduction of oxygen to water in the respiratory chain and is localized in the inner mitochondrial membrane.

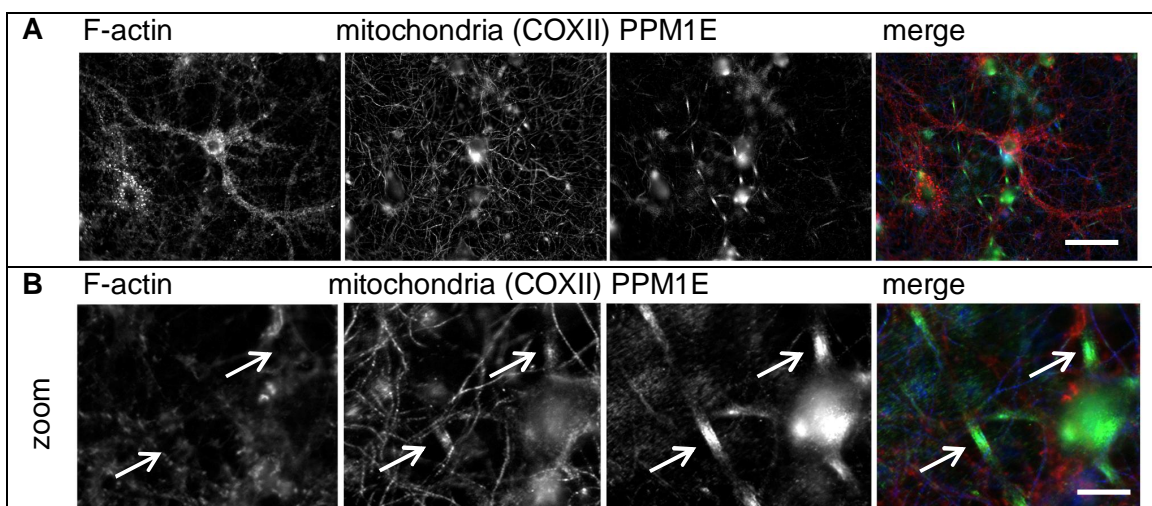


Figure 3.23: PPM1E is co-localized with the mitochondrial protein COXII and not enriched at sites of F-actin accumulation in DIV 21 dissociated hippocampal neurons. Immunolabeling with anti-PPM1E(ENS) and anti-COXII antibodies and phalloidin (F-actin labeling). Merge: PPM1E green; COXII blue; F-actin (phalloidin) red. Scale bar 50 μm , (B) zoom: 12 μm .

All three proposed target kinases of PPM1E are regulators of the actin cytoskeleton. Therefore the distribution of F-actin and PPM1E were compared. In the same culture the co-immunolabeling of F-actin with phalloidin showed that no accumulation of PPM1E at F-actin-rich sites was detected (Figure 3.23).

3.3 Effects of PPM1E *in vitro* and in primary neuronal culture

3.3.1 Eukaryotically expressed PPM1E exhibits phosphatase activity *in vitro*

The activity of PPM1E was determined previously *in vitro* in a cell-free system for rat but not for human PPM1E (Takeuchi et al., 2001). Therefore, and to enable future screens for PPM1E inhibitors, the activity of human PPM1E, encoded by NM_014906, was analyzed in an *in vitro* phosphatase assay.

His_hPPM1E protein expression, purification and activity determination.

The phosphatase was expressed in the *Spodoptera frugiperda* cell line Sf9 with an amino-terminal His-tag (Figure 3.4, lane 12). PPM1E was also expressed in different *E.coli* strains, but although the proteins solubility, size and truncation were identical in immunoblots, the protein was inactive (data not shown). His-PPM1E containing protein lysates were harvested from Sf9 cell culture 72 h after induction of expression. His-PPM1E was then purified with Ni-NTA affinity chromatographic columns in physiological pH values and salt concentrations. The resulting purity of His_PPM1E was approximately 80% as judged from Coomassie-stained gel electrophoresis (data not shown). Subsequently tested size-exclusion chromatography led to a higher purity of PPM1E (compare: "Expression, purification and characterisation of PPM1E and PPM1F", Bachelor's Thesis D.Siebert, excerpt in Appendix A 8).

The design of the phosphatase activity assay was based on an established assay for PPM1E (Takeuchi et al., 2001) and adapted to a 96-well medium-throughput screening format. The assay made use of a phosphorylated target peptide and the detection of phosphate released from this peptide.

The peptide contains a phosphorylated threonine (pT) and has a length of 12 amino acids YGGMHRQE_pTVDC. These mimick the CaMKII α/β autophosphorylation

site around threonine 286/287. The peptide was readily dephosphorylated after 30 min incubation at 30°C by increasing concentrations of purified His_PPM1E as indicated by

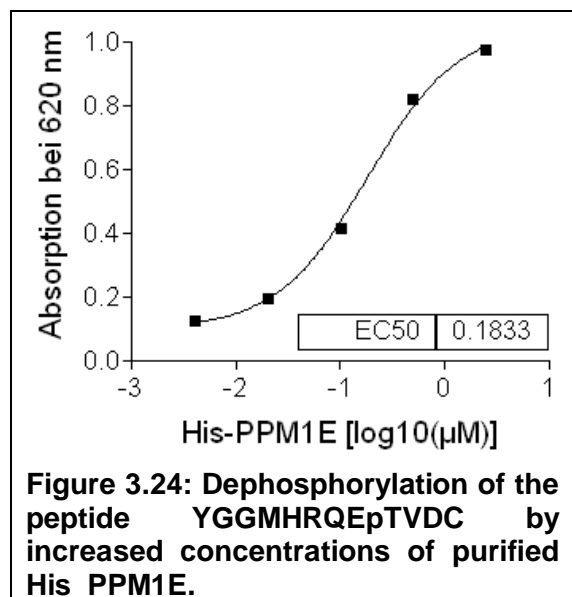


Figure 3.24: Dephosphorylation of the peptide YGGMHRQE_pTVDC by increased concentrations of purified His_PPM1E.

increased amounts of inorganic phosphate (Figure 3.24). In this assay inorganic phosphate is detected by its binding to molybdate, which then complexes in the solution with malachite green. This complex has an peak absorption at 620 nm. Ideal peptide concentrations were determined by titration. The half maximal effective concentration (EC_{50}) for PPM1E in this activity assay is 180 nM.

3.3.2 PPM1F levels do not compensate for PPM1E overexpression

The endogenous expression of the closest PPM1E homolog PPM1F was monitored in primary hippocampal neurons which ectopically expressed PPM1E, to detect potential compensatory effects in the cells. Mature DIV 17 hippocampal neurons showed no difference in their PPM1F expression after 10 days of ectopic PPM1E expression and a visibly increased PPM1E expression (Figure 3.25). Therefore the effects of ectopic PPM1E expression on PPM1F were not investigated further.

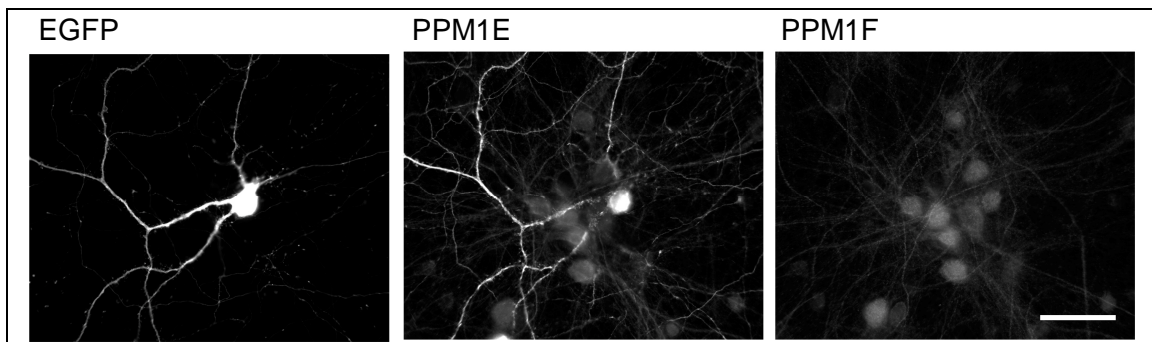


Figure 3.25: PPM1F expression is independent from PPM1E expression under experimental conditions. DIV 17 hippocampal neurons, transfected with 0.2 μ g pAAV / EGFP and pAAV / PPM1E each on DIV 7. Immunolabeling with anti-PPM1E(ENS)- and anti-PPM1F-antibodies and DAPI. Scale bar 50 μ m.

3.3.3 Dephosphorylation of downstream kinases in primary neuronal culture

Three target kinases for the PPM1E phosphatase activity have been proposed (Takeuchi et al., 2001; Koh et al., 2002; Kitani et al., 2003). However, the PPM1E activity on PAK1 at threonine 422 has been suggested indirectly on the basis that the closest homolog PPM1F dephosphorylates PAK1 *in vitro*, and that PPM1F and PPM1E both are able to inhibit PAK1 induced stress-fiber formation and Cdc42-based PAK1 activation in HeLa¹⁹ and COS-7 cells (Koh et al., 2002). Also the dephosphorylation of CaMKIV and a phosphopeptide modelled after the CaMKII phosphorylation site has been shown *in vitro* (Takeuchi et al., 2001). However for none of the kinases it was shown that PPM1E is able to dephosphorylate them in a neuronal cellular model. In

¹⁹ HeLa was the first human cell line and was derived from a cervical cancer from the patient Henrietta Lacks in 1951.

this study rat primary neuronal culture was employed as a relatively simple but sufficiently complex cellular model to analyze whether PPM1E actively dephosphorylates CaMKIV, CaMKII and PAK1.

3.3.3.1 Design and expression of PPM1E activity mutants

Design of PPM1E mutants

Functionally inactive single-amino acid mutants of PPM1E were employed as negative controls, where it was possible, in the following experiments. Thereby the possibility that effects of PPM1E overexpression are caused by mechanisms other than the phosphatase activity of PPM1E was excluded.

The exchanged amino acids arginine 241 and aspartate 479 are highly conserved in the PP2C family of phosphatases (Jackson et al., 2003; Kusuda et al., 1998) (Figure 3.26). The mutated sites were chosen analogue to previously described single amino acid exchanges in the PPM1E homolog PPM1F (Tada et al., 2006). The resulting PPM1E mutants R241A and D479N correspond to the previously characterized PPM1F mutants R162A and D400N, which are inactive *in vitro*, and to the amino acids arginine 33 and aspartate 282 in PP2C α (Figure 3.26; Appendix A 1). The PP2C α X-ray model by Das et al. (1996) predicts that both residues are part of the active phosphatase site. The active site of PP2C α is composed of several invariant amino acids in the PP2C family of phosphatases, which may serve as metal-coordinating and phosphate-binding residues and as a general acid during catalysis. Arginine 241 (R162 in PPM1F; R33 in PP2C α) is thought to be an inorganic phosphate-binding residue and aspartate 479 (D400 in PPM1F; D286 in PP2C α) may coordinate two divalent ions in the active center (Das et al., 1996).

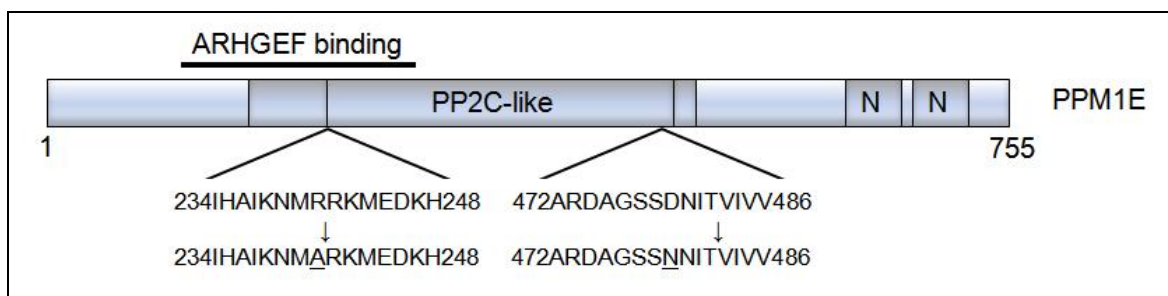


Figure 3.26: PPM1E activity mutants. Schematic view of the PPM1E protein, including the location of point mutations. PP2C phosphatase and E/Fhd domains shaded in grey, N: nuclear localization signal. ARHGEF binding site is indicated. Arrows indicate the location of single amino acid mutations in the PPM1E phosphatase.

Expression of PPM1E activity mutants

Transient expression of PPM1E and the activity mutants in HEK cells confirmed that the mutants are truncated in the same manner as the active phosphatase (Figure 3.27 B). Moreover, after transfection of dissociated hippocampal neurons PPM1E and the PPM1E mutants are all mainly expressed in the cytoplasm and in neurites (Figure 3.27 A). The levels of the expressed proteins were comparable for PPM1E mutants and PPM1E transfected neurons. The expression of PPM1E and the mutants appeared in some cultures fragmented in the neurites (see Figure 3.27 A, expression of PPM1E and PPM1E(R241A)). However this fragmented distribution of PPM1E in the dendrites was not conserved in all experiments as discussed above.

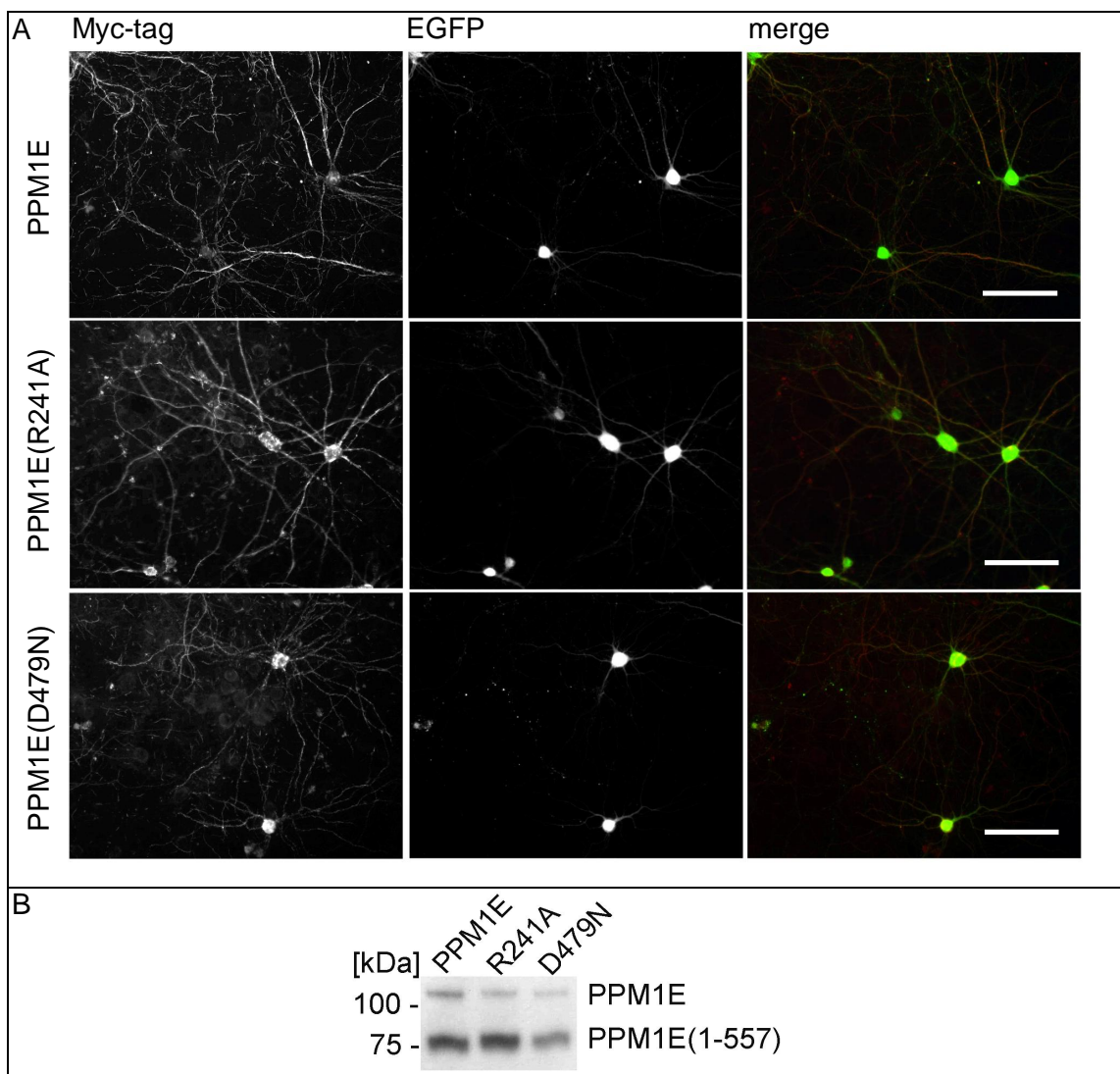


Figure 3.27: Expression of PPM1E and the activity mutants Myc_PPM1E(R241A) and Myc_PPM1E(D479N). (A) Dissociated hippocampal neurons on DIV 21, transfection on DIV 7. (B) Truncation of PPM1E and the activity mutants Myc_PPM1E(R241A) and Myc_PPM1E(D479N) in HEK cells after transfection. Scale bar 60 μ m.

3.3.3.2 PPM1E overexpression in neuronal culture with rAAV

The relative phosphorylation of CaMKII/IV and PAK1 was analyzed in rAAV_PPM1E infected primary neuronal cell culture and normalized to the total expression of the respective kinase. For this biochemical analysis primary hippocampal neurons were infected with recombinant adeno-associated viruses (rAAV) on DIV 7 and cellular lysates were analyzed on DIV 21. PPM1E or EGFP are expressed under control of the neuron-specific promoter for human synapsin (hSYN) which induces exclusively neuronal expression (Kügler et al., 2003). The expression of EGFP-encoding rAAV became gradually visible 48 hours after viral infection and did reach comparable protein expression levels achieved by transfection as judged from visual inspection of EGFP autofluorescence (Figure 3.28 A). 72 hours after infection of neurons, the expression of the desired gene was detected in all neurons that means that the number of target gene expressing neurons is considerably higher than after transfection (Figure 3.28 A).

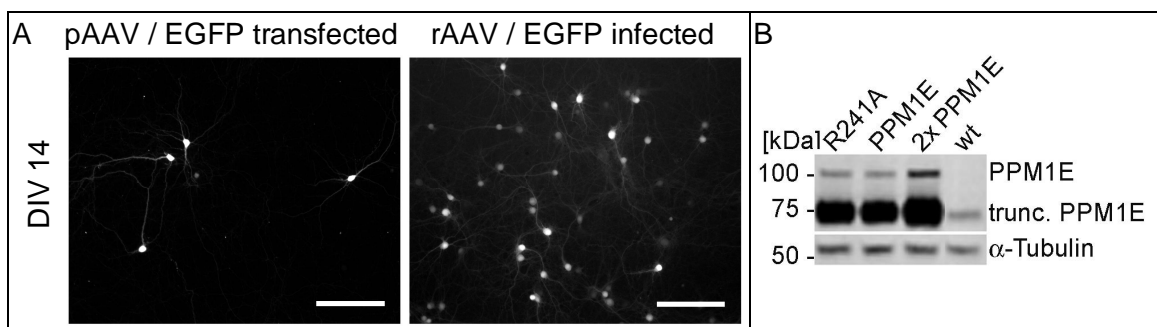


Figure 3.28: Efficiency of rAAV induced protein expression. (A) Representative example pictures of EGFP autofluorescence, demonstrating the transfection and rAAV-infection efficiency in medium-dense DIV 14 neuronal culture. Transfected / infected on DIV 7 with $0.2 \mu\text{g}$ pAAV / EGFP or $3 \cdot 10^8$ Dcvp per 1.9 cm^2 culture. (B) Overexpression of the encoded protein in dissociated hippocampal cell culture after infection with respective rAAVs on DIV 7 with $3 \cdot 10^8$ or $6 \cdot 10^8$ (2x) Dcvp per 1.9 cm^2 culture. Dcvp: DNA-containing viral particles. (A) Scale bar $200 \mu\text{m}$.

Purified viral vectors were able to induce a high overexpression of PPM1E or other encoded genes, in a rAAV-concentration dependent manner (Figure 3.28 B). The mutant PPM1E(R241A) was used as negative control for rAAV / PPM1E expression and also in this context the mutant was truncated in the same manner as the active phosphatase (Figure 3.28 B).

3.3.3.3 Immunoblot quantification of protein levels

To analyse the PPM1E effects on the target kinases, five- to three-step dilution series of cell lysates were blotted on PVDF membranes and detected quantitatively with fluorescently labelled antibodies as described above for the detection of PPM1E levels in human brain samples (compare also Figure 3.29 A). This relatively laborious method was chosen because

standard chemiluminescence detection allows only a snapshot of the enzymatic detection reaction and is therefore highly dependent on timing and exposure

and not suitable for quantitative Western blot detection (Gassmann et al., 2009; Dickinson and Fowler, 2002). The dynamic range, in which the signal is directly proportional to the amount of target is very limited. Compared to this standard detection the quantitative detection used in this study offers two advantages which broaden the dynamic range of detection: Firstly the samples are loaded in dilution series, which compensates for expression differences between different samples on the same blot and inter-experiment variation, and secondly the detection with antibodies which are conjugated to a fluorophor offers inherently a more stable signal than the detection through an enzymatic reaction.

From fluorescence scans the signal intensities for CaMKII, phosphoCaMKII α/β (threonine 286/7), CaMKIV, phosphoCaMKIV (threonine 196), PAK1 and phosphoPAK (threonine 423) were quantified with ImageJ software. The signals were plotted with

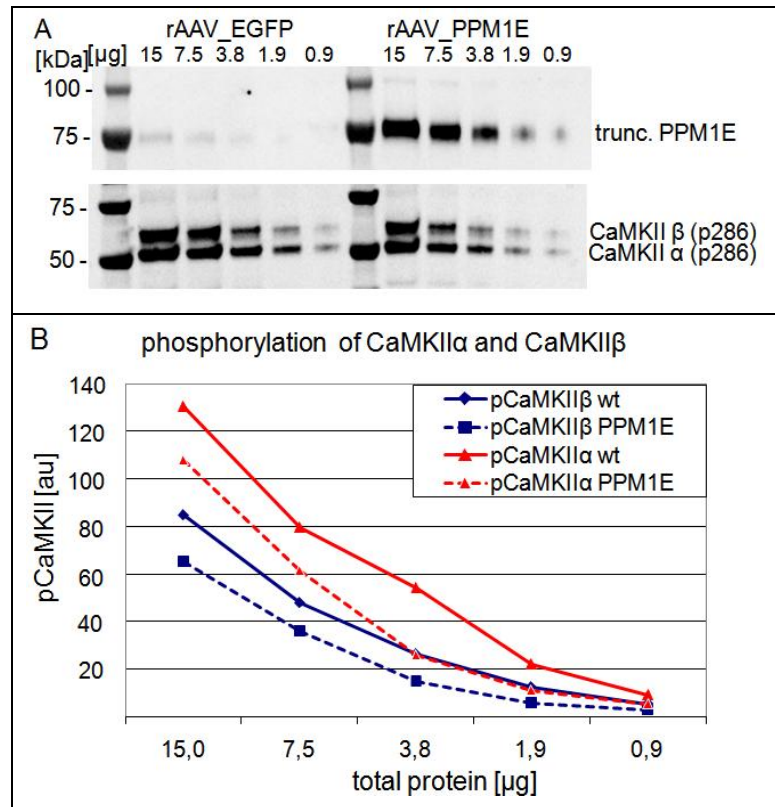


Figure 3.29: Reduction of CaMKII α and β phosphorylation in dissociated wt and PPM1E overexpressing cortical neuronal cell culture. (A) Example blots for PPM1E overexpression and CaMKII phosphorylation. (B) Examples for plotting of signal intensities of phosphorylated CaMKII, measured with ImageJ. DIV 21 neurons, infected on DIV 7. wt: uninfected, wildtype neurons; au: arbitrary units.

Microsoft® Office Excel® (Figure 3.29 B), and those in the dynamic range were averaged and normalized to similarly derived housekeeping protein levels.

Exemplified, an immunoblot for the quantitative detection of PPM1E and phosphorylated CaMKII α and β isoforms (threonine 286 and 287 respectively) is shown (Figure 3.29 A). The isoform CaMKII β with about 57 kDa and the isoform CaMKII α with about 50 kDa are both detected by this phosphorylation-specific antibody (Figure 3.29 A, lower blot).

These loaded cell extracts are derived from DIV 21 hippocampal culture infected rAAV-EGFP or with rAAV-PPM1E and are analysed in dilution series between 15 and 0.9 μ g per lane. Densitometric quantification of the bands with ImageJ shows a weaker phosphorylation of CaMKII α as well as of CaMKII β in this experimental batch of PPM1E overexpressing cells (Figure 3.29 B).

In the following analyses the characterized protein or phosphorylation level were normalized against equally derived values for the expression of a 'housekeeping protein', either cyclophilin B or GAPDH (glyceraldehyde 3-phosphate dehydrogenase). All three are highly abundant, consistently expressed proteins and thus suitable for the normalization.

3.3.3.4 PPM1E affects CaMKII α expression and potentially its phosphorylation at T286

The large-scale analysis of PPM1E effects on CaMKII was focussed on the isoform CaMKII α for simplification. However, initial experiments did not show a difference in the influence of PPM1E on the α - or the β -CaMKII isoform (compare immunoblot example in Figure 3.29).

The values for CaMKII α phosphorylation and expression were normalized to the levels of the GAPDH protein (Figure 3.30 A). The variability between the experiments was high, which is a relatively common problem in the analysis of primary neuronal culture (Chen et al., 2008; Maximov et al., 2007). Therefore all derived values were additionally normalized to the wildtype values of the same culture batch.

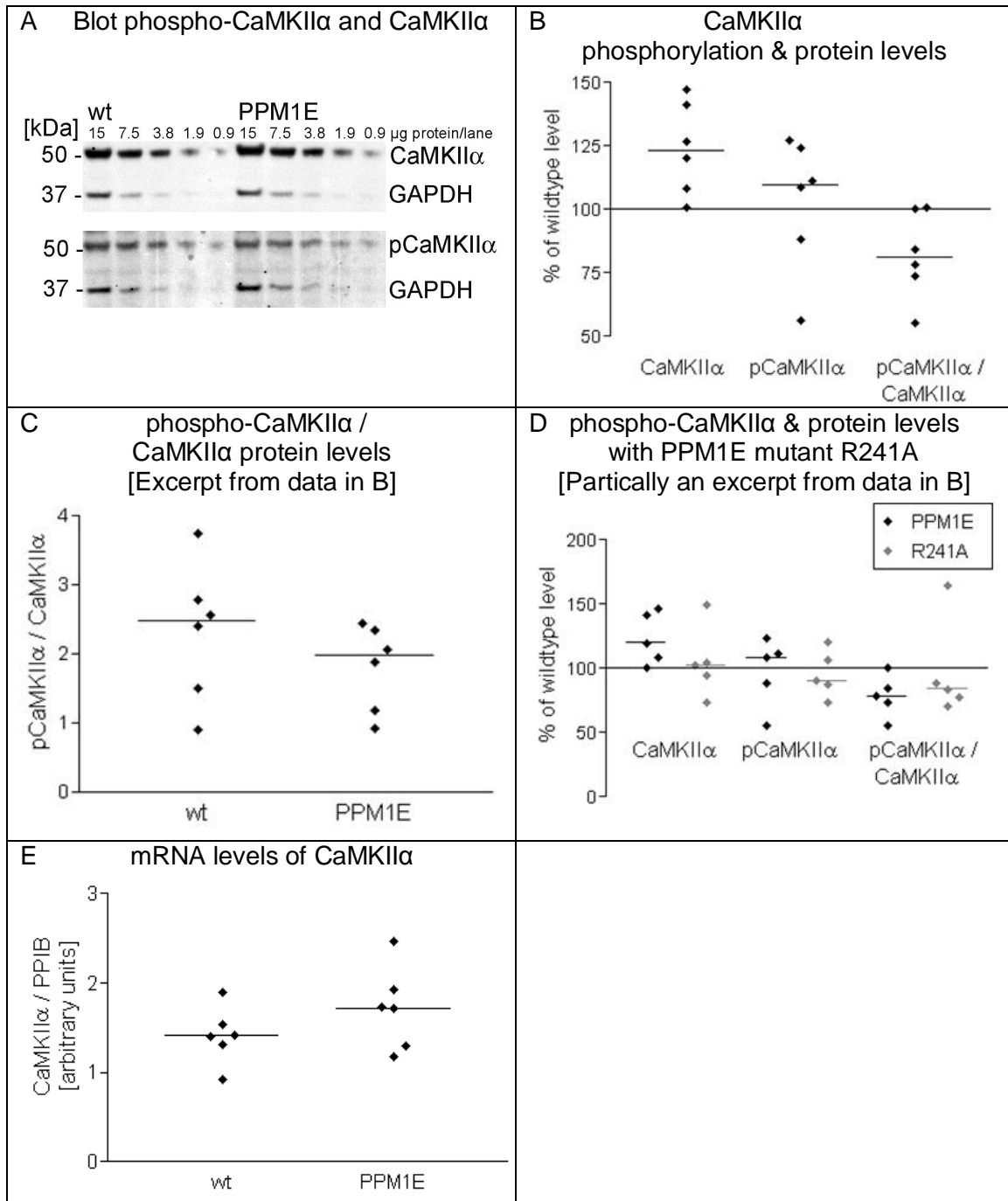


Figure 3.30: Influence of ectopic PPM1E expression on CaMKII α expression and phosphorylation in primary hippocampal culture. (A) Quantitative example blot, detected with anti-CaMKII α - or -phospho CaMKII α - and -GAPDH-antibody, with 5-step dilution series of wt and rAAV-PPM1E infected hippocampal culture (infection with 3×10^8 Dcvp rAAV / PPM1E). (B) Quantitative changes in CaMKII α phosphorylation and expression in wildtype and rAAV-PPM1E infected hippocampal culture expressed as % of wildtype. n=6 (C) Quantitative phospho-CaMKII α / CaMKII α levels. n=6 (D) Quantitative changes in CaMKII α phosphorylation and expression in wildtype, rAAV-PPM1E and -PPM1E(R241A) infected hippocampal culture expressed as % of wt. n=5 (E) CaMKII α mRNA levels, normalized against cyclophilin B (PPIB). n=6 from one experiment. Horizontal bars represent the median. Mature neurons (between DIV 17 and DIV 21) infected on DIV 7. wt: wildtype culture. pCaMKII α : CaMKII α phosphorylated at threonine 286. Statistical test: Wilcoxon matched pairs test, 95 % confidence interval (no significance for any of the above experiments).

The phosphorylation of CaMKII α at threonine 286, normalized to total CaMKII α levels, showed a trend towards a reduction in PPM1E overexpressing hippocampal compared with wildtype culture. The median of six experiments was 21.4 % lower than that of wildtype (Figure 3.30 B, C). However, this was a result from a slight increase in the median level of CaMKII α phosphorylation (8.7 %) and a considerable increase in the median of the total CaMKII α expression (20 %) (Figure 3.30 B). The number of experiments which could be conducted was limited, therefore it has to be noted that no significant change was determined between wildtype and ectopically PPM1E expressing cultures. However, the trend towards a changes CaMKII α expression in ectopically PPM1E expressing cultures was not present in PPM1E(R241A) expressing cultures (Figure 3.30 D). PPM1E(R241A) expressing hippocampal cultures show a similar deviation of the median, although in the opposite direction, from the wildtype levels in respect to phosphorylation of CaMKII α , but they do not have an effect on total CaMKII α expression. This indicates that ectopic PPM1E expression might have an effect on CaMKII expression rather than on phosphorylation.

Ectopically PPM1E expressing primary hippocampal cultures were also analysed for their CaMKII α mRNA levels and interestingly they are increased by trend compared to wildtype (Figure 3.30 E), providing potentially a basis for the same trend on the protein level.

Evaluation of CaMKII α phosphorylation in immunolabeled primary neurons

To get a better impression of – potentially only localized – differences in CaMKII α phosphorylation and expression, both parameters were initially also evaluated by immunolabeling of transfected cultures in which only single neurons express PPM1E in high levels. However, due to the density of the neuritic network, the investigation of CaMKII, CaMKIV and PAK and their phosphorylation in detail was not possible, because they are all expressed throughout the dendritic and axonal compartment (Figure 3.31 A), while PPM1E is only visibly expressed in dendrites. The resolution of single dendrites from the surrounding axons in the medium-dense cultures was not satisfying. Therefore the analysis was proceeded biochemically.

However, in single cultures a reduction in phosphorylated CaMKII α was visible in PPM1E transfected neurons (Figure 3.31). Although the network of pCaMKII(Thr286) positive neurites is very dense, the strong reduction became apparent in thicker secondary dendrites (Figure 3.31 B, arrows).

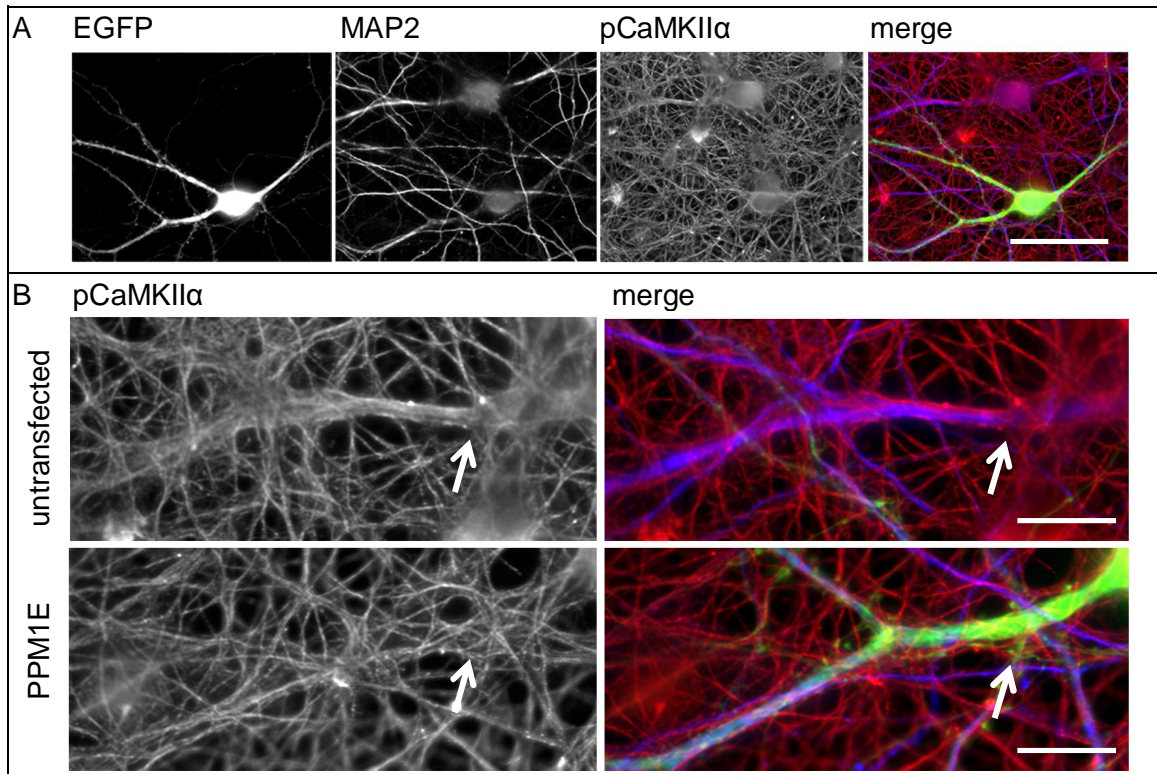


Figure 3.31: CaMKII α phosphorylation is visibly reduced in secondary dendrites which overexpress PPM1E. Mature primary hippocampal neuronal culture, transfected on DIV 7 with 0.2 μ g pAAV / EGFP and 0.2 μ g pAAV / PPM1E per 1.9 cm² culture. (A) EGFP autofluorescence, MAP2 labeling of neurons, pCaMKII(threonine 286) detection. Merge: EGFP green, MAP2 blue, pCaMKII(T286) red. (B) Zooms into A on two dendrites from a (top) untransfected control neuron and (B) transfected neuron. Merge and pCaMKII(T286) labeling. Same colouring as in A. Scale bar (A) 50 μ m; (B) 10 μ m.

3.3.3.5 PPM1E affects CaMKIV expression and phosphorylation at threonine 196

CaMKIV expression and phosphorylation was analysed with quantitative immunoblots as described for CaMKII α above (Figure 3.32 A). All derived values were normalized to GAPDH and subsequently to the wildtype values of the same culture batch because the inter-culture variations were high. The phosphorylation of CaMKIV at threonine 196 normalized against total CaMKIV expression, was significantly reduced in primary hippocampal cultures which ectopically expressed PPM1E (32.8 %, $p = 0.0313$) (Figure 3.32 B, C). This was a result of the overall levels of CaMKIV, which were slightly increased by trend compared with wildtype levels (10 %) and the phosphorylation of CaMKIV which was decreased by trend (27 %) (Figure 3.32 B).

In one experiment the inactive mutant PPM1E(R241A) was tested for its effect on CaMKIV expression and phosphorylation. Due to problems in the manufacture of the rAAV-PPM1E(R241A), only the limited number of one experiment could be conducted and can therefore only deliver a first indication for the reliability of the previous experiments.

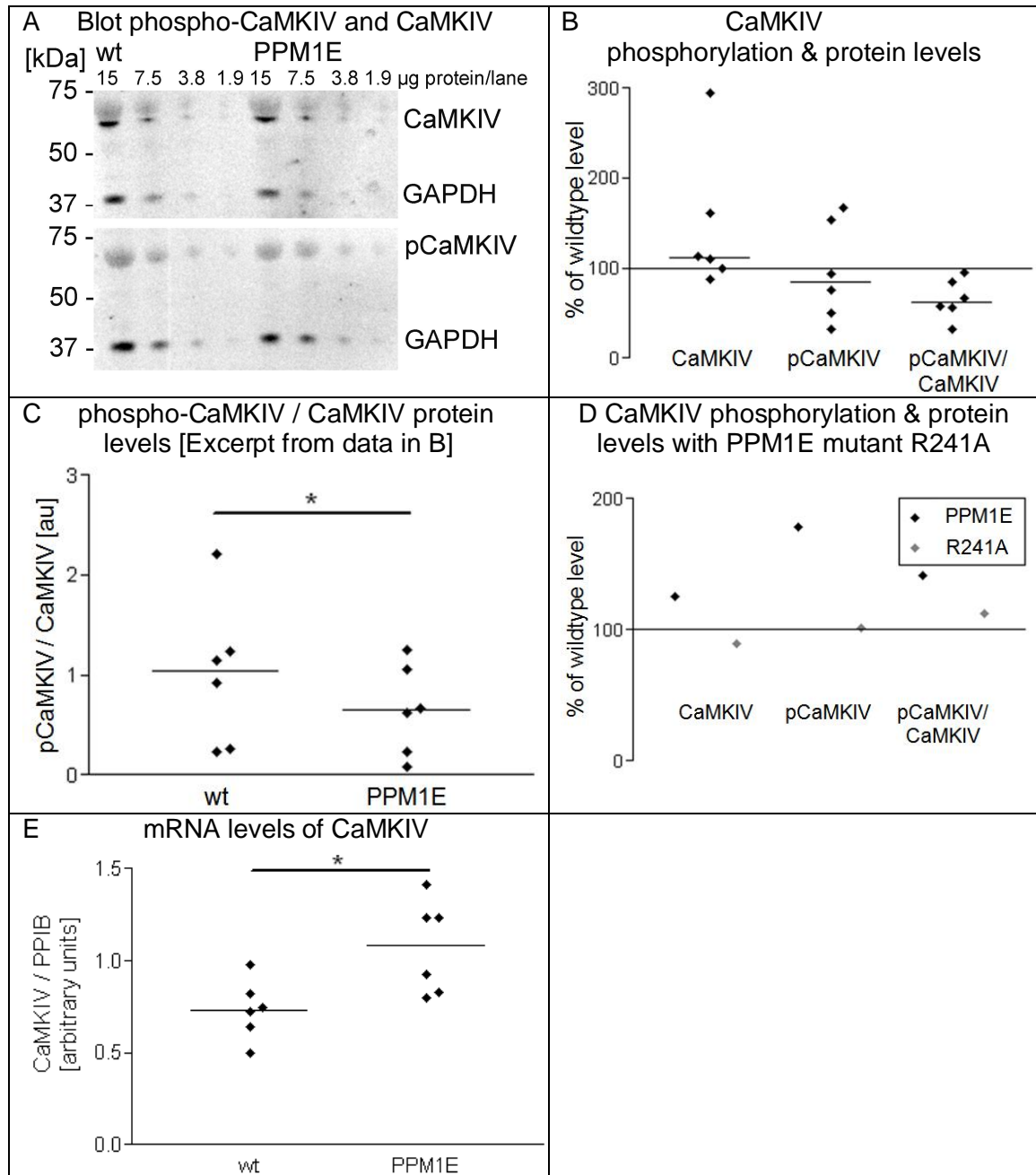


Figure 3.32: Influence of ectopic PPM1E expression on CaMKIV expression and phosphorylation in primary hippocampal culture. (A) Quantitative example blot, detected with anti-CaMKIV- or anti-phospho CaMKIV- and anti-GAPDH-antibody, with 4-step dilution series of wildtype and rAAV-PPM1E infected hippocampal culture (infection with 3×10^8 Dcvp rAAV / PPM1E). (B) Quantitative changes in CaMKIV phosphorylation and expression in wildtype and rAAV-PPM1E infected hippocampal culture expressed as % of wildtype. $n=6$ (C) Quantitative phospho CaMKIV / CaMKIV levels. $n=6$ ($p=0.0313$, 95 % confidence interval, Wilcoxon matched pairs test) (D) Quantitative changes in CaMKIV phosphorylation and expression in wildtype, rAAV-PPM1E and rAAV-PPM1E(R241A) infected hippocampal culture expressed as % of wildtype. $n=1$ (E) CaMKIV mRNA levels, normalized against cyclophilin B (PPIB). $n=6$ from one experiment. ($p=0.0260$, 95 % confidence interval, Mann-Whitney-U-test) Horizontal bars represent the median. Mature neurons (between DIV 17 and DIV 21) infected on DIV 7. wt: wildtype culture. pCaMKIV: CaMKIV phosphorylated at threonine 196. Statistical test: Wilcoxon matched pairs test, 95 % confidence interval (no significance for any of the above experiments).

However, the trend towards an increase of CaMKIV expression in ectopically PPM1E expressing cultures was not present in the PPM1E(R241A) expressing culture (Figure 3.32 D). However the phosphorylation of CaMKIV in the ectopically PPM1E expressing culture differed a lot from the median of all analysed cultures. Therefore no speculation can be made here with respect to the influence of PPM1E(R241A) on the phosphorylation of CaMKIV.

Interestingly the CaMKIV levels are regulated on the mRNA level. Ectopically PPM1E expressing hippocampal cultures show a significant increase in CaMKIV mRNA by 47.2 % compared with wildtype cultures (Figure 3.32 E, $p=0.0260$).

Overall, the CaMKIV protein levels by trend do not increase as much as those of CaMKII α after ectopic PPM1E expression, and additionally the phosphorylation is reduced in all experiments. Thus the predicted PPM1E target kinase CaMKIV might well be directly dephosphorylated by PPM1E also in primary neurons as proposed for other cell types before. However these experiments cannot exclude that the effect is only indirectly mediated by ectopic PPM1E expression.

3.3.3.6 PPM1E affects PAK1 expression but not phosphorylation

In a third approach the effect of ectopic PPM1E expression on PAK was analysed. A potential challenge with regard to the p21-activated kinase 1 (PAK1) was that phospho-specific antibodies against phospho-threonine 423 of PAK1 do also detect PAK2 and PAK3. Therefore it is important to note that only one band was observed on the immunoblots. However, the rat PAK1, PAK2 and PAK3 have similar predicted molecular weights of 60.59, 58 and 60.72 kDa respectively. Therefore PAK2 as well as PAK3 could have been detected due to overlap of their bands. However, it has been described before that in dissociated cortical cultures PAK1 is the predominant isoform of group I PAK kinases (Jacobs et al., 2007). Hence in the following experiments the effects of PPM1E on PAK1 were investigated in cortical instead of hippocampal dissociated culture.

All derived values were normalized to Cyclophilin B and subsequently to wildtype values of the same culture batch to compensate for inter-culture variations. No decrease in PAK phosphorylation with increased PPM1E expression was observed in DIV 17 primary cortical culture, which was infected with rAAV / PPM1E on DIV 7 (Figure 3.33). Instead, the median PAK1 expression was by trend lowered (31.5 %), whereas the overall median phosphorylation was slightly by trend reduced (9.3 %).

This resulted by trend in an overall increase in the phosphorylated PAK / PAK1 ratio (33.6 %).

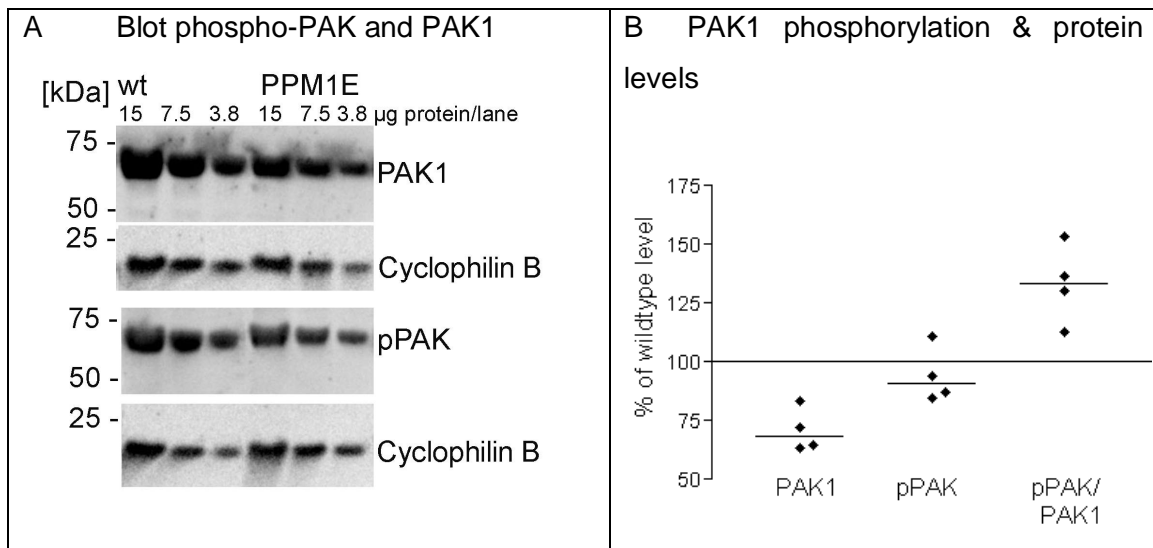


Figure 3.33: Influence of ectopic PPM1E expression on PAK1 expression and PAK phosphorylation in primary cortical culture. Infection with 3×10^8 Dcvp rAAV / PPM1E (A) by trend decreased the total expression of PAK1, by trend decreased the phosphorylation of PAK at threonine 423 and (C) by trend increased the ratio of pPAK / PAK1 to approximately 33.6 % of wildtype level. Horizontal bars represent the median. DIV 17 neurons, infected on DIV 7. wt: wildtype culture. pPAK: PAK phosphorylated at threonine 423. n=4, from three independent neuronal cultures.

Due to problems in the manufacture of the rAAV-PPM1E(R241A), only the experiments could not be repeated with the inactive mutant as control and can therefore only deliver a first indication. Although none of the described trends is significant, it is apparent that the ectopic PPM1E expression would influence PAK1 differently than expected, from previous literature data.

3.3.4 Increased PPM1E levels reduce mushroom spine density and dendritic arborization

rAAV infected neuronal cultures are unsuited for morphological analyses on single neurons because close to 100 % of all neurons are expressing the protein of interest, in this case EGFP. The neuritic network would therefore be too dense to differentiate between single neurons and to differentiate single spines. Therefore the neuronal cultures are instead transfected with the respective construct.

Transfection and co-transfection efficiency in primary neuronal culture

Most primary neurons are differentiated, post-mitotic cells which cannot be transfected as readily as immortalized, mitotic cell lines. However in recent years efficient methods

for transfection of primary neurons have been developed. In this study optimized protocols for lipid-mediated DNA transfection efficiently transfected around 7 % of all neurons in hippocampal culture. Co-transfection of two plasmids encoding different proteins led in all examined cultures also to the co-expression of both proteins. Transfected neurons showed EGFP autofluorescence after 24 hours.

3.3.4.1 PPM1E has a deteriorating effect on dendritic spines

To examine the effects of increased PPM1E levels on neurogenesis and synaptic plasticity, the spine number and morphology was evaluated in primary rat hippocampal neuronal cultures, which were transfected on DIV 7 and analyzed on DIV 21. EGFP was co-expressed with all constructs to visualize the dendritic spines. Three-dimensional, confocal images of the dendrites were deconvolved from z-stacks, and the spine number was analyzed with NeuronStudio software with the investigator being blind to the transfection condition.

Effects of PPM1E and PPM1E activity mutants on dendritic spine number

Changes in the spine number between PPM1E and EGFP or PPM1E mutant transfected neurons were analyzed semi-automated with the NeuroStudio software and the investigator was blind to the transfection condition.

On DIV 21, 14 days after transfection, the mushroom spine density in PPM1E expressing cells was severely decreased by 34 % (0.6 μ g pAAV / PPM1E per 1.9 cm² culture), compared to control EGFP expressing neurons (Figure 3.34 A; $p < 0.0122$). The mushroom spines are believed to have the greatest synaptic capacity (Ethell and Pasquale, 2005). PPM1E did not change the numbers of stubby or thin spines significantly. Meanwhile the neurons that were expressing either one of the PPM1E mutants (0.6 μ g pAAV / PPM1E mutant per 1.9 cm² culture) did not show a difference to the EGFP control neurons in any of the morphologically differentiated groups of spines (Figure 3.34 A-C). Thus, effects on dendritic mushroom spines observed between the neurons expressing PPM1E and control groups are indeed attributable to increased levels of PPM1E phosphatase activity.

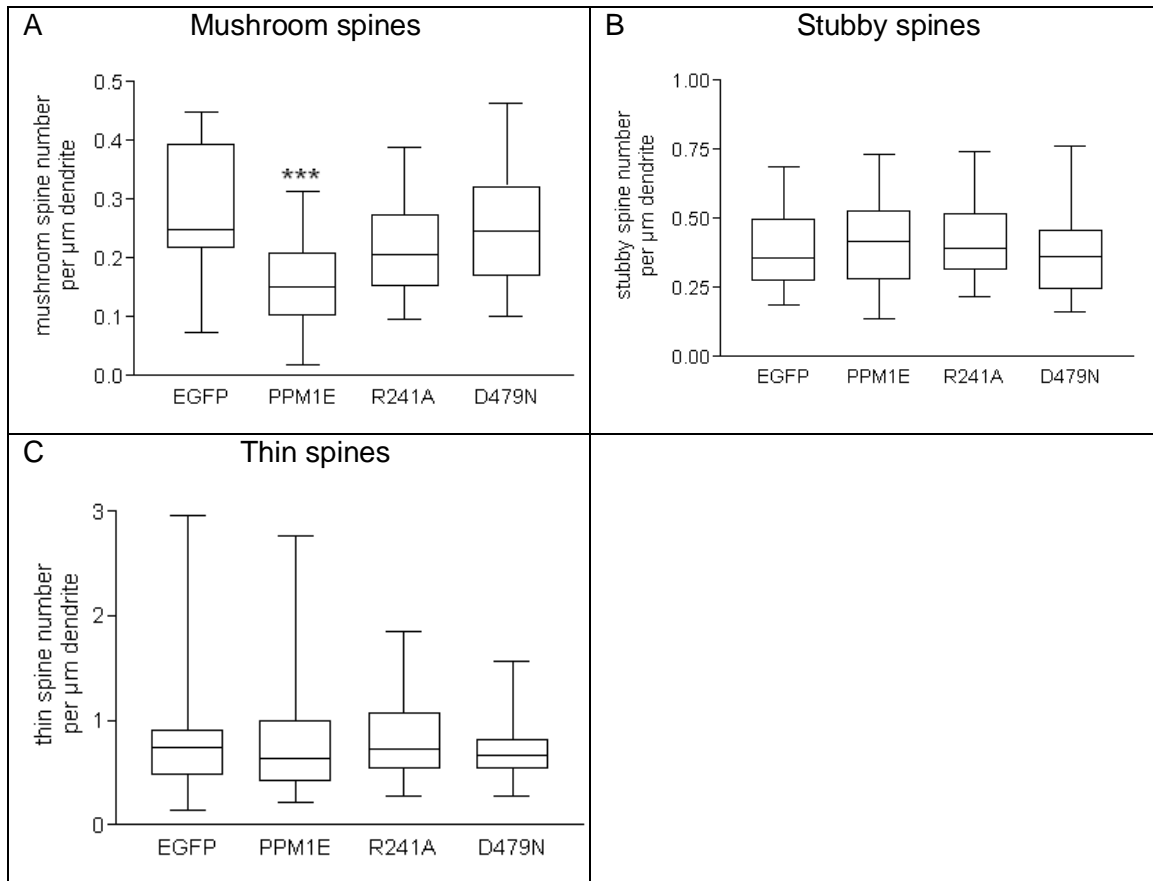


Figure 3.34: PPM1E reduces the number of mushroom spines in hippocampal neurons. Ectopic expression of functionally phosphatase-inactive PPM1E mutants does not affect the numbers of (A) mushroom, (B) stubby or (C) thin spines on mature hippocampal neurons. (A) hPPM1E expressing neurons show a significant decrease in mushroom spine number per μm of dendrite compared to EGFP control and PPM1E mutant transfected neurons by 34% ($p < 0.0122$), two-tailed Mann-Whitney U-test. DIV 21 neurons, transfected on DIV 7 with $0.2 \mu\text{g}$ pAAV / EGFP or $0.6 \mu\text{g}$ pAAV / PPM1E or / PPM1E_mutant construct per 1.9 cm^2 culture. $n=30$ neurons from 3 independent experiments. D479N: PPM1E(D479N); R241A: PPM1E(R241A).

Effects of PPM1E and inactive PPM1E mutants on spine morphology

Also the spine length and spine head diameter were determined in the semi-automated detection of spines with NeuronStudio software (Figure 3.35). The median head diameter is unchanged in all groups of spines between PPM1E expressing and control neurons (Figure 3.35 A). Additionally the spine length of mushroom and thin spines is consistent between the control groups of EGFP and PPM1E mutant expressing neurons. However neurons with increased PPM1E expression show a decrease in the length of stubby spines by 11.8 % compared with the group of EGFP transfected neurons.

In summary, PPM1E has a deteriorating effect on mushroom spine number and the group of stubby spines is shorter than spines in control groups.

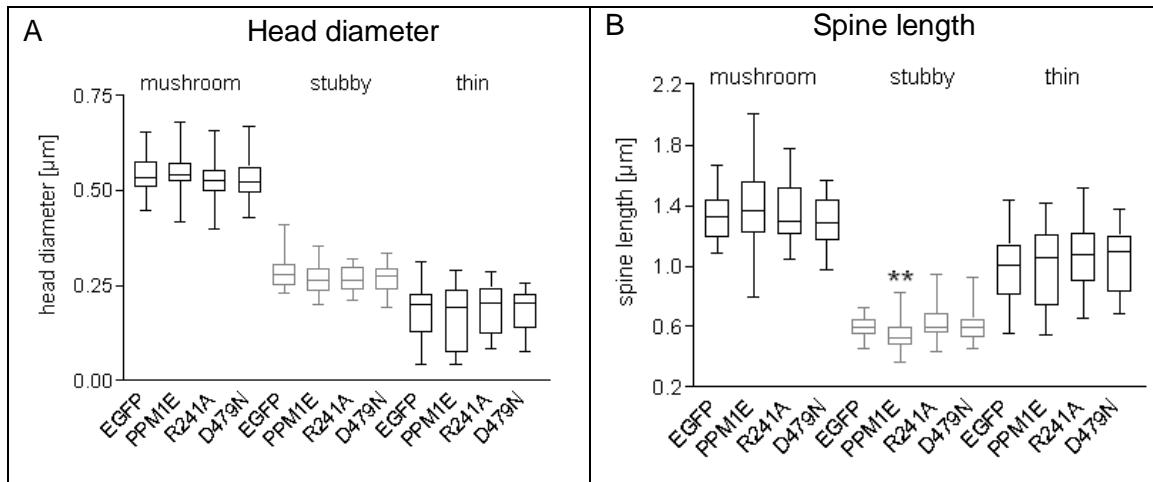


Figure 3.35: Effects of EGFP, PPM1E and PPM1E(D479) expression on the (A) head diameter and (B) the spine length on hippocampal neurons. Effects on mushroom, stubby or thin spines. Statistical test and p-values derived with two-tailed Mann-Whitney U-test. DIV 21 neurons, transfected on DIV 7 with 0.2 μg pAAV / EGFP or 0.6 μg pAAV / PPM1E or / PPM1E_mutant construct per 1.9 cm^2 culture. n=30 neurons from 3 independent experiments. ** significance p=0.0042, reduction of stubby spine length by 11.8 %.

3.3.4.2 PPM1E effect on dendritic spines is concentration-dependent

To support these results, three levels of ectopic PPM1E expression were induced in hippocampal neurons to evaluate whether the deteriorating on mushroom spines in concentration-dependent. The number of spines was evaluated manually and the investigator was blind to the transfection conditions.

Indeed the number of mushroom spines was reduced by 23%, 47% and 59% compared to control neurons, depending on the concentration of pAAV / PPM1E plasmid in the transfection (0.2, 0.6 and 0.8 μg pAAV / PPM1E per 1.9 cm^2 culture respectively; Figure 3.36). Again the variability between cultures was high as visible from large deviations from the median.

The neurons which were transfected with the highest concentration of PPM1E showed additionally a considerably increased number in filopodia-like long protrusions without spine head (not shown). These were not included in the evaluation.

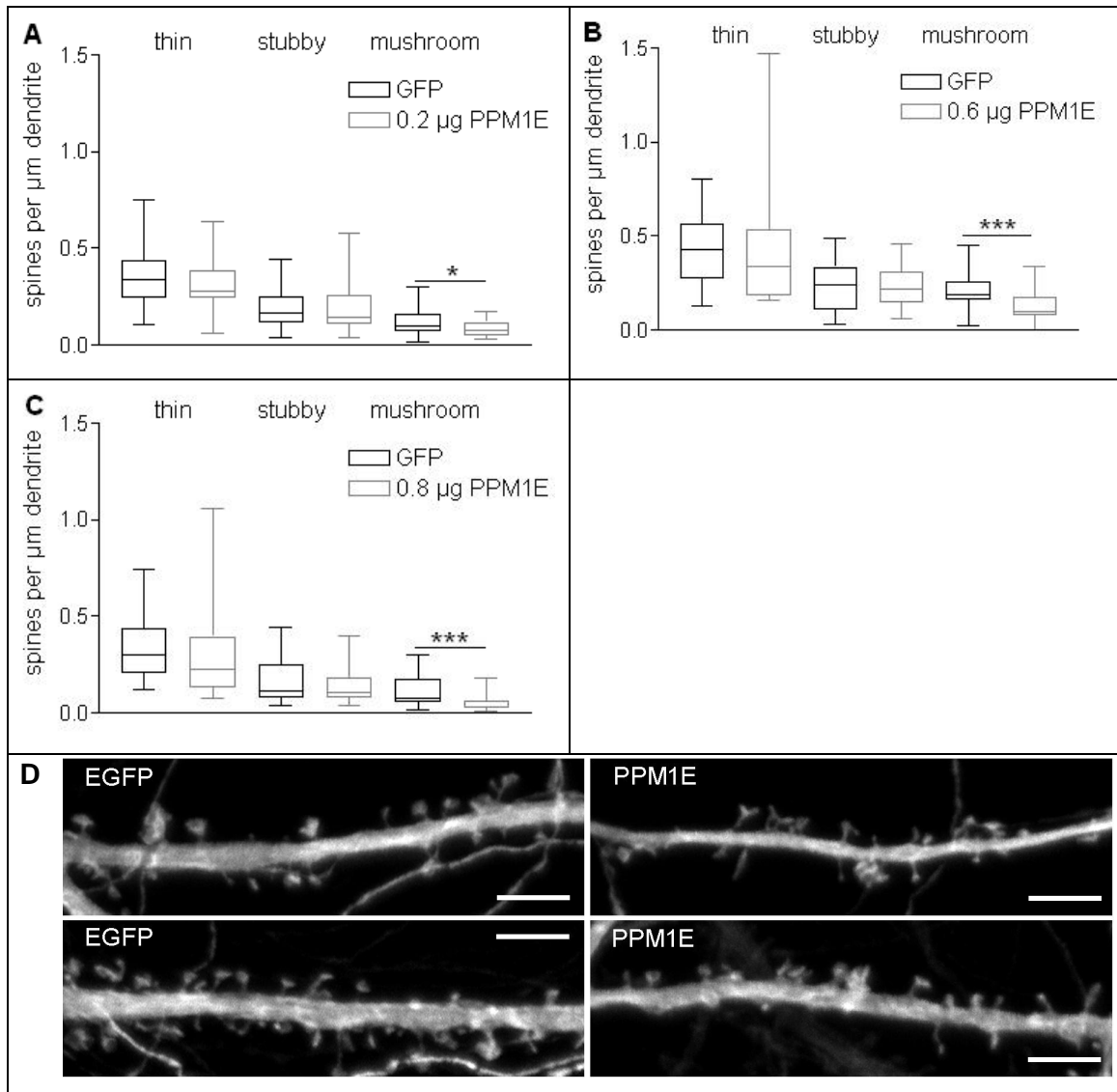


Figure 3.36: PPM1E expression decreases the number of mushroom-shaped spines in a concentration-dependent manner. PPM1E expressing neurons show a significant and concentration dependent decrease in the number of mushroom-shaped spines per μm dendrite compared to EGFP control neurons. DIV 21 neurons, transfected on DIV 7 with (A) 0.2 μg , (B) 0.6 μg and (C) 0.8 μg pAAV / PPM1E per 1.9 cm^2 culture. $n=30$ neurons from 3 independent experiments. Reduction of mushroom-shaped spines compared to control (A) 23% ($p=0.0178$), (B) 34% ($p=0.0122$), (C) 59% ($p=0.0001$), two-tailed Mann-Whitney U-test. (D) example pictures from dendrites transfected with (D) EGFP and PPM1E. EGFP autofluorescence. Scale bar 4 μm .

3.3.4.3 Effects of PPM1E and inactive PPM1E mutants on dendritic arborization

The putative PPM1E target kinase CaMKIV was reported to affect dendrite outgrowth in neurons (Takemura et al., 2009). Therefore the dendritic arborisation in PPM1E and PPM1E mutant expressing neurons was evaluated. The arborisation of DIV 21 neurons which express the PPM1E activity mutants is not affected (Figure 3.37). They show no difference compared with the EGFP control group.

Although it was shown that PPM1E is enriched at the postsynaptic density (Kitani et al., 2006 and above), PPM1E is ubiquitous in the cytoplasm of mature neurons in the brain and in primary neuronal culture and might therefore affect additional molecules, like the proposed PPM1E target kinase CaMKIV. Since CaMKIV regulates neuriteogenesis potential effects of PPM1E on neuritic arborisation were investigated.

Densely seeded hippocampal primary neurons (40 000 / 0.9 cm²) were transfected with PPM1E on DIV 7 and analyzed on DIV 17 and DIV 21. The number of primary dendrites branching off from a neuronal soma (roots) and the total length of neurites were determined. The dendritic arborisation was evaluated in a semi-automated manner with the 'Neurite' script (Acapella).

The number of roots and neurites in PPM1E overexpressing neurons is reduced by 30.7 % and 36.7 % respectively, as described above (Figure 3.37, compare also independent experiments in Figure 3.38).

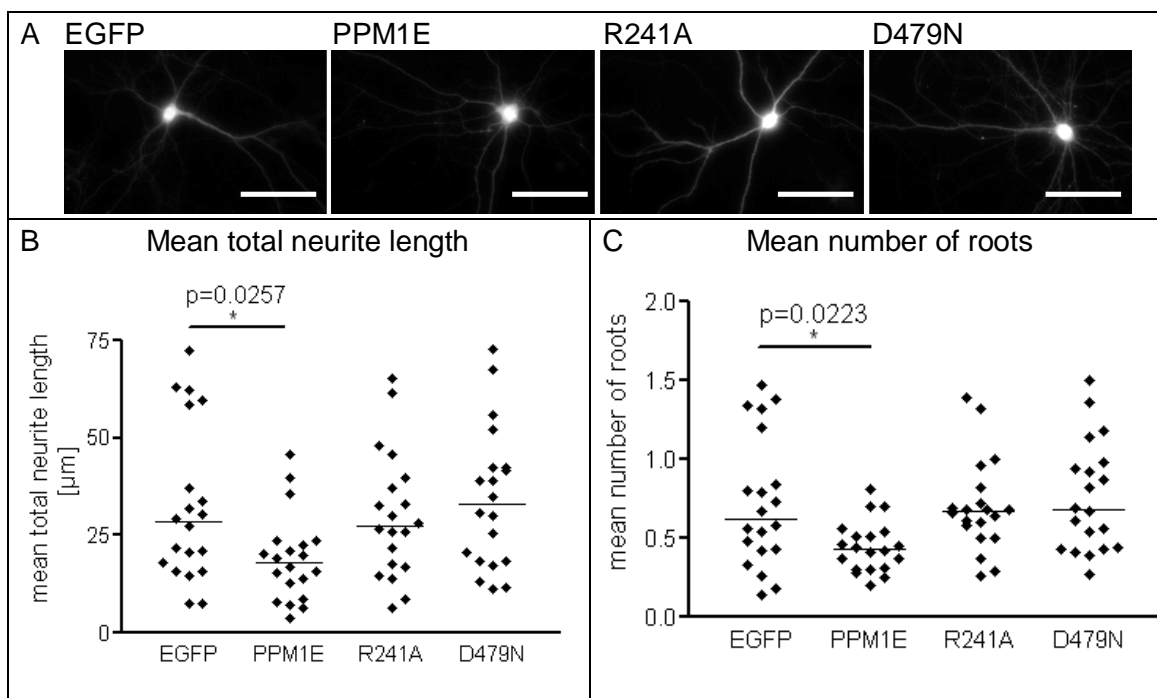


Figure 3.37: PPM1E activity mutants have no influence on the arborization of primary hippocampal neurons. (A) Example pictures. Scale bar 60 µm. (B) Mean number of roots (= primary dendrites). (C) Mean total neurite length. Each dot represents the mean from 17 pictures from one culture well. Horizontal bars represent the median. Reduction compared to EGFP control after transfection of 0.1 pAAV / PPM1E per 0.9 cm²: Roots: 30.7%. Mean total neurite length: 36.7 %. Statistical test with Mann-Whitney-U-test. Transfection with 0.1 µg pAAV / EGFP and 0.3 µg of pAAV / PPM1E, / PPM1E(R241A) or /PPM1E(D479N) on DIV 7 per 0.9 cm² hippocampal culture on DIV 7. Analysis on DIV21. n=20, from 2 independent experiments.

3.3.4.4 PPM1E effect on neuritic arbour is concentration-dependent

Additionally the effects of PPM1E on the number of primary dendrites and the total neurite length are strengthened with increased PPM1E expression (Figure 3.38). This effect is dependent on the amount of transfected pAAV / PPM1E and the maturity of the culture. Two different culture ages were tested to analyse whether the effect is rather an outgrowth-inhibiting or retraction-promoting effect. Interestingly at DIV 17 no significant differences in the number of roots and the mean total neurite length can be found, whereas the neurite length appears to be slightly reduced. Analysis on DIV 21 revealed that PPM1E expression has a concentration-dependent negative influence on the number of roots (Figure 3.38 A). These are reduced by 20 % and 38 % after transfection of 0.2 μg and 0.8 μg pAAV / PPM1E per 1.9 cm^2 culture. Moreover the PPM1E expressing neurons also had a by 25 % and 40 % shortened neuritic arbor than control neurons respectively (Figure 3.38 B).

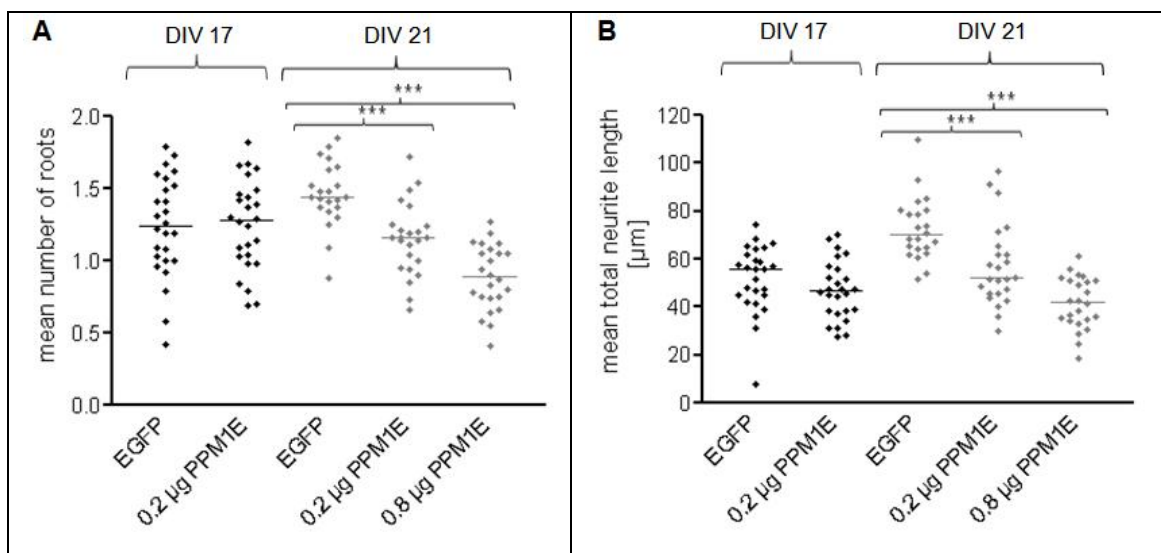


Figure 3.38: PPM1E overexpression significantly and concentration-dependent reduced the number of roots and the total neurite length. Transfection with 0.1 μg pAAV / EGFP and 0.1 μg or 0.4 μg of pAAV / PPM1E on DIV 7 per 0.9 cm^2 hippocampal culture on DIV 7. Analysis on DIV 17 or 21. $n > 22$, from three independent experiments. Each dot represents the mean from 17 pictures from one culture well. Horizontal bars represent the median. Reduction compared to EGFP control after transfection of 0.1 μg and 0.4 μg pAAV / PPM1E per 0.9 cm^2 : Roots: 20 % and 38 % ($p = 0.0002$ and < 0.0001) respectively. Mean total neurite length: 25 % and 40 % ($p = 0.0007$ and < 0.0001) respectively. Statistical test with Mann-Whitney-U-test.

PPM1E overexpression clearly decreases the branching in the neuronal arbour at DIV 21. However, PPM1E overexpressing neurons at DIV 17 show no reduction in roots or neurite length (Figure 3.38), hence this effect has its onset between these culture days. It might be facilitated by increase of the neurite retraction mediated through PPM1E.

3.3.5 Down-regulation of PPM1E with RNA interference affects spines and dendritic arborization

RNA interference is a powerful tool for the down-regulation of endogenous protein expression. However, *in silico* designed short hairpin RNAs (shRNA) can have unexpected side effects (Alvarez et al., 2006). These can be due to reactivity with other genes than the target gene or to overburdening of the endogenous micro RNA processing machinery. Therefore several shRNAs which were directed against PPM1E and two control shRNAs were tested for their down-regulation efficiencies and secondary effects on primary neurons.

3.3.5.1 Validation of shRNA constructs against rat PPM1E

The knock-down efficiencies of shRNA constructs which targeted rat PPM1E (rshRNA) were assessed by co-expression of rat PPM1E and shRNAs in a HEK cell line under control of the mammalian CMV and H1 promoters respectively, because no cell line was identified which expresses considerable amounts of endogenous rat PPM1E as described above. One scrambled shRNA sequence (scram_shRNA) (Vlachos et al., 2009), and one shRNA directed against human PPM1E (hshRNA4) with similar nucleotide composition to rshRNA4 served as control constructs. All plasmid constructs for shRNA expression also encode the EGFP protein, hence positive transfection of a neuron could be concluded from EGFP autofluorescence. Scram_shRNA had no effect on rat PPM1E expression in HEK cells (data not shown), however this scrambled shRNA obviously had deteriorating effects on the vitality of transfected neurons. Very few transfected neurons survived until DIV 21 and those showed a weak and fragmented expression of the co-expressed EGFP protein (Figure 3.39 A). Therefore hshRNA4 was employed as negative control in the following experiments.

In HEK cells the transfection efficiency was – in contrast to transfection of neurons - high enough to enable evaluation of the rat PPM1E levels through immunoblotting (Figure 3.39 B). The shRNA constructs rshRNA4 and rshRNA6 were directed against the rat PPM1E mRNA sequence and efficiently lowered the PPM1E expression while the control construct hshRNA4 had no effect on PPM1E.

These shRNA constructs were subsequently tested in primary neuronal culture by co-immunolabeling of endogenous PPM1E and MAP2 (Figure 3.39 C). The shRNAs number 4 and 6 against rat PPM1E (rshRNA4 and rshRNA6 respectively) also visibly reduced the expression of rat PPM1E (rPPM1E) in primary neuronal cells while the

control construct hshRNA4 had no effect on ratPPM1E expression primary neuronal culture (Figure 3.39 C).

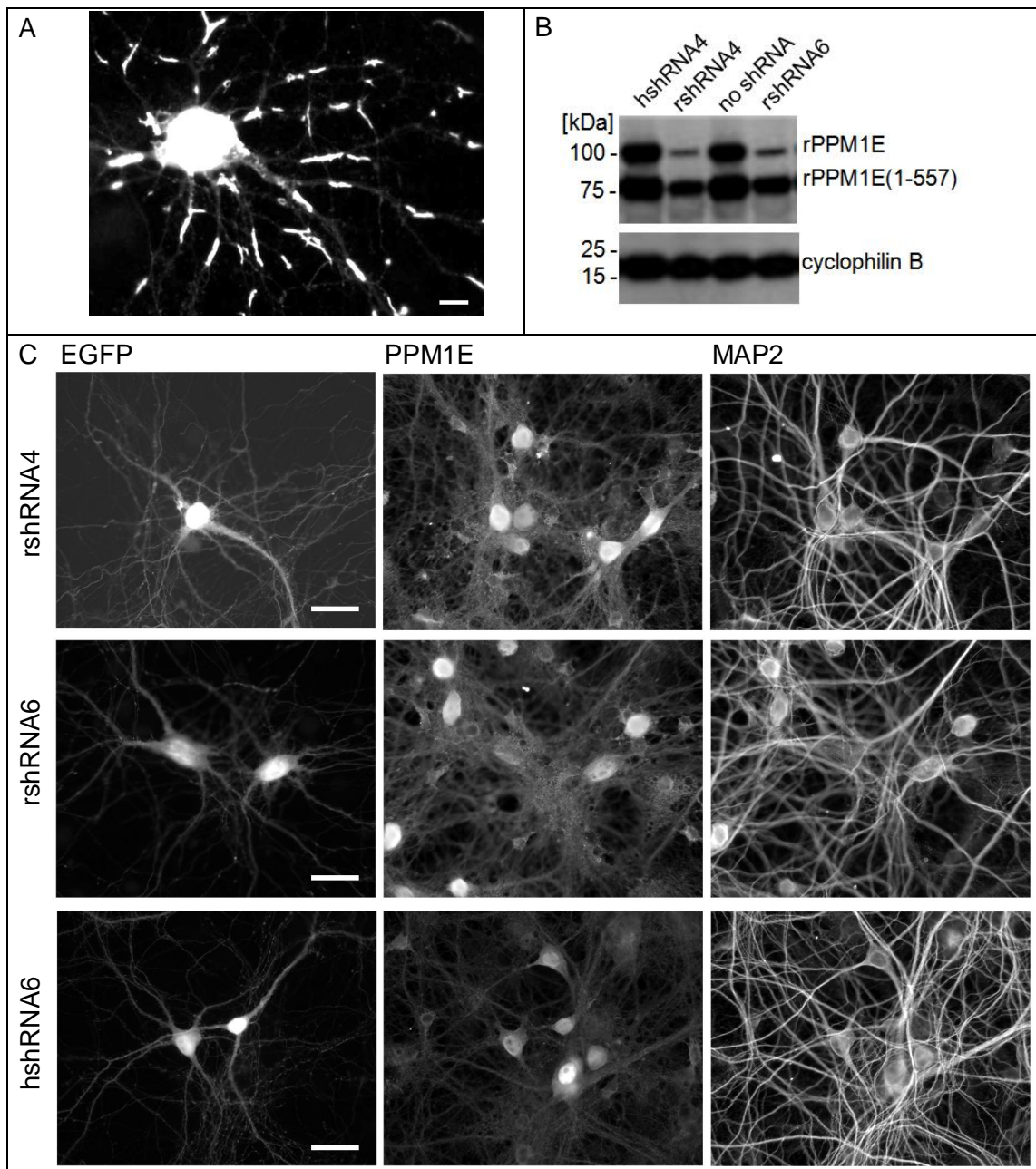
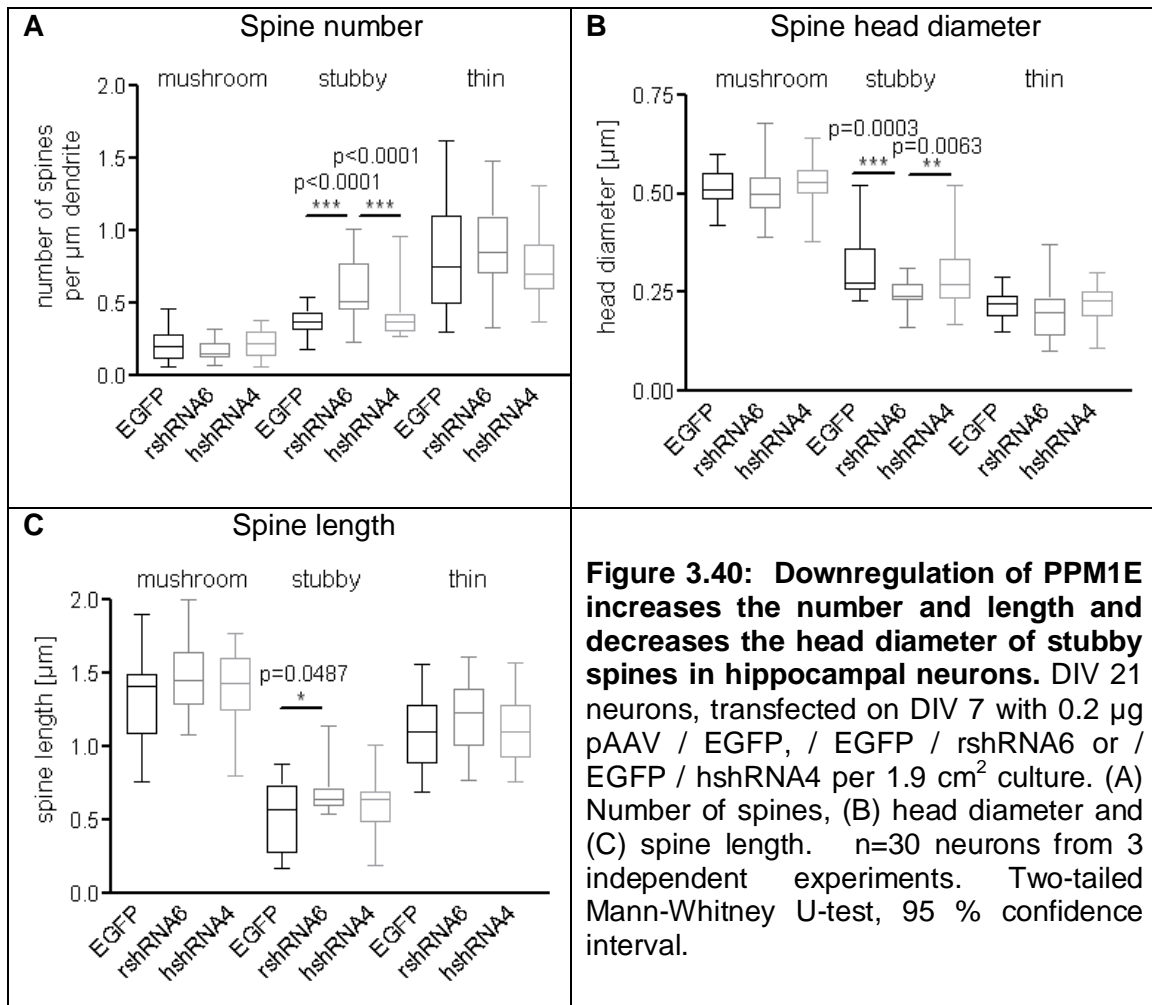


Figure 3.39: shRNA constructs down-regulate the expression of rat PPM1E. (A) Fragmented EGFP autofluorescence induced by co-expression of a scrambled shRNA construct. (B) Transient co-expression of different shRNAs with rat PPM1E in a HEK 293 GP cell line. Scale bar 10 μ m. (C) anti-human-PPM1E hshRNA4 has no effect on endogenous PPM1E expression in rat primary neurons, while anti-rat-PPM1E rshRNA4 and rshRNA6 down-regulate the endogenous PPM1E expression. (A, C) DIV 21 neurons transfected with 0.2 μ g pAAV/EGFP/shRNA per 7.5×10^4 neurons on DIV 7. Detected with anti-PPM1E(ENS) and anti-MAP2 antibodies. Scale bar: 23 μ m.

3.3.5.2 Effects of PPM1E down-regulation on dendritic spines

The endogenous rat PPM1E expression was down-regulated to test which effect the reverse regulation of PPM1E had on the spine number. The spine length and spine head diameter were determined again in a semi-automated manner with NeuronStudio software (Figure 3.40).



Along with the knockdown of PPM1E in single neurons by transfection (0.2 μg pAAV / GFP / rshRNA6 per 7.5×10^4 cells) a significant 38 % increase in stubby spine number from 0.37 to 0.51 spines per μm dendrite was determined (Figure 3.40 A). The numbers of mushroom and thin spines were not affected. Furthermore, the morphology of spines was affected in those neurons in which PPM1E expression was suppressed (Figures 3.38 B, C). The head diameter of stubby spines was significantly decreased by 13 % and 11 % compared to the control groups of EGFP and hshRNA4 transfected neurons respectively (Figure 3.40 B). The length of stubby spines was significantly increased by 11 % compared with the control group of EGFP transfected neurons (Figure 3.40 C). The length of stubby spine in neurons which express the control

hshRNA4 was however not comparable with that of the second control EGFP. The variance in both control groups was high. The morphology of mushroom and thin spines was not affected.

The shRNA4-hPPM1E control shRNA had no influence on the spines number, head diameter or length compared to the EGFP transfected control group, thus the effect is presumably specifically attributable to loss or reduction of endogenous PPM1E expression.

In summary, PPM1E downregulation has a positive influence on the number of stubby spines. The resulting group of stubby spines however has a smaller head diameter and increased length.

3.3.5.3 Effects of PPM1E down-regulation on neuritic arborisation

The effects of PPM1E downregulation on dendritic arborisation were investigated in a semi-automated manner with the 'Neurite' script (Acapella). Surprisingly the arborisation of DIV21 neurons was affected by the downregulation of PPM1E in a similar magnitude as by PPM1E overexpression (Figure 3.41, compare Figure 3.37).

In this experiment the transfection of two shRNAs against rat PPM1E (rshRNA4 and rshRNA6) was compared with EGFP control and PPM1E overexpressing neurons. No ineffective shRNA was accompanying, instead the control of the experiment was constituted by two shRNAs against the rat PPM1E which would be compared. Both shRNA constructs had similar deteriorating effect on the neuritic arbour and reduced the number of roots significantly by 35.8 % and 18.7 % and the total neuritic arbour length by 39.1 % and 13.2 %. PPM1E overexpression reduced the number of roots in a similar magnitude by 24.6 % and the neuritic arbour length by 20.4 %.

Although the down-regulation of PPM1E seems to have a positive influence on spine development, in that it increases the stubby spine number, it apparently has a negative influence on the stability of the neuritic arbour.

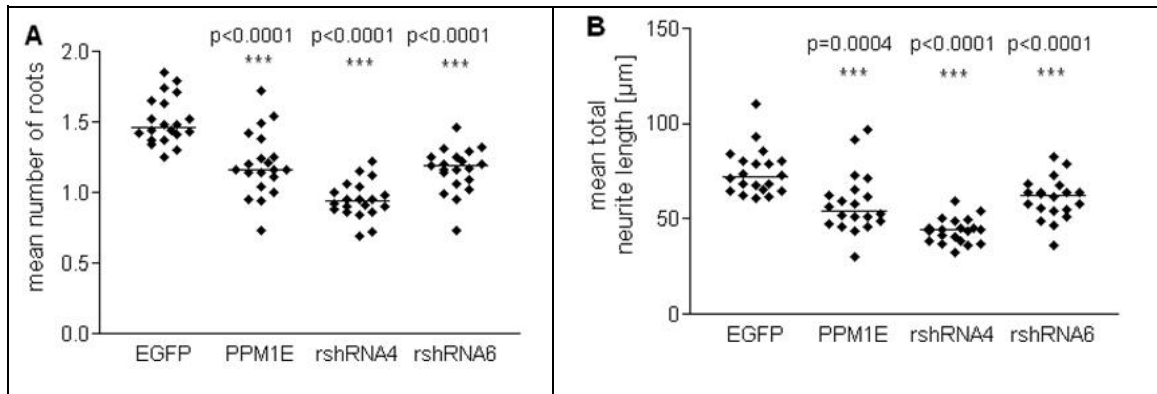


Figure 3.41: PPM1E overexpression as well as down-regulation reduce neuritic arborization. Transfection with 0.1 μg pAAV / EGFP or 0.1 μg of pAAV / PPM1E, / EGFP / rshRNA4 or // EGFP / rshRNA6 on DIV 7 per 0.9 cm² hippocampal culture on DIV 7. Analysis on DIV21. n=20, from 2 independent experiments. Each dot represents the mean from 17 pictures from one culture well. Horizontal bars represent the median. Reduction compared to EGFP control after transfection in PPM1E, rshRNA4 and rshRNA6 groups: Roots: 20.4 %, 35.8 % and 18.7 % respectively. Mean total neurite length: 24.6 %, 39.1 % and 13.2% respectively. Statistical test with Mann-Whitney-U-test.

3.3.6 Coexpression of hARHGEF6 had no effect on dendritic spines

ARHGEFs supposedly enable negative regulation of PAK1 function through PPM1E by acting as a molecular linker between PAK1 and PPM1E (Koh et al., 2002). Therefore this study tested whether concomitant expression of PPM1E and ARHGEF6 in dissociated primary neurons leads to a modulation of the PPM1E induced phenotype.

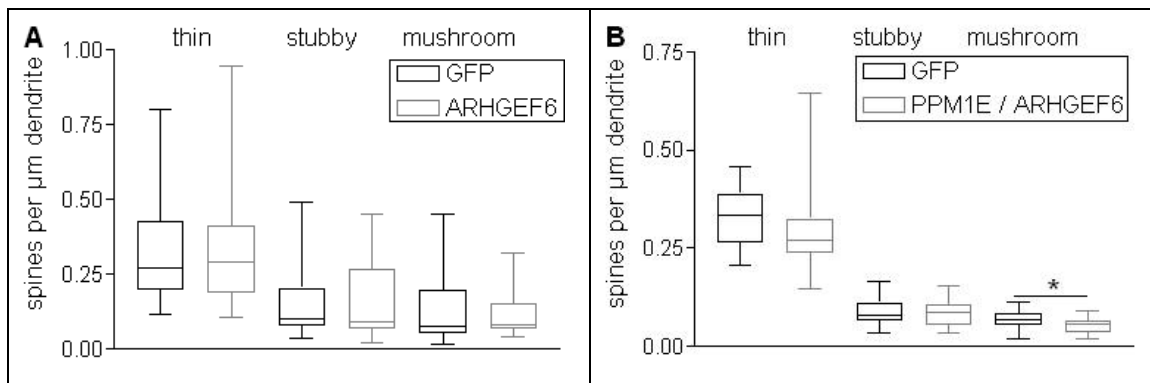


Figure 3.42: Overexpression of ARHGEF6 does not affect the number of spines nor does it increase the effect of PPM1E overexpression in mature hippocampal neurons. (A) ARHGEF6 expressing neurons show no changes in spine numbers compared to EGFP control. (B) PPM1E expressing neurons show a decrease in mushroom spine number by 22% ($p = 0.023$) comparable with that of PPM1E alone. DIV 21 neurons, transfected on DIV 7 with 0.2 μg pAAV / EGFP or (A) pAAV / ARHGEF6 or (B) / PPM1E and / ARHGEF6 per 1.9 cm² culture. (A) n=30 neurons from 3 independent experiments; (B) n=20 neurons from 2 independent experiments.

Moderate overexpression of ARHGEF6 alone from DIV 7 had no effect on the spine number in DIV 21 hippocampal neurons (Figure 3.42 A). Subsequently PPM1E and ARHGEF6 were co-expressed. Near-equimolar expression with 0.2 μg of both constructs per 1.9 cm^2 culture resulted in a reduction in mushroom-shaped spine number by 22% ($p=0.023$) compared to 23% by induced by 0.2 μg of pAAV / hPPM1E alone (Figure 3.42 B). The induced changes in spine density did therefore not differ from those induced by PPM1E expression alone (compare Figure 3.36 A and 3.42 B).

4 DISCUSSION

The protein phosphatase PPM1E was found to be up-regulated in early Braak stages in a screen for genes which are differentially regulated in early Alzheimer's disease (von der Kammer, 2009). PPM1E had not been correlated with neurodegenerative diseases before. The brain-specific phosphatase was initially identified as the closest homolog of the protein phosphatase PPM1F and described to be a regulator of the kinases CaMKII, CaMKIV and PAK1 (Koh et al., 2002; Takeuchi et al., 2001). Consequently, the research so far focussed on the influence of PPM1E on these kinases and related pathways *in-vitro* and in eukaryotic cell culture. This study aimed to complement these results by focussing on PPM1E properties in the native brain and PPM1E effects in the relevant model system of primary dissociated neuronal cell culture.

4.1 Characterization of PPM1E

4.1.1 Assessment of differential PPM1E expression is based on well-characterized human brain samples

The quality of human brain samples which are available for research has to be critically evaluated. Mainly due to a big variability in dissection and treatment protocols the quality of many available brain samples is low (Hulette, 2003). This is especially critical for mRNA analysis. Therefore the mRNA and protein quality of the samples used in this study has been evaluated prior to this study in a careful manner (von der Kammer, 2009). Although the quality of the human brain samples was satisfactory, this study started with the re-evaluation of potential correlations between PPM1E expression and different factors which might have been influenced by brain preparation. Others had found a correlation between the post-mortem time and the mRNA levels of certain groups of genes (Catts et al., 2005). The lack of a correlation of the PPM1E mRNA level with the post-mortem time, the pH of the interstitial fluid and the donor age, substantiated that the results of a differential PPM1E expression in early Braak stages is trustworthy (Figure 3.5).

Moreover, this study determined that the PPM1E(1-557) protein levels are correlated with its mRNA levels in a linear manner (Figure 3.9). Although proteins are also subjected to specific and unspecific degradation by proteases, they are usually considered to be more stable than RNAs. Even if both, PPM1E mRNA and protein were subjected to considerable degradation, it would be highly unlikely that protein and

mRNA and their normalization factors Cyclophilin B (mRNA) and α -Tubulin (protein) would be degraded in a concerted manner. Thus the correlation of protein and mRNA levels of PPM1E further substantiates that PPM1E is involved in or regulated by early Alzheimer's disease development as represented by Braak staging.

4.1.2 The truncation of PPM1E is conserved in all investigated organisms

Among the available insight into PPM1E one important point is that PPM1E is C-terminally truncated in such a manner that two nuclear localization sites are cleaved off from the rest of the phosphatase, which then still contains the catalytic domain and also N-terminal regions which are presumably required for substrate and cofactor interaction (Kitani et al., 2006). Such a truncation offers the very efficient possibility to determine the site of PPM1E activity – nucleus or cytoplasm - by cleavage of the protein. Therefore this study aimed to gain further insight into PPM1E truncation.

Rat PPM1E is carboxy-terminally truncated after proline 554, which was demonstrated by mass spectrometric analysis (Kitani et al., 2006). Rat PPM1E proline 554 is analog to proline 557 in the human PPM1E sequence. This study demonstrated *vice versa* that introduced vectors, which encode for full-length human PPM1E or only the truncated human PPM1E(1-557), result indeed in expression of proteins which run at the same height of approximately 80 kDa in electrophoresis (Figure 3.6). This complements the mass spectrometric data and indicates that the truncation mechanism is conserved in rat and human PPM1E.

Meanwhile the mechanism of the truncation remains mostly in the dark. Interestingly, the truncation mechanism is not restricted to neuronal or even mammalian cells but was also found in Sf9 cells and even *E.coli* cells which ectopically expressed full-length PPM1E (Figure 3.4; expression in *E.coli* not shown). Although others found a predominance of the full length PPM1E form in Sf9 cells (Kitani et al., 2006), the Sf9 cells and expression conditions in this study yielded predominantly truncated PPM1E. The truncation mechanism therefore might be either autoproteolytic or dependent on the presence of a protease, which is conserved in pro- and eukaryotes. Additionally, the mechanism is most likely a truncation on the protein level and does not represent the presence of mRNA splice variants because others have shown that only one transcript for full length PPM1E is detectable in Northern Blot analysis (Takeuchi et al., 2001).

Both the full-length and the truncated PPM1E run slower in the gelelectrophoresis than their actual molecular weight would indicate (Kitani et al., 2006). It has been suggested before that this indicates abnormal behaviour of PPM1E on SDS-PAGE (Kitani et al., 2003). In SDS-PAGE proteins are subjected to a denaturing heating step and then saturated with negatively charged SDS molecules according to the protein size. Usually thereby a separation of molecules according to their size is facilitated. The slower running behaviour of PPM1E and PPM1E(1-557) might for example indicate a reduced negative overall charge of both proteins or a denaturation-insensitive complex formation with another protein. One structural feature in the PPM1E sequence which might contribute to a reduced negative charge is a glutamate-rich, highly acid stretch in the N-terminal region of PPM1E (Appendix A 1).

Presumably the truncation of PPM1E regulates whether the phosphatase is transported into the nucleus or resides in the cytosol and thereby allows regional distribution of PPM1E activity. Here it is interesting to note, that the extend of post-translational removal of the C-terminal end differs between cell types (Figure 3.4). The ratio between truncated and full length PPM1E is for example greater in COS-7 cells than in Sf9 cells (Kitani et al., 2006). The present study found that the ratio is especially changed in favour of PPM1E(1-557) in H4 neuroglioma cells, in which no full length form is detectable (Figure 3.4). Although others found that PPM1E in the rat brain is not detectable in the full length form at all (Kitani et al., 2006), the anti-PPM1E(ENS) antibody, which was generated on behalf of this study, was able to detect also the full length form of PPM1E in rat brain extracts (Figure 3.10). This indicates that a lack of the full length form, in presence of the truncated PPM1E, might be attributable to the limited sensitivity of the respective antibody.

4.1.3 The levels of PPM1E are comparable in *R. norvegicus* and *H. sapiens*

PPM1E(1-557) is in all analysed human and rat brain samples the predominant PPM1E form (Figure 3.7). While the variability in the ratio between full length and truncated PPM1E in human brain samples seemed to be high, as determined by visual assessment, the direct comparison with adult rat brain samples indicated that human and rat PPM1E are comparable in that the truncated form is the predominant form and in that the ratio between full-length and truncated PPM1E appears to be in the same range.

This study analysed sub-samples (~60 mg) from human brain, which were broadly classified from the Netherlands Brain Bank (NBB) as frontal or temporal cortex. It is therefore possible that intra-cortical differences in the human frontal cortex, might be one reason for the apparent variability between the PPM1E/PPM1E(1-557) ratios of different donors. Therefore this variability might either indicate that the extent of full length PPM1E is highly variable in different areas of frontal cortex, or that the variability exists between donors.

No final statement can be made about differences in the absolute levels of PPM1E in rat and in human brain specimen, because it cannot be assumed that the anti-PPM1E(AGC) antibody binds to both proteins with the same affinity. However, the anti-PPM1E(AGC) antibody was derived to an immunization peptide against the very first 18 N-terminal amino acids of PPM1E which are identical in rat and human PPM1E (Table 2.8 and Appendix A 3). Therefore it is at least likely that the antibody binds to both proteins with similar affinity. The same careful assumption can be made for the full length and the truncated form of PPM1E. The statement that the truncated form of PPM1E is the predominant one is based on the assumption that the anti-PPM1E(AGC) antibody binds to the full-length and the truncated form with the same affinity. However, others have also seen a dominance of the truncated PPM1E form over the full-length form with antibodies, which were directed against different antigenic sequences in PPM1E (Kitani et al., 2006). It is therefore likely that any statement about the ratio between PPM1E and PPM1E(1-557) is not biased due to differential affinities of the antibody.

4.1.4 The PPM1E expression rises during development

The PPM1E expression in rat embryos on embryonal day (E) 9, 13 and 17 is considerably lower than in the adult rat (Figure 3.10). However PPM1E(1-554) expression is nevertheless clearly detectable in immunoblot analysis of E17 hippocampus and other E17 brain samples (Figure 3.10). The PPM1E(1-554) level in E13 embryos was lower than that in E17 embryos and no expression could be detected on embryonal day 9 (Figure 3.10). It is interesting to note the initial development of synapses and dendritic spines was described to fall between the embryonal days E9 and E10 (Li and Sheng, 2003).

A third anti-PPM1E(AGC) antibody-positive signal was detected in the immunoblots of E9 and E13 embryos and in E17 olfactory bulb (Figure 3.10). It has a size of

approximately 207 kDa and might therefore correspond to several multimeric variants of PPM1E(1-554) or PPM1E. However, no assumptions about the nature of the multimer can be made here because the two already existing PPM1E forms and the abnormal running behaviour of both forms in SDS-PAGE pose too many potential explanations.

Interestingly, in dissociated hippocampal culture no expression of PPM1E(1-554) can be found one day after the preparation of the culture from rat E17 hippocampi (Figure 3.11). This might indicate a reduction in PPM1E expression as a consequence of the disruption of the cellular network during culture preparation. This thought finds further basis in the fact, that the PPM1E expression in the neuronal culture rises with maturation of the culture considerably. The expression then stays constant approximately between day-*in-vitro* (DIV) 8 and DIV 20. With respect to data from Kitani et al. (2006), which showed that PPM1E is accumulated in the postsynaptic compartment, it is noteworthy that dissociated neurons exhibit considerably different spine morphology during the first week than in more mature cultures: During the first week in culture, the majority of dendritic spine-like structures resemble long filopodia without synaptic contacts and the majority of synapses are on short stubby-shaped spines (Biederer and Scheiffele, 2007; Papa et al., 1995). In contrast, in weeks two, three and four of the cultures, headless spines constitute a progressively smaller fraction of the population and are, on average, shorter than spines with heads.

For this study much effort was put into establishing reproducibly wealthy dissociated cultures. However, as described by others before, it was frequently observed that the mature hippocampal cultures started to deteriorate after DIV 21 (Banker and Goslin, 2002). A rising PPM1E expression was also observed usually at or after DIV 21 (Figure 3.11). The deterioration in old hippocampal cultures, which is associated with a loss in the integrity of the neuritic network and even a progressing detachment of neuronal soma from the growth substrate, could have influenced PPM1E expression levels.

Interestingly, a second side project to this study found that the PPM1E expression level is also dependent on the growth substrate: PPM1E levels were lower on the favoured substrate polystyrol than on glass slides, on which the neuronal network tends to be not as well as on polystyrol as determined by visual inspection (Diploma thesis D. Kampmann 2010, Appendix A 10).

4.1.5 PPM1E changes its localization during development

PPM1E is localized mainly in the cytoplasm and weakly also in the nucleus in adult rat and human neurons (Figures 3.12 and 3.15). This had already been shown by Kitani et al. (2006) who also made a detailed analysis of several human brain areas. The authors found additionally that very few large neurons of the mesencephalic trigeminal and facial nuclei instead showed an accumulation of PPM1E expression in the nucleus. This study showed that the cytoplasmic concentration of PPM1E is conserved between *Homo sapiens* and *Rattus norvegicus* and moreover also in the model system of dissociated rat neuronal culture after a certain level of culture maturation has been reached (Figures 3.12, 3.15 and 3.17).

Kitani et al. (2006) had proposed on the basis of immunolabeling of young DIV 6 hippocampal neurons that PPM1E is enriched in the neuronal nucleus. This provided the basis for the hypothesis that PPM1E and PPM1F act as nuclear and cytoplasmic equivalents and that the main target kinase for PPM1E is the nuclear CaMKIV. Interestingly this hypothesis now will have to be amended. This study confirmed that PPM1E is concentrated in the nucleus of young dissociated neurons and showed that this is a temporary phenomenon (Figure 3.17). During maturation of the neuronal culture the predominant localization of PPM1E is gradually changed towards the cytoplasm. The exact timepoint during maturation and also the extend to which the nucleus was depleted of PPM1E, varied between culture batches. Provided that indeed CaMKIV and CaMKII are target kinases of PPM1E as proposed by Takeuchi et al. (2001) and Kitani et al. (2006), PPM1E would have the chance to dephosphorylate both kinases at different timepoints during the neuronal maturation. PAK1 is mainly localized in the cytoplasm and can be recruited for example to focal adhesions upon its activation and would therefore also be a potential target of PPM1E in later differentiation stages of the neuronal culture (Kreis and Barrier, 2009; Dharmawardhane et al., 1999).

In one aspect, this study was interested in finding out whether this situation in primary neuronal culture finds an equivalent in the development of the intact rat brain. It was indeed found that PPM1E is enriched in the nucleus of E17 rat brain specimen, in contrast to the predominantly cytoplasmatic localization in the adult animal (Figure 3.16). Although no intermediate ages have been investigated it is reassuring for the choice of model system that the young dissociated, cultured neurons show the same

PPM1E expression pattern than seen in the embryonic E17 brain of which they were prepared.

The detected PPM1E expression in the younger embryonal stages E9 and E13 is very weak (Figure 3.10 and 3.16). However it seems that the slight PPM1E expression in these ages is not as restricted to the nucleus as on E17. Due to the very weak signal of the anti-PPM1E(ENS) antibody no conclusion is drawn from this. More sensitive methods like the *in situ* hybridization of short nucleotides, which are complementary to the PPM1E mRNA sequence, to rat embryonic brain samples, might gain reliable insight into PPM1E expression in these young embryonal ages in the future.

Although the localization of PPM1E changes with increasing culture maturity, the ratio between full length and truncated PPM1E remains largely unchanged as discussed above (Figure 3.11). This indicates that the truncation is not the mechanism which solely regulates the localization of PPM1E activity. While presumably only the full length form of PPM1E can be transported into the nucleus, it has been suggested on the basis of cellular fractionates that the truncation can also happen inside the nucleus (Kitani et al., 2006). Western blot analysis of cellular fractionates of rat brain demonstrated that truncated PPM1E is endogenously also present in the nucleus of cells (Kitani et al., 2006). The authors further showed that the full length form of PPM1E was found in the nucleus as well as in the cytoplasm.

4.1.6 PPM1E is enriched in the post-synaptic compartment and at sites of high metabolic activity

It has been suggested that PPM1E is enriched at synaptic sites because electron microscopic analyses with anti-PPM1E antibodies showed a stronger signal in the post-synaptic compartment of dendritic spines in rat hippocampus (Kitani et al., 2006). Indeed this localization was conserved in the human brain and in rat hippocampal culture: In human frontal cortex small globular sites, which were enriched in PPM1E, were co-localized with the high affinity glutamate transporter 'excitatory amino acid carrier 1' (EAAC1) which is responsible for re-uptake of the neurotransmitter glutamate from the synaptic cleft (Figure 3.18). Moreover, PPM1E was not co-localized with the pre-synaptic protein GAD67 (glutamic acid decarboxylase 67-kDa isoform) indicating a strictly post-synaptic localization also in the human brain (Figure 3.19).

The analysis of postsynaptic PPM1E localization was repeated in dissociated neuronal culture, to validate the culture further as a suitable model system. Small globular enrichment of PPM1E can also be found here opposed to the presynaptic marker Synaptophysin and in close spatial correlation with dendritic spines (Figure 3.22). The conserved localization of PPM1E in human and rat brain as well as in rat dissociated hippocampal culture strengthens the argument that phenotypic effects of PPM1E observed in primary culture allow conclusions about potential effects in brain.

To shed light on the cause for the occasionally occurring fragmented expression pattern of PPM1E in neurites (compare Figure 3.2), the potential co-localization of PPM1E with larger sub-cellular structures was investigated. PPM1E was not found to co-localize with endoplasmic reticulum, the golgi apparatus or F-actin. However, sites of globular enrichment of PPM1E showed also accumulation of mitochondria (Figure 3.23). The PPM1E globules are not co-localized with the mitochondria, but merely enriched in the same neuritic section. This might indicate that PPM1E is enriched at sites of high metabolic activity. Interestingly, growing evidence suggests that mitochondrial dysfunction is one of the key intracellular lesions associated with the pathogenesis of Alzheimer's disease (Eckert et al., 2003; Castellani et al., 2002). Therefore a potential connection between PPM1E and mitochondrial activity could be an interesting research subject for the future.

This study investigated the effects of PPM1E on dendritic spines (see below), therefore it has to be stated that mitochondria are rarely found within spines in mature neurons but that they are essential for the formation and maintenance of spines and synapses (Li et al., 2004). Molecular manipulations, which reduced mitochondria content in dendrites, lead to a loss of spines and synapses in primary dissociated hippocampal neurons, while an increase in dendritic mitochondria enhanced the number and plasticity of spines and synapses (Li et al., 2004). Thus, dendritic mitochondria seem to be essential for the support of synapses.

The globular structure of the PPM1E enriched sites in the neuritic compartment suggests that PPM1E might be located inside a vesicle. This was not analysed in further detail in the current study, however a number of vesicular structures come into consideration. For example mitochondria-derived vesicles (MDVs), which have recently been shown to transport cargo from the mitochondria to the peroxisomes (Neuspiel et al., 2008). Other types of vesicles which might accumulate together with mitochondria at sites of high metabolic activity might also be candidates for the PPM1E transport.

Life-imaging would enable the researcher to follow the route of PPM1E transport, and it will be interesting to investigate in the future whether vesicular structures facilitate the transport of PPM1E.

4.2 Effects of PPM1E

A gene like PPM1E, which is transcriptionally up-regulated in early Alzheimer's disease could be part of an adaptive answer of the cell to even earlier changes in the brain, but could also be involved in the early steps of disease development. In case the gene would be up-regulated as part of an adaptive signaling cascade, the gene might have a neuroprotective effect or, in contrast, trigger apoptotic cascades. Both effects could be protective for the underlying cellular network. In the present study no pro-apoptotic effect of PPM1E was observed. Therefore the characterization of PPM1E as potential drug target for Alzheimer's disease continued with the analysis of whether PPM1E is neuroprotective or induces Alzheimer-like degenerative phenotypes in primary neuronal culture.

4.2.1 Suitability of rat primary neurons as a model system

The identification of suitable model systems is a major issue for the Alzheimer's disease research community. Many resources have been spent on the establishment of mouse models, and none of them can model the complete Alzheimer's disease phenotype found in humans. This is not surprising because even closer relatives of *Homo sapiens*, like non-human primates, do not develop the whole range of Alzheimer's disease related changes in the brain (Rosen et al., 2009). Thus, the dissociated primary neuronal model used in this study has not the pretence to investigate more than the concerned PPM1E-mediated pathway of spine- and neuritogenesis. Additionally, primary neuronal culture can of course not claim to make any predictions of cognitive phenotypes, but can solely draw analogies.

The primary culture is a valid model for the investigation of neuritic arborization and spine development. The fact that aspects of PPM1E truncation and localization were comparable between the culture and human and rat brain as discussed above, strengthens the relevance of the culture in the investigation of PPM1E effects.

These considerations are especially important for the investigation of PPM1E because the phosphatase is not conserved in *Drosophila melanogaster*²⁰, another model system which is frequently used to analyse neurodegenerative diseases (Cauchi and Van Den Heuvel, 2006; Ghosh and Feany, 2004; Muqit and Feany, 2002). Moreover, although other members of the putative PPM1E signaling pathway, like dPAK, dPIX and CaMKII, are conserved in the fruitfly, ectopic PPM1E expression did not lead to considerable phenotypic effects on neuronal development in the fly eye or the central nervous system (Appendix A 9).

4.2.2 Ectopic PPM1E expression affects the expression levels of CaMKIV and potentially of CaMKII α and PAK1

Although three target kinases, CaMKIV, CaMKII and PAK1, have been proposed for PPM1E, for none of them the PPM1E activity has been shown in a model in which neurodegeneration was investigated. The most relevant *in vivo* result showed that knock-down of PPM1E during zebrafish embryogenesis leads to an increase in apoptotic cells in brain and spinal cord (Nimura et al., 2007). This was assigned to the regulation of CaMKIV by PPM1E, because it has been found that CaMKIV is important for the regulation of apoptotic events (Walters et al., 2002; Wayman et al., 2000; McGinnis et al., 1998). Moreover, the authors stated that PPM1E significantly decreased phospho-CaMKIV in ionomycin-stimulated Neuro2a cells (Nimura et al., 2007). Ionomycin stimulation of Neuro2a cells leads to an erratic rise of CaMKIV phosphorylation.

The *in vitro* activity of human PPM1E on a phosphorylated peptide modeled after the CaMKII phosphorylation site was confirmed in this study (Figure 3.24). Additionally the phosphorylation of CaMKIV, CaMKII and PAK1 was investigated with quantitative immunoblots in lysates of primary neuronal cultures which ectopically expressed considerable amounts of PPM1E (Figure 3.29 to to Figure 3.33). Phosphorylation-specific antibodies were available for all kinases, although the anti-phosphoPAK antibody recognized also other Type I PAKs (PAK2 and PAK3) as discussed below.

A faster investigation of the phosphorylation of the kinases for example by immunolabeling of fixed monolayer cell culture was not feasible because all three

²⁰ compare sequence alignment with closest homolog of PPM1E (Ppm1-PA) in *Drosophila melanogaster* in Appendix A 6.

kinases²¹ were expressed throughout the network of dendrites and axons in mature neurons. Meanwhile PPM1E was only visibly expressed in the dendrites. The dense axonal meshwork around the dendrites did not allow a proper visualization of the extend of phosphorylation in the dendrite (Figure 3.31 for phospho CaMKII α immunolabeling).

Surprisingly, quantitative immunoblots of ectopically PPM1E expressing and control cultures revealed no significant difference in the phosphorylation level of these kinases (Figures 3.30, 3.32 and 3.33). Instead, the expression of the kinases itself appeared to be influenced by the PPM1E expression considerably. CaMKIV expression was significantly higher on the mRNA level and also by trend increased on the protein level in cultures with a higher PPM1E level, whereas the expression of CaMKII α was only by trend higher on the mRNA and protein level. The levels of PAK1 were also not significantly affected but showed a strong trend toward a decrease on the protein level. The overall level of phosphorylated protein was for all three kinases not significantly affected, and only for CaMKIV the levels of phosphorylated kinase were significantly reduced when they were normalized to the overall expression level of the protein.

PAK1 is highly related to PAK2 and PAK3 (together they are referred to as Group I Pak), with which it shares conserved phosphorylation sites (Bokoch, 2003). PAK1 phosphorylation was investigated in cortical instead of hippocampal culture because others found that PAK1 here is the main PAK species (Jacobs et al., 2007). It can therefore validly be claimed that, although the phospho-PAK-specific antibody would also recognized PAK2 and PAK3, their contribution can be neglected in this case.

Notably, it can be concluded that the phosphorylation levels of the kinases were clearly not as affected as their expression levels. This unexpected effect did however show that PPM1E levels do have a severe influence on the investigated pathway. The effects on the expression levels of CaMKII α and PAK1 seem contradictory because a rising CaMKII α concentration exerts positive influence on the stabilization of filamentous actin, while decreased levels of PAK1 could have the opposite effect (compare pathway in Figure 1.6). This might indicate a compensatory mechanism of the cell. However, both kinases have multiple functions therefore no conclusion can be drawn at this point. Moreover, the absolute levels of phosphorylated, active forms were not strongly affected for any of the three proposed effector kinases.

²¹ Several publications state that CaMKIV is expressed exclusively in the nuclei of brain. However this study observed that CaMKIV is located in the nucleus during the first two weeks of a primary neuronal culture and then translocates, similar to PPM1E, into the cytoplasm (data not shown).

An additional technical problem with the manufacture of highly concentrated adeno-associated viruses (AAV), encoding the PPM1E activity mutant R241A, interfered in the present study with the proper incorporation of equal numbers of negative controls into the immunoblot quantification of kinases (Figures 3.30, 3.32 and 3.33). The low yield of rAAV_PPM1E(R241A) virus after purification was most likely associated with the vector DNA molecule: The virus particle number from the mutant-encoding virus preparation was considerably lower in all but one virus preparation than that from PPM1E-encoding viruses. Meanwhile the concerned activity mutant constructs were sequenced and did not show any nucleotide exchanges. Moreover the concerned constructs led to a comparable expression level of the mutants in transfected neurons as determined by anti-Myc-tag labelling (Figure 3.27), and the integrity of the PPM1E(R241A) protein is not affected as shown in a successful highly concentrated virus preparation which was able to induce a high level of PPM1E(R241A) expression (Figure 3.28). This preparation and one that was slightly less concentrated were successfully used for a number of infections of the neuronal culture (Figures 3.30 D and 3.32 D).

These few successful controls at least indicate that the effects on CaMKII α and CaMKIV are true effects. In summary, clearly this study cannot confirm prior data from *in vitro* and cell line experiments, which showed a reduction in phosphorylation of these kinases by PPM1E. Rather, a modulatory effect for kinase expression is suggested by these results. Surprisingly the trends in expression of CaMKs and PAK1 are oppositional, although all three kinases in their active state act as positive stabilizers or modulators on the actin cytoskeleton. Most likely, this adaptation of the kinase expression could represent a compensatory reaction of the cellular metabolism. This would not be surprising in the case of these three kinases because they are all crucial for several functions of the cell. For example, PAK1 controls the correct morphology, orientation, and radial migration of neurons in the cerebral cortex (Causeret et al., 2009). CaMKII α and CaMKIV fulfil additional functions in the structural stabilization of spines and in the CREB-mediated transcription initiation respectively (Jourdain et al., 2003; Pratt et al., 2003; Silva et al., 1998a; Silva et al., 1998b).

4.2.3 PPM1E expression affects the stabilization of dendritic spines

Ectopic PPM1E expression in dissociated hippocampal neurons led specifically to a decrease in the number of mushroom-shaped spines and a decrease in the length of the group of stubby spines (Figures 3.34 and 3.35). Expression of the PPM1E activity

mutants of PPM1E(R241A) and PPM1E(D479N) had no effect on the dendritic spines compared with EGFP expressing control neurons.

A loss of spines has also been observed very early during the development of Alzheimer's disease (Selkoe, 2002a). Therefore the reduced mushroom spine number in cultured neurons which have higher levels of PPM1E shows an interesting analogy to the increased PPM1E levels in AD-affected individuals (von der Kammer, 2009). Mushroom spines are considered to be the most stabilized spine structures and have also been referred to as "memory" spines, because they putatively facilitate the long-term stabilization of neuronal circuits which are crucial for memory retention (Tackenberg et al., 2009).

The putative PPM1E target kinases CaMKII and PAK1 are involved in the regulation of F-actin in the dendritic spines (compare pathway in Figure 1.6; (Saneyoshi et al., 2010)). They positively influence the stabilization of F-actin by promoting the phosphorylation-mediated inactivation of the F-actin-severing protein cofilin. Cofilin and a related actin depolymerising factor (ADF) bind to actin filaments and thereby induce structural changes that promote depolymerisation and severing of actin filaments (Bamburg, 1999; McGough and Chiu, 1999; McGough et al., 1997). A lack of mushroom spines and a reduction in stubby spine length in mature primary neurons due to increased levels of PPM1E, indicates that the phosphatase negatively influences the stabilized F-actin cytoskeleton in these spines.

Inversely, the down-regulation of PPM1E influenced only the group of stubby spines while the numbers and morphology of thin and mushroom-shaped spines was not affected (Figure 3.40). Stubby spines of neurons with a lower endogenous PPM1E level were shorter and had a smaller head size. Additionally the overall stubby spine number was increased in these neurons considerably. The reduction of PPM1E levels in these neurons appears to have enhanced new spine formation, although these new spines obviously do not develop into highly stabilized, large or long spine structures. Since spines are dependent on pre-synaptic input for their stabilization, the lack of this input might have hindered the stabilization of the new spine structures.

A particular cause for concern in the use of RNA interference is that shRNA molecules mimic precursors of another class of small RNA molecules, the microRNAs, and thereby might cause side effects attributable to competition for endogenous microRNAs processing molecules. Off-target mRNA degradation as well as induction of interferon

response have been reported for shRNA use (Jackson and Linsley, 2004; Persengiev et al., 2004). Therefore this study included a negative control shRNA. This negative control shRNA (hshRNA4) did not show any effect on dendritic spines compared with untreated controls (Figure 3.40). This suggests that the effects of anti-PPM1E shRNAs have a basis in the down-regulation of PPM1E expression.

It remains unclear whether PPM1E requires the activity of the guanosine exchange factor ARHGEF6 for its putative activity on PAK1 (Koh et al., 2002), because a complementary increase in ARHGEF6 expression in the neurons did not lead to a stronger effect on the dendritic spines (Figure 3.42). This might indicate that the endogenous concentration of ARHGEF6 was not limiting to PPM1E activity or that the primary mode of action which influences the spine number and morphology is not mediated through PPM1E activity on PAK1 but on CaMKII.

A moderate increase in ARHGEF6 levels had no effect on dendritic spines in the present study (Figure 3.42). However, mutations in ARHGEF6 are associated with degenerative spine phenotypes *in vivo* in the nonspecific X-linked and X-chromosomal specific mental retardation (Govek et al., 2004; Kutsche et al., 2000; Yntema et al., 1998).

A number of other members of the same F-actin regulating pathway exhibit similar deteriorating influence on dendritic spines like PPM1E. For example, the experimental enhancement of CaMKII signaling induces spine formation and increases synapse number (Jourdain et al., 2003; Bienvenu et al., 2000; Allen et al., 1998). Phenotypically, PAK1 has also been implicated in regulating dendritic spine shapes (Penzes et al., 2003; Meng et al., 2002).

Defects in some of pathway members are also associated with mental retardation: In Angelman syndrome, a disorder in which a maternal null mutation of the Ube3a ubiquitin ligase gene causes mental retardation and for which the mechanism is still unclear, a misregulation of CaMKII localization and function has been implicated (Weeber et al., 2003). Additionally, mutations in the CaMKII/IV effector LIMK-1 have been linked to William's syndrome, a mental disorder with abnormal spine morphology (Kaufmann and Moser, 2000; Bellugi et al., 1999; Bamberg, 1999; Frangiskakis et al., 1996). PAK family members have been genetically linked to several forms of mental retardation and spine dysgenesis in humans (Newey et al., 2005; Ramakers, 2002). Non-functional PAKs that impact dendritic spine morphogenesis are described for

several PAK family members in conjunction with AD (PAK1: (Zhao et al., 2006); PAK3: (McPhie et al., 2003); PAK5: (Matenia et al., 2005)), and X-linked mental retardation (PAK3: (Gedeon et al., 2003; Bienvenu et al., 2000; Allen et al., 1998)).

The relevance of the pathway is further emphasized by the connection of the actin-binding proteins cofilin and the isoform A of drebrin to Alzheimer's disease: Cofilin and the related actin depolymerising factor (ADF) bind to actin filaments and thereby induce structural changes that promote depolymerisation and severing of actin filaments (Bamburg, 1999; McGough and Chiu, 1999; McGough et al., 1997). It has been shown that soluble A β peptides, which are also discussed as causative factors for AD, activate the actin depolymerising factor cofilin (Maloney and Bamburg, 2007). Moreover, the level of the F-actin stabilizing protein drebrin A is markedly reduced in the brains of AD patients (Counts et al., 2006; Hatanpää et al., 1999; Harigaya et al., 1996). In mature hippocampal culture, A β peptides have been shown to down-regulate the levels of drebrin A (Lacor et al., 2007; Hatanpää et al., 1999). Additional studies indicate that drebrin is involved in the pathogenesis of the disease (Lacor et al., 2007; Zhao et al., 2006; Mahadomrongkul et al., 2005; Calon et al., 2004).

The abnormally modulated numbers and distorted morphologies of dendritic spines in AD and in other mental disorders indicate that fully functional dendritic spines are required for proper brain function (Selkoe, 2002a). PPM1E levels exert a strong influence specifically on the group of mushroom spines, which are thought to be especially important for the retention of memory. This indicates that elevated PPM1E levels might indeed play a role in the progressive deterioration of dendritic spine number and morphology which is found in Alzheimer's disease.

4.2.4 PPM1E expression affects the complexity of the dendritic arbor

The proposed PPM1E target kinase CaMKIV enables in concert with the activation of LIMK-1 the neurite outgrowth in a Neuro-2a murine neuroblastoma cell line (Takemura et al., 2009). Therefore the dendrite arbor in neurons with an increased PPM1E expression was investigated, although the morphology in neurons with moderate increases in PPM1E expression was not strikingly changed at the first visual impression (Figure 3.37 A). The PPM1E expression was experimentally dysregulated on DIV 7 in the neurons. After approximately 2 weeks of PPM1E dysregulated expression the dendritic arbor was analysed. Higher levels of PPM1E decreased the number of primary dendrites, which are defined as dendrites which branch off directly

from the neuronal soma, significantly and in a concentration-dependent manner. Meanwhile PPM1E active site mutants did not influence the neuronal arbor compared with EGFP expressing control neurons (Figures 3.37). Moreover the arbor was not significantly affected on DIV 17, while the number of roots was significantly reduced by DIV 21 (Figure 3.38). The reduction in primary dendrites in neurons with higher PPM1E expression is accompanied by a reduced overall length of the dendritic arbor. Due to the maturity of the primary culture at the date of analysis and the onset of the effect only after DIV 17, it is highly likely that the visible effects on primary dendrite number are attributable rather to retraction of existing dendrites than to outgrowth of new neurites.

Interestingly, also the down-regulation of PPM1E activity by shRNAs, which were directed against endogenous PPM1E, negatively affected the number of primary dendrites (Figure 3.41). For the analysis of dendrite arborization two shRNAs against rat PPM1E were employed to control the specificity of the effect. Both shRNAs reduced the number of primary dendrites to different extends. The variation of the severity of this effect between the two anti-PPM1E shRNAs, might be attributable to different extends of PPM1E downregulation (Figure 3.41). This different extend of downregulation might for example result from different affinities of the shRNA sequences to the mRNA of rat PPM1E.

A similar bi-directionally negative effect on the neurite outgrowth of neurons has been shown for the CaMKIV target kinase LIMK-1. Knockdown or inhibition, but also overexpression of LIMK-1 suppress neurite outgrowth and it was shown that these effects involve the phosphorylation of the actin-filament disassembling factor cofilin (Endo et al., 2007;Tursun et al., 2005;Rosso et al., 2004;Endo et al., 2003). Cofilin is inactivated by LIMK-1 mediated phosphorylation. The fact that deregulation of LIMK-1 or PPM1E in both directions causes similar effects, indicates that a proper balance of the activity of this pathway is required for homeostasis of the dendritic arbor.

PPM1E apparently has a dual functionality in the regulation of the actin cytoskeleton in spines and in the dendrites. Dystrophic dendrites are frequently found also in the brains of Alzheimer's disease patients. They are especially enriched close to amyloid plaques. The fact that both of the investigated neuronal phenotypes find analogs in the AD-affected brain, substantiates the hypothesis that PPM1E might play a role in early disease developments.

5 CONCLUSIONS AND OUTLOOK

Suitability of PPM1E as drug target for neurodegenerative diseases

The present study showed that increased levels of PPM1E have a degenerative effect on the number of dendritic mushroom spines and on the dendritic arbor. Additionally it was demonstrated that the previously shown elevation of PPM1E mRNA levels in early stages of Alzheimer's disease is also reflected on the protein level. This indicates that the phosphatase might play a role in AD disease development.

PPM1E could be recommended as a potential drug target for the treatment of Alzheimer's disease, because its expression is brain and neuron-specific. Thus it would be feasible to specifically address neuronal signalling pathways through the inhibition of PPM1E. However, low amounts of PPM1E expression have been found in Northern Blot analysis of testis (Kitani et al., 2003; Takeuchi et al., 2001). Side effects on this organ should therefore be critically examined. Additionally, the inhibition of PPM1E would have to be dosed carefully to avoid side effects on the sensitive LIMK-1 / cofilin signaling pathway which regulates neuritic arborisation and which has negative regulatory effects when it is overtly overstimulated but also when it is strongly inhibited.

A problem might be posed by the development of suitable PPM1E inhibitors. In the past the identification of phosphatase inhibitors has been proven difficult, due to their relatively large catalytic site. However, the substrate specificity of PPM1E and PPM1F is presumably facilitated by specific binding to the respective substrate with that part of the E/Fhd domain, which is not part of the PP2C domain region. Additionally PPM1E contains N- and C-terminal stretches which are exclusive for PPM1E and not present in PPM1F. It should therefore be feasible to identify a molecule which specifically inhibits PPM1E, based on these distinct structural features.

Additionally it would be a most interesting research subject for the future to further elucidate the correlation between the truncation of PPM1E and its subcellular localization. Moreover, an investigation of the tight spatial association of PPM1E and enrichment of mitochondria in dendrites might be interesting for the Alzheimer research community, because it has been suggested that defects in mitochondria are associated with AD.

Clearly, many challenges remain, but the present study has shown that PPM1E is potentially threatening for the maintenance of proper spine and dendritic arbor morphology in the AD-affected brain. Therefore PPM1E might be a promising new drug target for Alzheimer's disease.

APPENDIX

A 1. Alignment of human PPM1E and PPM1F protein sequences

PPM1F	-----	
PPM1E	MAGCIPEEKTYRRFLELFL GEFRGPCGGGEPEPEPEPEPEPEPEPEPEPELVEAEAAE	60
PPM1F	MSSGAPQKSSPMASGAEEETPGFLDTLLQDFPALLNPED-----	38
PPM1E	ASVEEPGEEAATVAATEEGDQE QDPEPEEEAAVEGEEEEGAATAAAAPGHSAVPPPPQ	120
	* * :.:. :.:.:** * . :. :.*: . *:	
PPM1F	--PLP--WKAPGTVLSQEEVEGELAEELAMGFLGSRKAPPPLAAALAHEAVSQLLQTDLSE	94
PPM1E	LPPLPPLRPLSERITREEVEGESLDLCLQQLYKYNCPFLAAALARATSDEVLQSDLSA	180
	*** :. . :. :***** :*:. * . :.*. *****: :. :.***:**	
	Glu cluster in PPM1F	
PPM1F	FRKLPREEEEEEDDDEEEKAPVTLLEDAQSLAQSFNRLWEVAGQWQKQVPLAARASQRQ	154
PPM1E	H-YIPKETDGTGEG ----- TVEIETVKLARSVFSKLHEIC CSWVKDFPLRRRP-QLY	229
	. :** : * . . :. :. :***:*.*:* *:. * **:** * . *	
PPM1F	WLVSIIHAIRNTRKMEDRHVSLPSFNQLFGLSDPVNRA YFAVFDGHG GVDAARYAAVHVH	214
PPM1E	YETSIIHAIKNMRKMEDKHVCIPDFNMLFNLEDQEEQAYFAVFDGHG GVDAAIYASIIHLH	289
	: .*****:* *****:* .:*.* **.* * :*****:***** * :.***:	
PPM1F	TNAARQPELPTDPEGALREAFRRTDQMFRLKAKRERLQSGTTGVCALIAGATLHVAVLGD	274
PPM1E	VNLVVRQEMFPHDPAEALCRAFRVTDERFVQKAARESLRCGTGVVTFIRGNMLHVAVVGD	349
	. * .** :* ** ** .*** ** : :.*** ** * :.***** :.* * *****:**	
PPM1F	SQVILVQQGQVVKLMEPHRPERQDEKARIEALGGFVSHMDCWRVNGTLAVSRAIGDVFOK	334
PPM1E	SQVMLVRKGAVELMKPHKPDREDEKQRIEALGGCVVWFGAWRVNGSLVSRRAIGDAEHK	409
	:**:*.* ::**:*:*:* * ***** * :. .*****:***** . :*	
PPM1F	PYVSGEADAASRALTGSSEYLLACDGFDFVPHQEVVGLVQSHLTRQQGSGLRVAEELV	394
PPM1E	PYICGDADSASTVLDGTEDYLILACDGFYDTPNPDEAVKVVSDHLKENNGDSSMVAHKL	469
	** :.*:**:* * * :*****:*****:* * :.* :.* .*. . :. . . * . :**	
PPM1F	AAARERGSHDNITVMVFLRDP -----QELLEGGNQEGD-----	429
PPM1E	ASARDAGSSDNITVIIVFLRDMNKAVNVSEESDWT ENSFQGGQEDGGDDKENHGECK RPW	529
	*:** : * *****:***** :. :.*:**. * *	
	▼	
PPM1F	PQAEG-----	434
PPM1E	PQHQCSAPADLGYDGRVDSFTDRTSLSPGSQINVLEDPGYLDTQIEASKPHSAQFLLPV	589
	** :	
PPM1F	-----RRQDLPSSLPEP-----ETQAPPR	453
PPM1E	EMFGPGAPKKANLINELMMEKKSQVQSSLPEWSGAGEFPTAFNLGSGTEQIYRMQSLSPVC	649
	. :. :. : ***** :. : *	
PPM1F	S-----	454
PPM1E	SGLENEQFKSPGNRVS RLSHLRHHYSKKWHFRFRFNPKFYSFLSAQEPSHK IGTSLSSLTG	709
	*	
PPM1F	-----	
PPM1E	SGKRNRIRSSLPWRQNSWKGYSENMRKLRK TH DIPCPDLPWSYKIE	755

Symbols: "*" the residues in that column are identical in all sequences in the alignment. "." conserved substitutions as defined in Material and Methods section. "." semi-conserved substitutions as defined in Material and Methods section.

PPM1E/1F homology domain (E/Fhd) as defined by Kitani et al. (2006) shaded in light grey. Catalytic PP2C phosphatase domain in bold letters (Tada et al., 2006). Protein phosphatase 2C motif shaded in yellow. Sequences complementary to immunization peptides used in antibody production in red letters. Nucleotides required for ARHGEF7 binding are underlined (Koh et al., 2002). The carboxyl terminal proline of truncated PPM1E(1-557) is indicated by an arrowhead (▼) (Kitani et al., 2006). Nuclear localization sites are shaded in black (Takeuchi et al., 2004). Sites that have been

Symbols: “*” the residues in that column are identical in all sequences in the alignment. “:” conserved substitutions as defined in Material and Methods section. “.” semi-conserved substitutions as defined in Material and Methods section.

PPM1E/1F homology domain (E/Fhd) as defined by Kitani et al. (2006) shaded in light grey. Catalytic PP2C phosphatase domain in bold letters (Tada et al., 2006). Protein phosphatase 2C motif shaded in yellow. Sequences complementary to immunization peptides used in antibody production in red letters. Nucleotides required for ARHGEF7 binding are underlined (Koh et al., 2002). The carboxyl terminal proline of truncated PPM1E(1-557) is indicated by an arrowhead (▼) (Kitani et al., 2006). Nuclear localization sites are shaded in black (Takeuchi et al., 2004).

A 4. Alignment of human and rat ARHGEF6 protein sequences

humanARHGEF6	MNPEEQIVTWLISLGVLESPKKTICDPEEFKSSSLKNGVVLCKLINRLMPGSVEKFCCLDP	60
ratARHGEF6	MNPEERVVTWVLSLGVLESPKKTICDPEEFKSSSLKNGVVLCKLISRLLPGSVEKYCQEP	60
	*****:*****.***:*****:*	
humanARHGEF6	QTEADCINNINDFLKGCATLQVEIFDPDDLYSGVNF SKVLST LLAVNKATEDQLSERPCG	120
ratARHGEF6	QTEADCIDNINDFLKGCATLQVEVFPDDLYSGANF SKVLNT LLAVNKATEDQLSERPCG	120
	*****:*****.*:*****.*****.*****	
humanARHGEF6	RSSLS SAANTSQTNPQGA VSVSTVSGLQ RQSKT VEMTENGSHQLI VKARFNFKQTNEDELS	180
ratARHGEF6	RSSLS SATSSQTNPQA AVPSTTPEQQSEKAAEMTENGSHQLI VKARFNFKQTNEDELS	180
	*****:.*:*****.*.*. * :.*:*****	
humanARHGEF6	VCKGDIIVVTRVEEGGWEGTLNGRTGWFP SNYVREIKSSERPLSPKAVKGFETAPLTKN	240
ratARHGEF6	VCKGDIIVVTRVEEGGWEGTLNGRTGWFP SNYVREIKPSERPLSPKAVKGFDTAPLTKN	240
	*****:*****.*****:*****	
humanARHGEF6	YYTVVLQNILDTEKEYAKELQSLLVTYLRPLQSN NNLSTVEVTSLLGNFEEVCTFQQTLC	300
ratARHGEF6	YYTVVLQNILDTEKEYAKELQSLLVTYLRPLQSN NNLSTVEFTCLLGNFEEVCTFQQTLC	300
	*****:*****.*.*****	
humanARHGEF6	QALEECSKFPENQHVKVGGCLLSLMPHFKSMYLA YCANHPSAVNVLTQHSDELEQFMENQG	360
ratARHGEF6	QALEECSKSPENQHVKVGGCLLNLMPHFKSMYLA YCANHPSAVNVLTQHSDDLRFMENQG	360
	***** *****.*****:***:*****	
humanARHGEF6	ASSPGILILTTNLSKPFMRLEKYVTLQLQELERH MEDTHPDHQDILKAIIVAFKTLMGQCQD	420
ratARHGEF6	ASSPGILILTTLSKPFMRLEKYVTLQLQELERH MEDTHPDHQDILKAIIVAFKSLMGQCQD	420
	*****.*****:***:*****	
humanARHGEF6	LRKRKQLELQILSEPIQAWEGEDIKNLGNVIFMS QVMVQYGACEEKEERYLMLFSNVLIM	480
ratARHGEF6	LRKRKQLELQILSEPIQAWEGDDIKTLGNVIFMS QVMVQYGACEEKEERYFLFSVLIM	480
	*****:***.*****:.*:*****:***.***	
humanARHGEF6	LSASPRMSGFIYQGKIPIAGTVVTRLDEIEGNDCT FEITGNTVERIVVHCNNNQDFQEWL	540
ratARHGEF6	LSASPRMSGFMYQGVPIAGMVVTRLDEIEGNDCT FEITGSTVERIVVHCNNNQDFQEWL	540
	*****:***:*** *****.*****:*****	
humanARHGEF6	EQLNRLIRGPASCSSSKTSSSSCSAHSSFSSTGQ PR GPLEPPQIIKPWSLSCLR PAPPL	600
ratARHGEF6	EQLNRLTKGPASCSSSKTSSSSCSHSSFSSTGQ PR GPLEPPQIIKPWSLSCLR PAPPL	600
	***** :*****:*****:*****	
humanARHGEF6	RPSAALGYKERMSYILKESKSPKTMKKFLHKKRKT ERKPSEEEYVIRKSTAAL EEDAQIL	660
ratARHGEF6	RPSAALGYKERMSYILKESKSPKTMKKFLHKKRKT ERKTSEEEYVIRKSTAAL EEDAQIL	660
	*****:*****.*****	
humanARHGEF6	KVIEAYCTSANFQQGHG SSSTRKDSIPQVLLPEE EKLIIEETRSNGQTIMEEKS LVDTVYA	720
ratARHGEF6	KVIEAYCTSASFQQG ---TRKDSVQVLLPEE EKLIIEETRSNGQTIIEEKS LVDTVYA	716
	*****.**** *****:*****:*****	
humanARHGEF6	LKDEVRELKQENKRMKQCLEEELK SRRDLEKLV RRLKQTDE CIRGESSKTSILP	776
ratARHGEF6	LKDEVKELKQENKMKQCLEEELKSRKDLEKLV RRLKQTDESIRAESSKTSILQ	772
	*****:*****:*****:*****:*****.*.*****	


```

hARHGEF7_t2 TYMSQVLIQCAGSEEKNERYL L L L F P N V L L M L S A S P R M S G F I Y Q G K L P T T G M T I T K L E D S E 519
hARHGEF7_t3 TYMSQVLIQCAGSEEKNERYL L L L F P N V L L M L S A S P R M S G F I Y Q G K L P T T G M T I T K L E D S E 540
hARHGEF7_t4 TYMSQVLIQCAGSEEKNERYL L L L F P N V L L M L S A S P R M S G F I Y Q G K L P T T G M T I T K L E D S E 490
hARHGEF7_t1 TYMSQVLIQCAGSEEKNERYL L L L F P N V L L M L S A S P R M S G F I Y Q G K L P T T G M T I T K L E D S E 362
hARHGEF6 IFMSQVMVQYGACEEKEERYL M L F S N V L I M L S A S P R M S G F I Y Q G K I P I A G T V V T R L D E I E 510
:****:* . . . ****:****:* . ****:*****:****:* : * . :****:*

hARHGEF7_t2 NHRNAFEISGSMIERILVSCNNQQDLQEWVEHLQKQTKVTSVGNPTIKPHSVPSHTLP SH 579
hARHGEF7_t3 NHRNAFEISGSMIERILVSCNNQQDLQEWVEHLQKQTKVTSVGNPTIKPHSVPSHTLP SH 600
hARHGEF7_t4 NHRNAFEISGSMIERILVSCNNQQDLQEWVEHLQKQTKVTSVGNPTIKPHSVPSHTLP SH 550
hARHGEF7_t1 NHRNAFEISGSMIERILVSCNNQQDLQEWVEHLQKQTKVTSVGNPTIKPHSVPSHTLP SH 422
hARHGEF6 GNDCTFEITGNTVERIVVHCNNNQDFQEWLEQLNRLIRG-----PASCSSLSK TSS 561
. : ****:* . ****:* ****:* ****:* ****:* ****:* : * * * . * : . *

hARHGEF7_t2 PVTPSSKHADSKPAPLTPAYHTLPHPSHHGTPHTTINWGPLEPPKTPKPWSLSCLR PAPP 639
hARHGEF7_t3 PVTPSSKHADSKPAPLTPAYHTLPHPSHHGTPHTTINWGPLEPPKTPKPWSLSCLR PAPP 660
hARHGEF7_t4 PVTPSSKHADSKPAPLTPAYHTLPHPSHHGTPHTTINWGPLEPPKTPKPWSLSCLR PAPP 610
hARHGEF7_t1 PVTPSSKHADSKPAPLTPAYHTLPHPSHHGTPHTTINWGPLEPPKTPKPWSLSCLR PAPP 482
hARHGEF6 --SSCSAHSS-----FSSSTGQPR-----GPLEPPQI I K P W S L S C L R P A P P 599
: . . * * : . * * * : * * * * : * * * * * * * * * * * * * * * * * * * * * * * *

hARHGEF7_t2 LRPSAALCY EDLS-----KSPKTMKLLPKRKP ERKP SDEEFASRKSTAALEEDAQI 692
hARHGEF7_t3 LRPSAALCY EDLS-----KSPKTMKLLPKRKP ERKP SDEEFASRKSTAALEEDAQI 713
hARHGEF7_t4 LRPSAALCY EDLS-----KSPKTMKLLPKRKP ERKP SDEEFASRKSTAALEEDAQI 663
hARHGEF7_t1 LRPSAALCY EDLS-----KSPKTMKLLPKRKP ERKP SDEEFASRKSTAALEEDAQI 535
hARHGEF6 LRPSAALGY ERMSYILKSSKSPKTMKFLHKKRTERKPS EEEYVIRKSTAALEEDAQI 659
***** ** * : * ****:* * * * . ****:* * * * : * * * * * * * * * * * * * * * * * *

hARHGEF7_t2 LKVI EAYCTSAKTRQTLNSTWQG---TDLMHN--HVLADDQPSLDSLGRSSLS---- 742
hARHGEF7_t3 LKVI EAYCTSAKTRQTLNSTWQG---TDLMHN--HVLADDQPSLDSLGRSSLS---- 763
hARHGEF7_t4 LKVI EAYCTSAKTRQTLNSTWQG---TDLMHN--HVLADDQPSLDSLGRSSLS---- 713
hARHGEF7_t1 LKVI EAYCTSAKTRQTLNSSSRKESAPQVLLPEEEKIIVEETKSNQGTVIEEKSLVDTVY 595
hARHGEF6 LKVI EAYCTSANFQQGHGSSTRKDSIPQVLLPEEEKLIEETRSNGQTIMEEKS LVDTVY 719
*****: * . * : : * : : : : : : : : : : : : : : : : . . . *

hARHGEF7_t2 --RLEPSDLS EDSYDYSIWTAHSYRMGSTSRKSCCSYISHQN----- 782
hARHGEF7_t3 --RLEPSDLS EDSYDYSIWTAHSYRMGSTSRKSCCSYISHQN----- 803
hARHGEF7_t4 --RLEPSDLS EDSYDYSIWTAHSYRMGSTSRKSCCSYISHQN----- 753
hARHGEF7_t1 ALKDEVQELRQDNKKMKKSL EEEQRARKDLEKLVKVLKNMNDPAWDETNL----- 646
hARHGEF6 ALKDEVRELKQENKRMKQCLEEELKSR R D L E K L V R F L L K Q T D E C I R G E S S S K T S I L P 776
: * * * : : . . . : . . : * : : : :

```

Sequences complementary to immunization peptides used in antibody production highlighted in grey. Sites required for binding of PPM1E and PPM1F are shaded yellow. hARHGEF7_t1 = hARHGEF7_t5 = β 1PIX.

Symbols and colours: Colours indicate different groups of amino acids: red: AVFPMILW = small (small and hydrophobic (incl. aromatic -Y)); blue: DE = acidic; magenta: RK = basic; green = STYHCNGQ = hydroxyl + amine + basic – Q. “*” the residues in that column are identical in all sequences in the alignment. “.” conserved substitutions as defined in Material and Methods section. “-” semi-conserved substitutions as defined in Material and Methods section. “t” : transcript number or ARHGEF7.

A 6. Alignment of human PPM1E with *D. melanogaster* CG10376-PA and Ppm1-PA

```

CG10376-PA -----MSSDAIPASECAHLMFEFK 18
hPPM1E MAGCIPEEKTYRRFLELFLGFRGPGCGGPEPEPEPEPEPEPESEPEPEPELVEAEAAE 60
Ppm1-PA -----

CG10376-PA RFLVSTA E K A A A V S E E V V S R S C V T R T A N E T Y K V S G E E R H A E L V S A I W K Q L E T R G ----- 72
hPPM1E ASVEEPGEAAATVAATFEQDQEQDPEPEEEAAVEGEEEEGAATAAAPGHSVPPPPPQ 120
Ppm1-PA -----

```


A 7. Alignment of human ARHGEF6 with *D. melanogaster* rtGEF-PC

```

hARHGEF6      -----MNPEEQIVTWLIS-----LG 15
rtGEF-PC      MDQPLVVQAEYSFMGSNNDELFCFQKGDVITVTQREDGGWEGTLNDKGTGWFPSPNYVNECK 60
                .. :: . * : *

hARHGEF6      VLESPKKTICDPE-----EFLKSSLKNGVVLCKLINRLMPGSVEKFCLDPQTEA 64
rtGEF-PC      VQLPLTETIRPPEEIQEYRSVVLKDLLDSERAHVAELQGLLENFLEPMQQTQILSQDEYA 120
                * . . : ** **          : : * . . : . * * : : : : . . * . : *

hARHGEF6      DCINNINDFLKGKCATLQVEIFDPDD-----LYSGVNF SKVLSTLLAVN-----K 108
rtGEF-PC      QLMCNFVEIVRTHEDLLIQIEECNDRVGKLF LTSAPLMKKVHQAYCAHPKCAIVILDKYK 180
                : : * : : : : * : * : : * * . . : ** . : * . : *

hARHGEF6      ATEDQLSERPCGRSSLSAANTSQTNPQGAVSSTVSGLQRQSKTVENTENG----- 160
rtGEF-PC      DELEKYMERQGAATPGLLVLTGLSKPFRRLDKYSAMLQELERHMESHPDRGDTQRSVA 240
                : : ** . : . * . . * . : : * . . : ** . : : * : . .

hARHGEF6      -HQLIVKARFNFKQTNEDELSVCKG-----DIIYVTRVEEGGWEG----- 200
rtGEF-PC      VYKDIAATCSATRRQKELELQVLTGVRGWGQELSTLGDIIHMGSVAVGADHRDRYFVL 300
                : : * . : . : : * ** * . * * * : : * * . .

hARHGEF6      -----TLNGRTGWFP SN-----YVREIKSSERPLSPKAVKGFETA 235
rtGEF-PC      FPQTLLFSLVSQRMSAFIYEGKPLPTGI IVNRLEDTDALKNAFEISSPLIDRIVAVCQGP 360
                : : . * . * : . : : . . ** : * : .

hARHGEF6      PLTKNYTIVV LQNILDTEKEYAKELQSLLVTYLRPLQSNNNLSTVEVTSL LGNFEEVCTF 295
rtGEF-PC      NEANKWVELLNANNPSLPMGIKRQLSNLSNSLGHNAHLSQHLD SRGYCTRFLCAYY 420
                : : : : : : * . : : * . * : * * : : . : : . * . : :

hARHGEF6      QQTLCQALEECSKFPENQHKVGGCLLSLMPHFK----- 328
rtGEF-PC      SSPPCHVRPLRVTLPPSNYPATAPYANLSAHFARLVKGGGLRSAIVKMLLYPQARQSIDL 480
                . . * . . : * . : : . . . * . **

hARHGEF6      -----SMYLAYCAN 337
rtGEF-PC      KRIALRKR RCHKASAKLKD LNTNQDSGQSELERQDAIELPTDSESYDDDFEDDFLHSCDS 540
                . : * * .

hARHGEF6      -----HPSAVNVLTQHSDELEQFMEN----- 358
rtGEF-PC      DPF EYVQFYQNKRNDSMCNSTGT FVDHGTGARRHCSSINLIK LDSADTDEVLALNELKKE 600
                * * : : : . . * : : : :

hARHGEF6      -----QGAS 362
rtGEF-PC      SLVIGSRALRALARKSTTRNSVHTSTATLELGVGGSITNCVEEPIKVKPFSFSLQQQS 660
                * *

hARHGEF6      SPGILILTTNLSKPFMRLEKYVTL LQELER----- 392
rtGEF-PC      SDASSIFAARLGGAFTACENLASMPDDL SRESSIQEPPTPLPASPTERHSMP TIFVGNRF 720
                * . * : : . * . * * : : : : * *

hARHGEF6      ----- 780
rtGEF-PC      NHSKNTEVYVPTWRDRQEMQNQSVDAKQDEELHSSSIDLPAACLSAPDKLQAE LLYNDE

hARHGEF6      ----- 840
rtGEF-PC      ILEKPLQLHRELTPFPGHNLNSDKRVSHKSDSPSTGNAKTDPNLATRSSTTELCIDTTS

hARHGEF6      ----- 900
rtGEF-PC      KKRTTPSERSRDSIRRCISYQFLQMSNRPPPPPPRRDPDLHLDTKCRCCENSQCPSPRS

hARHGEF6      -----HMEDTHPDHQDILKAI VAFKTLMGQCQDL 421
rtGEF-PC      SDSGMAGSCTITSPDPNPESYFPM EAAAGHDMLDNVEPERFDVCGMFRKFLTP EATQDV 960
                : : . . * : * : : * :

hARHGEF6      RKRKQLELQILSEPIQAWEGED--- IKNLGNVIFMSQVMVQYGACEEKEERYLMLFSNV 477
rtGEF-PC      VDLSEEQPQLSDEPTTPTNRKEEPTCITSAQVQVNTRSI FLPSSSSMDETNRNVPANNIL 1020
                . . : : * : ** . : : : * . . : : : . . : : * : . :

hARHGEF6      LIMLSASPRMSGFIYQG-----KIP-----IAGTVVTRLDEIEGND-----C 514
rtGEF-PC      FSSSSADQLEPQATFRSGMYAHWKKERLPPEVVRGIAHAYNKS LPSKDSKDSGVCSSC 1080
                : ** . . : : . : : * * : . * . : : * *

```

```

hARHGEF6      TFEITGNTVERIVVHCNNNQDFQEWLEQLNRLIR----- 548
rtGEF-PC      FCSLGASGYSEGALYCSVCQNCADYYNGSVTSTTNTTTTSSASCPLCSEDEGMIAPTHD 1140
               .: .. .:.*. *: :: :

hARHGEF6      -----
rtGEF-PC      SSSLDPCICNGRIASGAEEGKQSEMDRRPGNLRIPVEWYPVYLAGGMSPSSHILLPPGG 1200

hARHGEF6      -----GPASCSSLKTSSSSCSAHSSFSSTGQPRGPLEPPQI 585
rtGEF-PC      RPPATPSSIPAGSSSGGSHSQGSPATNSMHHKRSQSFNHHLSYNQYTPTQPPPHLHP 1260
               .**:* :. *.* . * *... .: * . :

hARHGEF6      IKPWSLSCLRPAAPLRPSAALGYKERMSYILKESKSPKTMKKFLHKKRTERK----- 638
rtGEF-PC      PQPPSLPSHLGASGPRSSSAQTPNSKTAAPLQASSMDASPAIQAAAAAAAAAAVGMGVPSPA 1320
               :* **.. * . *.*.* :.: : *:* ** .. . :

hARHGEF6      ---PSEEEYVIRKSTAAL EEDAQILKVI EAYCTS ANFQQGHGSSTR----- 681
rtGEF-PC      RKGSTKANWTISCLRPTPLRPSLLNATSGSGSGSGSGSGSSSNALASYCSGRKNQP 1380
               .: :.* .: .:*. . . :.: . * ***:

hARHGEF6      ---KDSIPQVLLPEEEKLIEETRSNGQTIMEEKSLVDTVYALKDEVRELKQENKRMKQC 738
rtGEF-PC      TYEEDALVLRVFEAYCAAYQNNARNTIHSGLENDMTPTLRQLWTAIRQMQQDMSQIKLQ 1440
               :*:: : : :*:.. : :*:..* * * :*:*: ::*

hARHGEF6      LEEELKSRRDLEKLVRRLLKQTDECIRGESSKTSILP 776
rtGEF-PC      INEERALRADLQQLLMQHLETSSVSSGANTPKC----- 1473
               ::* * **::*: : * :. . .:..

```

Symbols and colours: Colours indicate different groups of amino acids: red: AVFPMILW = small (small+ hydrophobic (incl.aromatic -Y)); blue: DE = acidic; magenta: RK = basic; green = STYHCNGQ = hydroxyl + amine + basic – Q. “*” the residues in that column are identical in all sequences in the alignment. “.” conserved substitutions as defined in Material and Methods section. “.” semi-conserved substitutions as defined in Material and Methods section. Sites required for binding of PPM1E and PPM1F are shaded yellow.

A 8. Comparison of His-PPM1E purification by Ni-NTA and by size-exclusion chromatography

Excerpt from: „Expression, purification and characterisation of PPM1E and PPM1F”; Bachelor-Thesis, Daniel Siebert, Hochschule Furtwangen University (Villingen-Schwenningen) and Evotec Neurosciences (Hamburg); 1st examiner Prof. Dr. Ulrike Salat, 2nd examiner M. Sc. Lene Jessen; Hamburg, August 27th 2009; from: Results 3.4 Purification of His-PPM1E, Myc-PPM1E mutants G276D, R241A, D273A, D479N and His-PPM1F.

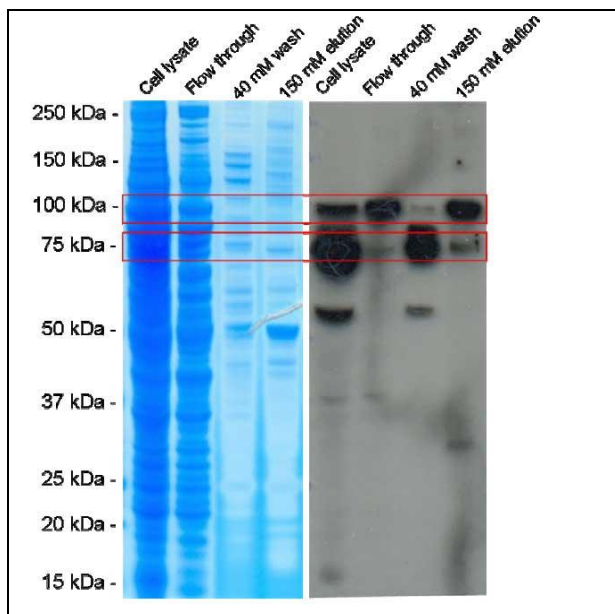


Figure DS12: SDS-PAGE and Western Blot of the His-PPM1E His-tag purification. Left side: Coomassie stained SDS-polyacrylamide gel (SimplyBlue™ SafeStain), no visible bands of 75 kDa and 100 kDa PPM1E species (framed in red), flow-through, 40 mM peak and also 150 mM elution lots of contaminations are visible. Right side: Western Blot (α-PPM1E, 1 min exposure time), cell lysate three significant bands (60 kDa, 75 kDa, 100 kDa), the flow-through almost only one significant band (100 kDa), 40 mM wash main band at 75 kDa and 150 mM elution main band at 100 kDa (framed in red). [page 59; emphasis added]

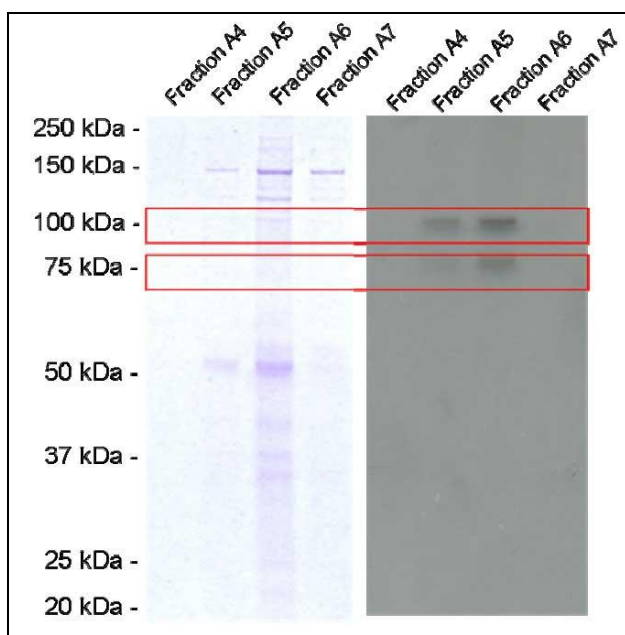


Figure DS14: SDS-PAGE and Western Blot of the His-PPM1E SEC with purified flow-through Left side: Coomassie stained SDS-polyacrylamide gel (PhastGel® Blue R), no visible bands of 75 kDa and 100 kDa PPM1E species (framed in red) visible. Right side: Western Blot (α-PPM1E, 20 min exposure time), two band detected (75 kDa and 100 kDa) in fraction A5 and A6 (framed in red). [Note: SEC: size-exclusion chromatography][page 61; emphasis added]

A 9. PPM1E has no macroscopic effect on *D. melanogaster* neuronal cells

***Drosophila melanogaster* as a model system**

A convenient model system for neurodegeneration is the fruit fly *Drosophila (D.) melanogaster* due to the relative ease with which it is amenable to genetic manipulation. It has been a useful genetic model for several neurodegenerative diseases in the past (Cauchi and Van Den Heuvel, 2006; Ghosh and Feany, 2004; Muqit and Feany, 2002). Additionally, several pathway members, among them PAK, ARHGEF and CaMK are conserved in the fly.

The *D. melanogaster* genome contains distantly related homologues of human PPM1E. The closest homologues, with absolute sequence identity of 27 % and 21 % to human PPM1E, are the PP2C-like serine/threonine phosphatase CG10376-PA and the predicted transcript Ppm1-PA (Appendix A 6). No function has been assigned to either one of them yet. Both show considerable sequence homology in the phosphatase domain and the CG10376-PA primary sequence is homologous in the amino-terminal ARHGEF binding motif. CG10376-PA and human PPM1E are 33 % identical and 68 % semi-conserved between the aa 150 and 490 in human PPM1E sequence. This stretch comprises the ARHGEF binding and the E/Fhd phosphatase domains. Neither of the proposed homologues is conserved in the carboxy-terminal PPM1E domain which encodes two nuclear localization signals.

The closest homolog of the human ARHGEF6 in *D. melanogaster* is rtGEF-PC, also referred to as dPIX, a rho-type guanine exchange factor with 31 % sequence identity (Appendix A 7). rtGEF-PC plays a major role in regulating postsynaptic structure and protein localization at the *Drosophila* glutamatergic neuromuscular junction (Parnas et al., 2001; Werner and Manseau, 1997). rtGEF-PC contains a pleckstrin homology, a RhoGEF and a SH3 domain which is required for dPAK binding. The SH3-domain, required for dPAK binding, is conserved (Parnas et al., 2001) and amino acids 578 to 719 (in human ARHGEF6), which are required for PPM1E binding, are semi-conserved by 92 % in rtGEF-PC.

Established *Drosophila melanogaster* transgenic lines

Drosophila (D.) melanogaster lines that contain P-element insertions with the human PPM1E gene were crossed to driver lines P{elav-GAL4} and P{gmr-GAL4} to overexpress hPPM1E in the complete central nervous system (Figure A9.1) and the eye respectively. The fly lines express hPPM1E(1-557) in the same truncated fashion

as described for the H4_PPM1E cell line and no full length form of PPM1E is detectable (Figure A9.1). The strength of protein expression depends on the location of the random P-element-mediated insertion on the chromosomes and is therefore variable between the fly lines (Figure A9.1; (Spradling et al., 1995)). Lines with different expression levels of PPM1E gene and PPM1E insertions on chromosome 2 (line 2.2 and 2.5 in Figure A9.1) or 3 (line 3.1 in Figure A9.1) were used for further experiments to assess the effect of PPM1E on *D.melanogaster* neurons.

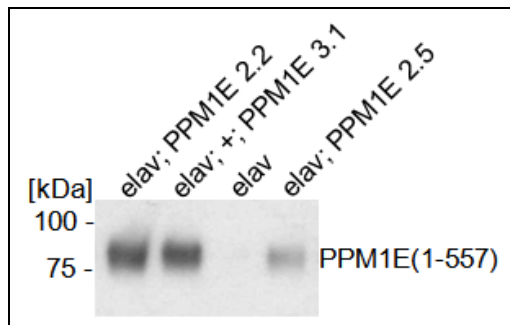


Figure A9.1: *D. melanogaster* PPM1E line crosses to elav-GAL4 express PPM1E(1-557). 15 μ g fly protein extracts per lane. Detection with anti-PPM1E(AGC). elav: elav-GAL4 coding chromosome; +: wildtype chromosome.

Ectopic PPM1E expression showed no effects in *D.melanogaster*

PPM1E expression was induced in crosses to the *gmr*-GAL4 driver line which drives expression under the control of the UAS promoter in all cells behind the morphogenic furrow of the fly eye, including photoreceptors (Freeman, 1996). Overexpression of PPM1E in the retinal tissue induced no eye phenotype (data not shown). The eye phenotype was assessed under the light microscope.

PPM1E expression was additionally induced in the complete central nervous system with the *elav* – GAL4 driver (Koushika et al., 1996). w^{1118} or *elav*-GAL4 driver line flies were crossed to three PPM1E lines. Larvae were normal in size and concession of developmental stages as visualized under the light microscope in comparison with *elav*-GAL4 crosses to w^{1118} . The flies showed no obvious deterioration in motor function. Therefore the lifespan of the flies was evaluated. The lifespan of 70 flies was recorded and no consistent difference in the lifespan in *elav*-GAL4 crosses to PPM1E fly lines was visible (Figure A9.2). A slight reduction in the lifespan of the crosses to the PPM1E lines 2.2 and 2.5 was not significant. PPM1E line 2.2 control crosses in w^{1118} background also showed a slight, however not significant reduction in life span.

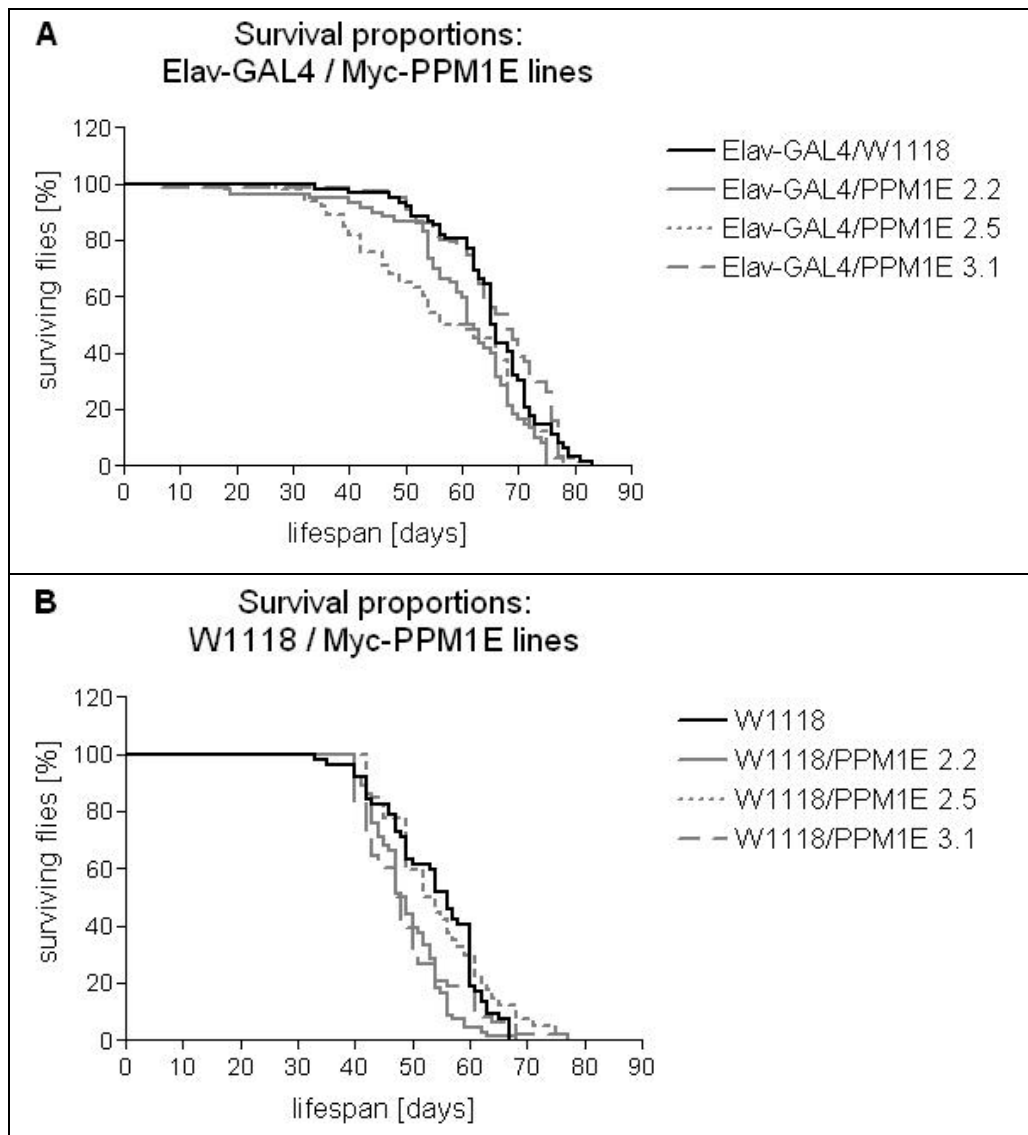
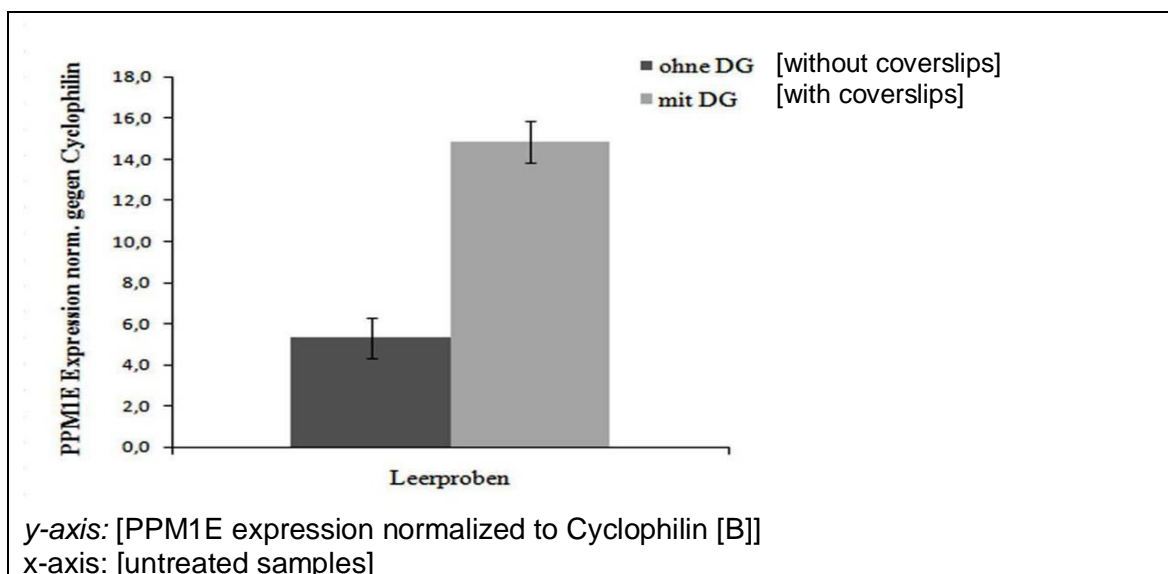


Figure A9.2: Survival of *D.melanogaster* PPM1E fly lines (A) without and (B) with induction of expression in the central nervous system by elav-GAL4. Lines 2.2 and 3.1: stronger PPM1E expression; line 2.5: weaker PPM1E expression. Lines 2.2 and 2.5 carry the PPM1E gene on chromosome 2; line 3.1 carries PPM1E gene on chromosome 3. n=70.

No further experiments were conducted with the established PPM1E fly lines.

A 10. Influence of growth substrate on PPM1E expression in primary hippocampal culture

Excerpt from: „Untersuchungen zum Einfluss von Stressfaktoren wie beta-Amyloid Oligomeren auf die Phosphatase PPM1E in neuronaler Primärzellkultur“ (“Analysis of the influence of stress factors like beta-amyloid oligomers on the phosphatase PPM1E in primary neuronal cell culture”); Diploma-Thesis (Fachhochschule), Dorothee Kampmann, Hochschule für Angewandte Wissenschaften Hamburg and Evotec AG (Hamburg); 1st examiner Prof. Dr. Ernst A. Sanders, 2nd examiner Dr. Heinz von der Kammer; Hamburg, March 23rd 2010



German description of figure (original):

„**Abb. 1:** PPM1E-mRNA-Expressionsunterschied von unbehandelten DIV 24-Primärneuronen auf unterschiedlichen Wachstumsuntergrundbedingungen. Wachstumsuntergrundbedingungen: ohne DG oder mit DG Marienfeld (Mar). Mittelwerte \pm Standardabweichung nach qRT-PCR über 8 Wells einer 24-well Zellkulturplatte (mit oder ohne DG), normalisiert gegen Cyclophilin; n=8. „

English description of figure (translation):

“**Figure 24:** Difference in PPM1E mRNA expression in untreated DIV 24 primary neurons on different growth substrate conditions. Growth substrate conditions: without [glass] coverslips [on cell culture dish plastic] or with [glass] coverslips obtained from Marienfeld (Mar). Mean values \pm standard deviation after qRT-PCR with > 8 samples from one 24 well cell culture dish (with or without coverslips), normalized to Cyclophilin; n=8.”

REFERENCE LIST

- Abo A, Qu J, Cammarano MS, Dan C, Fritsch A, Baud V, Belisle B, Minden A (1998) PAK4, a novel effector for Cdc42Hs, is implicated in the reorganization of the actin cytoskeleton and in the formation of filopodia. *EMBO Journal* 17:6527-6540.
- Abràmoff MD, Magalhães PJ, Ram SJ (2004) Image processing with imageJ. *Biophotonics International* 11:36-41.
- Adalbert R, Gilley J, Coleman MP (2007) Abeta, tau and ApoE4 in Alzheimer's disease: the axonal connection. *Trends in Molecular Medicine* 13:135-142.
- Ahmed T, Shea K, Masters JRW, Jones GE, Wells CM (2008) A PAK4-LIMK1 pathway drives prostate cancer cell migration downstream of HGF. *Cellular Signalling* 20:1320-1328.
- Allen KM, Gleeson JG, Bagrodia S, Partington MW, MacMillan JC, Cerione RA, Mulley JC, Walsh CA (1998) PAK3 mutation in nonsyndromic X-linked mental retardation. *Nature Genetics* 20:25-30.
- Allison DW, Chervin AS, Gelfand VI, Craig AM (2000) Postsynaptic scaffolds of excitatory and inhibitory synapses in hippocampal neurons: Maintenance of core components independent of actin filaments and microtubules. *J Neurosci* 20:4545-4554.
- Altschul SF, Madden TL, Schäffer AA, Zhang J, Zhang Z, Miller W, Lipman DJ (1997) Gapped BLAST and PSI-BLAST: A new generation of protein database search programs. *Nucleic Acids Research* 25:3389-3402.
- Alvarez VA, Ridenour DA, Sabatini BL (2006) Retraction of synapses and dendritic spines induced by off-target effects of RNA interference. *J Neurosci* 26:7820-7825.
- Arriagada PV, Growdon JH, Hedley-Whyte ET, Hyman BT (1992) Neurofibrillary tangles but not senile plaques parallel duration and severity of Alzheimer's disease. *Neurology* 42:631-639.
- Ball MJ, Murdoch GH (1997) Neuropathological criteria for the diagnosis of Alzheimer's disease: Are we really ready yet? *Neurobiology of Aging* 18.
- Ballatore C, Lee VMY, Trojanowski JQ (2007) Tau-mediated neurodegeneration in Alzheimer's disease and related disorders. *Nat Rev Neurosci* 8:663-672.
- Baloyannis SJ, Costa V, Mauroudis I, Psaroulis D, Manolidis SL, Manolidis LS (2007) Dendritic and spinal pathology in the acoustic cortex in Alzheimer's disease: Morphological and morphometric estimation by Golgi technique and electron microscopy. *Acta Oto-Laryngologica* 127:351-354.
- Baloyannis SJ, Manolidis SL, Manolidis LS (1992) The acoustic cortex in Alzheimer's disease. *Acta Oto-Laryngologica*, Supplement1-13.
- Bamburg JR (1999) Proteins of the ADF/cofilin family: Essential regulators of actin dynamics. pp 185-230.
- Banker G, Goslin K (2002) *Culturing nerve cells*. Cambridge, Massachusetts: The MIT Press.
- Barford D (1996) Molecular mechanisms of the protein serine/threonine phosphatases. *Trends in Biochemical Sciences* 21:407-412.
- Barford D, Das AK, Egloff MP (1998) The structure and mechanism of protein phosphatases: Insights into catalysis and regulation. pp 133-164.

- Bayer KU, De Koninck P, Leonard AS, Hell JW, Schulman H (2001) Interaction with the NMDA receptor locks CaMKII in an active conformation. *Nature* 411:801-805.
- Baykov AA, Evtushenko OA, Avaeva SM (1988) A malachite green procedure for orthophosphate determination and its use in alkaline phosphatase-based enzyme immunoassay. *Analytical Biochemistry* 171:266-270.
- Bellugi U, Lichtenberger L, Mills D, Galaburda A, Korenberg JR (1999) Bridging cognition, the brain and molecular genetics: Evidence from Williams syndrome. *Trends Neurosci* 22:197-207.
- Bianchini M, Martinelli G, Renzulli M, Gonzalez Cid M, Larripa I (2007) cDNA microarray study to identify expression changes relevant for apoptosis in K562 cells co-treated with amifostine and imatinib. *Cancer Chemotherapy and Pharmacology* 59:349-360.
- Biederer T, Scheiffele P (2007) Mixed-culture assays for analyzing neuronal synapse formation. *Nat Protocols* 2:670-676.
- Bienvenu T, Des Portes V, McDonell N, Carrié A, Zemni R, Couvert P, Ropers HH, Moraine C, Van Bokhoven H, Fryns JP, Allen K, Walsh CA, Boué J, Kahn A, Chelly J, Beldjord C (2000) Missense mutation in PAK3, R67C, causes X-linked nonspecific mental retardation. *American Journal of Medical Genetics* 93:294-298.
- Bito H, Deisseroth K, Tsien RW (1996a) CREB phosphorylation and dephosphorylation: A Ca²⁺- and stimulus duration-dependent switch for hippocampal gene expression. *Cell* 87:1203-1214.
- Bito H, Deisseroth K, Tsien RW (1996b) Signaling from synapse to nucleus: Ca²⁺-dependent control at hippocampal synapses of nuclear creb phosphorylation. *FASEB Journal* 10.
- Blennow K, Hampel H, Weiner M, Zetterberg H (2010) Cerebrospinal fluid and plasma biomarkers in Alzheimer disease. *Nature Reviews Neurology* 6:131-144.
- Bokoch GM (2003) Biology of the p21-activated kinases. *Annual Review of Biochemistry* 72:743-781.
- Bokoch GM, Wang Y, Bohl BP, Sells MA, Quilliam LA, Knaus UG (1996) Interaction of the Nck adapter protein with p21-activated kinase (PAK1). *Journal of Biological Chemistry* 271:25746-25749.
- Bollen M, Beullens M (2002) Signaling by protein phosphatases in the nucleus. *Trends Cell Biol* 12:138-145.
- Bouras C, Hof PR, Giannakopoulos P, Michel JP, Morrison JH (1994) Regional distribution of neurofibrillary tangles and senile plaques in the cerebral cortex of elderly patients: A quantitative evaluation of a one-year autopsy population from a geriatric hospital. *Cerebral Cortex* 4:138-150.
- Bourne JN, Harris KM (2008) Balancing structure and function at hippocampal dendritic spines. pp 47-67.
- Braak H, Braak E (1991) Neuropathological staging of Alzheimer-related changes. *Acta Neuropathologica* 82:239-259.
- Braak H, Braak E (1998) Evolution of neuronal changes in the course of Alzheimer's disease. *Journal of Neural Transmission, Supplement* 127-140.
- Brand AH, Perrimon N (1993) Targeted gene expression as a means of altering cell fates and generating dominant phenotypes. *Development* 118:401-415.
- Brion JP, Anderton BH, Authelet M, Dayanandan R, Leroy K, Lovestone S, Octave JN, Pradier L, Touchet N, Tremp G (2001) Neurofibrillary tangles and tau phosphorylation. pp 81-88.

- Caceres A, Payne MR, Binder LI, Steward O (1983) Immunocytochemical localization of actin and microtubule-associated protein MAP2 in dendritic spines. *PROC NATL ACAD SCI U S A* 80:1738-1742.
- Calon F, Lim GP, Yang F, Morihara T, Teter B, Ubuda O, Rostaing P, Triller A, Salem J, Ashe KH, Frautschy SA, Cole GM (2004) Docosahexaenoic acid protects from dendritic pathology in an Alzheimer's disease mouse model. *Neuron* 43:633-645.
- Carlisle HJ, Kennedy MB (2005) Spine architecture and synaptic plasticity. *Trends Neurosci* 28:182-187.
- Carlisle HJ, Manzerra P, Marcora E, Kennedy MB (2008) SynGAP regulates steady-state and activity-dependent phosphorylation of cofilin. *J Neurosci* 28:13673-13683.
- Castellani R, Hirai K, Aliev G, Drew KL, Nunomura A, Takeda A, Cash AD, Obrenovich ME, Perry G, Smith MA (2002) Role of mitochondrial dysfunction in Alzheimer's disease. *Journal of Neuroscience Research* 70:357-360.
- Catala I, Ferrer I, Galofre E, Fabregues I (1988) Decreased numbers of dendritic spines on cortical pyramidal neurons in dementia. A quantitative Golgi study on biopsy samples. *Human neurobiology* 6:255-259.
- Catts VS, Catts SV, Fernandez HR, Taylor JM, Coulson EJ, Lutze-Mann LH (2005) A microarray study of post-mortem mRNA degradation in mouse brain tissue. *Molecular Brain Research* 138:164-177.
- Cauchi RJ, Van Den Heuvel M (2006) The fly as a model for neurodegenerative diseases: Is it worth the jump? *Neurodegenerative Diseases* 3:338-356.
- Chawla S, Hardingham GE, Quinn DR, Bading H (1998) CBP: A signal-regulated transcriptional coactivator controlled by nuclear calcium and CaM kinase IV. *Science* 281:1505-1509.
- Chen G, Chen KS, Knox J, Inglis J, Bernard A, Martin SJ, Justice A, Mcconlogue L, Games D, Freedman SB, Morris RGM (2000) A learning deficit related to age and beta-amyloid plaques in a mouse model of Alzheimer's disease. *Nature* 408:975-979.
- Chen HJ, Rojas-Soto M, Oguni A, Kennedy MB (1998) A synaptic Ras-GTPase activating protein (p135 SynGAP) inhibited by CaM kinase II. *Neuron* 20:895-904.
- Chen Y, Stevens B, Chang J, Milbrandt J, Barres BA, Hell JW (2008) NS21: Re-defined and modified supplement B27 for neuronal cultures. *Journal of Neuroscience Methods* 171:239-247.
- Christie BR, Cameron HA (2006) Neurogenesis in the adult hippocampus. *Hippocampus* 16:199-207.
- Chrivia JC, Kwok RPS, Lamb N, Hagiwara M, Montminy MR, Goodman RH (1993) Phosphorylated CREB binds specifically to the nuclear protein CBP. *Nature* 365:855-859.
- Cingolani LA, Goda Y (2008) Actin in action: The interplay between the actin cytoskeleton and synaptic efficacy (*Nature Reviews Neuroscience* (2008) 9, (344-356)). *Nat Rev Neurosci* 9:344--356.
- Cohen P (2000) The regulation of protein function by multisite phosphorylation - A 25 year update. *Trends in Biochemical Sciences* 25:596-601.
- Cohen P (2001) The role of protein phosphorylation in human health and disease: Delivered on June 30th 2001 at the FEBS meeting in Lisbon. *European Journal of Biochemistry* 268:5001-5010.

- Cohen RS, Chung SK, Pfaff DW (1985) Immunocytochemical localization of actin in dendritic spines of the cerebral cortex using colloidal gold as a probe. *Cellular and molecular neurobiology* 5:271-284.
- Colbran RJ, Brown AM (2004) Calcium/calmodulin-dependent protein kinase II and synaptic plasticity. *Curr Opin Neurobiol* 14:318-327.
- Coleman PD, Yao PJ (2003) Synaptic slaughter in Alzheimer's disease. *Neurobiology of Aging* 24:1023-1027.
- Counts SE, Nadeem M, Lad SP, Wu J, Mufson EJ (2006) Differential expression of synaptic proteins in the frontal and temporal cortex of elderly subjects with mild cognitive impairment. *Journal of Neuropathology and Experimental Neurology* 65:592-601.
- Dan C, Kelly A, Bernard O, Minden A (2001) Cytoskeletal Changes Regulated by the PAK4 Serine/Threonine Kinase Are Mediated by LIM Kinase 1 and Cofilin. *Journal of Biological Chemistry* 276:32115-32121.
- Das AK, Helps NR, Cohen PTW, Barford D (1996) Crystal structure of the protein serine/threonine phosphatase 2C at 2.0 Å resolution. *EMBO Journal* 15:6798-6809.
- De Roo M, Klauser P, Mendez P, Poglia L, Muller D (2008a) Activity-dependent PSD formation and stabilization of newly formed spines in hippocampal slice cultures. *Cerebral Cortex* 18:151-161.
- De Roo M, Klauser P, Muller D (2008b) LTP promotes a selective long-term stabilization and clustering of dendritic spines. *PLoS Biology* 6.
- De Ruiter JP, Uylings HBM (1987) Morphometric and dendritic analysis of fascia dentata granule cells in human aging and senile dementia. *Brain Research* 402:217-229.
- De Strooper B (2003) Aph-1, Pen-2, and Nicastrin with Presenilin generate an active gamma-Secretase complex. *Neuron* 38:9-12.
- Dharmawardhane S, Brownson D, Lennartz M, Bokoch GM (1999) Localization of p21-activated kinase 1 (PAK1) to pseudopodia, membrane ruffles, and phagocytic cups in activated human neutrophils. *Journal of Leukocyte Biology* 66:521-527.
- Dickinson J, Fowler SJ (2002) Quantification of Proteins on Western Blots Using ECL. In: *The Protein Protocols Handbook* (Walker JM, ed), pp 429-437. Humana Press.
- Dorkeld F, Bernheim A, Dessen P, Huret JL (1999) A database on cytogenetics in haematology and oncology. *Nucleic Acids Research* 27:353-354.
- Drew MR, Hen R (2007) Adult hippocampal neurogenesis as target for the treatment of depression. *CNS and Neurological Disorders - Drug Targets* 6:205-218.
- Dubois B, Feldman HH, Jacova C, DeKosky ST, Barberger-Gateau P, Cummings J, Delacourte A, Galasko D, Gauthier S, Jicha G, Meguro K, O'Brien J, Pasquier F, Robert P, Rossor M, Salloway S, Stern Y, Visser PJ, Scheltens P (2007) Research criteria for the diagnosis of Alzheimer's disease: revising the NINCDS-ADRDA criteria. *Lancet Neurology* 6:734-746.
- DuBridge RB, Tang P, Hsia HC (1987) Analysis of mutation in human cells by using an Epstein-Barr virus shuttle system. *Molecular and Cellular Biology* 7:379-387.
- Eckert A, Keil U, Marques CA, Bonert A, Frey C, Schüssel K, Müller WE (2003) Mitochondrial dysfunction, apoptotic cell death, and Alzheimer's disease. *Biochemical Pharmacology* 66:1627-1634.

- Edwards DC, Sanders LC, Bokoch GM, Gill GN (1999) Activation of LIM-kinase by Pak1 couples Rac/Cdc42 GTPase signalling to actin cytoskeletal dynamics. *Nature Cell Biology* 1:253-259.
- Ehrlich I, Klein M, Rumpel S, Malinow R (2007) PSD-95 is required for activity-driven synapse stabilization. *PROC NATL ACAD SCI U S A* 104:4176-4181.
- Ehrlich ME, Conti L, Toselli M, Taglietti L, Fiorillo E, Taglietti V, Ivkovic S, Guinea B, Tranberg A, Sipione S, Rigamonti D, Cattaneo E (2001) ST14A cells have properties of a medium-size spiny neuron. *Experimental Neurology* 167:215-226.
- Einstein G, Buranosky R, Crain BJ (1994) Dendritic pathology of granule cells in Alzheimer's disease is unrelated to neuritic plaques. *J Neurosci* 14:5077-5088.
- El Hachimi KH, Foncin JF (1990) Loss of dendritic spines in Alzheimer's disease. *Comptes Rendus de l'Academie des Sciences - Serie III* 311:397-402.
- Endo M, Ohashi K, Mizuno K (2007) LIM kinase and slingshot are critical for neurite extension. *Journal of Biological Chemistry* 282:13692-13702.
- Endo M, Ohashi K, Sasaki Y, Goshima Y, Niwa R, Uemura T, Mizuno K (2003) Control of growth cone motility and morphology by LIM kinase and slingshot via phosphorylation and dephosphorylation of cofilin. *J Neurosci* 23:2527-2537.
- Engert F, Bonhoeffer T (1999) Dendritic spine changes associated with hippocampal long-term synaptic plasticity. *Nature* 399:66-70.
- Esch FS, Keim PS, Beattie EC, Blacher RW, Culwell AR, Oltersdorf T, McClure D, Ward PJ (1990) Cleavage of amyloid β peptide during constitutive processing of its precursor. *Science* 248:1122-1124.
- Eswaran J, Soundararajan M, Kumar R, Knapp S (2008) UnPAKING the class differences among p21-activated kinases. *Trends in Biochemical Sciences* 33:394-403.
- Ethell IM, Pasquale EB (2005) Molecular mechanisms of dendritic spine development and remodeling. *Progress in Neurobiology* 75:161-205.
- Feng Q, Albeck JG, Cerione RA, Yang W (2002) Regulation of the Cool/Pix proteins. Key binding partners of the Cdc42/Rac targets, the p21-activated kinases. *Journal of Biological Chemistry* 277:5644-5650.
- Feng Q, Baird D, Cerione RA (2004) Novel regulatory mechanisms for the Dbl family guanine nucleotide exchange factor Cool-2/ α -Pix. *EMBO Journal* 23:3492-3504.
- Ferrer I, Gullotta F (1990) Down's syndrome and Alzheimer's disease: Dendritic spine counts in the hippocampus. *Acta Neuropathologica* 79:680-685.
- Fiala JC, Feinberg M, Popov V, Harris KM (1998) Synaptogenesis via dendritic filopodia in developing hippocampal area CA1. *J Neurosci* 18:8900-8911.
- Fifkova E, Delay RI (1982) Cytoplasmic actin in neuronal processes as a possible mediator of synaptic plasticity. *Journal of Cell Biology* 95:345-350.
- Fong AY, Stornetta RL, Foley CM, Potts JT (2005) Immunohistochemical localization of GAD67-expressing neurons and processes in the rat brainstem: Subregional distribution in the nucleus tractus solitarius. *Journal of Comparative Neurology* 493:274-290.
- Frangiskakis JM, Ewart AK, Morris CA, Mervis CB, Bertrand J, Robinson BF, Klein BP, Ensing GJ, Everett LA, Green ED, Pröschel C, Gutowski NJ, Noble M, Atkinson DL, Odelberg SJ,

- Keating MT (1996) LIM-kinase1 hemizyosity implicated in impaired visuospatial constructive cognition. *Cell* 86:59-69.
- Freeman M (1996) Reiterative use of the EGF receptor triggers differentiation of all cell types in the *Drosophila* eye. *Cell* 87:651-660.
- Gassmann M, Grenacher B, Rohde B, Vogel J (2009) Quantifying Western blots: Pitfalls of densitometry. *Electrophoresis* 30:1845-1855.
- Gatti A, Huang Z, Tuazon PT, Traugh JA (1999) Multisite autophosphorylation of p21-activated protein kinase γ -PAK as a function of activation. *Journal of Biological Chemistry* 274:8022-8028.
- Gedeon AK, Nelson J, cz J, Mulley JC (2003) X-linked mild non-syndromic mental retardation with neuropsychiatric problems and the missense mutation A365E in PAK3. *American Journal of Medical Genetics* 120 A:509-517.
- Gertz HJ, Cervos-Navarro J, Ewald V (1987) The septo-hippocampal pathway in patients suffering from senile dementia of Alzheimer's type. Evidence for neuronal plasticity? *Neuroscience Letters* 76:228-232.
- Ghosh S, Feany MB (2004) Comparison of pathways controlling toxicity in the eye and brain in *Drosophila* models of human neurodegenerative diseases. *Human Molecular Genetics* 13:2011-2018.
- Glabe CC (2005) Amyloid accumulation and pathogenesis of Alzheimer's disease: significance of monomeric, oligomeric and fibrillar A β . *Sub-cellular biochemistry* 38:167-177.
- Glenner GG, Wong CW (1984a) Alzheimer's disease and Down's syndrome: Sharing of a unique cerebrovascular amyloid fibril protein. *Biochemical and Biophysical Research Communications* 122:1131-1135.
- Glenner GG, Wong CW (1984b) Alzheimer's disease: Initial report of the purification and characterization of a novel cerebrovascular amyloid protein. *Biochemical and Biophysical Research Communications* 120:885-890.
- Goldman SA, Sim F (2005) Neural progenitor cells of the adult brain. pp 66-82.
- Gordon MN, King DL, Diamond DM, Jantzen PT, Boyett KV, Hope CE, Hatcher JM, DiCarlo G, Gottschall WPE, Morgan D, Arendash GW (2001) Correlation between cognitive deficits and A β deposits in transgenic APP+PS1 mice. *Neurobiology of Aging* 22:377-385.
- Govek EE, Newey SE, Akerman CJ, Cross JR, Der Veken LV, Van Aelst L (2004) The X-linked mental retardation protein oligophrenin-1 is required for dendritic spine morphogenesis. *Nature Neuroscience* 7:364-372.
- Graham FL, Smiley J, Russell WC, Nairn R (1977) Characteristics of a human cell line transformed by DNA from human adenovirus type 5. *Journal of General Virology* 36:59-72.
- Green S, Dobrjansky A, Carswell EA (1976) Partial purification of a serum factor that causes necrosis of tumors. *PROC NATL ACAD SCI U S A* 73:381-385.
- Grimm D, Kay MA, Kleinschmidt JA (2003) Helper virus-free, optically controllable, and two-plasmid-based production of adeno-associated virus vectors of serotypes 1 to 6. *Molecular Therapy* 7:839-850.
- Grimm D, Kern A, Rittner K, Kleinschmidt JA (1998) Novel tools for production and purification of recombinant adenoassociated virus vectors. *Human Gene Therapy* 9:2745-2760.
- Halpain S (2000) Actin and the agile spine: How and why do dendritic spines dance? *Trends Neurosci* 23:141-146.

- Hämäläinen RH, Joensuu T, Kallijärvi J, Lehesjoki AE (2006) Characterisation of the mulibrey nanism-associated TRIM37 gene: Transcription initiation, promoter region and alternative splicing. *Gene* 366:180-188.
- Hardy J (1997) Amyloid, the presenilins and Alzheimer's disease. *Trends Neurosci* 20:154-159.
- Hardy J (2009) The amyloid hypothesis for Alzheimer's disease: A critical reappraisal. *Journal of Neurochemistry* 110:1129-1134.
- Hardy J, Selkoe DJ (2002) The amyloid hypothesis of Alzheimer's disease: Progress and problems on the road to therapeutics. *Science* 297:353-356.
- Hardy JA, Higgins GA (1992) Alzheimer's disease: The amyloid cascade hypothesis. *Science* 256:184-185.
- Harigaya Y, Shoji M, Shirao T, Hirai S (1996) Disappearance of actin-binding protein, drebrin, from hippocampal synapses in Alzheimer's disease. *Journal of Neuroscience Research* 43:87-92.
- Harris KM, Kater SB (1994) Dendritic spines: Cellular specializations imparting both stability and flexibility to synaptic function. *Annual Review of Neuroscience* 17:341-371.
- Harris KM, Stevens JK (1988) Dendritic spines of rat cerebellar Purkinje cells: Serial electron microscopy with reference to their biophysical characteristics. *J Neurosci* 8:4455-4469.
- Harris KM, Stevens JK (1989) Dendritic spines of CA1 pyramidal cells in the rat hippocampus: Serial electron microscopy with reference to their biophysical characteristics. *J Neurosci* 9:2982-2997.
- Harvey BP, Banga SS, Ozer HL (2004) Regulation of the multifunctional Ca²⁺/calmodulin-dependent protein kinase II by the PP2C phosphatase PPM1F in fibroblasts. *Journal of Biological Chemistry* 279:24889-24898.
- Harvey CD, Svoboda K (2007) Locally dynamic synaptic learning rules in pyramidal neuron dendrites. *Nature* 450:1195-1200.
- Hatanpää K, Isaacs KR, Shirao T, Brady DR, Rapoport SI (1999) Loss of proteins regulating synaptic plasticity in normal aging of the human brain and in Alzheimer disease. *Journal of Neuropathology and Experimental Neurology* 58:637-643.
- Ho SN, Hunt HD, Horton RM, Pullen JK, Pease LR (1989) Site-directed mutagenesis by overlap extension using the polymerase chain reaction. *Gene* 77:51-59.
- Holtmaat A, Wilbrecht L, Knott GW, Welker E, Svoboda K (2006) Experience-dependent and cell-type-specific spine growth in the neocortex. *Nature* 441:979-983.
- Holtmaat AJGD, Trachtenberg JT, Wilbrecht L, Shepherd GM, Zhang X, Knott GW, Svoboda K (2005) Transient and persistent dendritic spines in the neocortex in vivo. *Neuron* 45:279-291.
- Honkura N, Matsuzaki M, Noguchi J, Ellis-Davies GCR, Kasai H (2008) The subspine organization of actin fibers regulates the structure and plasticity of dendritic spines. *Neuron* 57:719-729.
- Hosokawa T, Rusakov DA, Bliss TVP, Fine A (1995) Repeated confocal imaging of individual dendritic spines in the living hippocampal slice: Evidence for changes in length and orientation associated with chemically induced LTP. *J Neurosci* 15:5560-5573.
- Hulette CM (2003) Brain banking in the United States. *Journal of Neuropathology and Experimental Neurology* 62:715-722.

- Impey S, Fong AL, Wang Y, Cardinaux JR, Fass DM, Obrietan K, Wayman GA, Storm DR, Soderling TR, Goodman RH (2002) Phosphorylation of CBP mediates transcriptional activation by neural activity and CaM kinase IV. *Neuron* 34:235-244.
- Irwin SA, Galvez R, Greenough WT (2000) Dendritic spine structural anomalies in fragile-X mental retardation syndrome. *Cerebral Cortex* 10:1038-1044.
- Jackson AL, Linsley PS (2004) Noise amidst the silence: Off-target effects of siRNAs? *Trends in Genetics* 20:521-524.
- Jackson MD, Fjeld CC, Denu JM (2003) Probing the function of conserved residues in the serine/threonine phosphatase PP2C α . *Biochemistry* 42:8513-8521.
- Jacobs T, Causeret F, Nishimura YV, Terao M, Norman A, Hoshino M, Nikolic M (2007) Localized activation of p21-activated kinase controls neuronal polarity and morphology. *J Neurosci* 27:8604-8615.
- Jaffer ZM, Chernoff J (2002) p21-Activated kinases: Three more join the Pak. *International Journal of Biochemistry and Cell Biology* 34:713-717.
- Jensen KF, Ohmstede CA, Fisher RS, Sahyoun N (1991) Nuclear and axonal localization of Ca²⁺/calmodulin-dependent protein kinase type Gr in rat cerebellar cortex. *PROC NATL ACAD SCI U S A* 88:2850-2853.
- Joshi M, Jeoung NH, Popov KM, Harris RA (2007) Identification of a novel PP2C-type mitochondrial phosphatase. *Biochemical and Biophysical Research Communications* 356:38-44.
- Jourdain P, Fukunaga K, Muller D (2003) Calcium/calmodulin-dependent protein kinase II contributes to activity-dependent filopodia growth and spine formation. *J Neurosci* 23:10645-10649.
- Kaech S, Fischer M, Doll T, Matus A (1997) Isoform specificity in the relationship of actin to dendritic spines. *J Neurosci* 17:9565-9572.
- Kanaani J, Lissin D, Kash SF, Baekkeskov S (1999) The hydrophilic isoform of glutamate decarboxylase, GAD67, is targeted to membranes and nerve terminals independent of dimerization with the hydrophobic membrane-anchored isoform, GAD65. *Journal of Biological Chemistry* 274:37200-37209.
- Kao FT, Puck TT (1968) Genetics of somatic mammalian cells, VII. Induction and isolation of nutritional mutants in Chinese hamster cells. *PROC NATL ACAD SCI U S A* 60:1275-1281.
- Kasai H, Matsuzaki M, Noguchi J, Yasumatsu N, Nakahara H (2003) Structure-stability-function relationships of dendritic spines. *Trends Neurosci* 26:360-368.
- Kaufmann WE, Moser HW (2000) Dendritic anomalies in disorders associated with mental retardation. *Cerebral Cortex* 10:981-991.
- Kennedy MB (1997) The postsynaptic density at glutamatergic synapses. *Trends Neurosci* 20:264-268.
- Kennedy MB (2000) Signal-processing machines at the postsynaptic density. *Science* 290:750-754.
- Kim S, Kim T, Lee D, Park SH, Kim H, Park D (2000) Molecular cloning of neuronally expressed mouse β Pix isoforms. *Biochemical and Biophysical Research Communications* 272:721-725.

- Kim S, Lee SH, Park D (2001) Leucine zipper-mediated homodimerization of the p21-activated kinase-interacting factor, β Pix: Implication for a role in cytoskeletal reorganization. *Journal of Biological Chemistry* 276:10581-10584.
- Kirov SA, Harris KM (1999) Dendrites are more spiny on mature hippocampal neurons when synapses are inactivated. *Nature Neuroscience* 2:878-883.
- Kitani T, Okuno S, Nakamura Y, Tokuno H, Takeuchi M, Fujisawa H (2006) Post-translational excision of the carboxyl-terminal segment of CaM kinase phosphatase N and its cytosolic occurrence in the brain. *Journal of Neurochemistry* 96:374-384.
- Kitani T, Okuno S, Takeuchi M, Fujisawa H (2003) Subcellular distributions of rat CaM kinase phosphatase N and other members of the CaM kinase regulatory system. *Journal of Neurochemistry* 86:77-85.
- Klein WL, Krafft GA, Finch CE (2001) Targeting small Abeta oligomers: The solution to an Alzheimer's disease conundrum? *Trends Neurosci* 24:219-224.
- Klumpp S, Krieglstein J (2002) Serine/threonine protein phosphatases in apoptosis. *Current Opinion in Pharmacology* 2:458-462.
- Knott GW, Holtmaat A, Wilbrecht L, Welker E, Svoboda K (2006) Spine growth precedes synapse formation in the adult neocortex in vivo. *Nature Neuroscience* 9:1117-1124.
- Koh CG, Manser E, Zhao ZS, Ng CP, Lim L (2001) β 1PIX, the PAK-interacting exchange factor, requires localization via a coiled-coil region to promote microvillus-like structures and membrane ruffles. *Journal of Cell Science* 114:4239-4251.
- Koh CG, Tan EJ, Manser E, Lim L (2002) The p21-activated kinase PAK is negatively regulated by POPX1 and POPX2, a pair of serine/threonine phosphatases of the PP2C family. *Current Biology* 12:317-321.
- Komaki KI, Katsura K, Ohnishi M, Li MG, Sasaki M, Watanabe M, Kobayashi T, Tamura S (2003) Molecular cloning of PP2C η , a novel member of the protein phosphatase 2C family. *Biochimica et Biophysica Acta - Gene Structure and Expression* 1630:130-137.
- Korkotian E, Segal M (2000) Structure-function relations in dendritic spines: Is size important? *Hippocampus* 10:587-595.
- Kotera I, Sekimoto T, Miyamoto Y, Saiwaki T, Nagoshi E, Sakagami H, Kondo H, Yoneda Y (2005) Importin α transports CaMKIV to the nucleus without utilizing importin. *EMBO Journal* 24:942-951.
- Koushika SP, Lisbin MJ, White K (1996) ELAV, a Drosophila neuron-specific protein, mediates the generation of an alternatively spliced neural protein isoform. *Current Biology* 6:1634-1641.
- Kreis P, Barnier JV (2009) PAK signalling in neuronal physiology. *Cellular Signalling* 21:384-393.
- Kügler S, Lingor P, Schöll U, Zolotukhin S, Bähr M (2003) Differential transgene expression in brain cells in vivo and in vitro from AAV-2 vectors with small transcriptional control units. *Virology* 311:89-95.
- Kusuda K, Kobayashi T, Ikeda S, Ohnishi M, Chida N, Yanagawa Y, Shineha R, Nishihira T, Satomi S, Hiraga A, Tamura S (1998) Mutational analysis of the domain structure of mouse protein phosphatase 2Cbeta. *Biochemical Journal* 332:243-250.
- Kutsche K, Yntema H, Brandt A, Jantke I, Nothwang HG, Orth U, Boavida MG, David D, Chelly J, Fryns JP, Moraine C, Ropers HH, Hamel BCJ, Van Bokhoven H, Gal A (2000) Mutations in

- ARHGEF6, encoding a guanine nucleotide exchange factor for Rho GTPases, in patients with X-linked mental retardation. *Nature Genetics* 26:247-250.
- Lacor PN, Buniel MC, Furlow PW, Clemente AS, Velasco PT, Wood M, Viola KL, Klein WL (2007) Abeta oligomer-induced aberrations in synapse composition, shape, and density provide a molecular basis for loss of connectivity in Alzheimer's disease. *J Neurosci* 27:796-807.
- Landis DMD, Reese TS (1983) Cytoplasmic organization in cerebellar dendritic spines. *Journal of Cell Biology* 97:1169-1178.
- Larkin MA, Blackshields G, Brown NP, Chenna R, Mcgettigan PA, McWilliam H, Valentin F, Wallace IM, Wilm A, Lopez R, Thompson JD, Gibson TJ, Higgins DG (2007) Clustal W and Clustal X version 2.0. *Bioinformatics* 23:2947-2948.
- Lei M, Lu W, Meng W, Parrini MC, Eck MJ, Mayer BJ, Harrison SC (2000) Structure of PAK1 in an autoinhibited conformation reveals a multistage activation switch. *Cell* 102:387-397.
- Lendvai B, Stern EA, Chen B, Svoboda K (2000) Experience-dependent plasticity of dendritic spines in the developing rat barrel cortex in vivo. *Nature* 404:876-881.
- Levi A, Eldridge JD, Paterson BM (1985) Molecular cloning of a gene sequence regulated by nerve growth factor. *Science* 229:393-395.
- Li Z, Okamoto KI, Hayashi Y, Sheng M (2004) The importance of dendritic mitochondria in the morphogenesis and plasticity of spines and synapses. *Cell* 119:873-887.
- Li Z, Sheng M (2003) Some assembly required: The development of neuronal synapses. *Nature Reviews Molecular Cell Biology* 4:833-841.
- Lim L, Manser E, Leung T, Hall C (1996) Regulation of phosphorylation pathways by p21 GTPases. The p21 Ras-related Rho subfamily and its role in phosphorylation signalling pathways. *European Journal of Biochemistry* 242:171-185.
- Lisman J, Schulman H, Cline H (2002) The molecular basis of CaMKII function in synaptic and behavioural memory. *Nat Rev Neurosci* 3:175-190.
- Lohmann C, Bonhoeffer T (2008) A Role for Local Calcium Signaling in Rapid Synaptic Partner Selection by Dendritic Filopodia. *Neuron* 59:253-260.
- Loo TH, Ng YW, Lim L, Manser E (2004) GIT1 Activates p21-Activated Kinase through a Mechanism Independent of p21 Binding. *Molecular and Cellular Biology* 24:3849-3859.
- Lopez OL, DeKosky ST (2003) Neuropathology of Alzheimer's disease and mild cognitive impairment. *Revista de Neurologia* 37:155-163.
- Lue LF, Kuo YM, Roher AE, Brachova L, Shen Y, Sue L, Beach T, Kurth JH, Rydel RE, Rogers J (1999) Soluble amyloid β peptide concentration as a predictor of synaptic change in Alzheimer's disease. *American Journal of Pathology* 155:853-862.
- Luo L, Hensch TK, Ackerman L, Barbel S, Jan LY, Jan YN (1996) Differential effects of the Rac GTPase on Purkinje cell axons and dendritic trunks and spines. *Nature* 379:837-840.
- Maekawa M, Ishizaki T, Boku S, Watanabe N, Fujita A, Iwamatsu A, Obinata T, Ohashi K, Mizuno K, Narumiya S (1999) Signaling from Rho to the actin cytoskeleton through protein kinases ROCK and LIM-kinase. *Science* 285:895-898.
- Mahadomrongkul V, Huerta PT, Shirao T, Aoki C (2005) Stability of the distribution of spines containing drebrin A in the sensory cortex layer I of mice expressing mutated APP and PS1 genes. *Brain Research* 1064:66-74.

- Maletic-Savatic M, Malinow R, Svoboda K (1999) Rapid dendritic morphogenesis in CA1 hippocampal dendrites induced by synaptic activity. *Science* 283:1923-1927.
- Maloney MT, Bamberg JR (2007) Cofilin-mediated neurodegeneration in Alzheimer's disease and other amyloidopathies. *Mol Neurobiol* 35:21-43.
- Manser E, Leung T, Salihuddin H, Zhao ZS, Lim L (1994) A brain serine/threonine protein kinase activated by Cdc42 and Rac1. *Nature* 367:40-46.
- Manser E, Loo TH, Koh CG, Zhao ZS, Chen XQ, Tan L, Tan I, Leung T, Lim L (1998) PAK kinases are directly coupled to the PIX family of nucleotide exchange factors. *Molecular Cell* 1:183-192.
- Marchler-Bauer A, et al. (2009) CDD: Specific functional annotation with the Conserved Domain Database. *Nucleic Acids Research* 37.
- Marrs GS, Green SH, Dailey ME (2001) Rapid formation and remodeling of postsynaptic densities in developing dendrites. *Nature Neuroscience* 4:1006-1013.
- Masters CL, Simms G, Weinman NA (1985) Amyloid plaque core protein in Alzheimer disease and Down syndrome. *PROC NATL ACAD SCI U S A* 82:4245-4249.
- Matenia D, Griesshaber B, Li XY, Thiessen A, Johne C, Jiao J, Mandelkow E, Mandelkow EM (2005) PAK5 kinase is an inhibitor of MARK/Par-1, which leads to stable microtubules and dynamic actin. *Molecular Biology of the Cell* 16:4410-4422.
- Matsuzaki M, Ellis-Davies GCR, Nemoto T, Miyashita Y, Iino M, Kasai H (2001) Dendritic spine geometry is critical for AMPA receptor expression in hippocampal CA1 pyramidal neurons. *Nature Neuroscience* 4:1086-1092.
- Matsuzaki M, Honkura N, Ellis-Davies GCR, Kasai H (2004) Structural basis of long-term potentiation in single dendritic spines. *Nature* 429:761-766.
- Matthews RP, Guthrie CR, Wailes LM, Zhao X, Means AR, Mcknight GS (1994) Calcium/calmodulin-dependent protein kinase types II and IV differentially regulate CREB-dependent gene expression. *Molecular and Cellular Biology* 14:6107-6116.
- Matus A (1999) Postsynaptic actin and neuronal plasticity. *Curr Opin Neurobiol* 9:561-565.
- Matus A, Ackermann M, Pehling G (1982) High actin concentrations in brain dendritic spines and postsynaptic densities. *PROC NATL ACAD SCI U S A* 79:7590-7594.
- Mauceri D, Cattabeni F, Di Luca M, Gardoni F (2004) Phosphorylation drives synapse-associated protein 97 into spines. *Journal of Biological Chemistry* 279:23813-23821.
- Maximov A, Pang ZP, Tervo DGR, Südhof TC (2007) Monitoring synaptic transmission in primary neuronal cultures using local extracellular stimulation. *Journal of Neuroscience Methods* 161:75-87.
- McGinnis KM, Whitton MM, Gnegy ME, Wang KKW (1998) Calcium/calmodulin-dependent protein kinase IV is cleaved by caspase-3 and calpain in SH-SY5Y human neuroblastoma cells undergoing apoptosis. *Journal of Biological Chemistry* 273:19993-20000.
- McGough A, Chiu W (1999) ADF/cofilin weakens lateral contacts in the actin filament. *Journal of Molecular Biology* 291:513-519.
- McGough A, Pope B, Chiu W, Weeds A (1997) Cofilin changes the twist of F-actin: Implications for actin filament dynamics and cellular function. *Journal of Cell Biology* 138:771-781.

- McGowan CH, Cohen P (1988) Protein phosphatase-2C from rabbit skeletal muscle and liver: An Mg^{2+} -dependent enzyme. *Methods in Enzymology* 159:416-426.
- McLean CA, Cherny RA, Fraser FW, Fuller SJ, Smith MJ, Beyreuther K, Bush AI, Masters CL (1999) Soluble pool of A β amyloid as a determinant of severity of neurodegeneration in Alzheimer's disease. *Annals of Neurology* 46:860-866.
- McPhie DL, Coopersmith R, Hines-Peralta A, Chen Y, Ivins KJ, Manly SP, Kozlowski MR, Neve KA, Neve RL (2003) DNA synthesis and neuronal apoptosis caused by familial Alzheimer disease mutants of the amyloid precursor protein are mediated by the p21 activated kinase PAK3. *J Neurosci* 23:6914-6927.
- Meng Y, Zhang Y, Tregoubov V, Janus C, Cruz L, Jackson M, Lu WY, MacDonald JF, Wang JY, Falls DL, Jia Z (2002) Abnormal spine morphology and enhanced LTP in LIMK-1 knockout mice. *Neuron* 35:121-133.
- Miller AD (1997) Development and Applications of Retroviral Vectors. In: *Retroviruses* (Coffin JM, Hughes SH, Varmus HE, eds), pp 437-473. Plainview, NY: Cold Spring Harbor Laboratory Press.
- Mirra SS, Hart MN, Terry RD (1993) Making the diagnosis of Alzheimer's disease: A primer for practicing pathologists. *Archives of Pathology and Laboratory Medicine* 117:132-144.
- Mirra SS, Heyman A, McKeel D, Sumi SM, Crain BJ, Brownlee LM, Vogel FS, Hughes JP, Van Belle G, Berg L (1991) The Consortium to Establish a Registry for Alzheimer's Disease (CERAD). Part II. Standardization of the neuropathologic assessment of Alzheimer's disease. *Neurology* 41:479-486.
- Morreale A, Venkatesan M, Mott HR, Owen D, Nietlispach D, Lowe PN, Laue ED (2000) Structure of Cdc42 bound to the GTPase binding domain of PAK. *Nature Structural Biology* 7:384-388.
- Morris BJ, Johnston HM (1995) A role for hippocampal opioids in long-term functional plasticity. *Trends Neurosci* 18:350-355.
- Mullen RJ, Buck CR, Smith AM (1992) NeuN, a neuronal specific nuclear protein in vertebrates. *Development* 116:201-211.
- Muqit MMK, Feany MB (2002) Modelling neurodegenerative diseases in *Drosophila*: A fruitful approach? *Nat Rev Neurosci* 3:237-243.
- Nägerl UV, Köstinger G, Anderson JC, Martin KAC, Bonhoeffer T (2007) Protracted synaptogenesis after activity-dependent spinogenesis in hippocampal neurons. *J Neurosci* 27:8149-8156.
- Nakamura Y, Okuno S, Sato F, Fujisawa H (1995) An immunohistochemical study of Ca^{2+} /calmodulin-dependent protein kinase IV in the rat central nervous system: Light and electron microscopic observations. *Neuroscience* 68:181-194.
- Neuspiel M, Schauss AC, Braschi E, Zunino R, Rippstein P, Rachubinski RA, Andrade-Navarro MA, McBride HM (2008) Cargo-Selected Transport from the Mitochondria to Peroxisomes Is Mediated by Vesicular Carriers. *Current Biology* 18:102-108.
- Newey SE, Velamoor V, Govak EE, Van Aelst L (2005) Rho GTPases, dendritic structure, and mental retardation. *Journal of Neurobiology* 64:58-74.
- Nimchinsky EA, Sabatini BL, Svoboda K (2002) Structure and function of dendritic spines. pp 313-353.
- Nimura T, Sueyoshi N, Ishida A, Yoshimura Y, Ito M, Tokumitsu H, Shigeri Y, Nozaki N, Kameshita I (2007) Knockdown of nuclear Ca^{2+} /calmodulin-dependent protein kinase

- phosphatase causes developmental abnormalities in zebrafish. *Arch Biochem Biophys* 457:205-216.
- Nimura T, Sugiyama Y, Sueyoshi N, Shigeri Y, Ishida A, Kameshita I (2010) A minimum size homologue of Ca²⁺/calmodulin-dependent protein kinase IV naturally occurring in zebrafish. *Journal of Biochemistry* 147:857-865.
- Nordberg A, Rinne JO, Kadir A, Lngström B (2010) The use of PET in Alzheimer disease. *Nature Reviews Neurology* 6:78-87.
- Oh JS, Chen HJ, Rojas-Soto M, Oguni A, Kennedy MB (2002) Erratum: A synaptic Ras-GTPase activating protein [p135 synGap] inhibited by CaM kinase II (*Neuron* (May 1998) 20 (895-904)). *Neuron* 33:151.
- Ohashi K, Nagata K, Maekawa M, Ishizaki T, Narumiya S, Mizuno K (2000) Rho-associated kinase ROCK activates LIM-kinase 1 by phosphorylation at threonine 508 within the activation loop. *Journal of Biological Chemistry* 275:3577-3582.
- Pantaloni D, Le Clainche C, Carlier MF (2001) Mechanism of actin-based motility. *Science* 292:1502-1506.
- Papa M, Bundman MC, Greenberger V, Segal M (1995) Morphological analysis of dendritic spine development in primary cultures of hippocampal neurons. *J Neurosci* 15:1-11.
- Parnas D, Haghighi AP, Fetter RD, Kim SW, Goodman CS (2001) Regulation of postsynaptic structure and protein localization by the Rho-type guanine nucleotide exchange factor dPix. *Neuron* 32:415-424.
- Parrini MC, Lei M, Harrison SC, Mayer BJ (2002) Pak1 kinase homodimers are autoinhibited in trans and dissociated upon activation by Cdc42 and Rac1. *Molecular Cell* 9:73-83.
- Pärssinen J, Kuukasjärvi T, Karhu R, Kallioniemi A (2007) High-level amplification at 17q23 leads to coordinated overexpression of multiple adjacent genes in breast cancer. *British Journal of Cancer* 96:1258-1264.
- Penzes P, Beeser A, Chernoff J, Schiller MR, Eipper BA, Mains RE, Huganir RL (2003) Rapid induction of dendritic spine morphogenesis by trans-synaptic ephrinB-EphB receptor activation of the Rho-GEF kalirin. *Neuron* 37:263-274.
- Persengiev SP, Zhu X, Green MR (2004) Nonspecific, concentration-dependent stimulation and repression of mammalian gene expression by small interfering RNAs (siRNAs). *RNA* 10:12-18.
- Peters A, Kaiserman-Abramof IR (1970) The small pyramidal neuron of the rat cerebral cortex. The perikaryon, dendrites and spines. *American Journal of Anatomy* 127:321-355.
- Pimplikar SW (2009) Reassessing the amyloid cascade hypothesis of Alzheimer's disease. *International Journal of Biochemistry and Cell Biology* 41:1261-1268.
- Pollard TD, Borisy GG (2003) Cellular motility driven by assembly and disassembly of actin filaments. *Cell* 112:453-465.
- Pratt KG, Watt AJ, Griffith LC, Nelson SB, Turrigiano GG (2003) Activity-dependent remodeling of presynaptic inputs by postsynaptic expression of activated CaMKII. *Neuron* 39:269-281.
- Purpura DP, Bodick N, Suzuki K, Rapin I, Wurzelmann S (1982) Microtubule disarray in cortical dendrites and neurobehavioral failure. I. Golgi and electron microscopic studies. *Brain Research* 281:287-297.

- Puto LA, Pestonjamas K, King CC, Bokoch GM (2003) p21-activated kinase 1 (PAK1) interacts with the Grb2 adapter protein to couple to growth factor signaling. *Journal of Biological Chemistry* 278:9388-9393.
- Ramakers GJA (2002) Rho proteins, mental retardation and the cellular basis of cognition. *Trends Neurosci* 25:191-199.
- Rao A, Craig AM (2000) Signaling between the actin cytoskeleton and the postsynaptic density of dendritic spines. *Hippocampus* 10:527-541.
- Redmond L, Kashani AH, Ghosh A (2002) Calcium regulation of dendritic growth via CaM kinase IV and CREB-mediated transcription. *Neuron* 34:999-1010.
- Rhee S, Yang SJ, Lee SJ, Park D (2004) β Pix-b_L, a novel isoform of β Pix, is generated by alternative translation. *Biochemical and Biophysical Research Communications* 318:415-421.
- Rodriguez A, Ehlenberger DB, Dickstein DL, Hof PR, Wearne SL (2008) Automated three-dimensional detection and shape classification of dendritic spines from fluorescence microscopy images. *PLoS ONE* 3.
- Roelandse M, Matus A (2004) Hypothermia-associated loss of dendritic spines. *J Neurosci* 24:7843-7847.
- Roelandse M, Welman A, Wagner U, Hagmann J, Matus A (2003) Focal motility determines the geometry of dendritic spines. *Neuroscience* 121:39-49.
- Rosen RF, Walker LC, LeVine III H (2009) PIB binding in aged primate brain: Enrichment of high-affinity sites in humans with Alzheimer's disease.
- Rosenberg OS, Deindl S, Sung RJ, Nairn AC, Kuriyan J (2005) Structure of the autoinhibited kinase domain of CaMKII and SAXS analysis of the holoenzyme. *Cell* 123:849-860.
- Rosenberger G, Gal A, Kutsche K (2005) α PIX associates with calpain 4, the small subunit of calpain, and has a dual role in integrin-mediated cell spreading. *Journal of Biological Chemistry* 280:6879-6889.
- Rosenberger G, Jantke I, Gal A, Kutsche K (2003) Interaction of α PIX (ARHGEF6) with β -parvin (PARVB) suggests an involvement of α PIX in integrin-mediated signaling. *Human Molecular Genetics* 12:155-167.
- Rosso S, Bollati F, Bisbal M, Peretti D, Sumi T, Nakamura T, Quiroga S, Ferreira A, Cáceres A (2004) LIMK1 regulates Golgi dynamics, traffic of Golgi-derived vesicles, and process extension in primary cultured neurons. *Molecular Biology of the Cell* 15:3433-3449.
- Rubin GM, Spradling AC (1982) Genetic transformation of *Drosophila* with transposable element vectors. *Science* 218:348-353.
- Safer D, Golla R, Nachmias VT (1990) Isolation of a 5-kilodalton actin-sequestering peptide from human blood platelets. *PROC NATL ACAD SCI U S A* 87:2536-2540.
- Safer D, Nachmias VT (1994) Beta thymosins as actin binding peptides. *BioEssays* 16:590.
- Saito S, Matsui H, Kawano M, Kumagai K, Tomishige N, Hanada K, Echigo S, Tamura S, Kobayashi T (2008) Protein phosphatase 2C ϵ is an endoplasmic reticulum integral membrane protein that dephosphorylates the ceramide transport protein CERT to enhance its association with organelle membranes. *Journal of Biological Chemistry* 283:6584-6593.
- Sala C (2002) Molecular regulation of dendritic spine shape and function. *NeuroSignals* 11:213-223.

- Saneyoshi T, Fortin DA, Soderling TR (2010) Regulation of spine and synapse formation by activity-dependent intracellular signaling pathways. *Curr Opin Neurobiol* 20:108-115.
- Saneyoshi T, Wayman G, Fortin D, Davare M, Hoshi N, Nozaki N, Natsume T, Soderling TR (2008) Activity-Dependent Synaptogenesis: Regulation by a CaM-Kinase Kinase/CaM-Kinase I/ β PIX Signaling Complex. *Neuron* 57:94-107.
- Scannevin RH, Huganir RL (2000) Postsynaptic organization and regulation of excitatory synapses. *Nat Rev Neurosci* 1:133-141.
- Scheff SW, Price DA, Schmitt FA, DeKosky ST, Mufson EJ (2007) Synaptic alterations in CA1 in mild Alzheimer disease and mild cognitive impairment. *Neurology* 68:1501-1508.
- Scheibel AB (1979) Dendritic changes in senile and presenile dementias. *Research publications - Association for Research in Nervous and Mental Disease* 57:107-124.
- Scheibel AB (1983) Dendritic changes. In: *Alzheimer's Disease* (B.Reisberg, ed), pp 69-73. New York: The Free Press.
- Scheuner D, et al. (1996) Secreted amyloid β -protein similar to that in the senile plaques of Alzheimer's disease is increased in vivo by the presenilin 1 and 2 and APP mutations linked to familial Alzheimer's disease. *Nature Medicine* 2:864-870.
- Sée V, Boutillier AL, Bito H, Loeffler JP (2001) Calcium/calmodulin-dependent protein kinase type IV (CaMKIV) inhibits apoptosis induced by potassium deprivation in cerebellar granule neurons. *FASEB Journal* 15:134-144.
- Segev I, Rall W (1998) Excitable dendrites and spines: Earlier theoretical insights elucidate recent direct observations. *Trends Neurosci* 21:453-460.
- Sekino Y, Kojima N, Shirao T (2007) Role of actin cytoskeleton in dendritic spine morphogenesis. *Neurochemistry International* 51:92-104.
- Selkoe DJ (1991) The molecular pathology of Alzheimer's disease. *Neuron* 6:487-498.
- Selkoe DJ (2001) Alzheimer's disease: Genes, proteins, and therapy. *Physiological Reviews* 81:741-766.
- Selkoe DJ (2002a) Alzheimer's disease is a synaptic failure. *Science* 298:789-791.
- Selkoe DJ (2002b) Deciphering the genesis and fate of amyloid β -protein yields novel therapies for Alzheimer disease. *Journal of Clinical Investigation* 110:1375-1381.
- Selkoe DJ, Schenk D (2003) Alzheimer's Disease: Molecular Understanding Predicts Amyloid-Based Therapeutics. pp 545-584.
- Selkoe DJ, Wolfe MS (2007) Presenilin: Running with scissors in the membrane. *Cell* 131:215-221.
- Sells MA, Chernoff J (1997) Emerging from the Pak: The p21-activated protein kinase family. *Trends Cell Biol* 7:162-167.
- Shen K, Meyer T (1999) Dynamic control of CaMKII translocation and localization in hippocampal neurons by NMDA receptor stimulation. *Science* 284:162-166.
- Shen K, Teruel MN, Connor JH, Shenolikar S, Meyer T (2000) Molecular memory by reversible translocation of calcium/calmodulin-dependent protein kinase II. *Nature Neuroscience* 3:881-886.

- Shen K, Teruel MN, Subramanian K, Meyer T (1998) CaMKII β functions as an F-actin targeting module that localizes CaMKII α/β heterooligomers to dendritic spines. *Neuron* 21:593-606.
- Shevtsova Z, Malik JMI, Michel U, Bähr M, Kügler S (2005) Promoters and serotypes: Targeting of adeno-associated virus vectors for gene transfer in the rat central nervous system in vitro and in vivo. *Experimental Physiology* 90:53-59.
- Silva AJ, Giese KP, Fedorov NB, Frankland PW, Kogan JH (1998a) Molecular, cellular, and neuroanatomical substrates of place learning. *Neurobiology of Learning and Memory* 70:44-61.
- Silva AJ, Kogan JH, Frankland PW, Kida S (1998b) CREB and memory. pp 127-148.
- Sisodia SS, Koo EH, Beyreuther K, Unterbeck A, Price DL (1990) Evidence that β -amyloid protein in Alzheimer's disease is not derived by normal processing. *Science* 248:492-495.
- Sisodia SS, St George-Hyslop PH (2002) γ -secretase, Notch, A β and Alzheimer's disease: Where do the presenilins fit in? *Nat Rev Neurosci* 3:281-290.
- Smith AD (2002) Imaging the progression of Alzheimer pathology through the brain. *PROC NATL ACAD SCI U S A* 99:4135-4137.
- Soderling TR, Stull JT (2001) Structure and regulation of calcium/calmodulin-dependent protein kinases. *Chem Rev* 101:2341-2351.
- Sorra KE, Harris KM (2000) Overview on the structure, composition, function, development, and plasticity of hippocampal dendritic spines. *Hippocampus* 10:501-511.
- Spacek J, Harris KM (1997) Three-dimensional organization of smooth endoplasmic reticulum in hippocampal CA1 dendrites and dendritic spines of the immature and mature rat. *J Neurosci* 17:190-203.
- Spradling AC, Rubin GM (1982) Transposition of cloned P elements into *Drosophila* germ line chromosomes. *Science* 218:341-347.
- Spradling AC, Stern DM, Kiss I, Roote J, Lavery T, Rubin GM (1995) Gene disruptions using P transposable elements: An integral component of the *Drosophila* genome project. *PROC NATL ACAD SCI U S A* 92:10824-10830.
- Star EN, Kwiatkowski DJ, Murthy VN (2002) Rapid turnover of actin in dendritic spines and its regulation by activity. *Nature Neuroscience* 5:239-246.
- Steiner P, Higley MJ, Xu W, Czervionke BL, Malenka RC, Sabatini BL (2008) Destabilization of the Postsynaptic Density by PSD-95 Serine 73 Phosphorylation Inhibits Spine Growth and Synaptic Plasticity. *Neuron* 60:788-802.
- Steward O, Schuman EM (2001) Protein synthesis at synaptic sites on dendrites. pp 299-325.
- Sueyoshi N, Takao T, Nimura T, Sugiyama Y, Numano T, Shigeri Y, Taniguchi T, Kameshita I, Ishida A (2007) Inhibitors of the Ca²⁺/calmodulin-dependent protein kinase phosphatase family (CaMKP and CaMKP-N). *Biochemical and Biophysical Research Communications* 363:715-721.
- Svoboda K, Tank DW, Denk W (1996) Direct measurement of coupling between dendritic spines and shafts. *Science* 272:716-719.
- Tackenberg C, Ghori A, Brandt R (2009) Thin, stubby or mushroom: Spine pathology in Alzheimer's disease. *Current Alzheimer Research* 6:261-268.

- Tada Y, Nimura T, Sueyoshi N, Ishida A, Shigeri Y, Kameshita I (2006) Mutational analysis of Ca²⁺/calmodulin-dependent protein kinase phosphatase (CaMKP). *Arch Biochem Biophys* 452:174-185.
- Takemura M, Mishima T, Wang Y, Kasahara J, Fukunaga K, Ohashi K, Mizuno K (2009) Ca²⁺/Calmodulin-dependent protein kinase IV-mediated LIM kinase activation is critical for calcium signal-induced neurite outgrowth. *Journal of Biological Chemistry* 284:28554-28562.
- Takeuchi M, Ishida A, Kameshita I, Kitani T, Okuno S, Fujisawa H (2001) Identification and characterization of CaMKP-N, nuclear calmodulin-dependent protein kinase phosphatase. *Journal of Biochemistry* 130:833-840.
- Takeuchi M, Taniguchi T, Fujisawa H (2004) Identification and characterization of nuclear localization signals of CaMKP-N. *Journal of Biochemistry* 136:183-188.
- Tanzi RE, Bertram L (2005) Twenty years of the Alzheimer's disease amyloid hypothesis: A genetic perspective. *Cell* 120:545-555.
- Tarrant SB, Routtenberg A (1979) Postsynaptic membrane and spine apparatus: Proximity in dendritic spines. *Neuroscience Letters* 11:289-294.
- Tashiro A, Yuste R (2003) Structure and molecular organization of dendritic spines. *Histology and Histopathology* 18:617-634.
- Terry RD, Masliah E, Salmon DP, Butters N, Deteresa R, Hill R, Hansen LA, Katzman R (1991) Physical basis of cognitive alterations in Alzheimer's disease: Synapse loss is the major correlate of cognitive impairment. *Annals of Neurology* 30:572-580.
- Thompson JD, Gibson TJ, Plewniak F, Jeanmougin F, Higgins DG (1997) The CLUSTAL X windows interface: Flexible strategies for multiple sequence alignment aided by quality analysis tools. *Nucleic Acids Research* 25:4876-4882.
- Trachtenberg JT, Chen BE, Knott GW, Feng G, Sanes JR, Welker E, Svoboda K (2002) Long-term in vivo imaging of experience-dependent synaptic plasticity in adult cortex. *Nature* 420:788-794.
- Tursun B, Schlüter A, Peters MA, Viehweger B, Ostendorff HP, Soosairajah J, Drung A, Bossenz M, Johnsen SA, Schweizer M, Bernard O, Bach I (2005) The ubiquitin ligase Rnf6 regulates local LIM kinase 1 levels in axonal growth cones. *Genes and Development* 19:2307-2319.
- Van Rossum D, Hanisch UK (1999) Cytoskeletal dynamics in dendritic spines: Direct modulation by glutamate receptors? *Trends Neurosci* 22:290-295.
- Vaughn JL, Goodwin RH, Tompkins GJ, McCawley P (1977) The establishment of two cell lines from the insect *Spodoptera frugiperda* (Lepidoptera; Noctuidae). *In Vitro* 13:213-217.
- Vincze T, Posfai J, Roberts RJ (2003) NEBcutter: A program to cleave DNA with restriction enzymes. *Nucleic Acids Research* 31:3688-3691.
- Vlachos A, Korkotian E, Schonfeld E, Copanaki E, Deller T, Segal M (2009) Synaptopodin regulates plasticity of dendritic spines in hippocampal neurons. *J Neurosci* 29:1017-1033.
- von der Kammer H (2009) PPM1E proteins and nucleic acids as targets for neurodegenerative diseases. Patent application PCT/EP2008/064446. Publication Date: 30.04.2009.
- Walsh DM, Selkoe DJ (2004) Deciphering the molecular basis of memory failure in Alzheimer's disease. *Neuron* 44:181-193.

- Walsh DM, Selkoe DJ (2007) A β oligomers - A decade of discovery. *Journal of Neurochemistry* 101:1172-1184.
- Walsh MJ, Kuruc N (1992) The postsynaptic density: Constituent and associated proteins characterized by electrophoresis, immunoblotting, and peptide sequencing. *Journal of Neurochemistry* 59:667-678.
- Walters MJ, Wayman GA, Notis JC, Goodman RH, Soderling TR, Christian JL (2002) Calmodulin-dependent protein kinase IV mediated antagonism of BMP signaling regulates lineage and survival of hematopoietic progenitors. *Development* 129:1455-1466.
- Wayman GA, Lee YS, Tokumitsu H, Silva A, Soderling TR (2008) Calmodulin-Kinases: Modulators of Neuronal Development and Plasticity. *Neuron* 59:914-931.
- Wayman GA, Walters MJ, Kolibaba K, Soderling TR, Christian JL (2000) CaM kinase IV regulates lineage commitment and survival of erythroid progenitors in a non-cell-autonomous manner. *Journal of Cell Biology* 151:811-824.
- Weeber EJ, Jiang YH, Elgersma Y, Varga AW, Carrasquillo Y, Brown SE, Christian JM, Mirmikjoo B, Silva A, Beaudet AL, Sweatt JD (2003) Derangements of hippocampal calcium/calmodulin-dependent protein kinase II in a mouse model for Angelman mental retardation syndrome. *J Neurosci* 23:2634-2644.
- Wei Z, Song MS, MacTavish D, Jhamandas JH, Kar S (2008) Role of calpain and caspase in β -amyloid-induced cell death in rat primary septal cultured neurons. *Neuropharmacology* 54:721-733.
- Werner LA, Manseau LJ (1997) A *Drosophila* gene with predicted rhoGEF, pleckstrin homology and SH3 domains is highly expressed in morphogenic tissues. *Gene* 187:107-114.
- Westrum LE, Jones DH, Gray EG, Barron J (1980) Microtubules, dendritic spines and spine apparatuses. *Cell and Tissue Research* 208:171-181.
- Wisniewski KE, Segan SM, Mizejeski CM, Sersen EA, Rudelli RD (1991) The fra(X) syndrome: Neurological, electrophysiological, and neuropathological abnormalities. *American Journal of Medical Genetics* 38:476-480.
- Wolf HK, Buslei R, Schmidt-Kastner R, Schmidt-Kastner PK, Pietsch T, Wiestler OD, Blümcke I (1996) NeuN: A useful neuronal marker for diagnostic histopathology. *Journal of Histochemistry and Cytochemistry* 44:1167-1171.
- Woodrum DT, Rich SA, Pollard TD (1975) Evidence for biased bidirectional polymerization of actin filaments using heavy meromyosin prepared by an improved method. *Journal of Cell Biology* 67:231-237.
- Woolley CS, Gould E, Frankfurt M, McEwen BS (1990) Naturally occurring fluctuation in dendritic spine density on adult hippocampal pyramidal neurons. *J Neurosci* 10:4035-4039.
- Wyszynski M, Lin J, Rao A, Nigh E, Beggs AH, Craig AM, Sheng M (1997) Competitive binding of α -actinin and calmodulin to the NMDA receptor. *Nature* 385:439-442.
- Xie Z, Photowala H, Cahill ME, Srivastava DP, Woolfrey KM, Shum CY, Haganir RL, Penzes P (2008) Coordination of synaptic adhesion with dendritic spine remodeling by aF-6 and kalirin-7. *J Neurosci* 28:6079-6091.
- Xie Z, Srivastava DP, Photowala H, Kai L, Cahill ME, Woolfrey KM, Shum CY, Surmeier DJ, Penzes P (2007) Kalirin-7 Controls Activity-Dependent Structural and Functional Plasticity of Dendritic Spines. *Neuron* 56:640-656.

- Yang N, Higuchi O, Mizuno K (1998a) Cytoplasmic localization of LIM-kinase 1 is directed by a short sequence within the PDZ domain. *Experimental Cell Research* 241:242-252.
- Yang N, Higuchi O, Ohashi K, Nagata K, Wada A, Kangawa K, Nishida E, Mizuno K (1998b) Cofilin phosphorylation by LIM-kinase 1 and its role in Rac-mediated actin reorganization. *Nature* 393:809-812.
- Yang N, Mizuno K (1999) Nuclear export of LIM-kinase 1, mediated by two leucine-rich nuclear-export signals within the PDZ domain. *Biochemical Journal* 338:793-798.
- Yntema HG, Hamel BCJ, Smits APT, Van Roosmalen T, Van Den Helm B, Kremer H, Ropers HH, Smeets DFCM, Van Bokhoven H (1998) Localisation of a gene for non-specific X linked mental retardation (MRX46) to Xq25-q26. *Journal of Medical Genetics* 35:801-805.
- Yoshihara Y, De Roo M, Muller D (2009) Dendritic spine formation and stabilization. *Curr Opin Neurobiol* 19:146-153.
- Yoshimura Y, Aoi C, Yamauchi T (2000) Investigation of protein substrates of Ca²⁺/calmodulin-dependent protein kinase II translocated to the postsynaptic density. *Molecular Brain Research* 81:118-128.
- Yu JS, Chen WJ, Ni MH, Chan WH, Yang SD (1998) Identification of the regulatory autophosphorylation site of autophosphorylation-dependent protein kinase (auto-kinase): Evidence that auto-kinase belongs to a member of the p21-activated kinase family. *Biochemical Journal* 334:121-131.
- Yuste R, Bonhoeffer T (2001) Morphological changes in dendritic spines associated with long-term synaptic plasticity. pp 1071-1089.
- Yuste R, Bonhoeffer T (2004) Genesis of dendritic spines: Insights from ultrastructural and imaging studies. *Nat Rev Neurosci* 5:24-34.
- Yuste R, Majewska A, Cash SS, Denk W (1999) Mechanisms of calcium influx into hippocampal spines: Heterogeneity among spines, coincidence detection by NMDA receptors, and optical quantal analysis. *J Neurosci* 19:1976-1987.
- Yuste R, Majewska A, Holthoff K (2000) From form to function: Calcium compartmentalization in dendritic spines. *Nature Neuroscience* 3:653-659.
- Zegers MMP, Forget MA, Chernoff J, Mostov KE, Ter Beest MBA, Hansen SH (2003) Pak1 and PIX regulate contact inhibition during epithelial wound healing. *EMBO Journal* 22:4155-4165.
- Zenke FT, King CC, Bohl BP, Bokoch GM (1999) Identification of a central phosphorylation site in p21-activated kinase regulating autoinhibition and kinase activity. *Journal of Biological Chemistry* 274:32565-32573.
- Zetterberg H, Blennow K, Hanse E (2010) Amyloid beta and APP as biomarkers for Alzheimer's disease. *Exp Gerontol* 45:23-29.
- Zhang H, Webb DJ, Asmussen H, Horwitz AF (2003) Synapse formation is regulated by the signaling adaptor GIT1. *Journal of Cell Biology* 161:131-142.
- Zhang H, Webb DJ, Asmussen H, Niu S, Horwitz AF (2005) A GIT1/PIX/Rac/PAK signaling module regulates spine morphogenesis and synapse formation through MLC. *J Neurosci* 25:3379-3388.
- Zhang W, Benson DL (2001) Stages of synapse development defined by dependence on F-actin. *J Neurosci* 21:5169-5181.

Zhao L, Ma QL, Calon F, Harris-White ME, Yang F, Lim GP, Morihara T, Ubeda OJ, Ambegaokar S, Hansen JE, Weisbart RH, Teter B, Frautschy SA, Cole GM (2006) Role of p21-activated kinase pathway defects in the cognitive deficits of Alzheimer disease. *Nature Neuroscience* 9:234-242.

Zhao ZS, Manser E, Chen XQ, Chong C, Leung T, Lim L (1998) A conserved negative regulatory region in α PAK: Inhibition of PAK kinases reveals their morphological roles downstream of Cdc42 and Rac1. *Molecular and Cellular Biology* 18:2153-2163.

Zheng WH, Bastianetto S, Mennicken F, Ma W, Kar S (2002) Amyloid β peptide induces tau phosphorylation and loss of cholinergic neurons in rat primary septal cultures. *Neuroscience* 115:201-211.

Zito K, Scheuss V, Knott G, Hill T, Svoboda K (2009) Rapid Functional Maturation of Nascent Dendritic Spines. *Neuron* 61:247-258.

Zolotukhin S, Byrne BJ, Mason E, Zolotukhin I, Potter M, Chesnut K, Summerford C, Samulski RJ, Muzyczka N (1999) Recombinant adeno-associated virus purification using novel methods improves infectious titer and yield. *Gene Therapy* 6:973-985.

Zuo Y, Lin A, Chang P, Gan WB (2005) Development of long-term dendritic spine stability in diverse regions of cerebral cortex. *Neuron* 46:181-189.

ACKNOWLEDGEMENT

First of all I wish to warmly thank Prof. Dr. Nils Brose for the supervision of this work, for his support and confidence in my work and for his critical input as head of my thesis committee.

I owe many thanks also to Prof. em. Dr. Rüdiger Hardeland, my second thesis committee member, for his collaboration and for valuable comments during my thesis committee meetings.

I also thank the other members of my defense committee Prof. Dr. André Fiala, Dr. Ralf Heinrich, Prof. Dr. Michael Hörner and Prof. Dr. Tomas Pieler for their interest in my doctoral thesis.

This study was carried out at Evotec Neurosciences GmbH, now Evotec AG. I would like to thank all of you at Evotec who have contributed to the existence of this thesis. Especially I would like to thank my supervisor Dr. Heinz von der Kammer for providing the opportunity to work with an interesting and challenging project and for always having time for my questions. Thank you Heinz, for all theoretical and technical advice, for giving me the chance to work independently and for welcoming me in your group.

I thank all past and present members of the Molecular Systems group at Evotec, especially Dr. Volker Mack for scientific discussions and for sharing your primary neuronal culture knowledge with me. I thank Maren Köhler for introducing the lab to me when I first started at Evotec and all the practical tips and help. Especially I also thank Christina Gabrysiak and Isabell Cardaun for your superb technical assistance, for all the help you have provided and for your admirable patience. I would like to thank Dr. Rita Reifegerste for sharing your knowledge about *D. melanogaster*. I thank Anika Beyn and Marion Biniszkievicz for teaching me the handling and anatomy of *D. melanogaster* when I started with this thesis. Furthermore I am grateful to Michaela Pirsch and Galina Bursova for their kind help in several practical matters over the years. Thank you!

At Evotec I would also like to thank Dr. Joachim Krämer for kindly introducing me to phosphatase assays and to the FCS research reader. I thank Dr. York Rudhard and Dr. Stefan Jäger for your technical guidance regarding the Opera measurements.

I warmly thank also Dr. Michaela Schweizer at ZMNH Hamburg for your help and advice regarding confocal microscopy and the reconstruction of 3D stacks.

Thanks go also to the former students in the lab, Nadine, Marco, Maria, Daniel and Dorothee, all of whom pushed different other aspects of the PPM1E project forward. Thank you for your enthusiasm!

I thank everyone at Evotec for making it a fun place to work. Especially I thank Nina, Svenja, Nadine, Ela, Christina, Isabell, Dörthe and Petra for all your help and support as well as for your company on the leisure time.

I owe great thanks also to Stefanie Steinert: Thank you for your help and support, even though you had your share of work.

I want to express my gratitude to my family for their constant support – it is way to seldom that I express my appreciation for all the things you have done for me. Thanks to Kolja, Nis and Gerburg, Morten and Marie, I greatly appreciate that you are always supporting me, no matter what.

Hamburg, 19th September

Lene Jessen

CURRICULUM VITAE**Personal Details**

Name	Anne <u>Lene</u> Jessen
E-mail	LeneJessen @ gmx.li
Nationality	german
Date of birth	4 May 1981

Education

07/2007 – 11/2010	Evotec AG, Hamburg / Georg-August-University Göttingen, Göttingen (Ph.D. Thesis) (Thesis supervisor: Prof.Dr.Nils Brose, MPI experimental medicine, Göttingen)
2004 - 2006	Molecular Life Science (Master of Science), University of Lübeck, Grade: good (1.7)
2001 - 2004	Molecular Biotechnology (Bachelor of Science), University of Lübeck, Grade: very good (1.4)

Work Experience I

04/2006 – 10/2006	Umeå Center for Molecular Pathogenesis, Umeå University, Sweden (Master's Thesis), Project: Structural Studies of the SRP (Signal Recognition Particle) Protein Targeting Pathway of <i>M. jannaschii</i>
08/2005 – 02/2006	Umeå Center for Molecular Pathogenesis, Umeå University, Sweden (Course for Future Graduate Students), Project: Structural Studies of the Alu domain from SRP of <i>M. jannaschii</i>
02/2005 – 03/2005	Molecular Phytopathology and Genetics, University of Hamburg
07/2004 – 09/2004	Division of Cell and Molecular Biophysics, King's College London, Great Britain (summer guest student)

Work Experience II

- 08/2003 – 01/2004 Cellular Allergology, Research Center Borstel (Bachelor's Thesis), Project: Recombinant Fragments of IPSE (IL-4 inducing principle from *Schistosoma mansoni* eggs): Cloning, Expression, Purification and functional Characterization
- 09/2003 Department of Medical Molecular Biology, University of Luebeck (assistant teacher)
- 09/2002 Department of Immunology, University of Luebeck (Internship)

Programme

- since 2008 NEURAD – Neurodegeneration in Alzheimer's disease, Marie Curie Ph.D. Graduate School

Posters

- 17 – 21/10/09 "Protein phosphatase 1E (PPM1E) expression is increased in early Braak stages and PPM1E overexpression in primary neuronal cells impairs dendritic spine morphogenesis"
Authors: Lene Jessen, Volker Mack, Christina Gabrysiak, Rita Reifegerste and Heinz von der Kammer; Evotec Neurosciences GmbH, Hamburg
Conference: Society for Neuroscience Annual Meeting 2009, Chicago, USA
- 15 – 22/05/09 "Validation of novel Alzheimer's Disease drug targets in primary neuronal cell culture"
Authors: Lene Jessen, Volker Mack, Christina Gabrysiak and Heinz von der Kammer; Evotec Neurosciences GmbH, Hamburg
Conference: Germany Gordon Research Conference & Seminar on Dendrites: Molecules, Structure & Function, Lucca, Italy

Göttingen, 21 September 2010